THE UNIVERSITY *of* EDINBURGH

Post-transcriptional regulation of fungal cell walls by RNA-binding proteins and untranslated regions

Marah Maan Jnied

Doctor of Philosophy
Institute of Cell and Molecular Biology
School of Biological Sciences
University of Edinburgh

2024

Dedication

To the family that made me,

and the family that found me.

Declaration

I declare that this thesis was composed by myself, that the work contained herein is my own except where explicitly stated otherwise in the text, and that this work has not been submitted for any other degree or professional qualification.

Marah Maan Jnied

2024

Acknowledgments

Firstly, I would like to thank my supervisors Dr. Edward Wallace and Dr. Atlanta Cook, and the chair of my thesis committee Dr. Amy Buck. You have all been inspiring over the past few years. Edward, thank you for giving me the opportunity to work in your lab, and for supporting and encouraging me to pursue the things I wanted to learn. Atlanta, thank you for your continued support and mentorship, and for always bringing in a fresh, clear perspective to every discussion I had with you. Amy, thank you for your comments and feedback on my project as it progressed. I learned so much from you all over the past few years.

There are many people to whom I owe the deepest gratitude for their help and support throughout this project. I will start with my friends and colleagues in the Wallace lab, past and present. The work in this thesis would not have been possible without them sharing their expertise and time and lab space with me.

Jamie, who was always incredibly supportive and genuine in her help, and who never tired of answering questions. I aspire to be as dedicated a scientist and mentor as you are. Liz, who has been a mentor and a support system and a dear friend. And above all: a true role model in every way possible. Laura, whose kindness and friendship and knowledge I always appreciate, and who made collaborating on a lab project so much fun. Sam, who is a dear friend and a brilliant person, generally speaking. Thank you for always making time to listen and help, and for enabling any idea involving food and drinks. Weronika, who is a brilliant scientist and a good friend, and who has an astonishing amount of knowledge both on lab and non-lab related things. And who I will always think of as my PhD-buddy, to her delight, I'm sure! Rachael, whose knowledge and dedication I always find truly inspiring, and who is my go-to person for questions on protein structure or R (or both). Domenico, who can always be counted upon to know everything technical, and who was a very fun and helpful lab-mate while we set up smFISH in the Wallace lab. Rosey, who started the Ssd1 work in the Wallace lab, and who I learned so much from during my project and lab work induction. James, for his advice and for looking over presentations and applications in the past when I asked him and Jamie for feedback. Amy, Flic, Sophie, Louis, and Benny whose comments and questions helped progress my project, and whose input I always appreciated.

The data in this thesis would not exist without the help of some great scientists.

The imaging in results chapter 3 was done at the University of Edinburgh with Dr. Ivan Clark's help and guidance. Some of the imaging in result chapter 3, and all of the smFISH imaging was done at the Vrije Universiteit in Amsterdam in collaboration with Dr. Evelina Tutucci. The work conducted at the Vrije Universiteit was funded by Scottish Universities Life Sciences Alliance, under the Saltire Emerging Researcher 2021 award.

Many heartfelt thanks to Dr. Evelina Tutucci for hosting me at her lab in at the Vrije Universiteit in Amsterdam, and for teaching me the smFISH technique. It remains one of the most fun and delightful things I learned during my PhD, and I'm truly

thankful for the experience. I would also like to thank Dr. Ivan Clark, whose kind guidance and help on the microscopy in this project I appreciate so much. And who was the first person to teach me fluorescent microscopy during my PhD.

The strain construction and some of the experimental design in result chapter 3 was done in collaboration with Dr. Weronika Danecka. I co-supervised two projects with Weronika, and I'm thankful for her insight and how fun and useful the entire experience was. I would also like to thank our students Ines Goncalves and Kexin Xiong for trusting us with their respective dissertation projects, and for being great students.

The analysis of the smFISH data in chapter 4 was done thanks to my student Carlotta Meyer constructing an analysis pipeline during her MSc project. Carlotta, thank you so much for all the hard work you put into the pipeline, and for putting up with endless comments and meetings to chat about the biology surrounding the project. You have done such a brilliant job with it!

The strain construction and phenotyping experiments in chapter 5 were done in collaboration with Dr. Laura Tuck, whose practicality and flexibility made the work easy. And who was genuinely just so much fun to plan and carry out a project with. I only regret that we couldn't do more work on it!

Thank you to Dr. Delma Childers at the University of Aberdeen, for being a mentor back when I was an MSc student at Aberdeen University, and again during my PhD.

I would also like to thank the Darwin Trust of Edinburgh for funding my PhD project, and all the Darwin Trust staff who worked tirelessly over the past few years to support students and help where they can. I really appreciate your efforts, and the opportunities you have given me.

The warmest and most sincere thanks to my friends whose support got me through the hardest parts of starting a PhD project just as the world fell apart. Hayarpi and Dima, who welcomed me into their home and beautiful family while I lived with them in Amsterdam, and whose friendship I cherish. Sam, again, for being a wonderful friend. Sofia and Jasmeet, who have been there since the first moment I decided I want to apply for a PhD. Ambra, my go-to pal in Edinburgh, who always makes time to listen and watch comfort movies. Adria, Nagham, Sara, Bonnie, Jaz, and Apple, who offered constant support and encouragement.

My most profuse and heartfelt gratitude to Bianca, who has been a best friend and a support system, and a cheerleader. Who listened, and understood, and kept me company, and whose presence and support never wavered.

Finally, my eternal gratitude to my family. Maan, Ghada, Laith, Hamza, and Salma. None of this would have been possible without your support and your belief. My dad and my mom, who have never let anything stand in their way. You inspire me and drive me to be a better person. My siblings, who are genuinely the best thing about my life, and whose resilience and kindness and support always ground me. Thank you for everything, truly.

Abstract

Cells grow and divide while maintaining spatial organisation, by controlling gene expression and subcellular RNA and protein localisation. Localised control of protein synthesis is important for establishment of cellular asymmetries, and for cell wall biogenesis at the growth tip leading to directional growth. Ssd1 is a conserved RNA-binding protein (RBP), required for tolerance of heat and cell wall stress in *Saccharomyces cerevisiae* and for virulence in *Candida albicans* and *Candida glabrata*. I hypothesize that Ssd1 is important for localised control of cell wall protein synthesis, thus contributing to directional growth and virulence.

Recent data from the Wallace lab show Ssd1 binding near the start codons of mRNAs encoding specific cell wall proteins. My research tests the hypothesis that Ssd1, alongside other RBPs of interest, control localised translation of target cell wall mRNAs near sites of cell wall synthesis. I employ single molecule fluorescence in situ hybridization (smFISH) to understand regulation of target mRNAs in *S. cerevisiae*. Using microscopy and flow cytometry, I also investigate the effect of Ssd1 and untranslated regions (UTRs) on the production and localisation of cell wall proteins fused to fluorescent tags. Lastly, I study conservation of Ssd1 molecular function in pathogenic fungi through genetic complementation with Ssd1 homologues from pathogens into *S. cerevisiae*.

I do not find clear evidence to support Ssd1 affecting protein localisation, however *SSD1* deletion leads to protein overproduction. Therefore, my results support the hypothesis that Ssd1 represses the translation of cell wall proteins to promote localised protein synthesis. My work shows that RNA targets of Ssd1 localise in a cell-cycle dependent manner. These findings in budding yeast can generate insight into post-transcriptional control of cell walls in pathogenic fungi, which pose major threats to human and crop health and rely on homologous systems of mRNA transport for growth and virulence.

Lay Summary

Fungal pathogens are major threats to human and crop health. The survival of fungi within the host, and its ability to cause harm, rely on its ability to grow and survive different types of stress. A key component in this process is the fungal cell wall, which shapes the cell and protects it from stressors. My research studies some of the elements that regulate the cell wall and enable it to function correctly. I study RNA-binding proteins (RBPs) which function in delivering, stabilizing, and enabling the translation of transcript mRNAs. The mRNAs I focus on are involved in strengthening the cell wall and allowing cell growth and continuity. I observe these mRNAs through a technique called single molecule fluorescence in situ hybridization (smFISH), which labels each single mRNA as a bright spot, to be observed in normal cells (wild-type) and mutated cells (RBPs deletions). Therefore, helping us infer the role of the RBP in its regulation. I also investigate the protein products of these target mRNAs with fluorescent microscopy, by observing where they localize in the cell and what affects that localization and abundance.

I use budding yeast, *Saccharomyces cerevisiae*, as a model organism to study these mechanisms and better understand how my RBPs of interest contribute to the integrity of the cell wall. In an effort to address how RBPs contribute to pathogenicity, I also investigate if some of the cell wall related functions of an RBP are conserved in other fungal species, beyond *S. cerevisiae*. This is because conservation of function might also indicate conservation of mechanism. If the function is conserved, then understanding these mechanisms in *S. cerevisiae* can be applied to fungal pathogens that threaten human health, which in turn paves the way for future studies to target these mechanisms and attenuate pathogenicity.

Contents

1 Introduction

The fungal cell wall is a dynamic organelle that is crucial for the cell's growth and survival. Cell survival relies on a combination of elements such as morphogenesis, virulence, biofilm formation, scavenging for nutrients, and an adequate stress response (Weissman and Kornitzer, 2004; Iraqui *et al.*, 2005; Kaur *et al.*, 2005; Verstrepen and Klis, 2006; Phan *et al.*, 2007). These elements are all connected to cell wall integrity and post-transcriptional regulation. The cell wall protects the cell from physical and environmental stress, preserves osmotic integrity within the cell, and confers resistance to antifungal drugs using the abovementioned process.

RNA-binding proteins (RBPs) post-transcriptionally regulate the expression and localization of cell wall proteins, which are involved in the biogenesis and maintenance of the fungal cell wall, by interacting with the untranslated regions (UTRs) of mRNAs. In this thesis, I investigate post-transcriptional regulation of cell wall mRNAs and their encoded proteins by RBPs and UTRs, in an effort to better understand how each component contributes to cell wall regulation. Using *Saccharomyces cerevisiae* as a model organism, I examine the effect of altered UTRs and RBP deletions, individually and in combination, on the localization and expression of cell wall proteins, and on the integrity of the cell wall.

1.1 The fungal cell wall shapes and protects the cell

The major components of the fungal cell wall are chitin, β-(1,3) glucan, β-(1,6) glucan, a mix of β-(1,3)/β-(1,4) glucan, α-(1,3) glucan, and mannan (**Fig. 1.1.**) (Orlean, 2012; Free, 2013; Gow, Latge and Munro, 2017; Stewart, 2017). Although this composition varies between fungal species, the cell wall is consistently made up of different layers with similar functions. For instance, the inner layer formed of chitin and beta-glucan, which exists in *S. cerevisiae*, *Candida albicans*, *Cryptococcus neoformans*, and *Aspergillus fumigatus* among others, gives the cell its shape and maintains rigidity and turgor pressure (Latgé, Beauvais and Chamilos, 2017; Patel and Free, 2019; Garcia-Rubio *et al.*, 2020). The innermost layer consists of covalently attached branched β-(1,3) glucan and chitin. The core layer of β-(1,3) glucan and chitin is fibrous due to the hydrogen bonds formed between the two components and acts as a scaffold for the remaining layers.

Plasma-membrane associated synthases make chitin through the use of UDP sugars as a substrate to synthesize polysaccharides. Chitin makes up between 1% and 15% of the cell wall mass, and significantly contributes to the integrity and strength of the cell wall (Free, 2013). Chitin is synthesized by chitin synthases which utilize cytoplasmic UDP-N-acetylglucosamine to produce linear chitin molecules (polymers of β-1,4-N-acetylglucosamine) (Cabib, 2004; Gow, Latge and Munro, 2017). The addition of N-acetylglucosamine elongates the chitin polymer, which is

expelled into the cell wall space during synthesis. Chitin polymers pass through the chitin synthase transmembrane domains which form a channel into the cell wall space. Most fungi have multiple genes encoding chitin synthases. For instance, *S. cerevisiae* has three genes encoding chitin synthases, while different filamentous fungi can have more than four (Mellado *et al.*, 2003; Munro *et al.*, 2003; Cabib, 2004; Banks *et al.*, 2005).

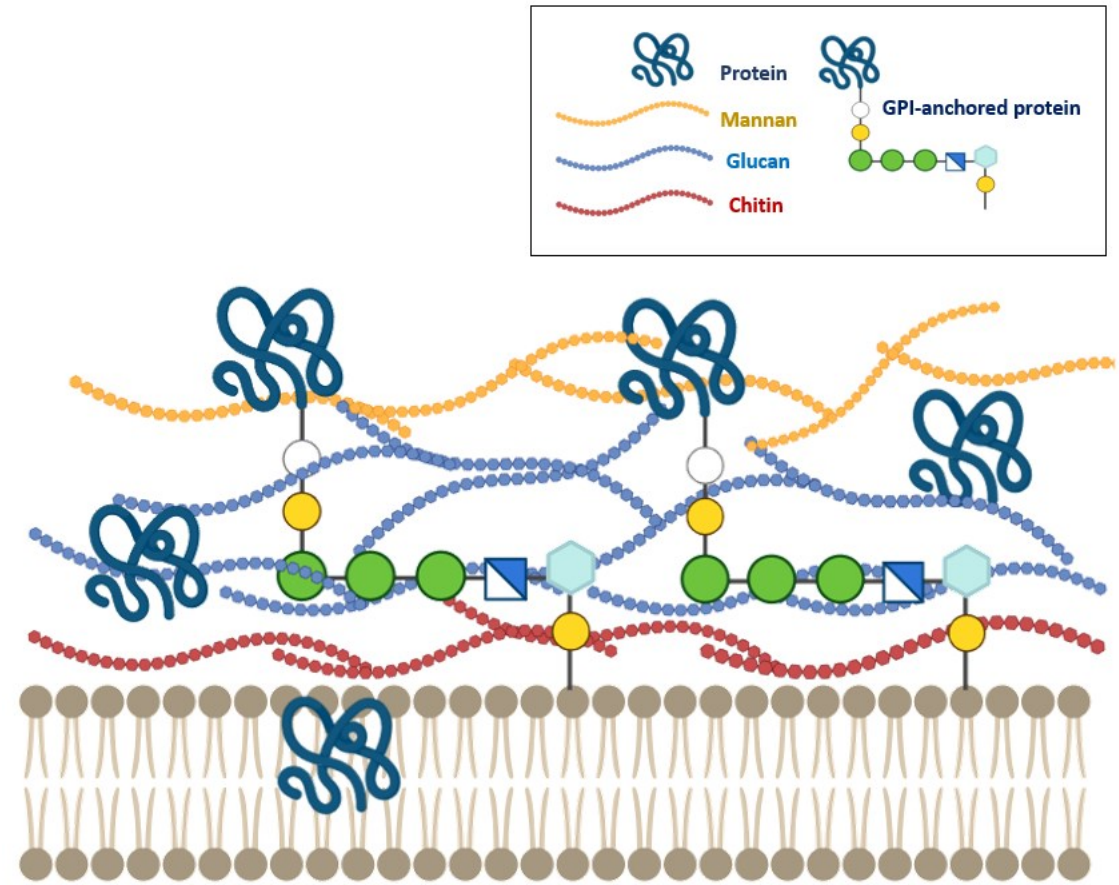

Figure 1.1. An overview of basic fungal cell wall structure. The chitin and glucan matrix forms the innermost, core layer of the cell wall and acts as a scaffold for the remaining layers. GPI-anchored proteins and non-anchored proteins are covalently attached to the cell wall. (Figure generated with BioRender)

β-(1,3) glucan makes up a major part of all of the characterized fungal cell walls, constituting 30% to 80% of the mass of the cell wall (Free, 2013). The glucan components are synthesized by glucan synthases associated with the plasma membrane, much like chitin synthases. Glucans are also polysaccharides, comprised of chains of glucose, linked by glycosidic bonds. Similar to the synthesis of Chitin, the β-(1,3) glucan synthase uses UDP-glucose from the cytoplasmic side of the membrane as a substrate to add glucose residues to the linear glucan polymer (Frost *et al.*, 1994; Klis, Boorsma and De Groot, 2006). Glucose is added to the nonreducing end of the polymer. As the polymer is synthesized, it gets extruded into the cell wall matrix through a channel formed by the transmembrane domains of the

glucan synthases. The glucans in the inner layer act as a scaffold for the glycosylated mannoproteins that form the outer layer (Kollár *et al.*, 1997; Orlean, 2012). These bound mannoproteins allow interaction with the external environment, mediating flocculation, adhesion, and invasion (Teunissen and Steensma, 1995; Guo *et al.*, 2000; Verstrepen and Klis, 2006; de Groot *et al.*, 2008).

In *S. cerevisiae*, cell surface proteins in the Flo family allow adherence to abiotic surfaces and mediate flocculation (Guo *et al.*, 2000; Verstrepen and Klis, 2006). Similarly, a number of cell wall proteins, such as Als proteins and Eap1 in *C. albicans* and Epa1 in *Candida glabrata*, have been implicated in facilitating adhesion to human tissues thus contributing to pathogenic survival in the human body (Cormack, Ghori and Falkow, 1999; Sundstrom, 2002; Li and Palecek, 2003; de Groot *et al.*, 2008). Furthermore, the mannoproteins in *C. albicans* also serve to mask the beta-glucans from the host, thus decreasing recognition to protect the cell from the host immune system (Galán-Díez *et al.*, 2010; Bain *et al.*, 2014).

mRNAs encoding a protein that is meant to be secreted to (or expressed on) the cell surface, contain a signal sequence at the protein's N-terminus which will direct it to the endoplasmic reticulum (ER). The signal sequence is recognized by the cell's protein-sorting apparatus, as soon as it emerges from the ribosome. The complex of ribosome, mRNA, and nascent protein are directed to the ER where the rest of the polypeptide chain is synthesized (Alberts *et al.*, 2022). Ribosomes in the ER synthesize cell wall glycoproteins and co-translationally release them into the ER lumen. As the cell wall proteins are released into the ER lumen, N-linked oligosaccharides are added onto aspargine residues, and are later further processed as these proteins pass through the ER and Golgi apparatus. Similarly, glycosylphosphatidylinositol (GPI) anchors are added to cell wall proteins as soon as they are released into the lumen of the ER. Addition of mannans and galactomannan (O-linked glycosylation) occurs as cell wall proteins pass through the ER and Golgi apparatus. Once these proteins are secreted into the cell wall to join the glucans and chitin, cell wall cross-linking enzymes join the components together with covalent bonds to generate the cell wall matrix (Free, 2013).

The cell wall is continuously maintained, during normal and stress conditions, through the highly conserved cell wall integrity (CWI) pathway (Dichtl, Samantaray and Wagener, 2016; García *et al.*, 2019). Activation of the CWI pathway under stress conditions starts at the cell surface in response to environmental stressors detected by transmembrane sensors. Upon activation as a stress response, this pathway protects the cell by enhancing synthesis and incorporation of chitin into the cell wall as a reinforcing polymer (Popolo *et al.*, 1997; Bulik *et al.*, 2003; Walker *et al.*, 2008). However, even under normal (non-stress) conditions, the CWI pathway contributes to cell wall biogenesis and cell integrity, due to its importance for cell growth and survival. In addition to conferring protection, the cell wall also determines the fungal cell shape during budding growth and hyphal or pseudohyphal formation, thus defining cell morphology. To enable this, the cell wall must be correctly synthesised and maintained throughout the cell cycle. This maintenance requires post-transcriptional regulation to permit correct production and localization of cell wall proteins.

RNA-binding proteins (RBPs) and untranslated regions (UTRs) regulate the translation and localization of messenger RNAs (mRNAs) encoding cell well proteins, thus regulating the synthesis and integrity of the fungal cell wall (Hall and Wallace, 2022). However, despite our knowledge of the fungal cell wall functions and composition, our understanding of some of its regulatory components are not well defined. For instance, it is unclear if some RBPs contribute to the localization of their target mRNAs and encoded proteins or merely act in a translational regulation capacity. Likewise, we do not fully understand the effect of UTRs on the expression and localization of certain proteins.

1.2 Post-transcriptional regulation

In eukaryotic cells, gene expression can be regulated spatially and temporally through a mechanism of mRNA localization and regulated translation within subcellular compartments. Post-transcriptional regulation enables the cell to spatially control the synthesis of proteins within the cytoplasm (Gonsalvez and Long, 2012). Post-transcriptional regulation functions in splicing, storage, localisation, and degradation of mRNA which consequently control protein translation and gene expression. This control is the result of RBPs interacting with pre-mRNA and mRNA in the cell to form ribonucleoprotein (RNP) complexes that affect the fate, transport, and function of RNA (Keene and Tenenbaum, 2002; Olivier *et al.*, 2005; König *et al.*, 2012; Marchese *et al.*, 2016; Hentze *et al.*, 2018).

1.2.1 Synthesis, processing, and export of mRNA

mRNA is a single-stranded molecule which contains the genetic information to make proteins. In eukaryotes, mRNA is synthesised through RNA polymerase II transcribing the information encoded in the DNA sequence to nascent mRNA. Several transcription factors for polymerase II (TFII) aid throughout transcription by positioning the RNA polymerase correctly at the DNA promoter, unwinding the DNA helix, and allowing initiation of elongation through releasing the RNA polymerase from the promoter (Alberts *et al.*, 2022). To start, RNA polymerase II forms a transcription initiation complex on the promoter DNA with the help of several transcription factors. The assembly of the transcription initiation complex is made possible through transcription factor II D (TFIID) binding to a short double-helical DNA sequence, which is known as the TATA box as it is primarily composed of T and A nucleotides. The binding causes a distortion which is thought to form a landmark for the location of the promoter. This distortion allows the assembly of the additional transcription factors along with RNA polymerase II, to form a transcription initiation complex. RNA polymerase II then gains access to the transcription start point with the help of Transcription factor II H (TFIIH). The unwinding is made possible through TFIIH using energy from ATP hydrolysis, to pull apart the DNA helix and expose the template strand. RNA polymerase II stays in place and synthesizes short lengths of RNA at the promoter region, until it goes through a series of

conformational changes that allow its movement along the template DNA. Once the polymerase starts moving, the elongation phase of transcription starts. At this point, most of the transcription factors are released from the DNA to be able to aid new RNA polymerase molecules initiate another round of the transcription.

mRNAs are processed while they are being synthesized. An important part of the change which facilitates RNA polymerase II movement is the addition of phosphate groups to the C-terminal domain (CTD) or the “tail” of the RNA polymerase II (Hsin and Manley, 2012; Alberts *et al.*, 2022). In addition to the phosphorylation of the CTD allowing elongation, it also functions to couple transcription to the processing of nascent mRNA. This phosphorylation causes components of the RNA-processing machinery to load onto the polymerase, thus facilitating the modification or processing of the transcribed mRNA as it arises from the polymerase. To produce a mature mRNA, transcription is accompanied by several other steps, including the modification of the 5' and 3' ends of the RNA, and the splicing or removal of intron sequences from the transcript. The 5' cap structure and the 3' poly(A) tail are features that distinguish mRNA from other RNAs. These features synergistically act to promote translation in the cytoplasm, and protect the mRNA against degradation (Pollard, 2024).

The cap is added as soon as transcription has been initiated, before the transcript reaches a length of 30 nucleotides. Capping starts with the addition of an extra guanosine to the 5′ end of the RNA. It involves a reaction carried out by the enzyme guanylyl transferase, between the 5′ triphosphate of the terminal nucleotide and the triphosphate of a GTP nucleotide, resulting in a 5′-5′ bond (Brown, 2002; Jurado *et al.*, 2014; Pollard, 2024). The following step is a modification catalysed by guanine methyltransferase, which converts the terminal guanosine into 7-methylguanosine by attachment of a methyl group to nitrogen number 7 of the purine ring. As discussed later in this introduction, a mature methylated cap is essential for recognition by the cap-binding complex (Jurado *et al.*, 2014).

A tail of adenosine residues (poly(A) tail) is added by poly(A) polymerase to the nascent mRNA during 3' end processing. Following transcription of the protein coding region of mRNA, polymerase II recognizes two sequence elements: AAUAAA and a GU-rich sequence element (Pollard, 2024). The two elements signal for the assembly of a large 3' processing complex, which leads to an endonuclease cleaving the nascent mRNA, releasing it from the transcription complex, and the addition of adenosine residues (polyadenylation) by the poly(A) polymerase (PAP) (Brown, 2002; Pollard, 2024). Polyadenylation is part of the mechanism for termination of transcription by RNA polymerase II, as it occurs simultaneously with transcription and the maturation of mRNA (Brown, 2002; Moore and Proudfoot, 2009; Pollard, 2024).

Mature mRNAs are selectively exported from the cell nucleus, following their synthesis and processing. Although the cell synthesizes a large number of pre-mRNA, only mature mRNAs which are useful to the cell are exported from the nucleus. These RNAs are identified by the proteins bound to them. As mRNAs are synthesized and processed for maturation and export, they are bound to RNA-binding proteins to form ribonucleoprotein particles (mRNPs). The Prescence (or absence) of certain proteins signal that an mRNA is successfully processed and ready to be guided through the nuclear pore complexes (NPCs) and into the cytosol (Xie and Ren, 2019; Alberts *et al.*, 2022). This means that co-transcriptional loading of RNA-binding proteins and the correct processing of mRNA are essential for the export of mature mRNAs. In yeast, this process requires the recruitment of the heterodimeric export receptor yeast Mex67-Mtr2 to signal the completion of nuclear mRNA assembly (Katahira *et al.*, 1999; Aibara *et al.*, 2015). The ATPase Sub2 recruits the export receptor Mex67-Mtr2 to assemble export-ready mRNPs (Zenklusen *et al.*, 2002; Rougemaille *et al.*, 2008). Mex67-Mtr2 mediates the translocation of the mRNP through the NPCs, which are aqueous channels in the nuclear membrane. Once it reaches the cytoplasmic side of the NPCs, Mex67-Mtr2 is displaced by the ATPase Dbp5 to release the mRNP into the cytoplasm (Alcázar-Román *et al.*, 2006).

1.2.2 Degradation and translation of mRNA

mRNA degradation is an essential part of regulating gene expression through regulating transcript and protein levels. As described in the previous section, the transcription, processing, and export of transcripts are highly regulated processes within the cell. This regulation extends to the decay of the transcript. Differential degradation of mRNA can control the level of mRNA expression, to allow environmental stimulation of mRNA levels and even localized translation of the encoded protein products. In yeast, cytoplasmic degradation of mRNAs occurs through general pathways, both of which utilise deadenylation which is the process of shortening the 3′ poly(A) tail (Muhlrad and Parker, 1992; Parker, 2012; Wahle and Winkler, 2013; Das, Sarkar and Das, 2017). Deadenylation is catalysed either by the major deadenylation machinery, the Ccr4/Pop2/Not complex, or by the Pan2/Pan3 complex, which is a subsidiary deadenylation machinery (Brown and Sachs, 1998; Tucker *et al.*, 2001). Following deadenylation, mRNAs can be degraded by the exosome in a 3′ to 5′ direction (Anderson and Parker, 1998), or they can be subjected to removal of the 5’-cap structure by the decapping complex consisting of Dcp1/Dcp2 (Dunckley and Parker, 1999; van Dijk *et al.*, 2002). The decapping reaction exposes the 5’-monophosphate of the terminal residue, which promotes the degradation of the transcript body by the cytoplasmic exoribonuclease Xrn1 in in a 5' to 3' direction (Hsu and Stevens, 1993; Muhlrad and Parker, 1994; Steiger *et al.*, 2003). Specialized decay pathways also exist in yeast to act in case of translation abnormalities. In such cases, mRNAs can be rapidly degraded in the 3' to 5'

direction, or subjected to deadenylation independent decapping, or cleaved by an endonuclease. Another level of regulation is the selective protection and localized degradation of mRNA. This mechanism provides selective protection of transcripts at their place of localization, while the mRNA is degraded everywhere else (Ding *et al.*, 1993). A well characterised example of this mechanism is heat shock protein 83 (*HSP83*) mRNA in *Drosophila*. *HSP83* mRNA is degraded everywhere in the cytoplasm, except in the posterior pole plasm of *Drosophila* embryos where it localizes. The degradation of *HSP83* mRNA involves binding of the RNA-binding protein Smaug, which recruits the Ccr4/Pop2/Not deadenylase complex, thus prompting deadenylation and destabilisation of transcripts (Semotok *et al.*, 2005). In *smaug* mutants, localization of *HSP83* does not occur due to lack of degradation of HSP83 mRNA. Smaug acts as a multifunctional RBP which prompts destabilization and localization of specific transcripts, and also acts as a translational repressor via indirect interaction with eIF4E, a component of the translation machinery.

Following the transcription, processing, maturation, and export of mRNA out of the nucleus, translation takes place to provide the cell with proteins. Protein synthesis starts with the initiation of translation. To begin the process of identifying the initiation codon by the eukaryotic translational machinery, the ternary complex (TC) binds to the small (40S) ribosomal subunit to form the 43S preinitiation complex (PIC). TC consists of initiator methionyl-tRNA (Met-tRNAi) and the GTP-bound form of eukaryotic initiation factor 2 (eIF2) (Poulin and Sonenberg, 2013). Physical interactions link eIFs 1, 3, 5, and TC into a multifactor complex (MFC), which works to enhance the formation or stability of the 43S PIC. The recruitment of the 43S complex to the 5' end of the mRNA is facilitated by eIF3 and the eIF4 factor (Hinnebusch and Lorsch, 2012). 43S PIC binds to the messenger RNA (mRNA) near the 5'-7-methylguanosine cap. Once bound, the 43S PIC starts scanning the 5' untranslated region starts, leading to recognition of the AUG codon. The initial event of codon recognition is the result of base pairing between the AUG in the peptidyl-tRNA (P) site of the 40S subunit and the anticodon of Met-tRNAi. Recognition of the AUG codon leads to the arrest of scanning PIC, and triggers assembly of the 80S ribosome (Lomakin *et al.*, 2006; Kolitz, Takacs and Lorsch, 2009). eIF2 in the TC is converted to its GDP-bound state via the release of gated phosphate and the action of GTPase-activating (GAP) factor eIF5. Following the release of GDP-bound eIF2 and other eIFS in the PIC, eIF5B catalyses the joining of the large subunit to produce an 80S initiation complex. This complex contains Met-tRNAi base-paired to AUG in the P site, and is ready to start the elongation phase (Hinnebusch, 2011; Hinnebusch and Lorsch, 2012). To start protein synthesis, mRNA translation requires adaptor molecules that are able to recognize the codons within the mRNA, and the corresponding amino acids. These adaptors consist of a set of RNA molecules known as transfer RNAs (tRNAs). The cloverleaf structure of the tRNA molecule folds to form a compact L-shape, which is held together by additional hydrogen bonds. This structure is important as it can bind to the codon on one site, and to the amino acid at another site of its surface (Brown, 2002; Alberts *et al.*, 2022). The anticodon region, a set of three consecutive nucleotides, pairs with the

complementary codon in an mRNA molecule. While the other region at the 3' end, consisting of short single-stranded region, binds the amino acid that matches the codon attached to the tRNA. The recognition and attachment of the correct amino acid relies on aminoacyl-tRNA synthetases, which covalently bond each amino acid to its appropriate set of tRNA molecules. Protein synthesis is performed through the use of tRNAs and the ribosome, which is a catalytic complex made from ribosomal proteins and ribosomal RNAs (rRNAs). The ribosome consists of a large subunit and a small subunit, which envelope the mRNAs. The small subunit acts as the framework which allows the tRNA to slot in and find a matching codon in the mRNA template, to deliver an amino acid. The large subunit acts as the enzyme which the peptide bonds that link the amino acids, thus facilitating the formation of a polypeptide chain. As protein synthesis goes on, a peptide bond forms between the carboxyl group at the end of the growing polypeptide chain and a free amino group on an incoming amino acid. A protein is consequently synthesized, one amino acid at a time, from its N-terminal end to its C-terminal end (Alberts *et al.*, 2022).

1.2.3 RNA-binding proteins

Every aspect of the mRNA progress throughout its life is decided by its complementary bound proteins. This can be achieved through translational repression and contributing to localized mRNA translation. A prominent example of such regulation can be seen with the RBPs Puf6 and Khd1 in the *ASH1* mRNA transport system (Deng, Singer and Gu, 2008). RBPs interact with mRNAs to form RNP complexes. The mRNA-containing RNPs (mRNPs) comprise tens of thousands of different RNA sequences, and hundreds of different RBPs in eukaryotes (Singh *et al.*, 2015). RBPs ensure that mRNA regions, such as 5' and 3' UTRs and the coding region, are covered or exposed to dictate appropriate mRNA processing.

RBPs represent a large force of post-transcriptional regulation across biology, including over 1500 human genes implementing proteins involved in human RNA metabolism (Dreyfuss, Choi and Adam, 1984; Piñol-Roma *et al.*, 1988; Gerstberger, Hafner and Tuschl, 2014; Dassi, 2017). The research surrounding RBPs has spanned decades, however, our knowledge of RBPs, their highly modular structure (Burd and Dreyfuss, 1994; Lunde, Moore and Varani, 2007), and their interactions with RNA has dramatically expanded only in recent years with the rapid development of high-throughput techniques. Despite these advances and a large number of RBP targets being characterised, a considerable number of verified RBPs remain poorly understood with functions yet to be discovered.

1.2.4 The conserved RNA-binding protein Ssd1

Ssd1 is an RNA binding protein that is highly conserved across fungi (Wanless, Lin and Weiss, 2014; Bayne *et al.*, 2022) and plays a number of essential roles. Ssd1 binds the 5'UTRs of a number of mRNAs encoding proteins that act in cell growth and control of the cell cycle, as well as cell wall biogenesis, and septum remodelling

in *S. cerevisiae* (Hogan *et al.*, 2008; Bayne *et al.*, 2022). mRNAs bound by Ssd1 include *SUN4, SIM1, UTH1, SCW4, CTS1, DSE2, CCW12* and *SRL1* (Hogan *et al.*, 2008; Jansen *et al.*, 2009; Hose *et al.*, 2020; Bayne *et al.*, 2022). As a result of its involvement with these transcripts, in *S. cerevisiae,* Ssd1 has roles in cell wall integrity and induced thermotolerance (Kaeberlein and Guarente, 2002; Mir, Fiedler and Cashikar, 2009; Bayne *et al.*, 2022), and is required for stationary phase viability (Werner-Washburne *et al.*, 1993). Previous studies also show that Ssd1 interacts with heat shock proteins, such as Hsp104, during heat stress and influences their aggregation (Mir, Fiedler and Cashikar, 2009). Consequently, the loss of this RBP results in the disruption of cell wall integrity and growth, leading to a disruption of virulence phenotypes. However, the mechanism behind the role of Ssd1 and *SSD1* deletion phenotypes remains unknown.

Homologs of Ssd1 have a role in virulence in the pathogenic fungi *C. glabrata, C. albicans*, and *A. fumigatus* (Yeaman *et al.*, 2004; Gank *et al.*, 2008; Schwarzmüller *et al.*, 2014; Thammahong *et al.*, 2019). In *C. albicans* a strain expressing higher levels of Ssd1 shows increased virulence in an animal model compared to other strains. Furthermore, in a murine model of disseminated candidiasis the ssd1 null mutants are significantly less virulent than the wild-type. This demonstrates that Ssd1 acts as a virulence factor in *C. albicans*, and highlights the importance of Ssd1 for resistance of *C. albicans* to host defence peptides (Yeaman *et al.*, 2004; Gank *et al.*, 2008). The Ssd1 homolog in *Schizosaccharomyces pombe,* Sts5, has a role in polarized cell growth and morphogenesis, as well as a role in actin patch localization during interphase (Toda *et al.*, 1996; Nuñez *et al.*, 2016). A homolog of Ssd1 acts in growth and morphology in the pathogenic *C. neoformans* (Gerik *et al.*, 2005; Ballou, Cook and Wallace, 2021). The conservation of Ssd1 function extends to plants; a homolog of Ssd1 in *Fusarium oxysporum*, encoded in FOR3, can complement the *S. cerevisiae* Ssd1, conferring resistance to the plant's defence protein osmotin to an osmotin-sensitive strain of *S. cerevisiae* (Lee *et al.*, 2010).

Ssd1 binds a CNYUCNYU motif at the 5′ UTR of its target mRNAs (Bayne *et al.*, 2022). Transcripts that are highly enriched in Ssd1 binding exhibit more than one CNYUCNYU motif in their 5' UTR. The current hypothesised mechanism of Ssd1 is that it acts as a translational repressor of its target mRNAs through binding this motif. Ssd1 co-localizes with the cell wall biogenesis kinase Cbk1, and is phosphorylated by it at a set of highly conserved phosphorylation sites on its N-terminus (Jansen *et al.*, 2009; Kurischko, Kim, *et al.*, 2011). It is thought that this phosphorylation leads to the release of Ssd1 from its bound target mRNA, thus permitting localized protein translation. Ohyama *et al.* (2010) show that Ssd1 stabilizes a subpopulation of *CLN2* mRNA, and postulate that Ssd1 might be escorting these transcripts to be translated locally following Ssd1 phosphorylation by Cbk1. In their study, they show that *CLN2* mRNA stabilized by Ssd1 (at 90 min after heat shock in *taf1-N568*Δ with a viable *SSD1* allele; SSD1-V) appears to be translationally inactive. Immunoblot analysis conducted on Cln2 protein (with an anti-HA for the HA epitope fused to the carboxy-terminus of

Cln2) showed that the protein was almost undetectable (Ohyama, Kasahara and Kokubo, 2010). This indicates that Ssd1 suppresses translation of Cln2, by binding to its transcript. Jansen *et al.* (2009) also show that Ssd1 associates with mRNAs that encode cell wall remodelling proteins, and that the translation of these messages is rapidly and specifically suppressed when Cbk1 is inhibited. They report that upon Cbk1 inhibition, Ssd1-associated mRNAs (*UTH1, SUN4, CTS1, SIM1, TOS1*) were dramatically depleted from polysome fractions. This suggests that the inability of Cbk1 to phosphorylate and release Ssd1 leads to the suppression of transcript translation. This is consistent with the role of Ssd1 as a translational repressor. Furthermore, the study found that Ssd1 affects Uth1 protein levels. Upon examining the levels of Uth1 protein in SSD1 and *ssd1*Δ strains, cell lysates on an SDS page showed that the abundance of Uth1 protein was lower in cells expressing functional Ssd1 (Jansen *et al.*, 2009). Additionally, a study by Hose *et al*. (2020) used quantitative proteomics to measure the effect of Ssd1 on the cellular proteome.They found that 301 the measured proteins were more abundant in the ssd1D aneuploid mutant versus the wild type (FDR < 0.05). The study accounted for nduced transcripts, and found that a large fraction of the abundant proteins were elevated beyond mRNA differences, and that several elevated proteins emerge from Ssd1 targets, including cell wall transcripts and nuclear transcripts that encode mitochondrial proteins (Hose *et al.*, 2020, p. 202).

Ssd1 genetically interacts with other RBPs including Mpt5. Ssd1 and Mpt5 function in parallel pathways to promote cell wall integrity (Kaeberlein and Guarente, 2002). Furthermore, Mpt5 binds the Ssd1 target mRNAs *SUN4* and *SRL1* (Kaeberlein and Guarente, 2002; Hogan *et al.*, 2008). However, while Ssd1 binds its targets at the 5' UTR, Mpt5 binds both mRNAs at the 3' end. This suggests that altering the 3' UTR in these mRNAs might alter their expression. The binding of the same mRNAs also indicates that Ssd1 and Mpt5 might be acting in cooperation to regulate select target mRNAs. However, the precise mechanism by which they act, and the timing of this regulation in reference to the cell cycle is not known. The connection of this regulation to the cell cycle is important to investigate. Partly due to the role of each mRNA in cell growth and cell wall integrity, and also due to *SUN4* and *SRL1* mRNA being bound by the RBP She2 (Oeffinger *et al.*, 2007), which is an essential part of the *ASH1* mRNA transport machinery (Long *et al.*, 2000). Each of the abovementioned elements will be discussed in more detail in the upcoming sections.

To clarify the mechanism of Ssd1, my research will investigate the conservation of this RBP's molecular function, and the role it plays in securing cell wall integrity through regulating cell wall mRNAs. My research will investigate the conservation of Ssd1 function by swapping *S. cerevisiae*'s Ssd1 with Ssd1 homologs from other fungi and testing them under phenotypic conditions. I will investigate if Ssd1 deletion causes mis-localization and mis-regulation of cell wall proteins and target mRNAs. I also investigate the role of other RBPs, such as Mpt5 and She2, in the localization of these cell wall encoding mRNAs. Finally, I will look into the role of the untranslated regions, precisely the 3' UTR, in the localization of cell wall mRNAs.

1.2.5 Untranslated regions

The noncoding portions of mRNA are predicted to direct post-transcriptional regulation of gene expression. Translation is affected by the 3' UTR and poly(A) tail downstream of the open reading frame (ORF), as well as by the transcript leader or 5' UTR upstream of the ORF. For instance, the 5' UTR is particularly important for translation initiation, the process in which the initiation codon is base-paired with initiator tRNA through assembly of elongation-competent 80S ribosomes. Pre-initiation complexes mostly bind the 5' cap of mRNA. In eukaryotes, a cap-binding complex known as eukaryotic initiation factor 4F (eIF4F) binds to the 5' UTR via the 5' methyl-7-guanosine (m^7G) cap, which in turn leads to forming a pre-initiation complex (PIC) through the employment of a small ribosomal subunit and its associated eukaryotic initiation factors (eIFs), this complex comprises a 40S subunit, the eIF2–GTP–Met-$tRNA^{Met}_i$ ternary complex (eIF2-TC), eIF3, eIF1, eIF1A, and likely eIF5 (Jackson, Hellen and Pestova, 2010). The PIC scans in a unidirectional manner from 5'-to-3' until it locates a start codon (AUG) to trigger complex rearrangements that results in the formation of an elongating 80S ribosome (Arribere and Gilbert, 2013).

The regulation of translation is dependent on a number of factors that can result in repression or initiation of translation of the protein-coding ORF, making the initiation mechanism context driven. For example, translation can be dependent on cellular internal ribosome entry sites (IRESs), which are untranslated segments of mRNA transcripts believed to respond to environmental stress that prevents canonical 5' cap–dependent translation, by initiating protein synthesis (Gilbert *et al.*, 2007). Gilbert *et al.* (2007) show that in yeast an unstructured A-rich element mediates internal initiation by employing the poly(A) binding protein (Pab1) to the 5′ UTR. Upon mutating the 5′ UTR, thus impairing IRES activity, invasive growth is compromised, which indicates that cap-independent translation is required for stress adaptation. Context driven initiation is also shown in the mRNA of the gene histone H4, where translation relies on RNA secondary structures within the ORF instead of the scanning mechanism (Martin *et al.*, 2011; Brar, 2016).

Another factor regulating translation through the 5' UTR is the presence of upstream AUGs (uAUGS). BRAC1 (breast cancer 1 gene) produces two different transcripts which display differences in their 5' UTR due to the utilisation of different promoters. The longer transcript is predominantly expressed in breast cancer, whereas the shorter transcript is expressed and efficiently translated in cancerous as well as noncancerous breast tissue. In this case, the presence of several uAUGs and a complex structure dramatically affects the translation of the longer transcript (Araujo *et al.*, 2012).

Additionally, the presence of binding sites for RBPs in UTRs forms an essential layer of translational regulation. A well characterized example of RBPs regulating translation through the 5' UTR is the iron regulatory proteins IRP1 and IRP2 which regulate ferritin and ferroportin (FPN1) among others. IRPs can act as enhancers or inhibitors of translation, however, during iron deficiency (Zhou and Tan, 2017), the

interaction between IRP and its binding motif in the 5' UTR of target mRNA hinders translation. In conditions of low cellular iron levels, IRP1 and IRP2 block translation of the downstream ORF through binding the iron responsive element (IRE). IRBs binds IREs, which are positioned close to the cap, to block the recruitment and binding of the 40s ribosomal subunits to the transcript, thus causing a steric hindrance. The IRE-IRP complex can also block ribosomal scanning when located further from the cap (Goss and Theil, 2011; Araujo *et al.*, 2012). Due to this role of binding sites of RBP in translation regulation, I hypothesize that my RBP of interest, Ssd1, might follow a similar mechanism of translational repression through binding to specific motifs in the 5' UTR transcript leader of its target mRNAs.

The 3′ UTR also plays an important role in determining the level of gene expression through regulating mRNA stability, localization, and translation (Mayya and Duchaine, 2019; Savinov *et al.*, 2021). The 3′ UTR interacts with several cellular regulatory factors, known as trans-acting factors, which can recognize specific features in the 3′ UTR and execute consequent activities. Sequence motifs and features occurring in the 3' UTR have been identified in yeast, humans, and zebrafish and implicated in mRNA stability and protein production (Shalem *et al.*, 2013; Zhao *et al.*, 2014; Rabani *et al.*, 2017; Savinov *et al.*, 2021). The sequence features in the 3' UTR can act as positioning elements (consensus AAWAAA, with W an A or U), cleavage and polyadenylation sites (YAN, with Y a C or U), or efficiency elements located upstream and downstream of the cleavage site (consensus UAUAUA) (Guo and Sherman, 1996; Savinov *et al.*, 2021). Due to the diversity of these sequence features, and the diverse regulatory elements (such as RBPs and miRNAs) acting on them; the 3' UTR plays different functional roles depending on cell type and cellular state (Jansen, 2001; Mayr, 2017).

RBPs enable regulation through binding cis-elements in the 3’ UTR. This allows mRNA localization followed by localized translation. An example of this is the chicken Zip-code binding protein 1 (Zbp1), which binds to a conserved 54-nucleotide element in the 3′ UTR of the β-actin mRNA. Zbp1 then represses the translation of β-actin mRNA by blocking translation initiation, in addition to playing a role in the localization of β-actin mRNA (Hüttelmaier *et al.*, 2005). The 3' UTR also contribute to mRNA localization in *Xenopus oocytes,* where localization occurs through a diffusion and entrapment-mediated mechanism (Kloc, Larabell and Etkin, 1996; Chang *et al.*, 2004; Oh and Houston, 2017). This mechanism leads to the localization of the germ plasm RNA Xcat2 during the early vegetal pathway by associating with a structure known as the mitochondrial cloud (MC) (Heasman, Quarmby and Wylie, 1984; Kloc and Etkin, 2005). Xcat2 transcripts localise to the MC through diffusion and remain entrapped there in a microtubule independent manner. Two distinct localization elements (LE) are encoded in the *XCAT2* 3′UTR, which are necessary for correct localization of the mRNA (Mosquera *et al.*, 1993; Kloc *et al.*, 2000). A detailed example of localized mRNA translation in yeast, through an RBP binding specific cis-elements found in the 3′ UTR, will be discussed in the upcoming section.

Due to the role and importance of these untranslated regions in mRNA localization and subsequent protein expression, my research accounts for these regions in the experimental design. I also investigate the combined and individual effects of RBPs of interest and the 3′ UTR.

1.3 RNA localization

The localization of mRNA is a powerful tool for gene regulation across biology. In eukaryotic cells, gene expression can be regulated spatially and temporally through a mechanism of mRNA localization and regulated translation within subcellular compartments. Post-transcriptional regulation enables the cell to spatially control the synthesis of proteins within the cytoplasm (Gonsalvez and Long, 2012). RNA localization is one of several existing mechanisms that achieve spatial sorting of specific proteins in eukaryotic cells. This localization is often governed by RBPs alongside other cellular components. The localization of RNA enables the cell to regulate the translation of mRNAs at specific locations within subcellular compartments, thus preventing ectopic protein translation and sorting proteins to distinct regions where they play specialized roles.

1.3.1 Mechanisms of mRNA localization

RNA localization can be achieved through various mechanisms such as active transport along the cytoskeleton using molecular motors, diffusion followed by entrapment of RNA by a localised anchor, or localised degradation (Fig. **1.2**).

Localization by active transport involves mRNA, RBPs, adaptor proteins, and motor proteins which shuttle the mRNA along cytoskeletal filaments. This process requires the recognition of mRNA by an RBP that binds it to form a ribonucleoprotein (RNP) complex. The RNP complex binds to a cytoskeletal motor protein, via the RBP or via an adaptor protein, to be transported to its destination, where the delivered RNA is tethered and locally translated. Active transport on the cytoskeletal tracks remains one of the best studied mechanisms of RNA localization, and has been reported in fungi such as *S. cerevisiae*, *Ustilago maydis*, and *C. albicans.*

Amongst the most prominent examples of this mechanism is the localization of the transcriptional repressor *ASH1* in *S. cerevisiae*. During mitosis, the mother cell undergoes genomic recombination which is mediated by the HO endonuclease. This recombination results in conversion of the mother cell's mating type (a to α or vice versa). *ASH1* mRNA is localized to the bud of the daughter cell where it inhibits mating type switching, through Ash1 selectively repressing the HO endonuclease in the daughter cell (Bobola *et al.*, 1996; Sil and Herskowitz, 1996). The localization of *ASH1* to the bud tip relies on the proteins She2, She3, the myosin Myo4, as well as several

cis-acting zip-codes that reside in the 3' UTR of the mRNA and bind *trans*-factors, including Puf6, Khd1, and She3 protein (Bashirullah, Cooperstock and Lipshitz, 1998; Kloc, Zearfoss and Etkin, 2002; Gonsalvez, Urbinati and Long, 2005).

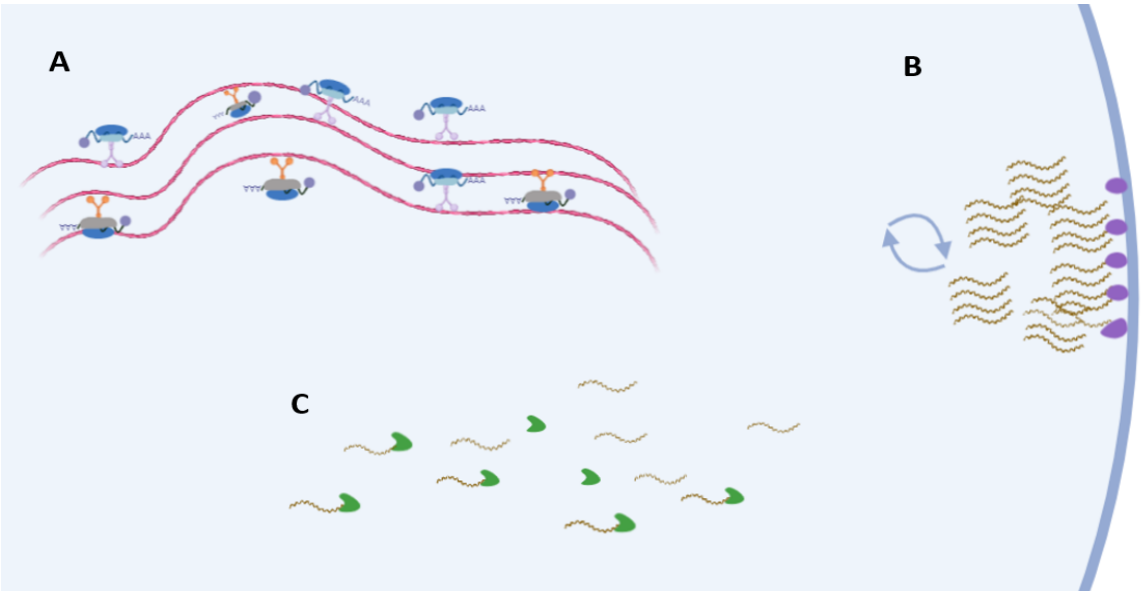

Figure 1.2: Mechanisms of RNA localization RNA localization is possible through mechanisms such as A) active transport in which the RNP complex binds to a cytoskeletal motor protein, via an adaptor protein, to be transported along actin or microtubules to its target destination for local translation, B) diffusion followed by entrapment of RNA by localised actin anchors, or C) selective protection and localised degradation of unprotected RNA. (Figure generated with BioRender)

She3 binds the 3' UTR and functions as an adaptor, connecting the *ASH1* mRNA to a myosin motor protein called Myo4. Myosin can transport the *ASH1* mRNA along the actin cytoskeleton into the bud tip (Fig. **1.3**). Meanwhile, *ASH1* mRNA is bound co-transcriptionally by She2p in the nucleus to form a complex, which binds the translational repressor proteins Puf6 and Khd1 during its transit to repress translation of *ASH1* mRNA (Deng, Singer and Gu, 2008). In the cytoplasm, the *ASH1*-She2p complex binds to Myo4/She3p complex (Long *et al.*, 2000). Following this, Myo4p transports the complex along the actin cytoskeleton and, once *ASH1* mRNA is localized, Puf6 and Khd1 are phosphorylated through kinases at the bud tip. Once the repressors Puf6 and Khd1 are inactivated, *ASH1* translation can begin (Paquin *et al.*, 2007; Deng, Singer and Gu, 2008). Thus, these RBPs regulate translation through a combination of translational repression and mRNA localization.

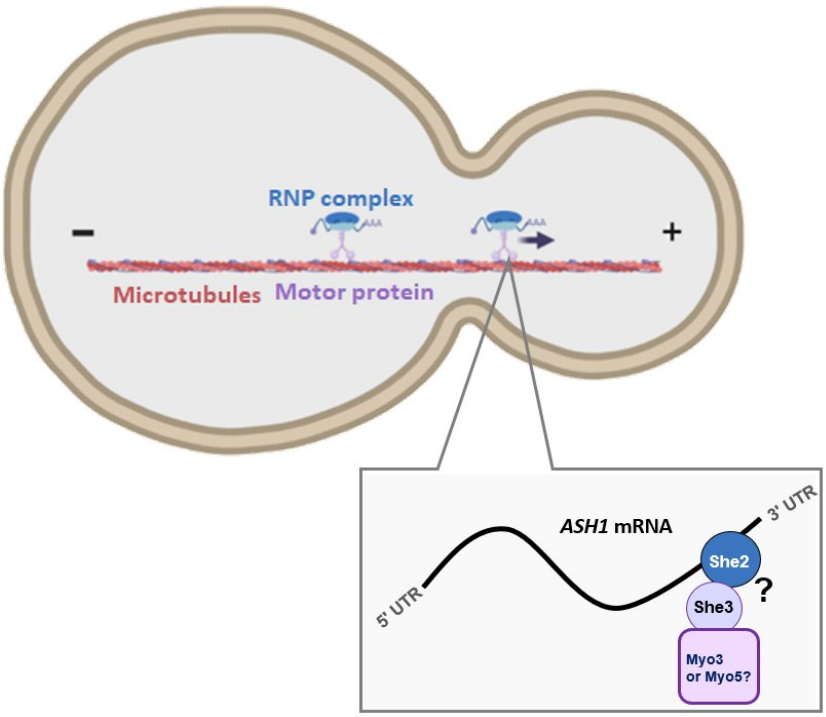

Figure 1.3: The localization mechanism of *ASH1* mRNA. A myosin motor transports the *ASH1* mRNA along the actin cytoskeleton into the daughter cell of budding yeast. She3 functions as an adaptor, connecting the *ASH1* mRNA to the motor protein Myo4 which transports *ASH1* mRNA, while the RBPs Puf6 and Khd1repress translation of Ash1 mRNA until it reaches its destination. (Figure generated with BioRender)

The role of RBPs in the abovementioned localization mechanism invokes the question on the role of other RBPs, such as Ssd1, in RNA localization and subsequent localized translation. The *ASH1* mRNA transport mechanism presents a viable model for how Ssd1 might affect the localization of its target mRNAs. The first possibility is that Ssd1 binds the RNA and acts as a connector protein to a motor protein, in order to facilitate the transport and localization of mRNA. The second, and more likely possibility, is that Ssd1 acts as part of the regulation mechanism but does not directly function in transportation. This means that Ssd1 could act similarly to Puf6 and Khd1 in the *ASH1* localization mechanism, where Ssd1 represses the translation of its target mRNA until the mRNA reaches the correct site of translation. This second possibility is supported by some studies reporting She2p binding some Ssd1 targets. This will be discussed in more details in the results section. It is also possible, however, that mRNAs are “hitchhiking” to the bud tip.

mRNAs encoding polarity factors might be hitchhiking or piggybacking to the bud on the ER during its transport (Schmid *et al.*, 2006; Aronov *et al.*, 2007; Christensen and Reck-Peterson, 2022) . In *S. cerevisiae*, some mRNAs might be transported through association with COPI vesicles. These are coatomer (a protein complex) coated vesicles which are generated at the Golgi apparatus (Taylor, Tagiltsev and Briggs, 2023). COPI vesicles transport cargo from the Golgi to the ER. The poly-A-binding protein Pab1, which associates with the 3′ end of mRNAs, was shown to form a complex with the GTP-bound form of Arf1 GTPase and coatomer on the surface of

COPI vesicles (Trautwein *et al.*, 2004). Knockout of secretory pathway components, such as Arf1 or coatomer, led to defects in the distribution of mRNA. This suggests that a subset of mRNAs might be hitchhiking on COPI vesicles, as an additional mechanism to ensure that mRNA reaches the bud and to prevent diffusion away from the bud tip (Trautwein *et al.*, 2004). Furthermore, Aronov et al. found that mutations that affect ER entry and bud anchoring also affect asymmetric localization of mRNA in S. cerevisiae. Co-fractionation showed an association between bud-localized mRNAs and ER microsomes, thus suggesting that mRNA transport and cortical ER inheritance are connected processes (Trautwein *et al.*, 2004; Christensen and Reck-Peterson, 2022).

mRNAs can also hitchhike on secretory vesicles to the hyphal tip in *C. albicans*. Secretory vesicles are transported to the hyphal tip during hyphal growth (Pruyne, Schott and Bretscher, 1998). In *C. albicans*, *SEC2* mRNA associates with the Sec2 protein on secretory vesicles, which suggests that *SEC2* mRNA might be piggybacking onto these secretory vesicles (Caballero-Lima *et al.*, 2014). Additionally, higher levels of *SEC2* mRNA associate with Sec2 protein in the hyphal state of *C. albicans* compared to its yeast state, thus suggesting that mRNA may be preferentially hitchhiking to the hyphal tip during hyphal growth (Caballero-Lima *et al.*, 2014; Christensen and Reck-Peterson, 2022).

It is vital to understand mechanisms of RNA transport and the role of RBP in them because these mechanisms determine the localization of mRNAs, and thus the way cells achieve polarity and direct asymmetric growth. Across eukaryotes, cell polarity underlies essential processes such as cell differentiation and cell division. In fact, cellular morphogenesis, and consequently pathogenesis in some fungi, is dependent on cell polarity. A clear example of this can be presented through hyphal growth.

1.3.2 Fungal Hyphae

The hyphae is a tubular structure in fungi which grows through apical extension. Although the evolution of hyphae remains poorly understood, several studies suggest that hyphae evolved in early fungi (the split of Blastocladio-, Chytridio- and Zoopagomycota, termed BCZ nodes), and indicates hyphae as the ancestral form of morphology from which yeasts evolved (Hibbett *et al.*, 2007; Dee *et al.*, 2015; Kiss *et al.*, 2019). Analyses performed by Kiss *et al*. (2019) suggest that hyphal morphogenesis genes are generally more essential than genes with other functions in yeast. Their data shows that fewer hypha morphogenesis genes (35–46%) were lost than genes with other functions, which in turn suggest that yeast-like fungi (Saccharomycotina, Taphrinomycotina, Pucciniomycotina, Ustilaginomycotina, and Tremellomycotina) preferentially retain multicellular growth.

Morphology switching, between yeast cells and multicellular form (hyphae), plays an essential role in pathogenicity and survival in the mammalian host. In fact, fungal hyphae function in niche colonization, the acquisition of nutrients, mating, and pathogenicity (Harris, 2011; Brand, 2012; Desai, 2018). For instance, the human pathogen *C. albicans* requires hyphal growth for pathogenesis in fatal systemic

infections, as well as in symptomatic infections such as oral thrush and vaginal candidiasis (Sudbery, 2011; Jabra-Rizk *et al.*, 2016), whereas thermally dimorphic pathogens such as *Histoplasma capsulatum* and *Blastomyces spp.* switch from hyphal growth to yeast cells in response to host stimuli such as elevated temperature (Li and Nielsen, 2017).

Hyphae grow apically in fungi (**Fig. 1.4**) and exhibit a difference in diameter among species. Their width can range from 3-4 to 30 µm or more, while their linear

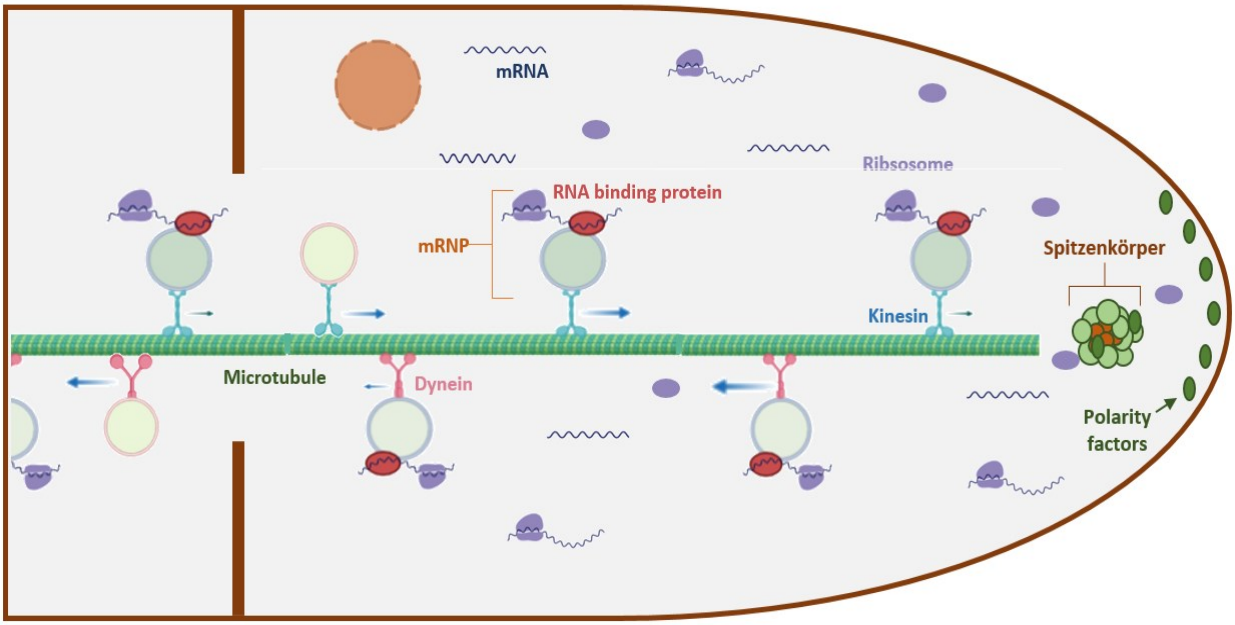

Figure 1.4. Apical Growth of Hyphae. A figure depicting apical growth in filamentous fungi, influenced by RNA localization and the Spitzenkörper (SPK) which produce polarity at the apical tip. This shows a microtubule-dependent mRNA transport system, where an RNA binding protein is shuttled by kinesin-3 and dynein along microtubules to facilitate long-distance mRNA transport. (Figure generated with BioRender)

elongation can reach an impressive rate of ~33 µm/min (López-Franco, Howard and Bracker, 1995; Kradin, 2017). The apical growth of hyphae depends on cell polarity, much like yeast cells, however this linear growth poses a challenge for transporting and localising RNA to the apical tip. Therefore, fungi such as *Ustilago maydis* developed a microtubule-dependent mRNA transport system. In *U. maydis*, the RNA binding protein Rrm4 is shuttled by kinesin-3 and dynein along microtubules to facilitate long-distance mRNA transport. This transport process determines polarity in infectious filaments (Becht, König and Feldbrügge, 2006; Baumann *et al.*, 2012).

Another clear example of cell polarity in filamentous fungi is the RNA transport system described in the human pathogen *C. albicans*, in which a She3-dependent RNA transport system binds to 40 mRNAs and transports them to yeast buds and to the tips of hyphae (Elson *et al.*, 2009). Elson *et al.* (2009) show that both the transport system and many of the genes encoded by transported mRNAs are

required for normal growth and function of hyphae, however, the RNA binding proteins operating this system remain unknown. Additionally, hyphal formation is slowed down by the absence of SR-like RNA-binding protein Slr1 which in turn decreases virulence. Slr1 is primarily a nuclear phosphoprotein, however, a fraction of Slr1 co-fractionates with translating ribosomes (80S ribosomes and polysomes), which suggests a cytoplasmic role. Interestingly, the slr1-6SA-GFP mutant protein is detected in a focus at the hyphal tip, in a manner that partially overlaps with the Spitzenkörper (SPK) (Ariyachet *et al.*, 2017). The Spitzenkörper is a collection of secretory vesicles and polarity-related proteins which direct the polarized growth of hyphae. This association suggests that post-transcriptional regulation plays a role in these processes, where Slr1 mRNA is shuttled to the hyphal tip to be locally translated, although the precise mechanism remains unknown. Another intriguing aspect in virulence and growth of hyphae is the Extent of Cell elongation (ECE1) gene. During epithelial infection *C. albicans* ECE1 is highly expressed by hyphae and is predicted to encode a secreted protein (Röhm *et al.*, 2013). Moyes *et al*. (2016) characterised the secretion of the ECE1-encoded toxin, Candidalysin, as essential for pathogenesis of *C. albicans*. Deletion of the Candidalysin encoding region from the ECE1 gene attenuated *C. albicans* virulence and eliminated its ability to damage epithelial cells (Moyes *et al.*, 2016). However, very little is understood about the transport mechanisms of Ece1 in hyphae. In fact, despite studies of RNA-binding proteins in *C. albicans* revealing some similarities, such as the reliance on She3 protein for RNA transport, to other fungal mRNA transport systems, the precise mechanism for mRNA transport in *C. albicans* remains to be understood.

The ability of *C. albicans* to undergo a morphological transition from oval budding yeast cells to pseudohyphal and hyphal filaments remains one of the most vital virulence traits possessed by this fungal pathogen (Kadosh, 2016). These observations highlight the importance of RNA localization and RBPs for fungal pathogenicity and illustrates the importance of examining the impact of RBPs, such as Ssd1, on virulence and pathogenicity in different fungal species.

1.4 Methods for measuring RNA localisation, translation, and RNA-protein interactions

1.4.1 Microscopy

Microscopy is an essential tool that offers invaluable insight into biology and morphology of the cell. In the field of cell biology and biomedical sciences, understanding the morphology of a cell can lead to important findings about its fate, function, and response to environmental stressors. Recent advances in microscopy also allow us to visualise what is happening within the cell, offering an essential

perspective on protein expression levels, RNA localization, and polarized growth of cells.

1.4.1.1 Fluorescence Microscopy

Amongst the most popular techniques in protein microscopy is fluorescence microscopy which served as a vital tool for protein visualization. Fluorescence microscopy employs an array of fluorophores that allow identification of cells and sub-microscopic cellular components with a high degree of specificity. The process of fluorescence occurs when a photon of light is absorbed by a 'fluorophore' and consequently re-emitted as a photon with a longer wavelength (Shashkova and Leake, 2017). In this method, proteins are tagged with a fluorophore (fluorescent probe), such as Green fluorescent protein GFP or mCherry, directly or via linkers. The linkers used are usually HALO/SNAP, which are probes consisting of a DNA repair protein (for SNAP) or a haloalkane dehalogenase enzyme (for HALO) (Keppler *et al.*, 2003; Los *et al.*, 2008), or fusion protein linkers (Chen, Zaro and Shen, 2013). The use of these linkers serves to avoid direct fluorescent labelling of the protein, which might lead to steric hindrance, thus impairing their physiological behaviour. In this method, the microscope has a filter and a dichoric mirror that allow light of a specific wavelength only to reach the florescence-tagged specimen. That radiation collides with the specimen, causing excitation of electrons followed by emission of light on a longer, lower energy wavelength. The fluorescence emitted from the sample is then separated from the excitation light through an emission filter and can then be visualised by the human eye through a detector. Fluorescence microscopy has been extensively used for imaging localization and aggregation of proteins within the cell. A prominent example is the research conducted by Huh et al (2003) to classify proteins into subcellular localization categories, through constructing a library of yeast strains expressing GFP-tagged proteins and performing microscopic analysis. This analysis allowed the classification of proteins representing 75% of the yeast proteome into 22 distinct subcellular localization categories, and provided localization information for 70% of proteins with previously unknown localization. Another example is a study conducted by Mir et al (2009), which showed the diffuse appearance of Hsp104 in wild-type cells versus a punctate pattern in *ssd1*Δ cells using fluorescence microscopy. In our research this method will be used to understand effect of Ssd1 on stress-protective proteins, such as Hsp104, by visualising its effect on the expression levels and localization of these proteins.

1.4.1.2 RNA Microscopy

A widely used RNA microscopy method is the m-TAG technique, which consists of the addition of MS2 stem loops into the 3' UTR of genes, followed by the co-expression of GFP fused to the RNA-binding MS2 coat protein (MS2-CP) (Haim-Vilmovsky and Gerst, 2009; Haimovich *et al.*, 2016). The m-TAG genome tagging

technique uses Cre recombinase to remove the selection marker used for genome integration, in order to maintain the 3' UTR associated with the ORF. This is important due to the role of the 3' UTR in mRNA localization and stability, thus allowing intracellular targeting of mRNA. The gene of interest is tagged with multiple binding sites for MS2 coat protein (MS2-CP) through PCR-based genomic-tagging and homologous recombination, and afterwards MS2-CP fused to GFP is expressed in cells. The binding of the tagged mRNA to this fusion protein produces an RNA granule that can be visualized using fluorescence microscopy. While other methods require cell fixation, this technique allows for robust, *in vivo* visualization of mRNA localization in live cells (George *et al.*, 2018). Despite its advantages, some controversy surrounds the m-tag technique as it is thought to impact upon mRNA production and stability. Therefore, the single molecule fluorescent *in situ* hybridization (smFISH) method presents an attractive alternative. In this method, cells are first fixed and permeabilized, and then they are hybridized with multiple single-stranded, short oligonucleotide probes that tile the length of the mRNA. Each oligo is conjugated with a fluorophore, and thus the binding of multiple probes to the same transcript produces a bright spot, indicating a single mRNA. The single-molecule resolution of this method permits precise quantification of gene expression levels (Haimovich and Gerst, 2018), however, smFISH doesn't allow for live imaging as cells need to be fixed. RNA microscopy allows the visualization of RNA transport and localization, thus providing valuable insight on co-localization, cell polarity, and important processes such as the stress-dependent formation of stress granules (Pizzinga *et al.*, 2019). In a recent study, Pizzinga *et al*. (2019) employ both of the abovementioned methods to examine translation factor mRNA localization. In our research, we can employ these methods to examine the effect of our RBPs of interest on the localization of RNA.

1.4.2 High-throughput techniques

Rapid technological progress presented high-throughput technologies for the study of biological systems on an unprecedented level. These advances led to invaluable findings in genomics and transcriptomics (Mardis, 2008; Reuter, Spacek and Snyder, 2015). RBPs control and interact with a wide array of targets, as revealed by techniques used in various studies such as DNA microarray performed by Hogan *et al*. (2008) to examine combinatorial binding of RBPs to specific recognition elements in mRNAs in yeast, or RNA-immunoprecipitation followed by sequencing (RIP-seq) and crosslinking followed by immunoprecipitation and sequencing (CLIP-seq) which were used to identify the RNA targets and specific binding sites of RBPs (Wheeler, Van Nostrand and Yeo, 2018). These techniques, among many other in vivo and in vitro techniques, were used to identify RBPs and their binding targets in a high-throughput manner.

One of the most prominent of these methods is ribosome profiling. Ribosome profiling is a deep-sequencing-based tool that determines the positions of ribosomes

on mRNAs are by sequencing ribosome-protected mRNA fragments (RPFs), which in turn facilitates detailed measurements of translation *in vivo* (Ingolia *et al.*, 2009). This approach depends on the sequencing of RPFs, known as ribosome footprints, which are nucleotides of an mRNA protected by translating ribosome from nuclease activity (Steitz, 1969; Brar and Weissman, 2015). This provides a precise record of the position of the ribosome when translation was stopped. Furthermore, protein synthesis can be measured through measuring the density of protected fragments on a specific transcript (Brar and Weissman, 2015). For example, ribosome profiling and RNA-Seq were used to investigate Puf3's functions in translational regulation in *S. cerevisiae* (Wang *et al.*, 2019)

Another proteomic approach is the proximity-dependent biotin identification (BioID). It is an approach based on generating a reactive biotin derivative which labels proteins in its vicinity through diffusion from the enzyme's active site. It is a technique of proximity-dependent labelling that was originally based on fusion of a promiscuous *Escherichia coli* biotin protein ligase to a targeting protein (Roux *et al.*, 2012). BioID is used for the proteomic characterization of protein clusters, protein-protein interactions, and spatially restricted proteins within an intracellular compartment (Jiang *et al.*, 2012; Rees *et al.*, 2015). This technique utilizes the short half-life of the enzyme-generated product to ensure labelling of proteins in the immediate vicinity of the enzyme (Rees *et al.*, 2015). BioID can be applied to a wide range of cellular proteins, including transcription factors and cytoskeletal components.

To understand RBPs and their functions, we need to investigate direct protein-RNA interactions and the mechanisms that govern regulation and specificity of RNA. The UV crosslinking and immunoprecipitation (CLIP) serves to purify short RNA fragments which crosslink to a specific protein, and then uses sequencing to identify these fragments (Lee and Ule, 2018). CLIP produces transcriptome-wide maps of RNA crosslink sites when combined with high-throughput sequencing. CLIP uses zero-length covalent protein-RNA crosslinking and RNA fragmentation to purify RNAs bound to a specific RBP under stringent conditions (Lee and Ule, 2018). This should ensure prevention of co-purification of free RNAs or unwanted RBPs, thus identifying the position of the direct RNA binding sites of the crosslinked RNA fragment. Crosslinking and cDNA analysis (CRAC) is a variation of CLIP, in which RBPs are tagged with C-terminal 6 × His, protein A tags, and tobacco etch virus (TEV) protease site. CRAC permits stringent, transcriptome-wide recovery of RNA–protein interaction sites in vivo at a base-pair resolution. The Tollervey lab used CRAC to map protein–RNA interaction sites for Hfq (an RNA chaperone) and ribonuclease RNase E in pathogenic *E. coli* (Sy *et al.*, 2018).

1.5 Research aims

My research investigates how Ssd1 regulates synthesis of the fungal cell wall, through binding mRNAs that encode secreted cell wall proteins. In this thesis, I set

out examine the role of Ssd1 and other RBPs in regulating the expression and localization of such mRNAs and their protein products. The aims of my project are to:

I. Investigate if RBPs of interest influences the proteins encoded by target mRNAs, by testing fluorescently tagged proteins for:
    a. Protein mis-localization in deletion strains, compared to wild-type and reference strains, using fluorescence microscopy.
    b. Protein expression in deletion strains, compared to wild-type and reference strains, using flowcytometry.
    c. Test the effect of altered UTRs on the localization and expression of these proteins.

II. Investigate if Ssd1 and other RBPs of interest (She2, She3, Mpt5) influence the localization of its target mRNAs by testing target mRNAs fluorescently labelled with smFISH probes for:
    a. mRNA mis-localization in RBP deletion strains, compared to wild-type, using RNA microscopy.
    b. mRNA expression in deletion strains, using BIGFISH quantification of mRNA spots in single cells for a whole population.

III. Explore conservation of Ssd1 function across fungi, by replacement of Ssd1 in *S. cerevisiae* with Ssd1 homologs and investigating cellular phenotypes.
    a. Investigate if *S. cerevisiae*'s Ssd1 might be suitable to study as a model for Ssd1 function in the fungal kingdom.

In this thesis, I attempt to address some of the elements regulating fungal cell walls by investigating their specific targets, and through examining the mechanisms by which these elements operate.

2 Materials and methods

2.1 Stock of oligonucleotides

Oligonucleotides used in this thesis were synthesised by Integrated DNA Technologies. Oligos were resuspend to a 100 µM stock concentration. This was done as per the manufacturer's recommendation, by multiplying the number of nanomoles listed for a particular oligo by a factor of 10, and then resuspending the dry DNA in that same number of microliters of sterile water. All primers used in this study can be found in the appendix.

2.2 Yeast strains

The yeast strain constructed in this thesis are listed per individual result chapter. All yeast strains were grown in YPD or Synthetic Complete media at 30 ºC, or grown in selection media (listed below) where appropriate. The background strains used for strains construction are listed below. An appendix at the end of this thesis includes all strains used.

Strain ID	Description	Genotype	Source
BY4741	Wild-type	*MATa; his3Δ1; leu2Δ0; met15Δ0; ura3Δ0;*	Jean Beggs
Δ*ssd1*	ΔYDR293C	*MATa; his3Δ1; leu2Δ0; met15Δ0; ura3Δ0; YDR293C::kanMX4*	H. Tekotte
Δ*mpt5*	ΔYGL178W	*MATa; his3Δ1; leu2Δ0; met15Δ0; ura3Δ0; YGL178W::kanMX4*	Edinburgh genome foundry
Δ*sec72*	ΔYLR292C	*MATa; his3Δ1; leu2Δ0; met15Δ0; ura3Δ0; YLR292C::kanMX4*	Edinburgh genome foundry
Δ*sun4*	ΔYNL066W	*MATa; his3Δ1; leu2Δ0; met15Δ0; ura3Δ0; YNL066W::kanMX4*	Edinburgh genome foundry

Table 2.1. Background strains used in this thesis. This is table shows all the main background strains used in this thesis for further strain construction.

2.3 Addgene plasmids

Plasmids used in this thesis were purchased from Addgene. Plasmids were streaked out from a bacterial stab onto an appropriate antibiotic supplemented plate, to isolate single colonies. Plates were stored at 37 ºC, then 3-5 ml overnights were set up at 37 ºC for each plasmid using a single colony. The overnights were used for creating

glycerol stocks (300 µl of overnight + 300 µl of 40% w/v glycerol, stored at -80 ºC). Overnights were also used for plasmid minipreps, by using the Zyppy Plasmid Miniprep Kit (Zymo) as per the manufacturer's protocol. Plasmid concentration and quality were checked on a DeNovix NanoDrop. All plasmids used can be found in the appendix.

2.4 Media

2.4.1 Preparation of YPD

Liquid YPD: 20 g Bacto peptone, 10 g Yeast extract, 50 ml of sterile 40% glucose, 950 ml Water. This was autoclaved.

YPD Agar: 20 g Bacto peptone, 10 g Yeast extract, 24 g Bacto agar, 950 ml Water. This was autoclaved.

2.4.2 Preparation of Synthetic Complete (SC) media

2.4.2.1 Synthetic complete liquid media

SC -Uracil media consisted of: 3.35 g of Yeast Nitrogen Base (YNB) without amino acids, 10 g glucose (or with 50 ml of 20% w/v glucose), and 0.963 g SC -Ura dropout mix (Kaiser), make up to 500 ml with ddH2O. This was filter sterilize.

SC -Histidine media consisted of: 3.35 g of Yeast Nitrogen Base (YNB) without amino acids, 10 g glucose (or with 50 ml of 20% w/v glucose), and 0.963 g SC -His dropout mix (Kaiser), make up to 500 ml with ddH2O. This was filter sterilize.

SC media consisted of: 3.35 g of Yeast Nitrogen Base (YNB) without amino acids, 10 g glucose (or with 50 ml of 20% w/v glucose), and 1 g SC dropout mix (Kaiser), make up to 500 ml with ddH2O. This was filter sterilize.

2.4.2.2 Synthetic complete agar plates

Synthetic complete (SC) selection plates were prepared by combining 2x of the relevant SC media and 2x (4%) agar for a final volume of 500 ml, as follows:

2x (4%) agar consisted of 10 g agar and 250 ml of sterile water, placed in a sterile bottle and autoclaved.

2x SC -Ura media consisted of: 3.35 g of Yeast Nitrogen Base (YNB) without amino acids, 10 g glucose (or with 50 ml of 20% w/v glucose), and 0.963 g SC -Ura dropout mix (Kaiser), make up to 250 ml with ddH2O. This was filter sterilize.

2x SC -His media consisted of: 3.35 g of Yeast Nitrogen Base (YNB) without amino acids, 10 g glucose (or with 50 ml of 20% w/v glucose), and 0.963 g SC -His dropout mix (Kaiser), make up to 250 ml with ddH2O. This was filter sterilize.

2x SC media consisted of: 3.35 g of Yeast Nitrogen Base (YNB) without amino acids, 10 g glucose (or with 50 ml of 20% w/v glucose), and 1 g SC dropout mix (Kaiser), make up to 250 ml with ddH2O. This was filter sterilize.

2.5 gRNA plasmids

CRISPR guide RNAs (gRNA) were all designed using the Benchling guide RNA online design tools, as single guides with 20 bp guide length and an NGG PAM sequence. A list of all gRNA oligos and plasmids can be found in the appendix. Each gRNA consisted of two annealed oligos, cloned into pML104 vectors as described below. The pML104 vector used in this study has a *URA* selection cassette (**Fig. 2.1.)**.

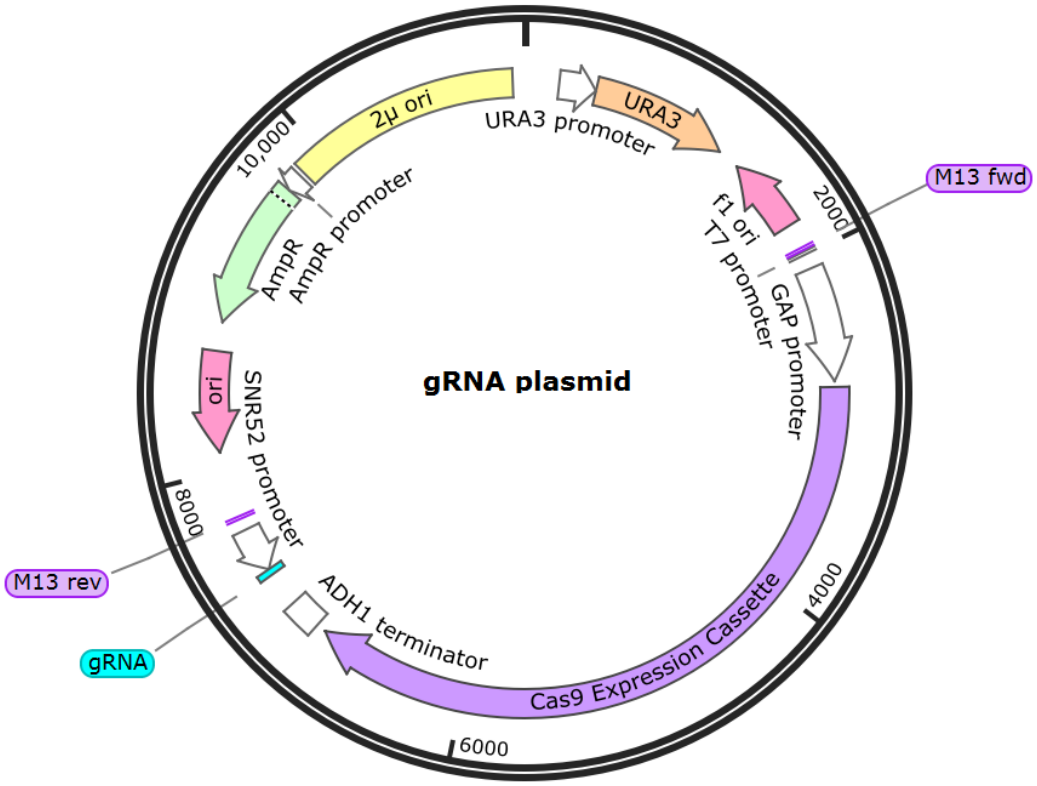

Figure. 2.1. Schematic of the gRNA plasmids used in this study. Plasmid map of the single guide RNA (sgRNA)/Cas9 expression vector pML104 (URA3 selection) (Laughery *et al.*, 2015). The plasmid is a yeast/*E. coli* shuttle vector containing an ampicillin resistance (AmpR) marker, and a yeast 2 micron (2μm) origin of replication. The vector contains the SNR52 promoter, a Cas9 expression cassette, and an sgRNA expression cassette containing unique *Bcl*I and *Swa*I restriction sites, to facilitate directional cloning of the user-designed guide sequence into the sgRNA expression cassette.

Guides were annealed by mixing the following: 3 µl oligo 1 (100uM), 3 µl oligo 2 (100uM), 10 µl T4 DNA Ligase buffer with ATP (Thermofisher), and 84 µl Nuclease Free Water. This was placed in a PCR tube and run at a temperature ramp down cycle in the thermocycler (95°C (5min), 85°C (9min), 65°C (9min), 55°C (9min), 45°C (9min), 35°C (9min), 25°C (9min), 10°C (hold)).

To acquire the necessary Saccharomyces cerevisiae strains for the study, CRISPR/Cas9 editing was performed using pML104 (Addgene), which is the plasmid required for expressing Cas9 and a gRNA. pML104 stock was stored in NEB5alpha *Escherichia coli* as recommended by Addgene. The stocks were streaked out and used for plasmid minipreps using the Zyppy Plasmid Miniprep Kit (Zymo) as per the manufacturer's protocol. The pML104 plasmid was then transformed into dam-, dcm- competent cells to prepare it for cloning gRNA into pML104.

Ampicillin resistant pML104 must be grown in a dam- strain (transformed into dam-, dcm- competent cells) so that it can be digested with the enzyme BclI (10 U/µL), which is dam methylation sensitive). For bacterial transformations, competent cells from New England Biolabs were used.

Single colonies were selected from transformation plates, and overnight were set up in Luria broth (LB) + Ampicillin (100 µg/mL), then plasmid minipreps performed as previously described.

*Swa*I digests were set up, by mixing the following: 5 µg of pML104, 5 µl NEB 3.1 buffer, 2 µl *Swa*I (10 U/µL), up to 50 µl water. This was incubated at 25 C for 15 hours, then *Swa*I inactivated at 65C for 20 minutes. 2 µl of *Bcl*I were added to the tube and set it up to incubate at 50 C for 120 minutes. Digests were checked on an agarose gel to check for correct digest size. The double digests were then purified using Zymo Clean & Concentrator kit as per the manufacturer's protocol.

Annealed oligos were then ligated with the double cut plasmid as follows: 2 µl Annealed oligo (3 µM), 2 µl *Swa*I/*Bcl*I cut pML104 (33ng/µl), 1 µl 10× T4 DNA ligase buffer with ATP, 0.5 µl T4 DNA ligase, and 4.5 µl water. Ligation was incubated at 25°C for 2 hours.

The ligation was transformed into competent NEB5alpha *E. coli,* then overnights made, and plasmid minipreps performed. The minipreps were sent for verification by sequencing at Dundee Sequencing Facility. Sequencing reactions were sent as 1.5 ml Eppendorf tubes containing 20 µl (30 ng/µl) aliquots. These were sequenced with standard M13 forward and reverse primers.

2.6 Bacterial transformations for plasmids

Cells were thawed on ice, then mixed gently, and 50 µl of cells were pipetted into each transformation tube on ice. 5 µl containing 1 pg-100 ng of plasmid DNA were added to the cell mixture. Tubes were gently flicked 4-5 times to mix cells and DNA (without using vortex). Reaction was incubated on ice for 30 minutes (Without

mixing). Reaction was then exposed to heat shock at exactly 42 °C for exactly 30 seconds in a water bath (Without mixing). Reaction was placed on ice for 5 minutes, then 950 µl of room temperature Super Optimal broth (SOC) pipetted into the mixture. This was mixed gently by pipetting up and down. Reaction was incubated at 37 °C for 60 minutes in a shaking incubator (250 rpm). Following incubation, cells were mixed thoroughly by flicking the tube and inverting, then serial dilutions were performed using SOC. Neat and 1:10 and 1:100 dilutions were then used for plating 50 µl of each dilution onto LB + Amp plates and incubated overnight at 37 ºC.

2.7 Yeast transformations

2.7.1 Stock solutions

1M LiOAc stock solution: 10.2 g of lithium acetate dihydrate was dissolved in 80 ml of sterile H2O and then made up to 100 ml. This was filter-sterilized.

Polyethylene glycol (PEG) 50%: 5 g of PEG 4000 was measured into a 50 ml falcon tube. 3 ml water was added and vortexed thoroughly. This was microwave for 10 seconds until dissolved, placed in a stand in the microwave with lid loose and stopped to check every two seconds (Tube could explode or boil over easily if left unchecked). Mixture was vortexed again then made up to 10 ml with sterile water (in 15 ml or 50 ml falcon tube). This was filter sterilized using 0.45 mm filter and a 10ml syringe into sterile 50 ml tube. Note that PEG 50% can seriously affect transformation efficiency, and so it is better to prepare it fresh and in small batches (5 - 10 ml). Autoclaving PEG 50% also affects the efficiency of yeast transformations, so this was filter sterilised each time and tube lid parafilmed when not in use.

2.7.2 Transformation protocol

5 ml of yeast cells were grown overnight in YPD at 30 C in a shaking incubator until saturated. A 1:10 dilution of the overnight (made in fresh YPDA) was checked on a spectrophotometer at OD600. The OD600 of this dilution was used to calculate the amount needed from the overnight, to make a subculture at a final OD600 of 0.2 in 15 ml of fresh YPD. Subcultures were inoculated (to final OD600 0.2 in 15 ml of YPD) in a flask or a 50 ml Falcon tube, then grown in a shaking incubator (at 30 ºC, 180 rpm) until reaching an OD600 0.5 - 0.8, which takes about 3 to 4 hours.

Once at correct OD, cells were pelleted by centrifugation at 3500 rpm for 3 minutes. Washed once with 10 ml of sterilised water, and centrifuged at 3500 rpm for 3 minutes, then washed once with 5 ml of 0.1M LiOAc and centrifuged at 3500 rpm for 3 minutes. LiOAc was discared, and cells were resuspended with 250 ul 0.1M LiOAc and used for transformation.

Salmon sperm DNA (SS DNA) (ThermoFisher) was boiled at 100 ºC for 10 minutes. The following master mix was prepared, per single reaction: 240 µl PEG (50%), 36 µl 1M LiOAc, 25 µl SS DNA (10 mg/ml), 19 µl sterile water. Master mix was vortexed, then 300 µl (per reaction) of the master mix were pipetted into labelled sterile eppendorf tubes. 2 ul of insert DNA (~100-250 ng) were added into their respective tubes, then mixed by vortexing. 50 µl of yeast competent cells were added on top, slowly. This was mixed by inverting the tube a few times, then incubated at 30 ºC (shaking incubator) for 30 minutes. 36 µl of DMSO were added, then immediately mixed well by inverting and incubated at 42 ºC for exactly 15 minutes. Tubes were centrifuged at 8000 rpm for 30 seconds. 280 µl of the supernatant was removed, without touching the pellet, then the the pellet was resuspended with the remaining liquid. Cells were then plated on appropriate selection plates by spreading transformants using a spreader or sterile small glass beads.

2.8 Genomic DNA (gDNA) extraction

0.2M lithium acetate and 1% SDS solution: 5 g sodium dodecyl sulphate was dissolved in 50 ml distilled sterile water. 10.2 g lithium acetate dehydrate was added, then volume made up to 500 ml with distilled water. This was filter sterilized.

200 µl of liquid overnight yeast culture was transferred to Eppendorf tube then pelleted. The supernatant was removed, and the pellet resuspend in 100 µl of 0.2M LiOAc/1% SDS solution. This was incubated for 5 minutes at 70 °C. Following incubation, 300 µl of 100% ethanol was added then mixture vortexed. This was centrifuge at 15,000 g for 3 minutes. Supernatant was discarded, and the pellet was washed with 70% ethanol then pelleted again. Ethanol was removed and the pellet dissolved thoroughly in 30 µl of nuclease free water. This was centrifuged at 15,000 g for 30 seconds. The supernatant was transferred to a new sterile tube, and used as input for PCR. Concentration and purity of each gDNA extraction was measured using Denovix Nanodrop.

3 Investigating the effect of RNA-binding proteins and untranslated regions on the localization of the proteins Sun4 and Srl1

3.1 Introduction

S. cerevisiae coordinates its cell wall construction with the cell cycle. This process requires cell polarity, and timely delivery and translation of the cell wall proteins involved in cell wall biogenesis and involved in cell cycle control. An example of this is the strict transcriptional regulation which ensures the arrival of *ASH1* mRNA in the daughter cell, untranslated, to enable mating type switching between mother and daughter cell. This is because mother and the developing bud in budding yeast have different mating type, sizes, and lifespans at the end of mitosis (Juanes and Piatti, 2016). The mother cell grows and starts budding in late G1/S stage. During this time of impending bud emergence, the cell chooses its presumptive bud site and deposits chitin as a ring at the bud site in late G1 stage (**Fig. 3.1**) (Baladrón *et al.*, 2002; Stewart, 2017). The chitin ring is anchored by attachment to 1-3-β-glucan chains in the existing glucan network (Cabib, 2004). The cell weakens at the bud site to allow bud emergence. Once the cell starts the process of budding, it is committed to cell

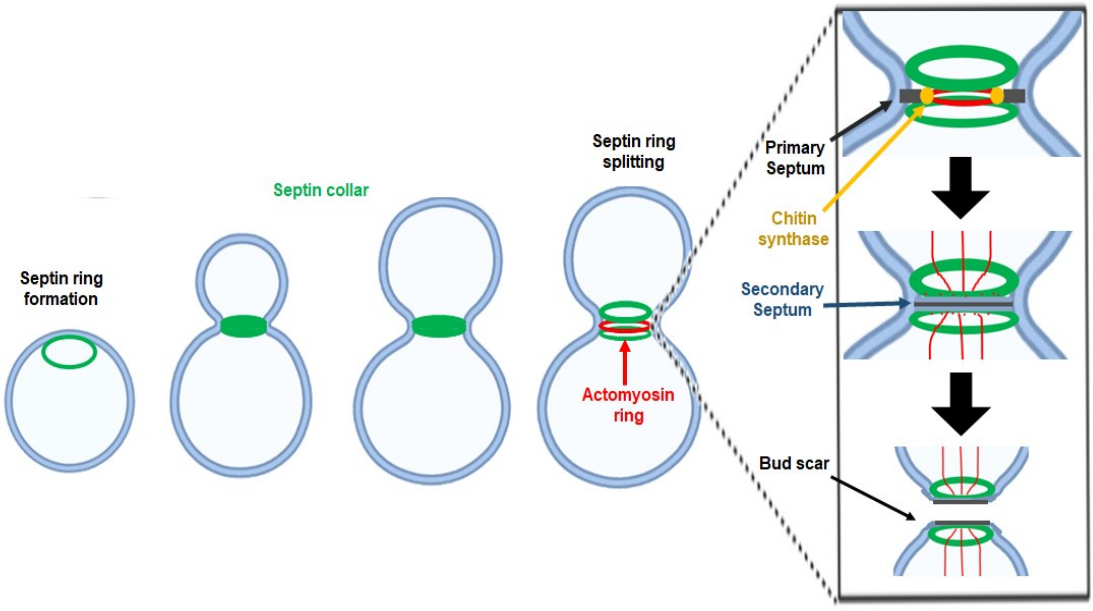

Figure 3.1. The formation of the septin ring leading up to budding and cytokinesis. This figure depicts septin ring formation, followed by budding and the formation of a septin collar. The formation of the contractile actomyosin ring (CAR) guides the formation of the primary septum which marks the daughter cell's independence from the mother. Once the secondary septum forms around the primary septum, chitinase secretion from the daughter cell dissolves the primary septum. Thus, enabling cytokinesis. Figure adapted from Juanes and Piatti (2016).

division (Zakhartsev and Reuss, 2018). At this stage, cell growth is restricted to the developing bud, while the mother duplicates and divides its contents. Signalling molecules establish an axis of polarity pointed at the bud site, to enable segregation of the cell content. As the bud grows apically and becomes larger, the motor protein myosin II and actin filaments make a contractile actomyosin ring (CAR), which guides the formation of the primary septum (Bi *et al.*, 1998; Rancati *et al.*, 2008). The bud then grows independent of the mother cell with the formation of a primary septum consisting of chitin growing from the chitin ring. The primary septum soon becomes covered with secondary septum on both sides, to allow chitinase secretion from the daughter cell; resulting in dissolving the primary septum (Juanes and Piatti, 2016). In collaboration with other enzymes degrading the cell wall, this allows cytokinesis and separation from the mother cell. Leaving the mother with a bud scar, and the daughter with a birth scar. Simultaneously to the cell cycle process, the cell traffics its mRNAs and regulates protein production to ensure asymmetric protein translation.

Previous studies documented cell wall protein families regulated in accordance with the yeast cell cycle, and proteins such as Crh2 localizing to the bud neck during the budding cycle (Rodríguez-Peña *et al.*, 2000; Baladrón *et al.*, 2002). Likewise, the SUN (SIM1, UTH1, NCA3) family proteins are secreted out of cells in different growth phases. Although the roles of these proteins aren't fully understood, they are thought to be connected to mitochondrial and cell wall functions (Kuznetsov *et al.*, 2013). For instance, cells lacking Uth1 have different β-D-glucan and chitin composition compared to wild-type cells, thus indicating a cell wall function for Uth1p (Ritch *et al.*, 2010). Another member of this family is the Sun4/Scw3 glucanase. Sun4 was reported to be involved in cell septation, where its absence results in inefficient mother-daughter cell separation (Mouassite *et al.*, 2000). However, the localization of Sun4 was not clearly defined at the time of this publication. In fact, until recently, the tagging and imaging of Sun4 in the available literature has been inconsistent. The available images came from studies tagging Sun4 with a green fluorescent protein (GFP) at the C'-terminal, or tagging it at the N' or C' terminals using the SWAT-GFP libraries (Huh *et al.*, 2003; Breker, Gymrek and Schuldiner, 2013). Proteins localize differently when tagged at the N' or C' terminal as a result of interfering with regulatory or targeting sequences, therefore, the data generated from these studies is inconsistent (Yofe *et al.*, 2016). The SWAT-GFP library images do not show clear localization of Sun4 to the yeast bud scar, which was shown in living cells using direct immunofluorescence (IF) and an HA tag on the C-terminal of Sun4 (Kuznetsov *et al.*, 2013). Because of the ambiguity of this protein's localization in the existing literature, and due to its role in cell septation and its association with three of my RBPs of interest (Ssd1, Mpt5, and She2); I chose this protein as my first target protein to investigate. My second target protein was Srl1; a cell wall mannoprotein that is required to compensate for cell wall instability (Hagen *et al.*, 2004). Srl1 is also bound by the RBPs Ssd1, Mpt5, and She2 (Oeffinger *et al.*, 2007; Hogan *et al.*, 2008), and *SRL1* mRNA was previously reported to mislocalize upon deletion of

Ssd1 (Kurischko, Kim, *et al.*, 2011). Srl1 localizes to the periphery of small buds (Shepard *et al.*, 2003), however, its precise function remains unknown.

Both Sun4 and Srl1 contain N-terminal signal sequences (Fundakowski, Hermesh and Jansen, 2012; Mori *et al.*, 2015). Secreted proteins are directed to the endoplasmic reticulum (ER) for biogenesis via a hydrophobic ER targeting sequence (Rapoport, 2007; Cross *et al.*, 2009). In eukaryotes, these sequences can be N'-terminal cleavable signal sequences (SS) and transmembrane domains (TM) which act as signal anchors(Ast, Cohen and Schuldiner, 2013). ER-targeting can be dependent on the signal recognition particle (SRP) to mediate co-translational translocation, or utilize an alternate SRP-independent translocation pathway. The SRP-independent pathway is utilised by short secretory proteins that are unable to recruit the SRP co-translationally, due to an insufficiently hydrophobic ER-targeting sequence (Ng, Brown and Walter, 1996; Lee and Bernstein, 2001). The translocation machinery for this pathway consists of a tetrameric complex including Sec62, Sec63, Sec66, and Sec72 (Feldheim and Schekman, 1994; Panzner *et al.*, 1995; Young *et al.*, 2001). Recent studies showed that the deletion of the translocon component Sec72 blocks secretion and leads to mis-localized protein aggregates in the cytoplasm for some Ssd1 targets, including Sun4 (Ast, Cohen and Schuldiner, 2013). This suggests that more of Ssd1 target cell wall proteins might be using an SRP-independent pathway for translocation.

My research investigates the localization and expression of the Sun4 and Srl1 proteins, within the context of post-transcriptional regulators. I follow an approach of tagging proteins at the C'-terminal as to not disrupt peptide signal sequences in the N'-terminal or Ssd1 binding sites at the 5' UTR. I also test tags which alter the 3'UTR or leaves it undisturbed, to understand the effect of this region on expression and localization. I also make 3' UTR alterations individually (wild-type background) and in combination with RBP deletions, to test the effect of each factor on cell wall proteins.

3.2 Methods

3.2.1 Strain construction

mNeonGreen was amplified from a plasmid (pFA6a-link-ymNeonGreen-SpHis5, Addgene) (Shaner *et al.*, 2013; Botman *et al.*, 2019) using amplification primers. The amplification primers (**Table 3.1**) consisted of ~40bp of homology both upstream and downstream of the target gene, plus 18bp of homology to the plasmid region.

Primer ID	Sequence
oMJ001_SUN4_mNG_FP	GTTTCCGTTACTGCTGGCAAAGCTAAGTTTGTTCTATACAACggtgacggtgctggttta
oMJ002_SUN4_mNG_RP	ATACAATCAACTTACTCAACTGTTGATGCGCCTAAGTTTAtcgatgaattcgagctcg
oMJ003_SRL1_mNG_FP	CAATGGTACAACACCACTTCGATTACTAATTCGACCAGTTGGggtgacggtgctggttta
oMJ004_SRL1_mNG_RP	CAAAAAGAACTTAAAAGGACACGTTTGAACTCATAATTCAtcgatgaattcgagctcg
oMJ118_Sun4_mNG_FP	CCGTTACTGCTGGCAAAGCTAAGTTTGTTCTATACAACatggtctctaaggtgaagaag
oMJ119_Sun4_mNG_RP	ATACAATCAACTTACTCAACTGTTGATGCGCCTAAGTTTActtgtacaattcgtccatac
oMJ120_SRL1_mNG_FP	GGTACAACACCACTTCGATTACTAATTCGACCAGTTGGatggtctctaaggtgaagaag
oMJ121_SRL1_mNG_RP	CAAAAAGAACTTAAAAGTACACGTTTGAACTCATAATTCActtgtacaattcgtccatac
oMJ010_SEQ_SUN4_FP	CAGTCAACGGTGAATGTATCTATG
oMJ011_SEQ_mNG_RP	ccatacccatgacgtcggtg
oMJ012_SEQ_SUN4_RP	CGGCGTGGGTTTTAGTGTATG
oMJ013_SEQ_HIS3_FP	ccaagcatacaaaccaaaaggg
oMJ014_SEQ_SRL1_FP	CGACTACACAATACGTTACTGtc
oMJ015_SEQ_SRL1_RP	CTGATGTATTTAGGTAGCAGAAGG
oMJ020_SUN4_CP_FP	CAAAATTGTCGCCGCTGATGAC
oMJ021_SUN4_CP_RP	GTCTGGAAGAATGATAAATAGAAACAAAG
oMJ022_SRL1_CP_FP	CAGTACGTTACAGTCACCCC
oMJ023_SRL1_CP_RP	GATAGTGAAAAATAAATACCAGTTGG

Table 3.1. Primers used for strain construction and verification. oMJ001-oMJ004 and oMJ118-oMJ121 were used to amplify the repair template from the mNeonGreen plasmid with homology to the named gene. Primers with “CP” in the name were used for verification and colony PCRs. Primers with “SEQ” in the name were used for verification by sequencing.

3.2.1.1 Strains with altered terminator region

To create the repair template, reverse primers were used. These primers amplified the HIS selection marker from the plasmid (**Fig. 3.2A**)**,** and added ~40bp of homology to the gene's 3'UTR. The forward amplification primers for this strategy consisted of ~40bp homology to the gene open reading frame (ORF), and homology to the linker region leading up to the fluorescent protein on the plasmid (**Fig. 3.2A, Fig.3.2B**). PCRs were performed using Phusion polymerase (NEB) according to the manufacturer's PCR protocol. PCR products were verified on agarose gel to confirm correct product size (**Fig. 3.2C**)**,** then digested with DpnI enzyme (New England Biolabs) to remove any remaining plasmid backbone and enhance transformation efficiency. Several PCR reactions were pooled and purified using Genomic DNA Clean & Concentrator-5 Kit (Zymo Research) to achieve a repair template concentration of around 100 ng/µl. Yeast transformations were performed (2.7.) using 250-500 ng/ul of insert DNA, and transformants were plated onto Sc-HIS plates. The repair template was inserted before the stop codon into the desired gene's ORF.

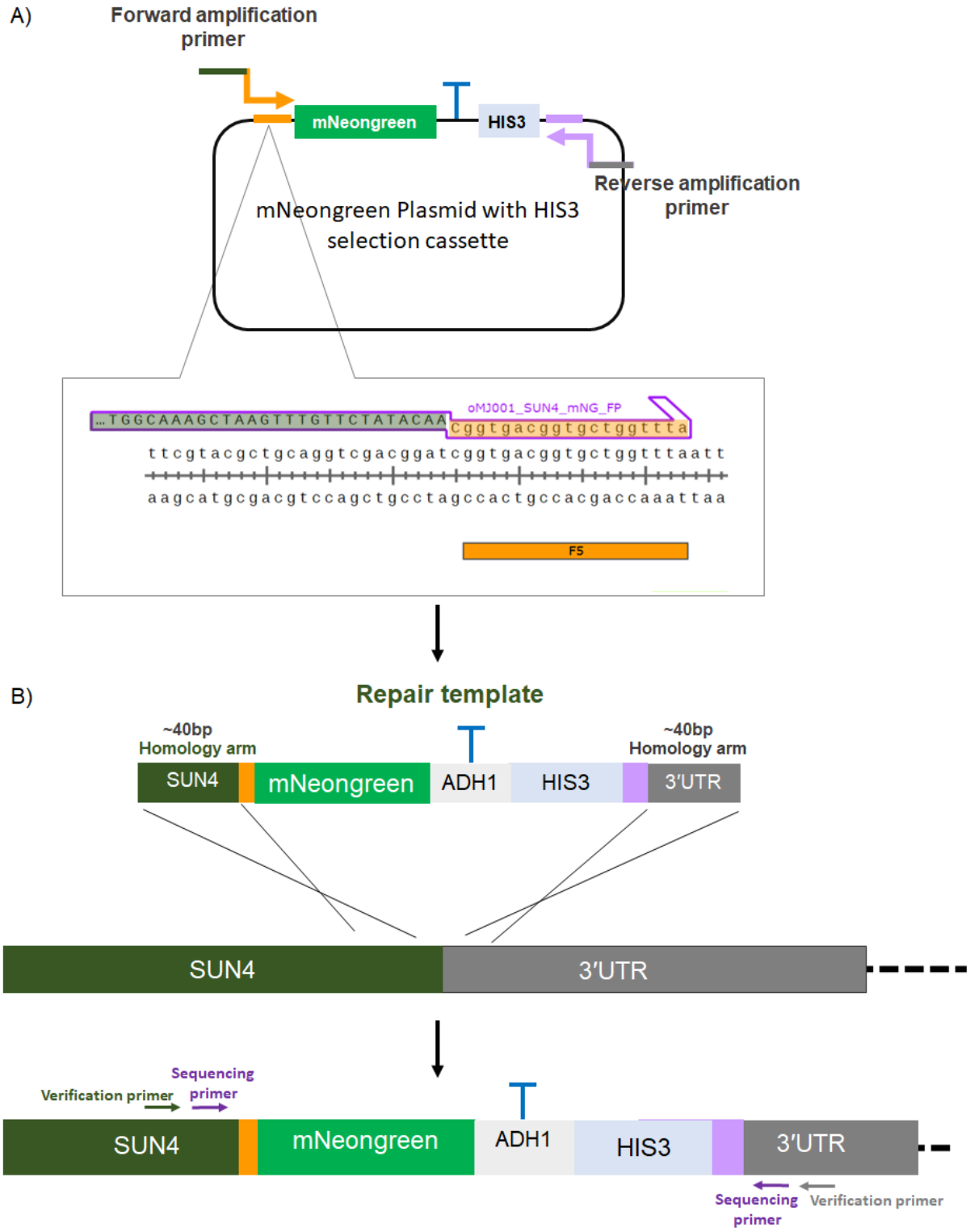
A)
Forward amplification primer
mNeongreen
HIS3
Reverse amplification primer
mNeongreen Plasmid with HIS3 selection cassette
oMJ001_SUN4_mNG_FP
…TGGCAAAGCTAAGTTTGTTCTATACAA
cggtgacggtgctggttta
ttcgtacgctgcaggtcgacggatcggtgacggtgctggtttaatt
aagcatgcgacgtccagctgcctagccactgccacgaccaaattaa
F5
B)
Repair template
~40bp Homology arm
SUN4
mNeongreen
ADH1
HIS3
~40bp Homology arm
3′UTR
SUN4
3′UTR
Sequencing primer
Verification primer
SUN4
mNeongreen
ADH1
HIS3
3′UTR
Sequencing primer
Verification primer

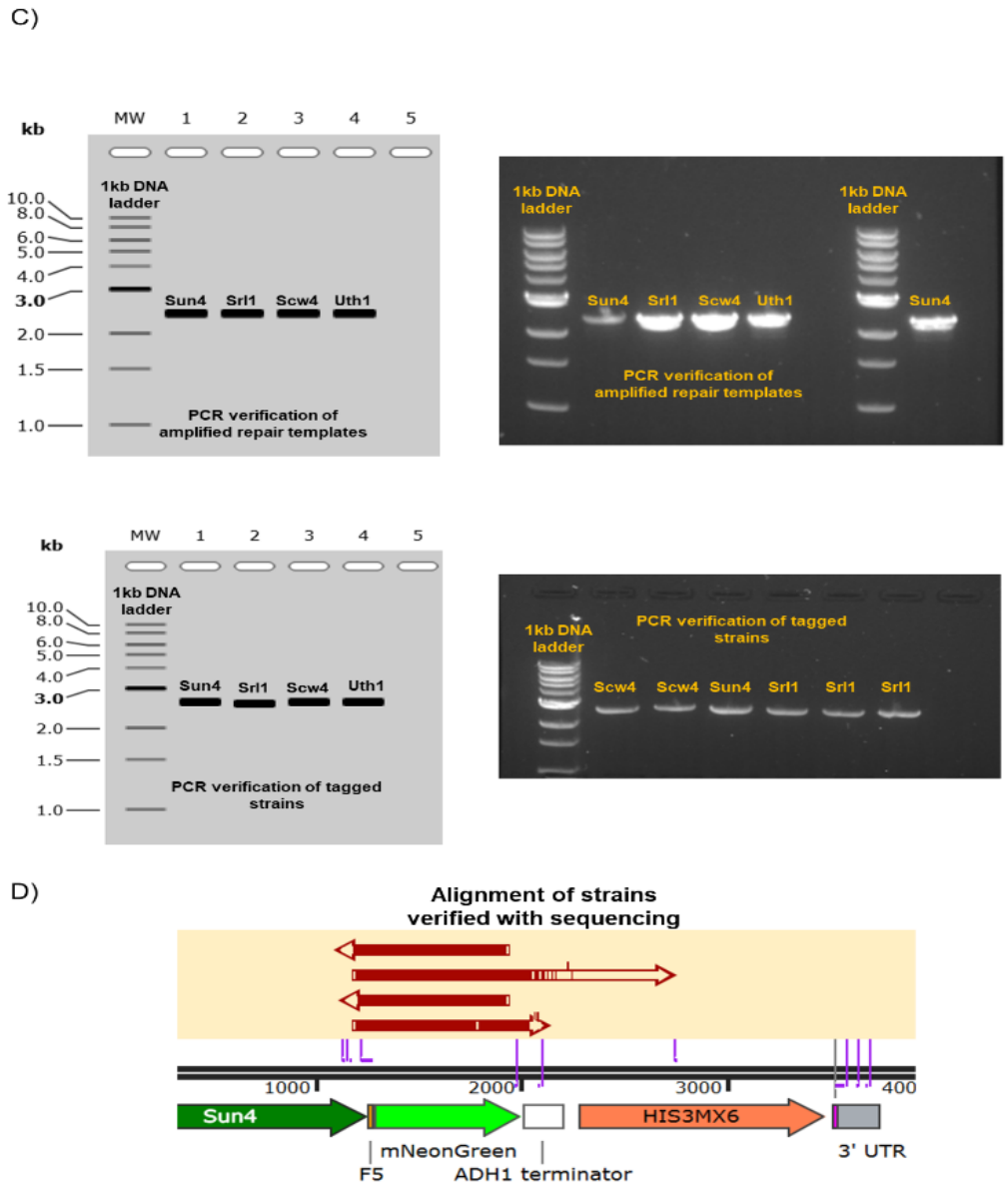

Figure 3.2. Construction and verification of proteins tagged with mNeonGreen under an altered terminator region. A) Amplification of the repair template with the addition of homology arms upstream and downstream of the gene. **B)** Insertion of the repair template with a new, altered terminator (tADH1). **C)** Verification PCRs of transformants. **D)** Aligned sequencing results to confirm correct insertion and unmutated mNeonGreen sequence.

3.2.1.2 Strains with the native terminator

The second strategy utilised a CRISPR/Cas9 approach (Laughery and Wyrick, 2019). The repair template was amplified using primer pairs that added homology arms on either side of the mNeonGreen ORF (**Fig. 3.3A**), while maintaining the linker region. Each primer consisted of ~40 bp of homology to the target gene's ORF and 3' UTR plus 18 bp of homology to the plasmid (**Fig. 3.3A, Fig.3.3B**). PCRs were

performed using Phusion polymerase (NEB) according to the manufacturer's PCR protocol, then verified on agarose gel to confirm correct product size (**Fig. 3.3C**).

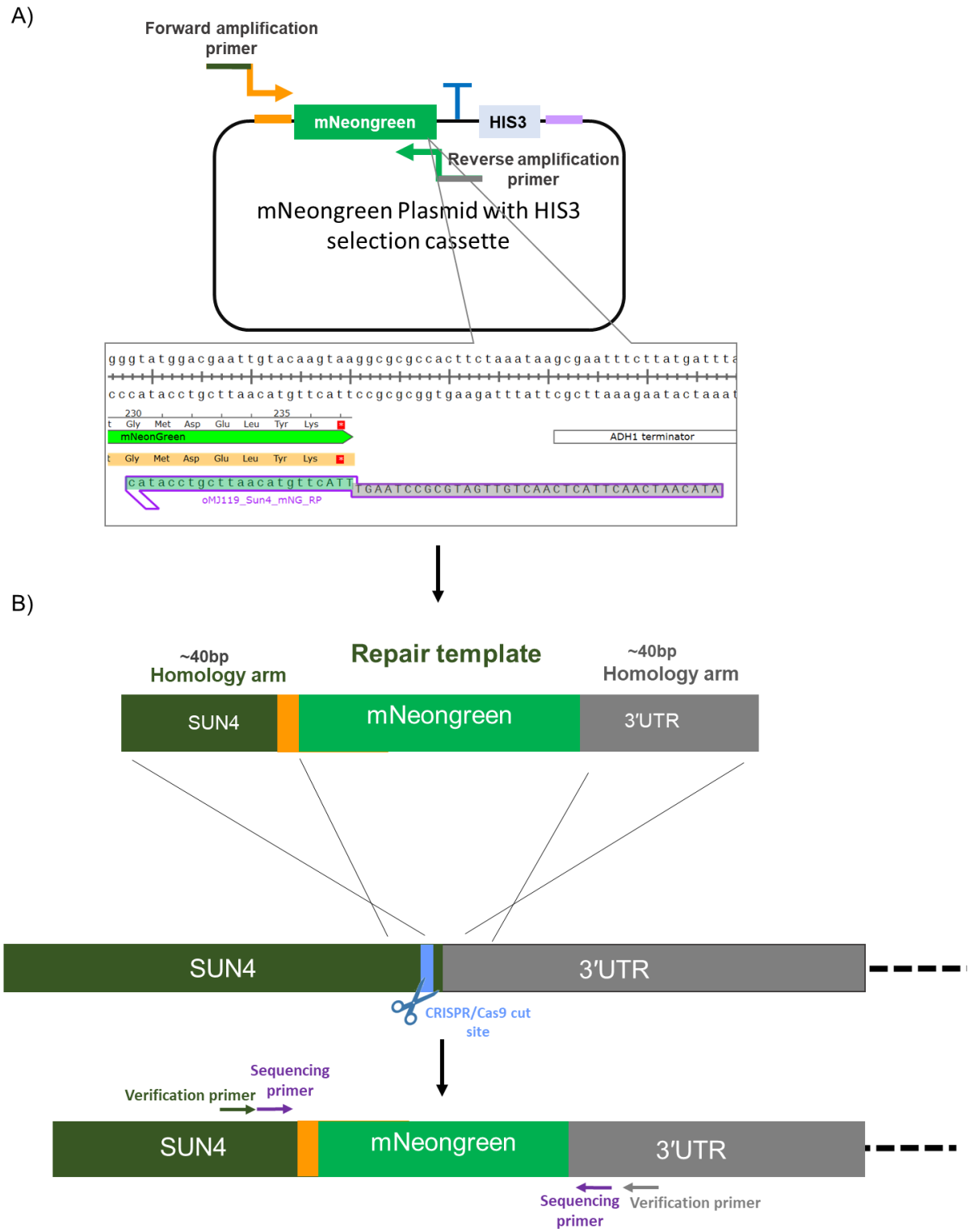

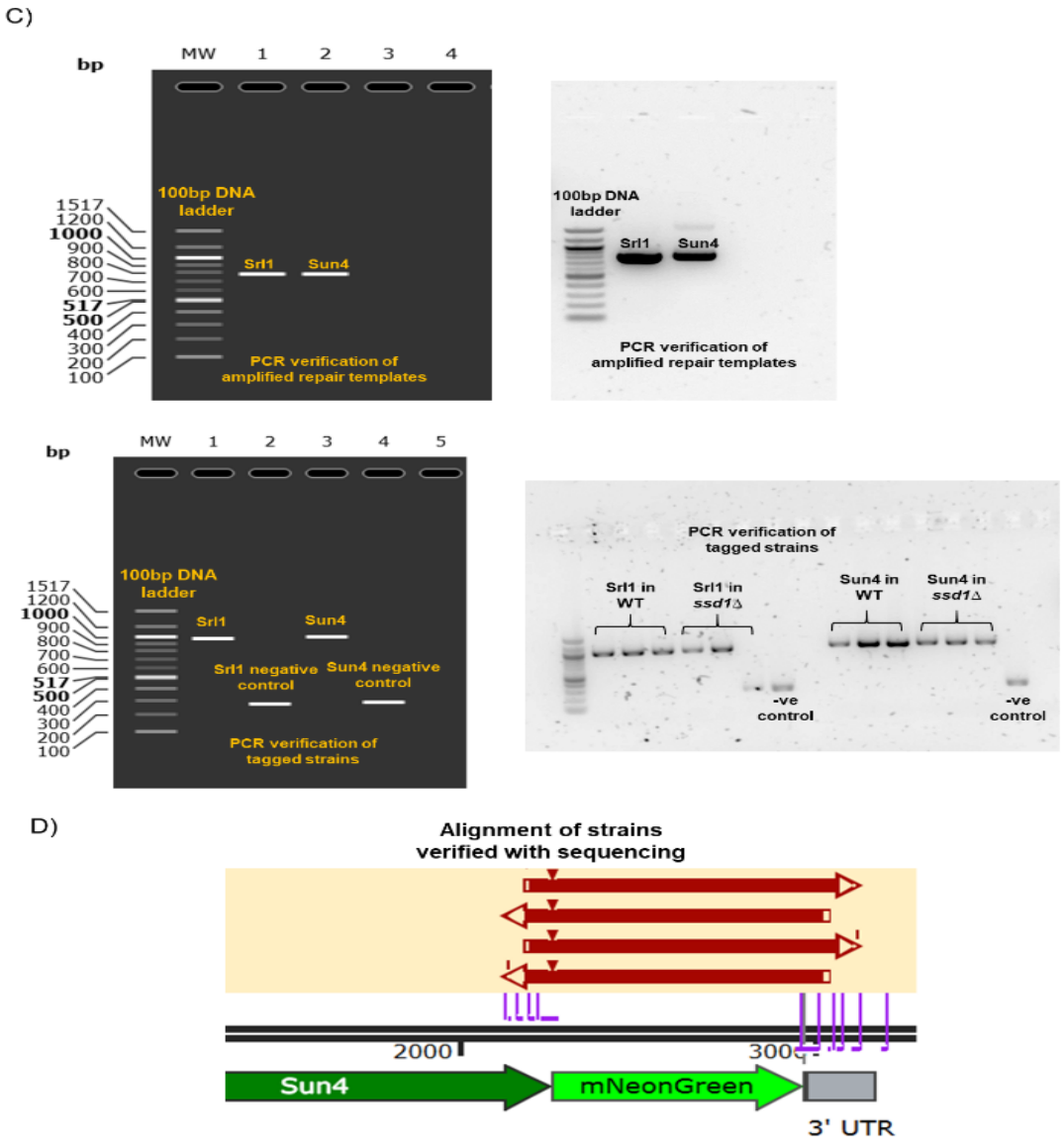

Figure 3.3. Construction and verification of proteins tagged with mNeonGreen under the native terminator region. A) Amplification of the repair template with the addition of homology arms upstream and downstream of the gene. B) Insertion of the repair template under the native gene's terminator, leaving the 3' UTR unaltered. **C)** Verification PCRs of transformants. **D)** Aligned sequencing results to confirm correct insertion and unmutated mNeonGreen sequence.

Purified PCR product was then transformed at a concentration of 250 ng/ul with 500 ng/ul of the relevant gRNA (**Table 3.2**). Transformants were plated on Sc-URA plates, due to gRNAs containing URA selection cassettes as previously described (general methods).

gRNA ID	gRNA+PAM sequence	Oligo 1	Oligo 2
gMJ001_Sun4_gRNA_3UTR	TGGACGGGCAGAAAAGAATGGGG	GATCTGGACGGGCAGAAAAGAATGGTTTTAGAGCTAG	CTAGCTCTAAAACCATTCTTTTCTGCCCGTCCA
gMJ002_Sun4_gRNA_orf_3UTR	TGTTCTATACAACTAAACTTAGG	GATCTGTTCTATACAACTAAACTTGTTTTAGAGCTAG	CTAGCTCTAAAACAAGTTTAGTTGTATAGAACA
gMJ003_SRL1_gRNA_orf_3UTR	TGAACTCATAATTCACCAACTGG	GATCTGAACTCATAATTCACCAACGTTTTAGAGCTAG	CTAGCTCTAAAACGTTGGTGAATTATGAGTTCA
gMJ004_SRL1_gRNA_3UTR	AGAAACAAAAAGAACTTAAAAGG	GATCAGAAACAAAAAGAACTTAAAGTTTTAGAGCTAG	CTAGCTCTAAAACTTTAAGTTCTTTTTGTTTCT

Table 3.2. gRNAs used for strain construction using CRISPR/Cas9. The table shows the gRNA and PAM sequence, plus the oligos used to create each gRNA

3.2.2 Strain verification

3.2.2.1 PCR verification

Constructed strains were verified using PCRs. gDNA extractions were performed from transformants successfully grown on HIS or URA selection plates to use as PCR template, as previously described (2.8.). For the first verification step, verification primers (**Table 3.1**) that anneal to the gene's ORF and 3' UTR outside of the tagged region were used (**Fig. 3.2B, Fig.3.3B**). Amplified PCR products were screened on Agarose gel for correct band size for each transformant. The initial verification PCRs were carried out using DreamTaq Green PCR Master Mix (Thermo Scientific) according to the manufacturer's protocol.

3.2.2.2 Verification with Sanger sequencing

Following the initial verification step, successful transformants were confirmed using Sanger sequencing. These PCRs were repeated using the previously mentioned verification primers and high fidelity Phusion polymerase (New England Biolabs), as per the manufacturer's protocol. PCR products were purified using Genomic DNA Clean & Concentrator-5 Kit (Zymo Research), and diluted to a DNA concentration of 32 ng/µl as per the sequencing facility's instructions. For sequencing, primers that bind within the ORF or 3' UTR of the amplified PCR product were designed and used (**Fig. 3.2B, Fig. 3.3B**). Tubes containing 20 µl of purified PCR product, alongside tubes containing 20 µl of the sequencing primer (3.2 µM), were sent to Dundee Sequencing facility for sequencing. Results were viewed and aligned using Snapgene software (**Fig. 3.2D, Fig. 3.3D**), and then glycerol stocks of the strains listed in **Table 3.3** were made.

ID	Description	Genotype
yMJ003	SUN4-mNG-tADH1, wild-type	*MATa ura3Δ0 leu2Δ0 his3Δ1 met15Δ0; SUN4-mNeonGreen-tADH1 HIS3MX*
yMJ008	SRL1-mNG-tADH1, wild-type	*MATa ura3Δ0 leu2Δ0 his3Δ1 met15Δ0; SRL1-mNeonGreen-tADH1 HIS3MX*

yMJ011	SUN4-mNG-tADH1, Δ*ssd1*	*MATa; his3Δ1; leu2Δ0; met15Δ0; ura3Δ0; YDR293c::kanMX4; SUN4-mNeonGreen-tADH1 HIS3MX*
yMJ012	SRL1-mNG-tADH1, Δ*ssd1*	*MATa; his3Δ1; leu2Δ0; met15Δ0; ura3Δ0; YDR293C::kanMX4; SRL1-mNeonGreen-tADH1 HIS3MX*
yMJ027	SUN4-mNG-tADH1, Δ*sec72*	MATa; his3Δ1; leu2Δ0; met15Δ0; ura3Δ0; YLR292C::kanMX4; SUN4-mNeonGreen-tADH1 HIS3MX
yMJ029	SRL1-mNG-tADH1, Δ*sec72*	MATa; his3Δ1; leu2Δ0; met15Δ0; ura3Δ0; YLR292C::kanMX4; SRL1-mNeonGreen-tADH1 HIS3MX
yMJ040	Sun4-mNeonGreen-tSun4, wild-type	BY4741; MATa; his3Δ1; leu2Δ0; met15Δ0; ura3Δ0; Sun4-mNeonGreen
yMJ041	Sun4-mNeonGreen-tSun4, Δ*ssd1*	BY4741; MATa; his3Δ1; leu2Δ0; met15Δ0; ura3Δ0; YDR293C::kanMX4 Sun4-mNeonGreen
yMJ044	Sun4-mNeonGreen-tSun4, Δmpt5	BY4741; MATa; his3Δ1; leu2Δ0; met15Δ0; ura3Δ0; YGL178W::kanMX4 Sun4-mNeonGreen
yMJ045	Sun4-mNeonGreen-tSun4, Δ*sec72*	BY4741; MATa; his3Δ1; leu2Δ0; met15Δ0; ura3Δ0; YLR292C::kanMX4 Sun4-mNeonGreen
yMJ050	Srl1-mNeonGreen-tSrl1, wild-type	BY4741; MATa; his3Δ1; leu2Δ0; met15Δ0; ura3Δ0; Srl1-mNeonGreen
yMJ051	Srl1-mNeonGreen -tSrl1, Δ*ssd1*	BY4741; MATa; his3Δ1; leu2Δ0; met15Δ0; ura3Δ0; YDR293C::kanMX4 Srl1-mNeonGreen
yMJ054	Srl1-mNeonGreen-tRrl1, Δ*mpt5*	BY4741; MATa; his3Δ1; leu2Δ0; met15Δ0; ura3Δ0; YGL178W::kanMX4 Srl1-mNeonGreen
yMJ055	Srl1-mNeonGreen-tSrl1, Δ*sec72*	BY4741; MATa; his3Δ1; leu2Δ0; met15Δ0; ura3Δ0; YLR292C::kanMX4 Srl1-mNeonGreen

Table 3.3. strains made for this chapter. The table shows the ID, description, and genotype of some of the strains constructed for this chapter. See chapter appendix for the full list of strains

3.2.3 Live protein microscopy

Images were acquired using Eclipse Ti Inverted epi-fluorescence microscopes (Nikon), with 60x/1.42NA and 100x/1.45NA Plan Apo Lambda D objective. Overnight cultures were grown in 5 ml of filtered SC complete media plus 2% glucose, then used for inoculation of new cultures (in SC + 2% glucose) the following morning. Cells were left to grow to mid exponential phase (OD0.4) then were spotted onto agarose pads or loaded into microfluidic devices (McDonald *et al.*, 2000; Crane *et al.*, 2014), courtesy of Dr. Ivan Clark, for live imaging. Agarose pads were placed in µ-Slide 4 Well Glass Bottom (Ibidi) to image multiple strains at once. For some of the imaging, SC + 2% glucose media at pH 6.0 was switched with SC + 2% glucose at pH 3.0 during imaging. The relevant conditions will be specified in the results section. The imaging software used for these experiments was NIS-Elements Viewer

(Nikon) or Micro-Manager software. Images were analysed using Fiji: ImageJ software.

3.2.4 Preparing Agarose pad slides

Agarose pads were prepared from 1.5% agarose medium, using filtered SC media + 2% glucose mixed with agarose powder. In sterile conditions, the agarose mixture was pipetted onto clean 18x18 mm Fisherbrand glass square coverslips (Fisher Scientific), followed by immediate placement of another clean coverslip on top of the agarose with a pair of tweezers. This ensures a flat agarose surface for spotting and imaging the cells later, so it is important to avoid creating air bubbles at this step. Agarose pads were left to dry for 30–60 minutes then cut with a razor to create pads of the appropriate size for the wells (µ-Slide 4 Well Glass Bottom). 5 µl of culture were spotted onto each pad, left to dry in the flow hood for a few seconds, then gently placed in each well with the cells facing down to the glass bottom. This set up ensures that cells are even in the field of view, and do not float out of focus during long periods of live imaging. Protocol was adapted from previous publications (Skinner *et al.*, 2013; Molino, 2020).

3.2.5 Flow cytometry

Protein levels were measured by quantifying the fluorescent intensity of the mNeonGreen tag (green fluorescent protein) using BD LSRFortessa SORP (BD Biosciences). Cells were grown overnight in SC media (2% glucose) in a 30°C shaking incubator. Cells were then diluted in fresh SC media (2% glucose) in a 96-well plate and left to grow, at 30°C in shaking incubator, for 3-4 hours before measurement. The 488 nm laser and 530/30 nm filter were used to measure mNeonGreen fluorescence, and at least 10,000 cells were counted for each sample. BD FACSDiva (version 8.0.1) software was used to gate and view the results. Data was gated for singlet cells by forward scatter width and area. Gated data contain roughly 20,000 singlet cells per sample. Fluorescence boxplots were extracted from the FITC-A channel, and plotted using the ggplot2 (version 3.5.0) geom_boxplot function in R (version 4.3.3). For each strain, two independent biological replicates were measured. The boxplots show the median of mNeonGreen fluorescence on log scale for each strain, by showing the interquartile range (25th, 50th, and 75th percentile) of fluorescence distribution within the box. The bars on either side of the box represent the smallest and largest values within 1.5 times of the interquartile range. The forward scatter area boxplots were extracted from the FSC-A measurements, and plotted using the ggplot2 (version 3.5.0) geom_boxplot function in R (version 4.3.3). The boxplots show the median of cell size for two biological replicates for each strain. These were plotted on linear scale, with the boxes showing the interquartile range and largest and smallest values as previously described.

3.3 Results

3.3.1 Strain construction to test the effect of post-transcriptional regulation elements on protein expression and localization

To examine the effect of RBPs and UTRs on cell wall protein expression and localization, I tagged target proteins with a green fluorescent protein. The use of the fluorescent tag allowed measurement of protein levels by measuring fluorescence, and the visualization of the location of the protein within the cell. Since my research investigates the effect of two different regulatory elements on cell wall proteins, it was important to design tagged-protein strains in a way that addresses each element individually and in combination (**Table 3.3**). It was also important to design these tags for the 3'UTR end, as to not alter or obstruct the 5' UTR where some of my RBPs of interest bind the targets I'm investigating. To construct the required strains for this section, I used the following design strategies.

3.3.2 Constructing strains with an altered 3' UTR and terminator region

In the first tagging strategy, I constructed strains with an altered 3' UTR region in both the wild-type and the RBP deletion backgrounds. For each construct, the repair template was added right before the stop codon within the gene's coding sequence. As previously explained (Fig. **3.2A, Fig.3.2B**), the repair template consisted of a ~40 bp homology arm to the coding sequence, a linker region followed by an mNeonGreen fluorophore, an *ADH1* terminator, a Histidine (HIS3) selection marker, and a 40~ bp homology arm to the 3' UTR. This construct design effectively alters the 3'UTR and assigns *ADH1* as the terminator region.Furthermore, by designing primers that use the linker regions within the plasmid; my strategy allows the use of my gene-specific primers with any other plasmids that have the pFA6 backbone plus a different fluorescent protein (Bähler *et al.*, 1998; Longtine *et al.*, 1998; Botman *et al.*, 2019). This allows use of different plasmids from this library, and tagging with differently coloured reporter tags, without the need for designing new primers.

These repair templates that alter the 3' UTR and terminator region were inserted in the wild-type strain BY4741, as well as RBP deletion strains**.** The combination of the altered region and deleted RBP background allowed for screening the combined effect of these regulatory elements, compared to the effect of the deleted RBP alone. While tagging in the wild-type background served to show the effect of the altered 3' UTR on expression and localization, compared to the native region in wild-type.

3.3.3 Constructing strains with a native 3' UTR and terminator region

The second design strategy aimed at achieving fluorescent tagging without altering the native 3' UTR and terminator region. To achieve this, I used CRISPR/Cas9 gRNAs to make precise cuts near the tag insertion site in the gene, and inserted the fluorescent tag before the stop codon within the coding sequence as previously shown (Fig. **3.3A, Fig.3.3B**). To ensure that the strains are comparable, the linker-mNeonGreen tag was amplified from the same plasmid I used for the other strains (Fig. **3.2A, Fig.3.3A**). This allowed me to "scarlessly" tag my proteins of interest

while keeping them under their native terminator, and without altering the 3' UTR. Through using this strategy to tag proteins in the wild-type and RBP deletion strains, I now had a set of strains that allowed testing protein expression as affected by individual RBPs. It also meant that I could now compare the effect of an altered terminator region versus a native one.

These specific strains were constructed by myself and Dr. Weronika Danecka, while co-supervising undergraduate students Ines Goncalves and Kexin Xiong on a lab project. The students' individual contributions to the lab work can be found in their theses.

3.3.4 Ssd1 deletion produces larger cell size

The tagging of Sun4 and Srl1 in the wild-type and Δ*ssd1* backgrounds was intended to elucidate the effect of Ssd1 on protein expression. The predicted model of Ssd1 mechanism is that Ssd1 acts as a translational repressor, and therefore the encoded proteins of its target mRNAs would be more abundant in an *SSD1* deletion strain. However, before delving into protein expression, the first notable result upon testing my tagged strains was related to cell size. Flow cytometry experiments conducted on Sun4 and Srl1 tagged with mNeonGreen show that cells in the Δ*ssd1* background are consistently bigger than cells in the wild-type. In flow cytometry, the forward scatter area (FSC-A) indicates the relative size of the cell, while the side scatter (SSC) indicates the granularity or the components and internal complexity of the cell. In my data, the FSC-A of two replicates for each of my strains show that Δ*ssd1* cells are bigger, regardless of the tagged protein or the 3' UTR region. Here I show one biological replicate for the tagged protein wild-type and Δ*ssd1* strains, under altered (tADH1) or native (tSun4 or tSrl1) terminators, plus one replicate each for the untagged background (**Fig. 3.4A**). The flow cytometry data shows two populations of cells, with an increased number of the second population in the wild-type compared to Δ*ssd1* strain. It is possible that these two populations represent budded cells versus unbudded/single cells in each background.

To visualize the difference in cell size between different backgrounds, I created boxplots of the FSC-A which show the interquartile range and median of cell size for two replicates of each strain (**Fig. 3.4B**). This visualization clearly shows a shift towards larger cell size in Δ*ssd1* compared to all other strains. With two biological replicates across five independent Δ*ssd1* strains, including an untagged control; these results are highly reproducible. Interestingly enough, the deletion of the translocon component Sec72 also seems to increase cell size in the tested strains.

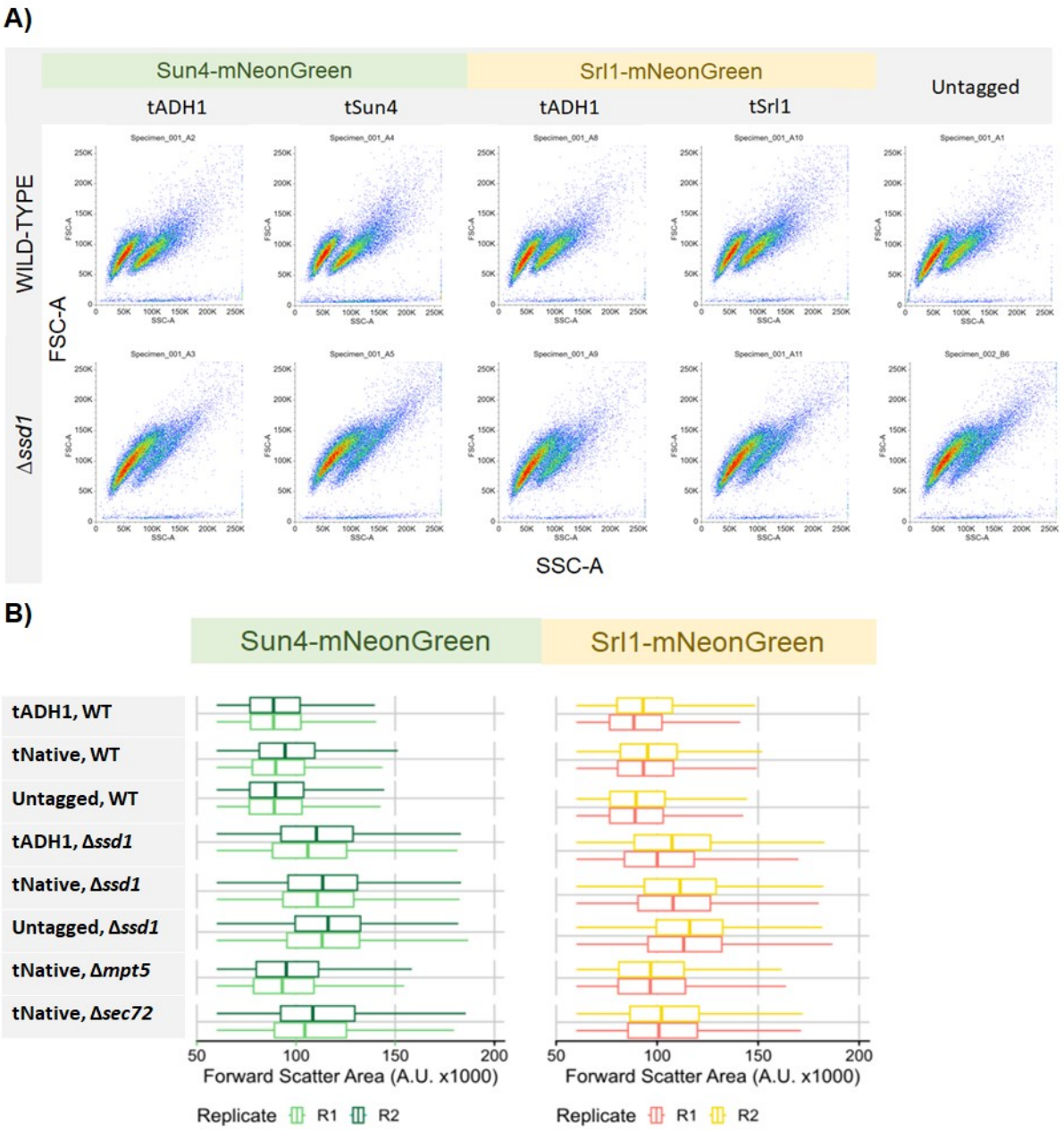

Figure 3.4. The deletion of Ssd1 leads to larger cell size. A) Flow cytometry forward scatter (FSC-A) on the Y axis against side scatter (SSC-A) on the X axis show that cells are consistently larger in Δ*ssd1* strains than the wild-type background. **B)** Box plots, generated from two biological replicates (R1, R2) for each strain, using FSC-A data show that the median (50th interquartile) cell size for Δ*ssd1* cells is bigger than that of the wild-type cells. Cells in the Δ*sec72* background are of comparable size to Δ*ssd1*, thus larger than the wild-type as well.

To confirm flow cytometry results, I conducted further analysis on microscopy images of Sun4-mNeonGreen in the wild-type and the Δ*ssd1* background. The analysis shows the size of the mother cells in each population, plotted against time points taken at 5 minute intervals (Pietsch *et al.*, 2023). Cells were left to grow to mid

exponential phase (OD0.4), and were then loaded into microfluidic devices (McDonald *et al.*, 2000; Crane *et al.*, 2014), courtesy of Dr. Ivan Clark, for live imaging. The microfluidic devices capture and hold the mother in place, enabling a measurement of the mean brightness of all the pixels within mother cells in a strain background. In **Fig. 3.5.** the mean of fluorescence values across the population of mothers is shown on the Y axis, across time points taken at 5-minute intervals. The X axis indicates the time point at which an image was taken (multiply by 5 to get the time in minutes). In agreement with flow cytometry results; this analysis (Fig. **3.5**) shows that mother cells are consistently larger in size in Δ*ssd1* than the wild-type,

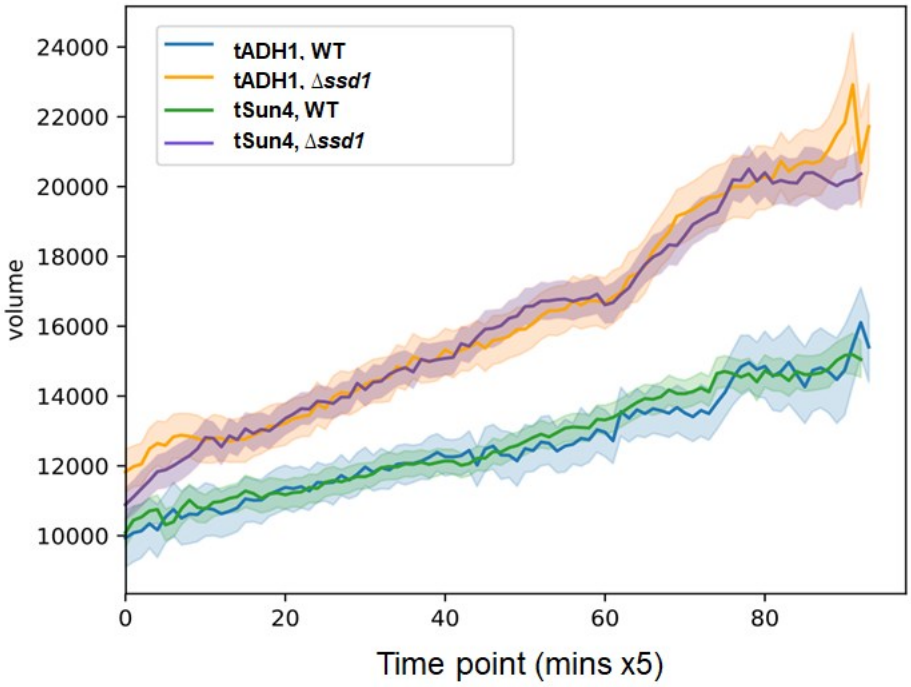

Figure 3.5. Analysis of mother cells in the wild-type and Δ*ssd1* confirms larger cells upon Ssd1 deletion. Analysis of Sun4-mNeonGreen microscopy images shows that the mother cell size is consistently larger in the *SSD1* deletion backgrounds compared to wild-type backgrounds. The terminator regions tADH1 and tSun4 do not affect cell size in either background. The volume unit for the Y axis is cubic pixels, and pixel size is 0.182 x 0.182, so multiplication by 0.182^3 (0.006) gives the size in μm^3 . The X axis indicates the time point at which a reading was taken (multiply by 5 to get the time in minutes).

under the native Sun4 terminator and an altered *ADH1* terminator.

Several published studies reported that cells lacking *ssd1* have cell wall integrity defects and are vulnerable to cell wall stressors such as CFW (Kaeberlein and Guarente, 2002; Bayne *et al.*, 2022). Thus, this phenotype of bigger cell size brings up the question of the relationship between cell size and cell wall integrity. Furthermore, it touches on the intriguing relationship between cell size and the cell cycle, where smaller cells spend a longer duration in G1 phase (Hartwell *et al.*, 1974;

Hartwell and Unger, 1977). This is especially interesting in light of Ssd1 binding cell cyclins mRNA such as *CLN2*, and other mRNAs involved in cell cycle control (Hogan *et al.*, 2008; Jansen *et al.*, 2009). This relationship is explored in detail in 4.1.1.

3.3.5 Ssd1 deletion leads to over-production of proteins encoded by its target mRNAs

The Ssd1 homolog Sts5 acts as translational repressor in *S. pombe* of mRNAs that encode proteins involved in cell growth and cytokinesis (Nuñez *et al.*, 2016). Previous studies conducted in *S. cerevisiae* also hypothesized that Ssd1 acts as a translational repressor on its target mRNAs (Jansen *et al.*, 2009). To test this hypothesis, I visualised fluorescently tagged Ssd1 target proteins, and quantified their fluorescence to measure protein expression.

To observe the individual effect of *SSD1* deletion, I start by showing Sun4 tagged with mNeonGreen, under the native Sun4 3' UTR/terminator region (tSun4) in the wild-type and Δ*ssd1* background. Samples were taken from cell cultures grown to mid exponential phase from overnights, and loaded onto microfluidic devices (SC + 2% glucose, pH 6.0) as previously described in 3.2.3. These live cell cultures were recorded at 5 minute intervals for the duration of ~3 cell cycles, which is around 5 hours.

Live microscopy shows higher fluorescence for the cell wall protein Sun4p in the Δ*ssd1* strain compared to the wild-type (**Fig. 3.6A**). Under the same acquisition and display settings, my results show that the protein is more abundant in the mother cells of Δ*ssd1* compared to the wild-type cells. Using ImageJ (Fiji) I analysed several fields of view from each sample, and found that the max pixel values were higher in Δ*ssd1* images than in the wild-type; indicating higher florescence and thus higher expression in the deletion background as shown in the histograms in **Fig. 3.6B**. Analysis of these images using ALIBY (Analyser of Live-cell Imaging for Budding Yeast) (González and Fernando, 2023) confirms higher fluorescence in the Δ*ssd1* background (**Fig. 3.6C**). The analysis measures the mean brightness of all the pixels within mother cells in a strain background, then plots the mean of fluorescence values across the population (Y axis), across time points taken at 5-minute intervals (X axis).

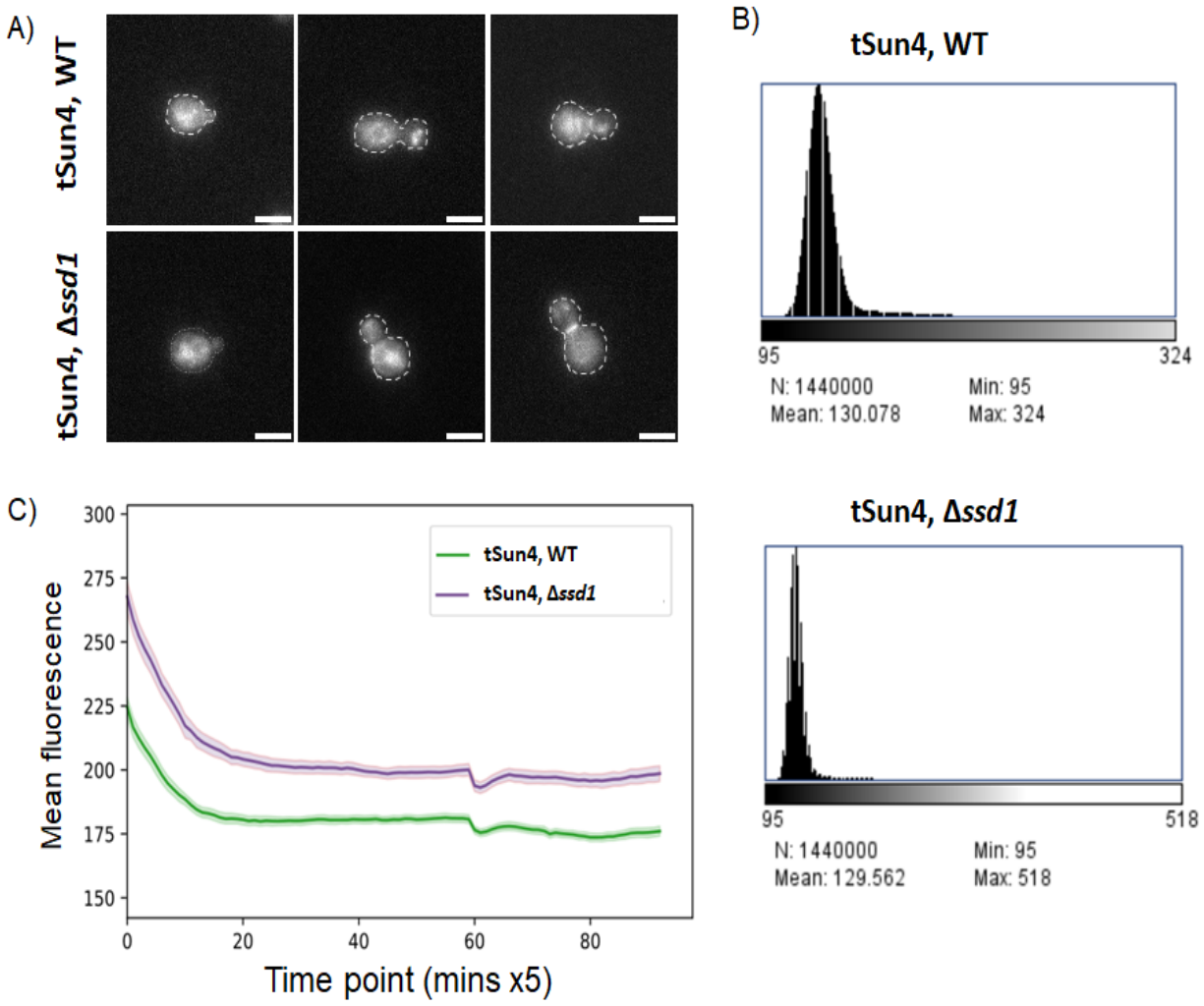

Figure 3.6. Sun4 protein is overexpressed upon deletion of Ssd1. A) Microscopy images of Sun4 tagged under the native terminator (tSun4) in the wild-type and Δ*ssd1* show higher fluorescence values as shown by **B)** histograms generated from these images using ImageJ. Scale bar is 5μm. **C)** Analysis of mean fluorescence values in mother cells (Y axis), across the population of each strain, display higher fluorescence and thus more protein production in the Δ*ssd1* background. The X axis displays the time point at which an image was taken (multiply by 5 for time in minutes).

To further check these results, I used flow cytometry to measure the fluorescence of the mNeonGreen tagged proteins in each strain background. Each flow cytometry experiment consisted of two biological replicates of the tagged protein in the wild-type and Δ*ssd1,* as well as an untagged wild-type and Δ*ssd1* strain as negative controls. In agreement with previous results, flow cytometry analysis confirmed that Sun4 under the native terminator (tSun4) is more fluorescent, and therefore more abundant, in Δ*ssd1* (**Fig. 3.7)**. Likewise, flow cytometry of Srl1 tagged with mNeonGreen under the native Srl1 terminator (tSrl1) also shows higher expression in the Δ*ssd1* background (**Fig. 3.7**). These results suggest that Ssd1 might be acting as a translational repressor of its target mRNAs. However, the bigger cell size of Δ*ssd1* clearly skews the result slightly towards “more fluorescence” as showed by

the untagged controls in this figure. For my results, it is most likely that the flow cytometry data is in fact representative of higher fluorescence, rather than an artefact of cell size. This is due to my microscopy results showing higher fluorescence and protein concentration in the same tagged strains, both visually and through quantification of fluorescence (using previously mentioned software). Still, the cell size variation is an issue that should be accounted for in any future work testing tagged protein expression in Δ*ssd1*.

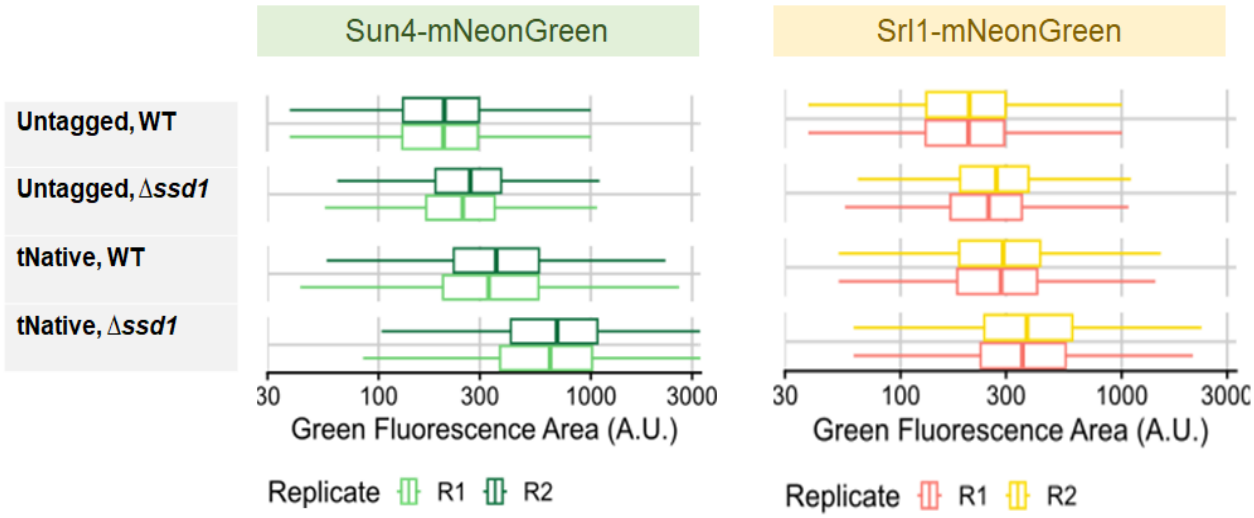

Figure 3.7. Flow cytometry results show higher fluorescence in the Δ*ssd1* background under the gene's native terminator. Box plots of flow cytometry results from the FITC-A channel show higher fluorescence in the Δ*ssd1* background for both Sun4 and Srl1 under their respective native terminators. The results show two biological replicates for each strain.

3.3.6 Sun4 localizes to the bud neck which is consistent with its role in septation

In addition to the informative results on protein expression, the live microscopy data sets provided valuable information on protein localization. Earlier in this thesis, I questioned whether Ssd1 is involved in localization of its target proteins. My results so far indicated that Ssd1 might be acting as a translational repressor, and so the next step was to investigate if *SSD1* deletion leads to mis-localization of Sun4 and Srl1.

I tested the localization of Sun4 in the wild-type and Δ*ssd1* strains using live microscopy. Cells were loaded into microfluidic devices as previously described and imaged at 5 minute intervals in SC media (2% glucose, pH 6.0). The resulting microscopy images in **Fig. 3.8A** clearly showed a pattern of Sun4-mNeonGreen localizing to the bud neck in larger budding cells. I estimate that these cells are in late G2, however future experiments should include cell markers and DAPI staining to pinpoint the cell cycle phase. Localization to the bud neck can be seen in the wild-type and Δ*ssd1* background, under the altered (tADH1) and native (tSun4) terminators alike (Fig. **3.8A**). This is consistent with the role of Sun4 in septation and separation of the daughter from the mother cell (Mouassite *et al.*, 2000). As for the other cells, Sun4 seems to localize to the cytoplasm in smaller budding cells, with some of the protein appearing near the apex of the developing bud. For these cells, I found it harder to define whether the wild-type and Δ*ssd1* were showing similar localization. In Δ*ssd1*, there seems to be masses or "blobs" of the protein in the cytoplasm, compared to what looks like ER localization in the wild-type (Fig. **3.9**). It is difficult to say whether these are in fact aggregates within the cytoplasm, or simply an overproduction of the protein obscuring its localization. This is another point in favour of future work testing the co-localization of this protein with known cell markers.

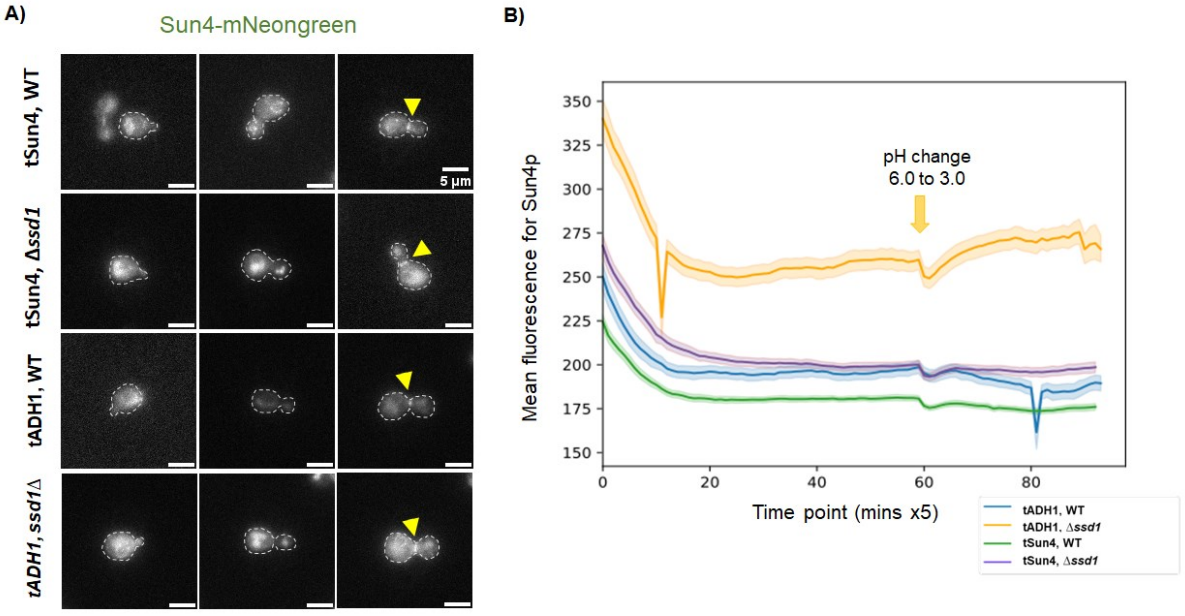

Figure 3.8. Sun4 localizes to the bud neck and the cell surface. A) Live microscopy images show Sun4 localizing to the bud neck in budding cells (yellow arrows) in both the wild-type and Δ*ssd1* strains. Cytoplasmic localization seems to be at the ER in tSun4 wild-type strain, while the Δ*ssd1* strain has foci of protein in the cytoplasm. **B)** Microscopy analysis figure showing the mean fluorescence of Sun4-mNeonGreen in the wild-type and Δ*ssd1* background, under native (tSun4) and altered (tADH1) terminators. There is an obvious dip in fluorescence at the point of switching media from pH 6.0 to pH 3.0.

The images shown in **Fig.3.8A** were acquired in SC media at pH 6.0. This is important to note because mNeonGreen is less fluorescent if exposed to acidic pH (Tutol, Kam and Dodani, 2019). From the microscopy experiments I conducted across my research project, it seemed that image quality was lower in unbuffered SC media. Such images displayed less fluorescence and were hard to decipher, despite trialling different microscopes and live imaging setups to acquire them. Therefore, Dr Ivan Clark and I imaged the above cells for 5 hours in pH 6.0, then switched the media to SC pH 3.0 while live imaging. The rationale behind this experiment was to test if switching the media from pH 6.0 to pH 3.0 affects mNeonGreen fluorescence. As shown in **Fig.3.8B**, this switch indeed caused a dip in fluorescence for all four tagged-Sun4 strains. This implies that Sun4, and consequently mNeonGreen, might have been exposed to the acidic media at the cell surface. This might indicate cell surface localization for Sun4, however; more experiments are needed to confirm this

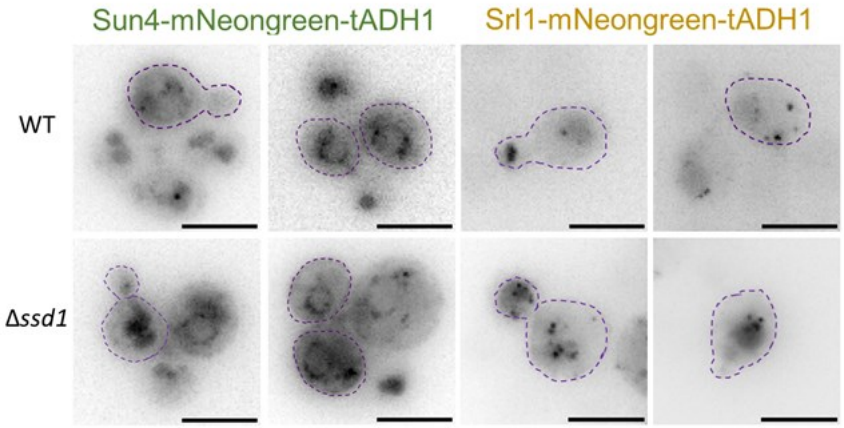

Figure 3.9. Srl1 localizes to the apex of the budding daughter. Right: Srl1 localizes to the apex of the budding daughter in both wild-type and Δ*ssd1* cells. In Δ*ssd1*, Srl1 can be seen in the cytoplasm of cells where the bud is about to emerge. Left: Live microscopy images show Sun4 localizing to the ER in unbudded wild-type cells. This localization can also be seen in unbudded Δ*ssd1* cells, whereas the budding cells have foci of protein in the cytoplasm. Both Sun4 and Srl1 protein are more abundant in the Δ*ssd1* background. These images were acquired in unbuffered SC+2% glucose media. The scale bar is 5 μm.

localization.

For the cell wall protein Srl1, I was only able to image the tagged protein with an altered terminator and in unbuffered SC media due to time constraints. This imaging was done by spotting cell cultures onto the previously described agarose pads. In the wild-type, under the *ADH1* terminator, microscopy images display localization to the periphery of the growing bud (**Fig. 3.9**). This localization can also be seen in the Δ*ssd1* background in cells of similar size. However, the localization of Srl1 should be imaged under the native terminator and at pH 6.0 to confirm the localization pattern shown in these experiments, and to test whether Srl1 is also a cell surface protein. Overall, combined with the Sun4 results, these results indicates that Ssd1 is unlikely to be involved in the localization of its target mRNA's encoded proteins. However,

this is by no means a definite conclusion without the abovementioned additional experiments to elucidate native localization patterns.

3.3.7 Altering the native 3' UTR and terminator region leads to increased Sun4 protein expression

The following set of experiments aimed to observe the effect of an altered terminator region on protein expression. To investigate the role of this region, I conducted live microscopy as previously described, to test Sun4 tagged with mNeonGreen under the ADH1 terminator in wild-type and Δ*ssd1*. Initial results reported on the combined effect of the deletion of Ssd1 and the altered terminator region. In agreement with previous results, there was higher fluorescence and more protein abundance in the *SSD1* deletion background compared to the wild-type **Fig. 3.9**.

As for the individual role of the terminator region; ALIBY analysis shown in **Fig. 3.8B**, clearly displays the highest fluorescence for Sun4-mNeonGreen-tADH1 in the Δ*ssd1* background. In the Sun4-mNeonGreen-tADH1 in the Δ*ssd1* background: Sun4-mNeonGreen-tADH1 shows higher fluorescence than Sun4-mNeonGreen under the native terminator tSun4. Similarly, Sun4-mNeonGreen-tADH1 in the wild-type has higher fluorescence mean values than Sun4-mNeonGreen-tSun4 in the same background.

To further investigate the independent role of the terminator, I collected flow cytometry data and compared protein expression between altered and native terminator regions within the same background strain. In the wild-type, data analysis shows that mNeonGreen-tagged Sun4 exhibited higher fluorescence under the ADH1 terminator than its native terminator (tSun4) in the wild-type strain (Fig. **3.10**)**.** This is also the case when comparing the fluorescence of Sun4-mNeonGreen under the native and altered terminator in Δ*ssd1* (**Fig**. **3.10)**. Thus, confirming that an altered terminator region also altered Sun4 protein expression. The increased expression is likely the result of hindering the binding of a *SUN4* post-transcriptional regulator upon altering the 3' UTR. For Srl1, however, flow cytometry results showed that an altered terminator region (t*ADH1*) did not affect protein expression. Unlike the Sun4 result, Srl1 tagged with mNeonGreen exhibits very similar expression levels under the *ADH1* terminator and native Srl1 terminator region (**Fig**. **3.10**). This can be seen when comparing tADH1 and tSrl1 in the wild-type or the Δ*ssd1* strain.

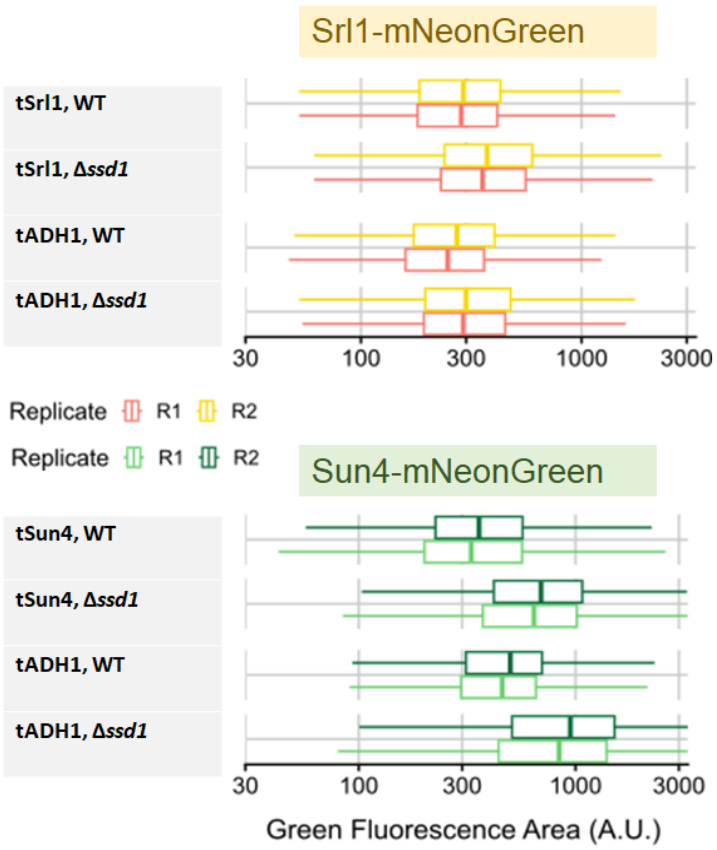

Figure 3.10. Sun4 displays higher expression under an altered terminator. Box plots of flow cytometry data (FITC-A) show increased protein expression for Sun4 under the ADH1 terminator both in the wild-type and Δ*ssd1.* Srl1 shows similar expression under its native terminator and tADH1 in both strains.

3.3.8 Deletion of the translocon component Sec72 leads to cytoplasmic aggregation of Sun4

Published studies show that deletion of Sec72 blocks secretion of some proteins encoded by Ssd1 targeted mRNAs and leads to mis-localized protein aggregates in the cytoplasm (Ast, Cohen and Schuldiner, 2013). Therefore, I tagged and imaged Sun4 in the Δ*sec72* background, with an ADH1 terminator to replicate these results. Similar to previously published data, Sun4-mNeonGreen showed a cytoplasmic aggregation phenotype upon Sec72 deletion (**Fig. 3.11A**). Next, I tagged both Srl1 and Sun4 with mNeonGreen under their respective native terminators. Flow cytometry measurement of fluorescence in these strains show higher protein expression in the Δ*sec72* background (**Fig**. **3.11B**) compared to the wild-type. Correlating this result with the known cytoplasmic aggregation pattern for Sun4 in this background, this suggests that the “higher fluorescence” might be indicative of these bright cytoplasmic aggregates. Flow cytometry results of tagged Srl1 in Δ*sec72* show an increase in fluorescence. This suggests that Srl1 might also be aggregating in the

cytoplasm upon Sec72 deletion, and utilising the translocation pathway facilitated by Sec72. This is a reasonable assumption to make in light of Srl1 having a signal peptide sequence in its N'-terminal. However, it is also worth noting that cell size plots shown earlier in this chapter showed bigger cell size for the Δ*sec72* background compared to the wild-type. Therefore, the increased fluorescence could be a result of increased cell size. Unfortunately, I was unable to image the Srl1-mNeonGreen Δ*sec72* strains I constructed due to time constraints, but this is something that can be pursued in future work to investigate whether this protein aggregates upon Sec72 deletion.

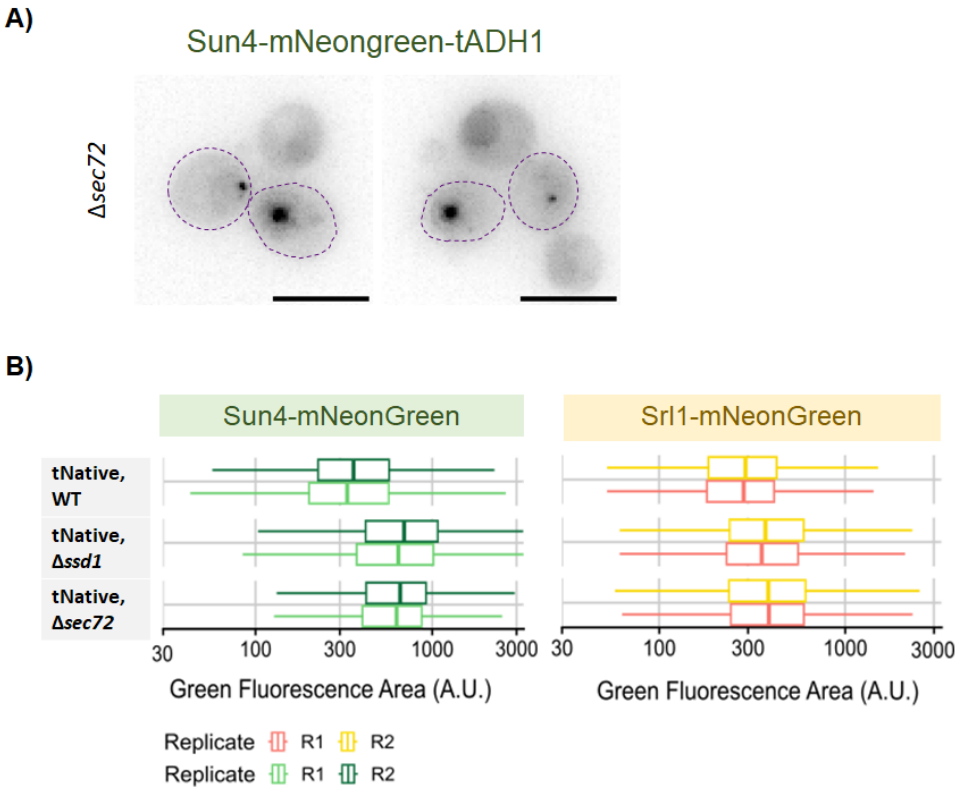

Figure 3.11. Flow cytometry data shows more fluorescence for Sun4 and Srl1 upon deletion of Sec72. A) Microscopy of Sun4-mNeonGreen under an altered terminator shows cytoplasmic aggregation in the Δ*sec72* background. Scale bar is 5 μm. **B)** Flow cytometry results (FITC-A) show higher fluorescence in Δ*sec72*, compared to the wild-type strain. Fluorescence in Δ*sec72* is comparable to Δ*ssd1*.

3.3.9 Deletion of the RBP Mpt5 leads to increased Sun4 expression

As previously mentioned, Ssd1 and Mpt5 act in parallel pathways, and therefore I wanted to test the individual effect of each on my proteins of interest. Furthermore, Mpt5 binds both *SRL1* and *SUN4* mRNA at the 3'UTR, and so it was intriguing to investigate if Mpt5 affects expression for either protein. Therefore, I measured fluorescence of the tagged Sun4 and Srl1 proteins in the Δ*mpt5* background.

Flow cytometry results show that Srl1-mNeonGreen, under the native terminator tSrl1, exhibits similar fluorescence in the Δ*mpt5* background compared to the wild-type background (**Fig. 3.12**). Whereas Sun4-mNeonGreen, under the native terminator tSun4, displays higher expression in Δ*mpt5* than the in the wild-type (Fig. **3.12**)**.** Thus, indicating higher Sun4 protein expression upon deletion of Mpt5. This suggests that Mpt5 might be strongly involved in the regulation of Sun4, either through translational repression or regulating mRNA turnover.

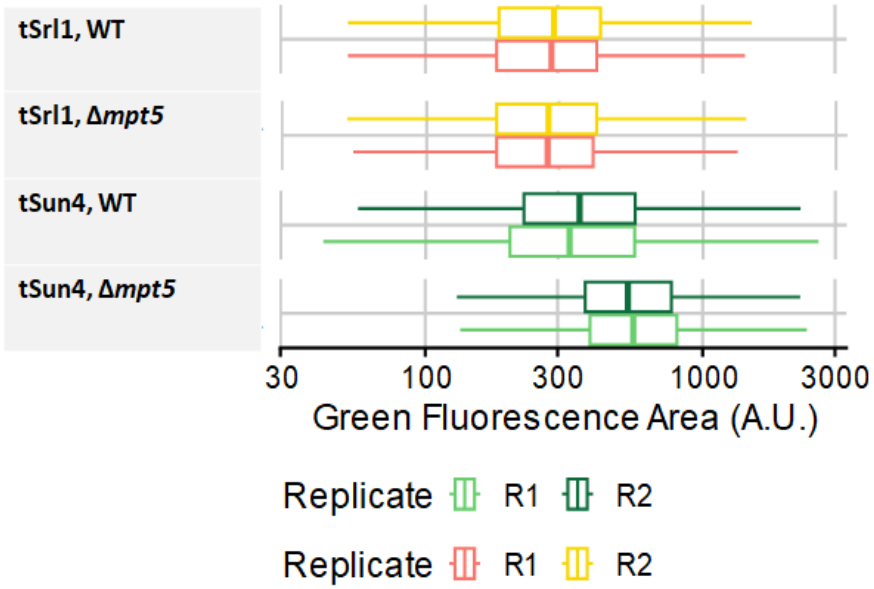

Figure 3.12. Sun4 displays higher fluorescence in the Δ*mpt5* background. Flow cytometry results show increased fluorescence for Sun4 (bottom; green box plots) under its native terminator, compared to the wild-type background. Whereas Srl1 (top; yellow box plots) is expressed similarly in the wild-type and Δ*mpt5* background.

3.4 Discussion

Previous studies show cell wall sensitivity phenotypes upon deletion of Ssd1 in *S. cerevisiae* or the deletion of its homologs in other species (Kaeberlein and Guarente, 2002; Healey *et al.*, 2020). This is not surprising considering that Ssd1 binds mRNAs encoding cell wall proteins, such as Srl1, Sun4, and Scw4, and cell cycle control proteins, including the cell cyclin CLN2 (Hogan *et al.*, 2008; Jansen *et al.*, 2009; Hose *et al.*, 2020; Bayne *et al.*, 2022). *S. cerevisiae*'s Ssd1 and its homolog in *S. pombe* were reported to act as translational repressors of these mRNAs involved in cell growth and cytokinesis (Jansen *et al.*, 2009; Nuñez *et al.*, 2016), however the precise mechanism by which Ssd1 acts is still unknown. In this chapter, I set out to examine if the role of Ssd1 extends to the localization of its target proteins, or if Ssd1 purely operates as a translational repressor.

3.4.1 The increased cell size in ∆*ssd1* might affect the cell cycle

My results show that the ∆*ssd1* background produces larger cells than the wild-type. Flow cytometry results conducted on tagged proteins in the ∆*ssd1* background consistently show larger budding yeast cells than in the wild-type. The larger cell size can also be seen in the untagged ∆*ssd1* strain, which confirms that the change in size is not an artefact of protein tagging. These results are replicated through analysis of microscopy images of the same strains, where analysing the mother cell size shows bigger cells in ∆*ssd1*. This phenotype of larger cells is particularly intriguing in light of the relationship between cell size and the cell cycle.

Smaller cells in *S. cerevisiae* delay the Start transition in late G1 (Hartwell *et al.*, 1974; Hartwell and Unger, 1977). Start is the checkpoint in the cell cycle where the cell fully commits to budding, or the point of "no return", meaning that the cell cycle goes forward from this point, regardless of environmental or nutritional changes following Start. The delay of Start in smaller cells indicates that initiation of the cell cycle is dependent on cell size. However, studies addressing molecular noise and cell size control show that cell size isn't the only factor affecting cell cycle initiation (Talia *et al.*, 2007). Previous studies showed that the timing of G1 in *S. cerevisiae* is variable regardless of cell size (Nurse, 1980; Lord and Wheals, 1981). To test the relationship, Talia *et al.* (2007) conducted experiments where they generate and control cell cycle variability. This led them to find that there are two modules controlling cell cycle initiation. The study reports that G1 phase is regulated through two independent modules; a cell size sensing module, and a subsequent size-independent module. The size-independent module is dependent on the (presumably molecular) noise, leading to variability in the duration of G1 in both mothers and daughters. However, they also find that size control accounts for about 30–40% of overall G1 variability in daughters. This suggests that the size-dependent cell cycle initiation is more relevant to budding daughters. It is worth noting that Talia et al. divide the G1 phase into two steps, step one "T1" marks the period between cytokinesis and the exit of the transcriptional repressor Whi5, while "T2" marks the period between Whi5 nuclear exit and budding. Data from this study show that G1

size control is restricted to T1, which is the period of Whi5 nuclear residence. Whereas T2, following Whi5 exit, is independent of cell size, and similar in mothers and daughters (Talia *et al.*, 2007). This suggests that if *SSD1* deletion was in fact causing cells to initiate cell cycle unprepared, then we need to measure the size of buds at birth and compare them in the wild-type versus deletion strains. And, in context of overall larger deltaSsd1 cells, it brings up the question on whether the deletion of Ssd1 "tricks" the daughter cells into shortening their G1 phase -thus impacting G1 duration and regulation. It brings up the question of which *SSD1* deletion-related phenotype might lead to the other, and if the two phenotypes are in fact related. Future experiments could utilize cell wall integrity assays to investigate if the cells are indeed bigger under these stress conditions. Following such experiments, the questions regarding cell size and a weakened cell wall could be pursued; do cells become bigger due to a weakened cell wall, or is the cell wall weakened as a result of bigger cells, or are the two the result of the cell going into this all-or-nothing state unprepared?

3.4.2 *SSD1* deletion leads to protein overproduction which is consistent with its role as a translational repressor

Talia *et al*. also factor in "molecular noise" in their study, and this suggests that protein overexpression might be worth considering here, but before addressing that, we must look at the Ssd1 target CLN2. Studies show that positive feedback by CLN1 and CLN2 for SBF/MBF dependent transcription ensures the cell's commitment to the cell cycle (Talia *et al.*, 2007; Skotheim *et al.*, 2008). Talia *et al.* report that increasing CLN2 gene dosage modestly decreases T2, meaning that it decreases the time to budding. Ohyama *et al.* (2010) show that there are at least two types of CLN2 mRNA, and that a minor population (approximately 20% after heat shock) is targeted and stabilized by Ssd1. This does not imply that there is an overproduction of Cln2 without Ssd1, however, the study posits that Ssd1 might be binding a subpopulation of CLN2 mRNA and escorting it to be translated at the bud cortex during bud emergence. They propose that Ssd1 might be working in analogous pathway to Whi3p, an RBP that binds G1 cyclins. Whi3p was proposed to bind CLN2 mRNA and facilitate apical cell growth at the bud apex (Colomina *et al.*, 2008, 2009). Intriguingly, two studies in later years detect physical interactions between SSD1 and WHI3 (Holmes *et al.*, 2013; Bayne *et al.*, 2022). Furthermore, although previous studies show that Ssd1 is not involved in cell cycle progression under nonstress conditions (Ohyama, Kasahara and Kokubo, 2010), they do not seem to look into or address the effect of Ssd1 on cell size. This suggests that future studies should further examine the regulation of CLN2 by Ssd1, and how Ssd1 might be acting in coordination with other RBPs involved in cell cycle regulation such as Whi3.

Cell size sensing and cell cycle initiation takes cell content into account. My results are suggestive that *SSD1* deletion leads to overproduction of the cell wall proteins Sun4 and Srl1. The increased fluorescence in Δ*ssd1* can be seen by eye in the microscopy images I corrected, and is seen clearly in the analysis performed on these images. Flow cytometry data also shows increased fluorescence; however, these results need interrogating to separate the effect of increased cell size from

increased fluorescence. At this point it is necessary to note the limitations of using fluorescence microscopy to estimate protein levels in wild-type and mutant strains (Markham and Conchello, 2001; Hickey *et al.*, 2022). Previous studies show that the large size of fluorescent proteins could perturb the normal functions of proteins (Stadler *et al.*, 2013), and that overexpression of fluorescent proteins can lead to the formation of aggregates (Zacharias *et al.*, 2002, p. 200; Cranfill *et al.*, 2016). The use of fluorescent proteins leads to high background fluorescence, and issues such as photobleaching; which is light-induced degradation of fluorophores leading to a gradual decrease in fluorescence intensity might also arise (Magidson and Khodjakov, 2013). Another limitation with using fluorescent proteins for quantification is fluorescence intermittency (also known as blinking), where the fluorophore stops emitting light under continuous excitation (Dickson *et al.*, 1997; Frantsuzov *et al.*, 2008). These issues could impact the robustness of the imaged fluorescence, and therefore impact the interpretation of protein quantity, distribution, and function. Furthermore, due to time constraints I was unable to perform a western blot to test that the fluorescent tag is not getting cleaved from the protein. If such cleavage occurred, it would also lead to misinterpretation of protein abundance and localization. Future experiments should address these limitations, however, the microscopy results I have and the model of Ssd1 operating as a translational repressor seem in favour of increased fluorescence being a true result rather than an artefact of cell size. In terms of the cell cycle and molecular noise; protein overproduction in ∆*ssd1* cells, combined with weakened cell walls and bigger cells, only leads me to more questions. Is it possible that an increase in cell content and molecular noise upon deletion of Ssd1 contributes to a shortened G1 phase, leading to pre-mature budding in the mother cells? The answer to this question could be addressed in comparing budding time between the wild-type and ∆*ssd1* strains (future work).

Another hypothesis arising from my data is that the weakened cell wall is a result of protein burden. Protein overexpression can cause growth defects, which are known as the protein burden, and can deplete the cell's limited resources for other protein production (Eguchi *et al.*, 2010). Ssd1 binds to up to 150 different mRNAs (Jansen *et al.*, 2009), and therefore its ensuing phenotypes of cell wall defect could be attributed to the overexpression of proteins draining the cell’s resources. The other possibility is that Ssd1 is involved in delivering its untranslated target mRNAs to the correct location for polarized translation. In this scenario, the defects could be attributed to Ssd1 contributing to localized protein translation, where *SSD1* deletion compromises this process. Further experiments on mRNA localization and the interactions between Ssd1 and other RBPs could clarify such a mechanism if it exists. This is chapter 3.

3.4.3 Sun4 localizes to the bud neck and to the cell surface in budding yeast

My results show that Sun4 localizes to the bud neck in both the wild-type and the ∆*ssd1* strain in large budding cells (possibly late G2 and M phase). This is consistent with previously published Sun4 localization patterns (Kuznetsov *et al.*, 2013) and the role of Sun4 in cell septation (Mouassite *et al.*, 2000). Although I find no immediately

clear evidence of mis-localization with Δ*ssd1*, it is still unclear if some of the proteins seen in my microscopy are in the cytoplasm or on the cell surface. In my results, the use of pH as a reporter of cell surface localization shows that Sun4 is localizing to the cell surface of budding yeast cells. However, the pH media switch happens all at once for the population. Meaning that there is no way to determine from my existing data if the protein is at the cell surface at some points of the cell cycle, but not others. To test this, future experiments might need to synchronise the cells, or isolate cells from pH 6.0 at certain stages of the cell cycle, and expose them to pH 3.0 media while live imaging. This would clarify how mNeonGreen fluorescence at these stages is affected by the pH switch, thus clarifying whether the protein is intracellular or on the cell surface.

Furthermore, I find that the localization in smaller budding cells (possibly early G2) is harder to decipher between the WT and Δ*ssd1* background. In the wild-type cells, I see Sun4 in the developing bud near the bud tip, and in the cytoplasm of the mother possibly in the ER. In Δ*ssd1*, I see the protein in the bud near the tip, although it looks more congealed together, while in the mother cell it is more concentrated in foci. It is hard to tell if this is a result of protein overproduction leading to a higher concentration of the protein obscuring the ER. Therefore, further examination is necessary to elucidate if there are multiple populations of this protein moving at different points of the cell cycle. It is also important to test the co-localization of Sun4 with cell markers. These experiments will be addressed in the future work section.

Meanwhile, Srl1 seems to localize near the tip of the growing bud in budding cells in both wild-type and Δ*ssd1* strains. While smaller cells show cytoplasmic Srl1 localization in both backgrounds. However, as previously noted, imaging of Srl1 in this thesis was done in unbuffered SC which is acidic. Previous studies identified Srl1 as an extracellular protein (Terashima *et al.*, 2002). Therefore, future experiments should test Srl1-mNeonGreen under pH 6.0 and pH 3.0 at different points of the cell cycle, to determine the point of cell surface localization.

3.4.4 Deletion of the RBP Mpt5 increases Sun4 expression

My results show that the deletion of the RBP Mpt5 causes increased fluorescence, and thus increased expression, of the protein Sun4. Whereas, Srl1 levels seem unaffected by Mpt5 deletion. We know that Mpt5/Puf5 binds both SRL1 and SUN4 transcript mRNAs, therefore it is acting either as a second translational repressor for both mRNAs or is acting to enhance their decay (Wickens *et al.*, 2002). Previous studies show that Mpt5 has two binding sites in the *SUN4* 3'UTR, and one binding site in *SRL1* 3'UTR. These binding sites, combined with the flow cytometry results, suggests that Mpt5 plays a bigger role in repressing *SUN4* translation than it does for *SRL1*. The role of Mpt5 in regulating Sun4 translation might be connected to the different points of the cell cycle where each mRNA is produced and transported for localization. I have previously described the *ASH1* transport machinery utilizing Puf6 and Khd1 as translational repressors to be released upon the mRNA reaching its destination. *ASH1* mRNAs has a very specialised role which requires complete repression of translation until the mRNA reaches the daughter cell. Although *SRL1*

and *SUN4* mRNA do not have a role as specialised as *ASH1* mRNA, thus they do not need as stringent a repression; both of the Srl1 and Sun4 proteins act in cell continuity and integrity through contributing to bud septation and cell wall integrity. Therefore, we can assume that these proteins are needed at specific points of the cell cycle. Furthermore, both of the mRNA transcripts are bound by She2 and localize to the growing bud or near the bud. Therefore, I propose that there might be different populations of these proteins translated at different points in the cell cycle to serve the cell's needs at the time. It is possible that Mpt5 and Ssd1 repress the translation of these mRNAs in coordination and at different times, or that Ssd1 represses translation at some point while Mpt5 impacts mRNA turnover upon release of Ssd1 by phosphorylation.

3.4.5 Sec72 is involved in protein translocation for Sun4 and possibly Srl1

Both of my proteins of interest seem to be targets of the Sec72 translocation pathway. In my flow cytometry results, Sec72 deletion seems to increase Srl1p expression. The increased fluorescence of Srl1 in ∆*sec72* flow cytometry could be indicative of aggregates in the cytoplasm, similar to what we see of Sun4 increased fluorescence in ∆*sec72*. Although I could not image Srl1 in the ∆*sec72* due to time constraints, published studies show that Srl1 co-localizes with the protein conducting channel Sec61 on the ER membrane (Toikkanen *et al.*, 2003; Cohen, Aviram and Schuldiner, 2023). Combined with the higher fluorescence of Srl1 in ∆*sec72* background, and other Ssd1 target proteins aggregating in the cytoplasm in ∆*sec72;* it is reasonable to assume that Srl1 might be similarly aggregating. This indicates that several of the Ssd1 targets are utilising the SRP-independent translocation pathway. It also implies that Ssd1 and Mpt5, in addition to other RBPs, might act as part of the transport machinery to regulate translation while a population of mRNAs is shuttled to the ER to be translated and used for biosynthesis. While another population of mRNA is taken to the bud neck and budding daughter to be translated at the septum (Sun4) or in the growing bud to contribute to cell wall biogenesis (Srl1).

3.4.6 Altering the 3' UTR alters protein expression for Sun4

Replacement of the 3' UTR leads to increased expression of Sun4 but not Srl1. Flow cytometry data shows higher fluorescence for Sun4-mNeonGreen-tADH1 compared to Sun4-mNeonGreen under its native terminator, while Srl1-mNeonGreen is the same in both strains. This is interesting because Sun4 and Srl1 encoding mRNAs are both targets for Puf2 (Porter *et al.*, 2015). I searched for the Puf2 binding motif UAAUNNNUAAU (Yosefzon *et al.*, 2011) for each gene using Snapgene, and found that Srl1 has this binding motif within its coding sequence near the 3' end, whereas Sun4 has the motif in its actual 3' UTR (note that the motif is off by a single mismatch for both). This could mean that Srl1 is still getting bound and translationally regulated by Puf2 regardless of the altered 3' UTR, however, more experiments are needed to test that hypothesis. As for Sun4, the binding site is lost, hence; its overproduction with an ADH1 terminator and an altered 3' region. These results further prove the importance of an altered 3' UTR when investigating protein expression. As for

localization, I see no clear difference in Sun4 localization to the bud neck between the native and altered 3' UTR strains. However, it is worth noting that this is only the case for localization in larger budding cells with a clear band around the neck.

4 Testing the effect of RNA-binding proteins of interest on the localization of the mRNAs *SUN4* and *SRL1*

4.1 Introduction

Cells grow and divide while maintaining their spatial organisation, by controlling the subcellular localisation of their RNA and proteins. The localization of RNA enables the cell to regulate the translation of mRNAs at specific locations within subcellular compartments, thus preventing ectopic protein translation and sorting proteins to distinct regions where they play specialized roles. Due to this level of regulation in eukaryotes, the next step following the investigation into localization of the Sun4 and Srl1 was to examine the localization of the mRNAs encoding them. My aim was to identify the localization patterns of mRNAs of interest in the wild-type, and then test which RBPs, if any, contribute to the transport machinery of these mRNAs.

As previously discussed in this thesis, RNA-binding proteins play a role in gene regulation through involvement in the translation, stability, and localization of mRNAs. RBPs such as Ssd1 bind target mRNAs at a region with a binding motif. However, it is unclear whether such binding is merely for post-transcriptional regulation through translational repression, or if these RBPs also play a role in the transport machinery for mRNAs.

Some examples of RNA-binding proteins playing roles in mRNA transport are the previously mentioned Puf6, Khd1, and She2 proteins acting in *ASH1* mRNA shuttling. While Puf6 and Khd1 act as translational repressors for *ASH1*, the She2 and She3 proteins are involved in the tethering of the mRNA to Myo4 for transport

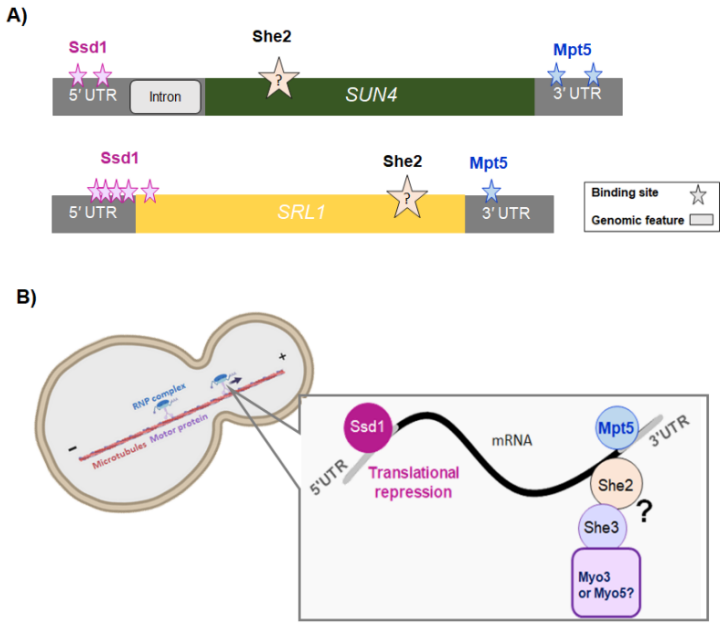

Figure 4.1. Shared elements of RNA-protein binding of *SRL1* and *SUN4* indicate the possibility of a shared mRNA transport mechanism. A) *SUN4* and *SRL1* RNA are both bound by the RBPs Ssd1, She2, and Mpt5. **B)** A cartoon of possible RNA transport machinery delivering transcript RNA, where She2 binds the RNA and connects it to the She3-Myo protein complex to be shuttled to the budding daughter.

along the actin cytoskeleton (Gonsalvez, Urbinati and Long, 2005; Deng, Singer and Gu, 2008; Shen *et al.*, 2009). This example is particularly interesting to me, because RNA affinity capture shows that *SUN4* and *SRL1* both interact with the RBP She2p (**Fig. 4.1A**) (Oeffinger *et al.*, 2007).

I previously showed the localization of Sun4 to the bud neck of *S. cerevisiae.* Previous studies show that Sun4 is also localised to the cell wall and the birth scar of budding yeast cells. This is consistent with the role of Sun4 in septation of the daughter and mother cell, and the phenotype of the mother and daughter cell failing to separate upon completion of the budding daughter cell wall in the absence of Sun4 (Mouassite *et al.*, 2000; Kuznetsov, Váchová and Palková, 2016). However, despite this clear role of the protein in the cell cycle of budding yeast; there is little data on the localization of the *SUN4* transcript mRNA. In fact, I find no evidence in the literature of *SUN4* mRNA localization having been observed in context of She2p at the time of writing this. The combination of Sun4's role in daughter-mother separation and its affiliation with the She2 protein poses a question about the localization and transport mechanism of *SUN4* mRNA.

Following this logic, the same question applies to the localization of the She2p target *SRL1*. Previous studies showed that *SRL1* mRNA localizes in a She2 dependent

manner (Shepard *et al.*, 2003; Jambhekar *et al.*, 2005). *SRL1* mRNA localizes to the bud tip (Kurischko, Kim, *et al.*, 2011; Fundakowski, Hermesh and Jansen, 2012), and the Srl1 protein localizes to the budding daughter periphery (Shepard *et al.*, 2003). However, the mechanism of *SRL1* mRNA transport is unclear.

Multiple datasets have reported specific proteins that bind both *SRL1* and *SUN4* mRNA. Ssd1 binding to of SUN4 and SRL1 mRNA was proven through tandem affinity purification (TAP)-tagged proteins and microarray analysis (Hogan *et al.*, 2008), as well as through Cross-linking and cDNA analysis (CRAC), followed by RNA-sequencing (Bayne *et al.*, 2022). High-throughput sequencing of U-tagged RNA (Lapointe *et al.*, 2017), and RNA immunoprecipitation (RIP) and high-throughput RIP- sequencing (Miller *et al.*, 2017) were also used to show that Mpt5 binds both mRNAs (**Fig. 4.1A**).

This binding is particularly interesting in light of Ssd1 genetically interacting with RBPs including Mpt5. As previously mentioned in this thesis, studies report that deletion of both Ssd1 and Mpt5 is lethal under cell wall stress, but both single deletions are viable (Kaeberlein and Guarente, 2002). Ssd1 and Mpt5 bind *SRL1* mRNA similarly to their binding of *SUN4;* with Ssd1 binding the 5' UTR, while Mpt5 binds the 3' UTR (**Fig. 4.1A**) (Kaeberlein and Guarente, 2002; Hogan *et al.*, 2008; Bayne *et al.*, 2022). It is not known if the interaction between these RBPs is due to Ssd1 and Mpt5 regulating the same mRNAs within the same pathway, or if they differentially regulate different target mRNAs.

In this chapter, I aim to investigate if She2p shuttles these mRNAs of interest in a manner similar to the *ASH1* mechanism, and I ask whether the RBPs Ssd1 and Mpt5 might be involved in this localization (**Fig. 4.1B**). I predict a localization mechanism where Ssd1 are involved in transcriptional regulation, while She2 operates as part of the machinery shuttling these mRNAs to the budding daughter (**Fig. 1B**). To study the effect each RBP's deletion on the localization of target mRNAs, I used single molecule fluorescent in situ hybridization (smFISH) to label mRNAs in fixed cells and investigate their localization. This allowed me to visualize the location of mRNAs at different points of the cell cycle, in reference to individual RBPs. Thus, elucidating the role of each of these RBPs in RNA transport.

4.2 Methods

4.2.1 smFISH probe design

smFISH probes were designed against the native coding sequence of *SUN4* and *SRL1* mRNA using the StellarisTM Probe Designer by LGC Biosearch Technologies, and purchased as pre-Dye labelled probes from Biosearch Technologies. Probe sets were comprised of a set of 39 probes for *SUN4* mRNA, and 25 probes for *SRL1* mRNA (**Table 4.1**). Each set of probes were BLASTed against *S. cerevisiae* using the NCBI alignment search tool (https://blast.ncbi.nlm.nih.gov/Blast.cgi). Probes with 16 or more nucleotides complementarity to non-target RNAs were eliminated from the set, as per the manufacturer's guidelines, to prevent off-target binding. Probe sets were labelled with: CAL Fluor Red 610 (CFR610), imaged using the CY3.5 filter for *SRL1* mRNA, and Quasar® 570 (Q570), imaged using the CY3 filter for *SUN4* mRNA. *ASH1* probes and *CLB2* probes, both labelled with Quasar 670 (Q670), and imaged using CY5 filter, were provided by Dr. Evelina Tutucci (Tutucci *et al.*, 2022).

ID	Probe sequence 5' to 3'	ID	Probe sequence 5' to 3'
SUN4_1	caatgaagccgcggtaagag	SRL1_1	atcgctgacacagaacttgc
SUN4_2	agcggaaacgattgtgctat	SRL1_2	gcgctaaagtggtagttgta
SUN4_3	tcaatatcagccgcatacgg	SRL1_3	cttggggcaccaaggagtag
SUN4_4	agcagtagtagtacatcctg	SRL1_4	gtcggcgtacgatatggtag
SUN4_5	tcttatgctggtgtgaacca	SRL1_5	gtagaccgttgaggtgacaa
SUN4_6	acgtatgtaactgcaacggc	SRL1_6	ttgaggtgaaccagctcgtg
SUN4_7	atcgacagtgactgtttcgt	SRL1_7	gcattggtaatggtggctga
SUN4_8	gagtgacggtctgaccattt	SRL1_8	ggtggacaaggaggaggagg
SUN4_9	agaagaggcttcagttgagg	SRL1_9	ttacagatccagaggccgaa
SUN4_10	tcagagtagtagtggaagca	SRL1_10	atttcatgggtggattctgg
SUN4_11	acttggtgaccgaagattcg	SRL1_11	cgtgatagtcgaggtggagg
SUN4_12	agcgatttgttcagtactct	SRL1_12	gaagggttagcagcaaagtg
SUN4_13	tttgagccgaagacgaggtg	SRL1_13	ggagacaaagtagtggagtc
SUN4_14	cacagaggattcgctagtag	SRL1_14	gacacttgctgcagtagatg
SUN4_15	ctgacccagatgtggaaata	SRL1_15	tgttgtttgaatcttcgtca
SUN4_16	gaagctgctgaagatgtgga	SRL1_16	aaggacttgacctttgcatc
SUN4_17	atggacctgaaaagtcagcc	SRL1_17	cattggaagttgaagcctgt
SUN4_18	aaggaatggtaccgtcttca	SRL1_18	aactttgtgattgggacgca
SUN4_19	ttcatctaaccagctgatgg	SRL1_19	taacgggctcattggtgaca
SUN4_20	gtattttcaacaccagacca	SRL1_20	ttggggtgactgtaacgtac
SUN4_21	tacaagagccacccgtagaa	SRL1_21	gtaacgtattgtgtagtcgt
SUN4_22	tatgagcagtaagacccttc	SRL1_22	taacagaaggtgcaccggtg
SUN4_23	cattgtgtcttggacatacc	SRL1_23	tacgttacctggagaggtag
SUN4_24	gtcagatggttggtcagaag	SRL1_24	tcgaagtggtgttgtaccat
SUN4_25	tttgaacggtacaggtagcc	SRL1_25	caccaactggtcgaattagt
SUN4_26	cccattcgcataaatagtca		
SUN4_27	ttcagagacgacgtaagcgg		
SUN4_28	cagatagcaacatcgttgct		
SUN4_29	ggtaaagagtcacctgcttg		
SUN4_30	aatccttgccaagtgtagta		
SUN4_31	aacgtagtattgcgcggatg		
SUN4_32	tcgacagaaataccggcatt		

SUN4_33	agaaccccaaacacaagcat		
SUN4_34	aattaccgacgcctgaactt		
SUN4_35	agcgccaaagttcaatggag		
SUN4_36	aggcgacaccatcagaagaa		
SUN4_37	caatgcgttaccgttgtttg		
SUN4_38	ctgaagctaccgttttcata		
SUN4_39	aaacttagctttgccagcag		

Table 4.1. smFISH probe sequences. This table shows the sequences of the smFISH probes designed for this chapter and used for imaging *SUN4* and *SRL1* mRNA.

4.2.2 Cell fixation and smFISH probe hybridization

smFISH fixation and hybridization was done following the Tutucci lab protocol (Tutucci and Singer, 2020). The protocol is summarized below.

4.2.2.1 Coverslip preparation

Round noncoated coverslips 0.13–0.17 mm thick; diameter 18 mm (Fisherbrand Cover Glasses) were washed with boiled water and 0.1 HCL, then autoclaved. Sterile coverslips were stored in 70% Ethanol at 4ºC until needed. Coverslips were coated with 0.01% (w/v) poly-L-lysine (Sigma-Aldrich) on the day of the experiment, then placed face-up in sterile 12-well plates with tweezers.

4.2.2.2 Cell fixation

S. cerevisiae strains of interest were grown in Synthetic complete medium (SC medium) + 2% glucose in a 30 ºC shaking incubator overnight, then diluted in 25 ml of fresh media and allowed to grow until OD_{600} 0.3–0.4. At this time, cells were fixed through incubation, at room temperature for 45 minutes, with Paraformaldehyde (Thermo Fisher Scientific) at a final concentration of 4% (w/v). Fixed cells were then washed twice with 10 ml of buffer B (1.2 M Sorbitol, 100 mM potassium phosphate buffer [pH 7.5]) at 2400 x g for 3 min at 4ºC then resuspended in 1 ml of the same buffer. Cells were digested and permeabilized using lyticase (Sigma-Aldrich) at 25 U lyticase per OD of cells, 20 mM ribonucleoside–vanadyl complex (VRC) (New England Biolabs), and 20mM β-mercaptoethanol and incubated in a water bath at 30 ºC for 5-7 minutes. Samples from the incubated cells were checked on a microscope every 2 minutes for cell wall digestion, and removed from water bath when 50% of the cells in the sample are opaque. Following digestion, cells were collected at 1300 x g at 4 ºC for 4 min then washed once with 1 ml of buffer B, and resuspended in the same buffer. Onto the coated coverslips, ~125 µL of cells were pipetted to coat each coverslip then incubated at 4 ºC for 30 min to an hour. Following the incubation, coverslips were gently washed once with 2 ml of cold buffer B, with the buffer carefully removed using a vacuum aspirator. 2 ml of cold 70% ethanol was gently added to each well for storage. Plates

were parafilmed and stored at -20 ºC at least for 3 hours or until ready to be used for probe hybridization.

4.2.2.3 Probe hybridization

For hybridization, coverslips were placed in a new 12-well plate and rehydrated with two washes of 2 ml 2x Saline sodium citrate (SSC) (diluted from 20x SSC: 3 M NaCl, 0.3 M sodium citrate-HCl, pH 7.0). Following these washes, coverslips were incubated for 30 min in 2 ml of 10% formamide/2xSSC at room temperature. For each coverslip: 0.125 µL of the probe stock (stock concentration is 25 µM) is needed to achieve a final concentration of 125 nM in 25 µL of the hybridization mix. To prevent pipetting errors, the probe mix was prepared for 4 coverslips by taking 0.5 ul of each probe and mixing with 1.5 ul water, then combined with 20 µL (5 µL per coverslip) of *E. coli* tRNA tRNA/ssDNA (10mg/ml) in a 1.5 ml Eppendorf tube. Probes with different colours were mixed in the same tube with the tRNA/ssDNA. Note that probes must be protected from light at all times by using foil to cover the tubes. The probe mix was lyophilized in a SpeedVac at 45 ºC, to be resuspended in the hybridization mix later –thus achieving the correct final concentration.

Following the lyophilization step, the hybridization mix was added to the probe mix in two steps. First, a solution containing 20% formamide and 10 mM NaHPO4 [pH 7.5] was added to the probe mix tube, at 12.5 µL per coverslip, then incubated at 95 ºC for 2 min then cooled at RT in the dark. Following this, 12.5 µL per coverslip of a solution containing 4xSSC, 2 mg/ml BSA, and 10 mM VRC of was added to the same tube. For each coverslip, 20 µL of the hybridization mix was pipetted onto parafilm placed in a hybridization chamber (square plate covered in foil). Using tweezers, coverslips were carefully placed on the hybridization mix with the cells facing down, then incubated at 37 ºC for 3 hours. A plastic cap filled with water was placed inside each hybridization chamber to create humidity.

Coverslips were placed back in the 12-well plates and washed twice with 2 ml of 10% formamide/2xSSC, and incubated at 37 ºC for 15 min each time. Following this, coverslips were washed once with 2 ml 2xSSC 0.1% Triton X-100 at RT (5 min), once with 2 ml of 2xSSC at RT (5 min), and a final wash with 2 ml of 1xSSC at RT (5 min). During the last incubation, glass slides were labelled with date, initials, and the strain name plus probe set used, then placed inside clean hybridization chambers. One drop of ProLong Diamond Antifade Mountant with DAPI (Thermo Fisher Scientific) was placed on each glass slide. Using tweezers, coverslips were transferred from the plate and onto the glass slide with cells facing down. Slides were incubated at RT overnight in the dark in the hybridization chambers, and sealed with clear nail polish in the morning. Following this, slides can be stored in the - 20 ºC for months.

4.2.3 Fixed cell imaging

Images were acquired using Olympus BX63 microscope with 100x/1.4NA UPLSAPO100XO objective, using CellSens imaging software. mRNA were imaged using the CY3.5 Narrow filter for SRL1 mRNA (CFR610 probes) at Ex/Em: 590/610 nm, the CY3 filter for SUN4 mRNA (Q570 probes) at Ex/Em: 548/566 nm, and the

CY5 filter for *ASH1* mRNA and CLB2 mRNA (Q670 probes) at Ex/Em: 647/670 nm, with an exposure time between 750 and 1000 ms to acquire each Z plane. For the DAPI channel 25–50 ms exposure was used for each Z plane. 41 Z plane images were acquired per channel, and a single plane differential interference contrast (DIC) image for 50–100 ms.

4.2.4 Analysis, pipeline management, and packages

RNA quantification in this chapter was done using Bigfish v 0.6.2 (Imbert *et al.*, 2022). For the analysis, I used Anaconda software for package management of the following packages:

- Python v 3.9 (van Rossum, 1995)
- Bigfish v 0.6.2
- Jupyter Lab v 3.5.0 (Kluyver *et al.*, 2016)
- Napari 0.4.17 (Ahlers *et al.*, 2023)
- OpenCV v 4.6.0 (Bradski, 2000)
- Cellpose 2.2.2 (Stringer *et al.*, 2021)
- Scikit-Image v 0.21.0 (Walt *et al.*, 2014)
- Numpy v 1.24.3 (Harris *et al.*, 2020)
- Pandas v 2.0.1
- Openpyxl v 3.1.2
- Xlsxwriter v 3.1.2
- Shapely v 2.0.1 (Gillies, 2023)

The smFISH analysis pipeline used in this chapter was created by MSc student Carlotta Meyer, during a master's project at the Wallace lab co-supervised by Dr. Edward Wallace and myself. This pipeline can be accessed on GitHub at https://github.com/carlottacode/smFISHImagePipeline. smFISH datasets (acquired in collaboration with Dr Evelina Tutucci) were used for development and testing of this pipeline. These datasets will be available in future publications.

Plots and images in this chapter were created using matplotlib (Droettboom *et al.*, 2015), Seaborn (Waskom, 2021), R (v 4.3.3) using ggplot, and Fiji(ImageJ). Statistics were performed using SciPy on Python.

4.3 Results

RNA localization is utilised by the cell to achieve spatial sorting of specific proteins. This process is often governed by RBPs and other cellular components. Thus, it is possible to understand mechanisms of spatial regulation through observing the localization of target RNAs in reference to RBPs. Single-Molecule Fluorescence In Situ Hybridization (smFISH) is a technique that allows the detection of individual mRNA molecules to study the localization, abundance, and transcription sites of mRNA (Raj *et al.*, 2008; Tutucci and Singer, 2020; Imbert *et al.*, 2022). I used this technique to label and image my mRNAs of interest, to observe how certain RBPs affect the localization of mRNA, and how this localization correlates with their protein localization.

smFISH enables mRNA detection through hybridization of multiple single-stranded oligonucleotide probes to single mRNAs, followed by visualization using microscopy (Femino *et al.*, 1998; Raj *et al.*, 2008; Tutucci and Singer, 2020). Each oligonucleotide is fluorescently labelled, and designed to bind to a designated region of the gene. Thus, the binding of multiple probes to a single transcript produces a clear bright spot representing a single mRNA. These spots can be imaged for localization in context of known cell compartments such as the nucleus, the cytoplasm, or the bud neck through the use of appropriate stains and cell markers (Maekiniemi, Singer and Tutucci, 2020; Tutucci and Singer, 2020). To achieve this spatial context, cells are imaged in the z-axis to produce a three-dimensional representation of the structures within the cell through z projections. Furthermore, smFISH allows for imaging of multiple mRNAs at once when using different

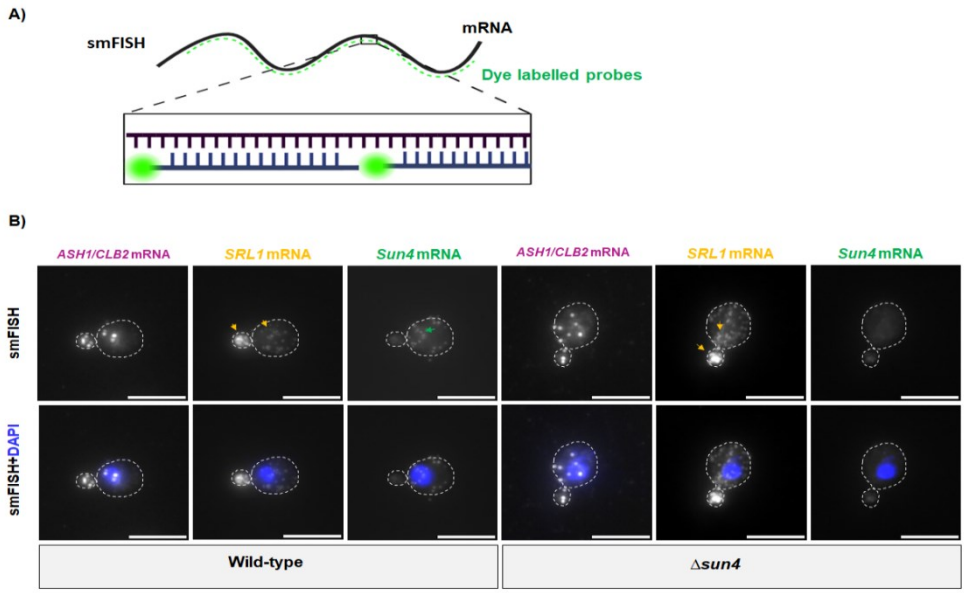

Figure 4.2. smFISH enables visualization of single mRNAs as bright spots in fixed cells. A) Dye labelled probes tile the length of the mRNA to create a bright spot **B)** Trialling my smFISH RNA probe sets in the wild-type and Δ*sun4* confirms that I have a working probe set, with specific binding to the target gene. The scale bar is 5 µm.

fluorescent dyes for each mRNA probe, to identify localization and co-localization of mRNAs.

I used smFISH to observe the localization of my target mRNAs, and to quantify their expression throughout the cell cycle. smFISH probes tile the length of mRNA to create fluorescent spots that indicate single mRNAs (**Fig. 4.2A**). I hybridized fluorescent probes to *SRL1* and *SUN4* mRNA in different colours, as described previously, to detect both mRNAs simultaneously. The smFISH technique was used successfully in various studies to investigate mRNA localization using smFISH alone or in combination with immunofluorescence (IF) (Pizzinga *et al.*, 2019; Tutucci and Singer, 2020; Tutucci *et al.*, 2022). Thus, I referred to some of these studies to choose my controls for this experiment. To monitor the localization of my target mRNAs in reference to the cell cycle, I used *ASH1* mRNA and *CLB2* mRNA as markers for localization to the growing bud (Shen *et al.*, 2009; Tutucci *et al.*, 2022).

4.3.1 Verification of smFISH technique and probe sets

To conduct a reliable screening of mRNA localization with smFISH, I started by controlling for the smFISH technique and for probe specificity. To ensure that my smFISH probes were hybridizing correctly, I started by imaging *ASH1/CLB2, SRL1,* and *SUN4* mRNA in the wild-type and in Δ*SUN4* strain. I used *ASH1* and *CLB2* probes labelled with Q670 (CY5 filter), because I did not need to tell these mRNAs apart as they only acted as a technical control. I followed this approach because my probe sets weren't tested in an experiment before, and so I used previously verified smFISH probes in the same experiment as a positive control to account for technique and probe design. This means that the *ASH1* and *CLB2* mRNA probes acted as a control that shows correct localization, correct hybridization, and fluorescence when hybridized and imaged; to ensure that I did not disturb mRNA localization through technical errors. My first set of results showed clear fluorescence from the *ASH1/CLB2* probes in the wild-type, and localization patterns to the budding daughter that match published data (**Fig. 4.2B**).

My next control accounted for probe specificity. The *SUN4* gene in *S. cerevisiae* has a paralogue called SIM1. When designing my probe sets, I used BLAST to check probe specificity and to avoid detecting SIM1. *SUN4* probes were BLASTed against the *S. cerevisiae* genome, and any non-specific probes were removed from the set, decreasing the number from the original 48 probes to the 39 probes listed in **Table 4.1**. I then checked it by experiment in the Δ*sun4* background, expecting to see no *SUN4* RNA spots at all in this background (**Fig. 4.2B**)**.** As for the *SRL1* probe set, the *SRL1* coding sequence was short, compared to *SUN4*, and so the probes had high specificity to the gene. Using the same method of checking this probe set against the *S. cerevisiae* genome in BLAST, I found none that required elimination from the set. The criteria for checking these probes is explained in methods (4.2.1). Due to the high specificity of the probes, I did not include a Δ*srl1* control.

To test for the efficiency of the probe sets, I imaged all four smFISH probes in the wild-type and ∆*sun4* background. In ∆*sun4,* I expected to see fluorescent spots in the Cy5 channel representing *ASH1/CLB2* mRNAs, and spots in the CY3.5 channel representing *SRL1* mRNA, but no spots for *SUN4* mRNA in the CY3 channel. My results matched these expectations; showing no *SUN4* smFISH in ∆*sun4* background, and clear *SUN4* mRNA spots in the wild-type, in addition to *ASH1/CLB2* and *SRL1* mRNA in both strains (**Fig. 4.2B**)**.**

Having verified the *SUN4* probe set and my smFISH technique, I then imaged and analysed the localization of my mRNAs of interest.

4.3.2 Analysis of smFISH images

4.3.2.1 Analysis overview

My data for this chapter consists of stacks of containing, per field of view: the four channels Cy5, Cy3.5 NAR, and Cy3 corresponding to *ASH1/CLB2, SRL1*, and *SUN4* mRNA respectively, and the DAPI channel which shows the cell nucleus (Fig. **4.3A**). For each of these channels, I took images of 41 Z-plane slices per field of view, as well as one single differential inference contrast (DIC) image. Thus, I had a stack of 164 images and 1 DIC image captured separately per field of view.

Tools such as FISH-quant (Mueller *et al.*, 2013; Imbert *et al.*, 2022) and Starfish (Axelrod *et al.*, 2021) are available for analysis of smFISH data. However, these tools are mainly trained for mammalian cells, and that entails separation of the segmentation and quantification steps when analysing yeast cells. Due to the large difference in size and shape between mammalian cells and budding yeast cells, software such as Cell profiler (Carpenter *et al.*, 2006), FIJI (ImageJ), or Cellpose (Stringer *et al.*, 2021) is more appropriate to use for cell segmentation prior to quantification. The analysis pipeline I used, combines the steps of segmentation using Cellpose and quantification using FISH-quant.

To quantify the mRNA in each single field of view, the pipeline starts with splitting the stacks of images into smaller stacks corresponding to individual channels. This generates a stack of Z projection images per channel (Fig. **4.3A**). mRNA spots are detected and counted for each channel (Fig. **4.3B, Fig.4.3C**) using Big-FISH (Imbert *et al.*, 2022). Accumulation of RNAs, at active transcription sites or areas of local translation, can lead to under-detection of RNAs; since such accumulations could mistakenly be counted as single RNAs. Big-FISH uses an analysis method based on Gaussian Mixture Models (GMM), where dense RNA regions are decomposed, and an estimated number of individual RNA molecules are counted (Samacoits *et al.*, 2018; Imbert *et al.*, 2022). Simultaneously, the pipeline uses pre-segmented models, generated from DAPI and DIC overlays, to identify and segment yeast cells within the data using Cellpose (Stringer *et al.*, 2021) (Fig. **4.3B**). Once the cells are identified, they are annotated with “masks” which are outlines that annotate a single cell. These masks are fed into the pipeline, and outlines are laid over the counted mRNA spots to generate counts per cells. The mRNA counts and localization co-ordinates are assigned for whole

cells (mother and bud counted as one cell) and segmented cells (mother and bud counted as one cell each) and written into an output file (Fig. **4.3C**).

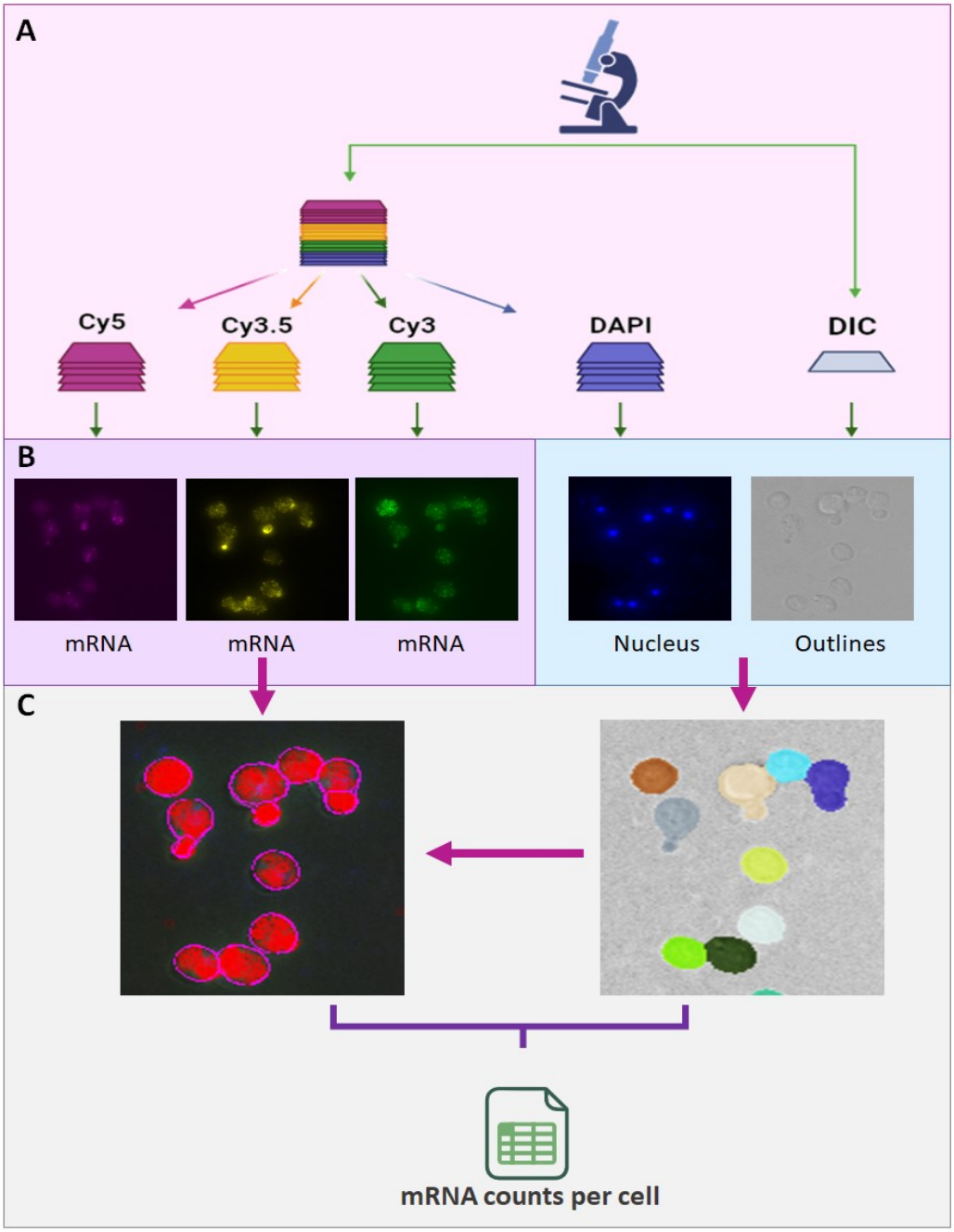

Figure 4.3. Overview of the image analysis pipeline. A) The microscope generates a stack of images containing the four channels Cy5, Cy3.5 NAR, and Cy3 consisting of 41 Z slices per channel, and one differential inference contrast (DIC) image thus generating a stack of 164 images plus DIC. The pipeline splits the original stack into stacks of Z projection slices. **B)** Max projection images are generated by taking the most in-focus slices of each channel, and mRNA spot counts and coordinates are detected with Bigfish for the fluorescent channels. DAPI and DIC channels are utilised for generating cell masks. **C)** Cell masks are laid over the detected mRNA spots to create an outlines and spots output. This output is recorded in an excel file containing the full mRNA quantification output.

4.3.2.2 Generating whole and segmented cell masks

My biological question concerns mRNAs which are involved in cell cycle control and cell wall biogenesis; therefore, the cell segmentation part of this analysis was essential. I needed an analysis pipeline segmentation step that is able to achieve accurate separation and annotation of “mother” vs “bud” cells, to correlate mRNA expression and location with the *S. cerevisiae* cell cycle.

For this purpose, I used Cellpose to cell annotations (masks) from a combined maximum intensity projection of the DAPI channel and the corresponding DIC image (**Fig. 4.3B**). Two Cellpose models for the same image, one with the mother and bud annotated as one cell (whole cell masks), and one with the mother and bud segmented and annotated as one cell each (segmented cell masks) (**Fig. 4.4**), were used as input to pre-train Cellpose to recognise and annotate whole and segmented cells. The workflow runs with pre-trained models fed in at the first step, and uses these to automatically generate cell masks.

As previously mentioned, this workflow was part of an MSc project that I co-supervised. My role in this project was to oversee the theoretical side of it, define the biological requirements, and ensure that the pipeline output addressed the biological

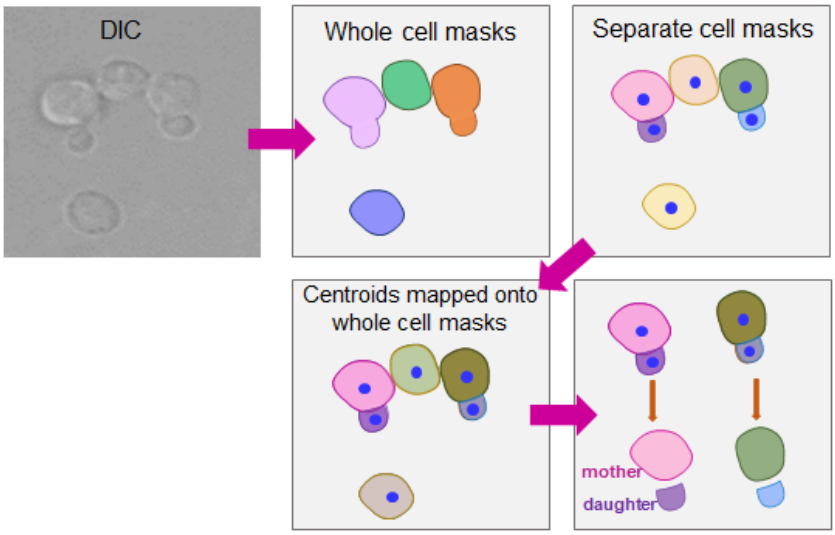

Figure 4.4. Centroids are calculated and mapped onto whole cell masks to identify mother and daughter cells. Cellpose generates whole and separate cells masks, then calculates centroids (the centre of the mask) for the separate masks. The calculated centroids are mapped onto the whole cell masks, and mother and daughter cells are then identified and labelled as separate components corresponding to the same “whole” cell.

question. Therefore, I worked to ensure that the cell annotations (masks) generated through this pipeline were accurate, by suggesting and trialling a human-in-the-loop step to allow mask corrections. Thus, the automatically generated masks can be viewed within the pipeline with Napari to allow user input and mask correction.

Via Napari viewer, two windows show the generated whole cell masks and segmented cell masks. In the segmented model, the cell masks are calculated using centroid (centre of the mask) information combined with information from the “whole” cell masks (**Fig4.4**). This way, the cells that have two centroids are flagged and identified as cells requiring separate masks. The size of the cells containing two centroids is then calculated, and the smaller cell is labelled as “daughter”, while the bigger mask is assigned as the “mother”. The above calculation and the Cellpose pre-trained models lead to fairly accurate auto-generated cell annotations, however smaller budding cells without a clear centroid are dismissed by this calculation, as shown by the blue arrows in **Fig.4.5**. Similarly, some cells in the “whole” cell masks annotation are segmented in the automatically generated masks and require manual correction (**Fig. 4.5**)**.** Cellpose can also mistakenly annotate background noise as small cells or include half cells on the edges of the field of view (**Fig**. **4.5**), therefore; having a human-in-the-loop step is important for viewing and correcting these mistakes. The auto-generated or manually corrected cell masks can also be stored and used for carrying out quantification in the pipeline, or stored for use in future analysis. Once the masks are corrected, mRNA quantification can be done. I used Big-FISH to quantify mRNA in my datasets using the mRNA spot detection (bigfish.detection) package (Tsanov *et al.*, 2016; Imbert *et al.*, 2022). Following the generation of cell outlines, Big-FISH detects mRNA spots, quantifies them, and stores them as an array of Z, Y, and X co-ordinates (Imbert *et al.*, 2022). The correction of cell annotations allows this quantification to happen within the outlines of the cell mask; thus, no data is lost through mis-annotation.

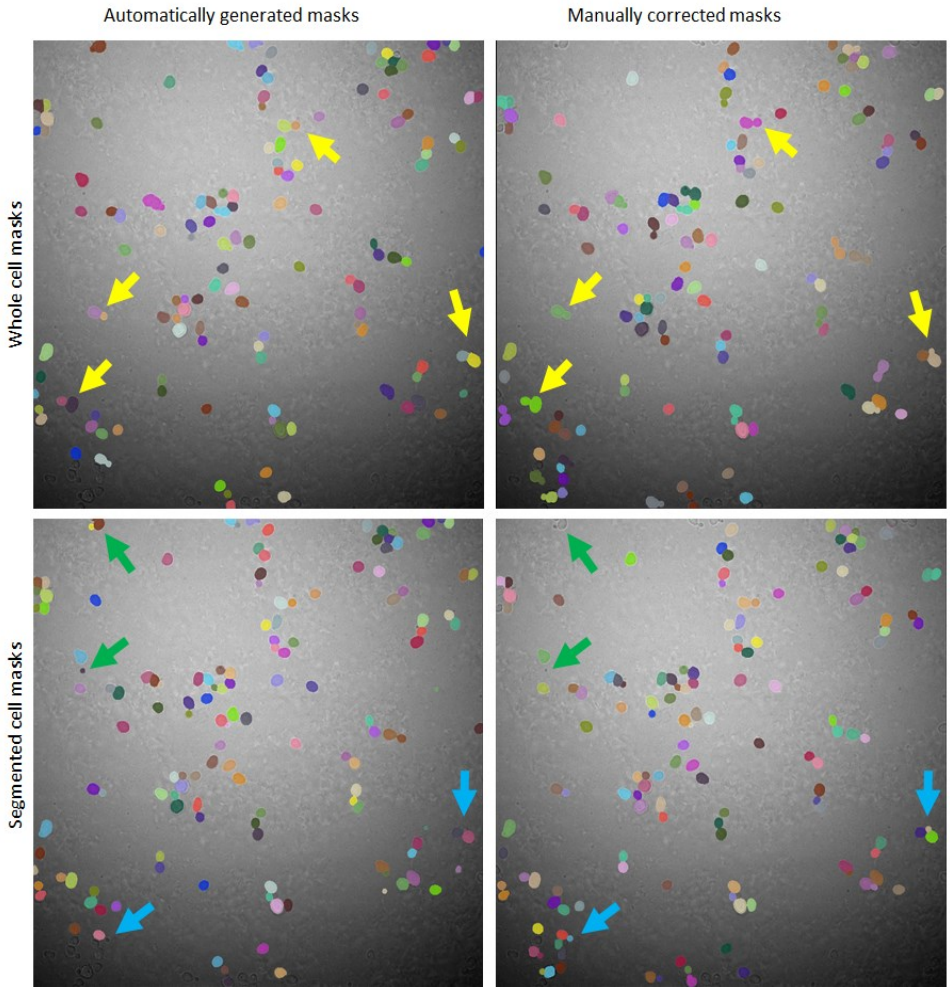

Figure 4.5. Manual correction of whole and segmented cell masks within the pipeline. Masks automatically generated with Cellpose can be manually corrected by the user to create accurate cell masks of whole and segmented cells. The automated annotation could miss small budding daughter cells (blue arrows), include half cells on the edge of the image and background noise (green arrows), or mistakenly annotate whole cells (yellow arrows).

4.3.3 *SUN4* mRNA and *SRL1* mRNA are expressed in a cell cycle dependent manner

To elucidate the localization patterns of my mRNAs of interest, I started by observing localization in the wild-type. Respective *SUN4* and *SRL1* smFISH showed that these mRNAs localize according to the cell cycle (**Fig. 4.6A**). I used *ASH1/CLB2* probes and the DAPI and DIC channels to determine the cell cycle stage by eye. I consulted previous studies on *ASH1/CLB2* mRNA localization at each stage of the cell cycle (Tutucci *et al.*, 2022), and referred to published literature on cell morphogenesis during

these stages (Tutucci and Singer, 2020), however; future experiments must utilize cell cycle markers for exact annotation. Through this analysis (**Fig. 4.6A**), I was able to determine that *SRL1* mRNA starts polarizing to the site of budding at late G1. This polarization continues through S phase with *SRL1* mRNA localizing to the emerging bud, and then to the apex of the developing bud during G2. It is worth noting that SRL1 mRNA seems more abundant from S phase and throughout G2. *SRL1* mRNA stays localized in the bud towards the apex of the bud during M phase (for early and late anaphase), however it seems less abundant at these stages. As for *SUN4* mRNA, it seems to be moving towards the budding site, in the cytoplasm of the mother, in late G1 to early G2 but it does not look as polarized as *SRL1* mRNA at these stages. However, from late G2 and into early anaphase: *SUN4* mRNA localizes to the bud neck and the growing bud as shown by the green arrows in **Fig. 4.6A**. As opposed to *SRL1*, *SUN4* mRNA seems most abundant in smaller cells i.e., earlier in the cell cycle.

My results showing cell cycle dependent localization of these mRNAs are consistent with published RNA-sequencing data on mRNA abundance (Kelliher *et al.*, 2016). To show this correlation in my data and previously published research, I used the Kelliher *et al* (2016) sequencing data to visualize the mRNA abundance of *SRL1* and *SUN4* mRNA against time from alpha factor release. I annotated the cell cycle stage corresponding to the time scale based on data from Kelliher *et al* showing synchronized *S. cerevisiae* (by alpha-factor mating pheromone) growth across time (Fig. **4.6B**).

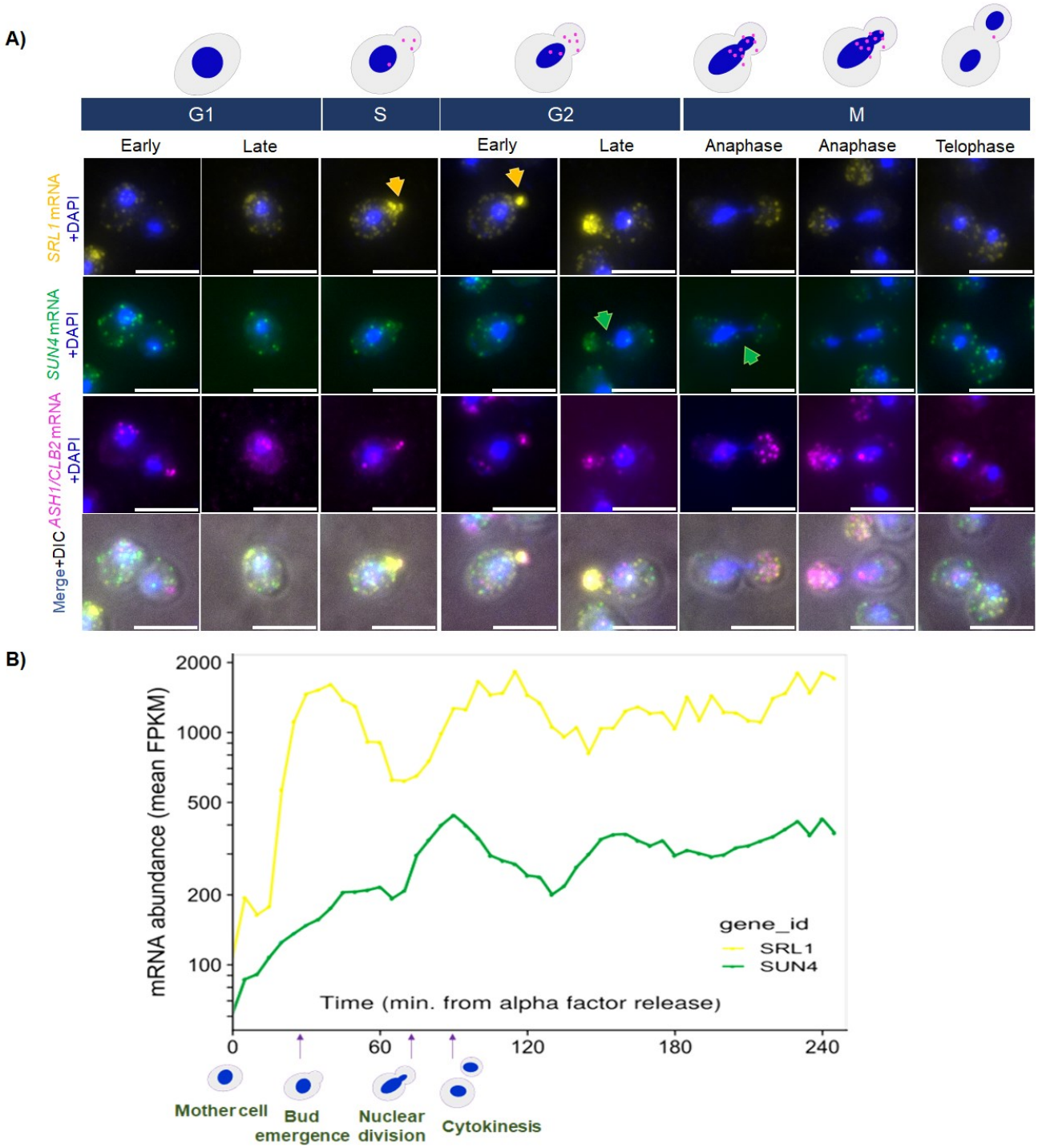

Figure 4.6. *SUN4* and *SRL1* localize in a cell cycle dependent manner, consistent with published sequencing data on RNA abundance. A) A figure showing mRNA localization in the wild-type, using smFISH, across stages of the cell cycle. *SRL1* mRNA polarizes towards the budding site at late G1, and through S phase with localization to the emerging bud, and then to the bud apex during G2 (yellow arrow). *SRL1* seems at its most abundant at this stage. Localization to the bud periphery can also be seen during anaphase and telophase. *SUN4* mRNA moves towards the bud in late G1 to early G2 (green arrow), but is not as abundant as *SRL1* mRNA. From late G2 into early anaphase: SUN4 mRNA localizes to the bud neck and the daughter cell. *ASH1/CLB2* mRNA, DAPI, and DIC were used to annotate the cell cycle stage. Scale bar is 5 μm. **B)** Visualisation of RNA-sequencing data (Kelliher *et al*., 2016) showing *SUN4* and *SRL1* mRNA abundance, with the cell cycle stage annotated at the X axis. The Y axis shows mRNA abundance, against time from alpha factors release (cells released from synchronisation).

The Kelliher *et al* data visualization shows a clear spike in *SRL1* mRNA abundance corresponding to bud emergence (**Fig. 4.6B**), which is in line with my observations in the wild-type. RNA-seq data also shows a steady increase of *SUN4* mRNA from the start of the cell cycle, till around budding time where *SUN4* plateaus (**Fig**. **4.6B**). This also correlates to my observations from microscopy images, and to plots generated from smFISH mRNA quantification. Plotting counts of *SUN4* and *SRL1* mRNAs against the cell size (**Fig. 4.7**) shows that *SUN4* mRNA is more abundant in smaller cells (early cell cycle stages), whereas *SRL1* abundance skews towards bigger cells (later cell cycle stages) in the wild-type. This data comes from 3 biological replicates, with around 1000 cells quantified. The top panel shows the cell count against cell area in μm^2. The

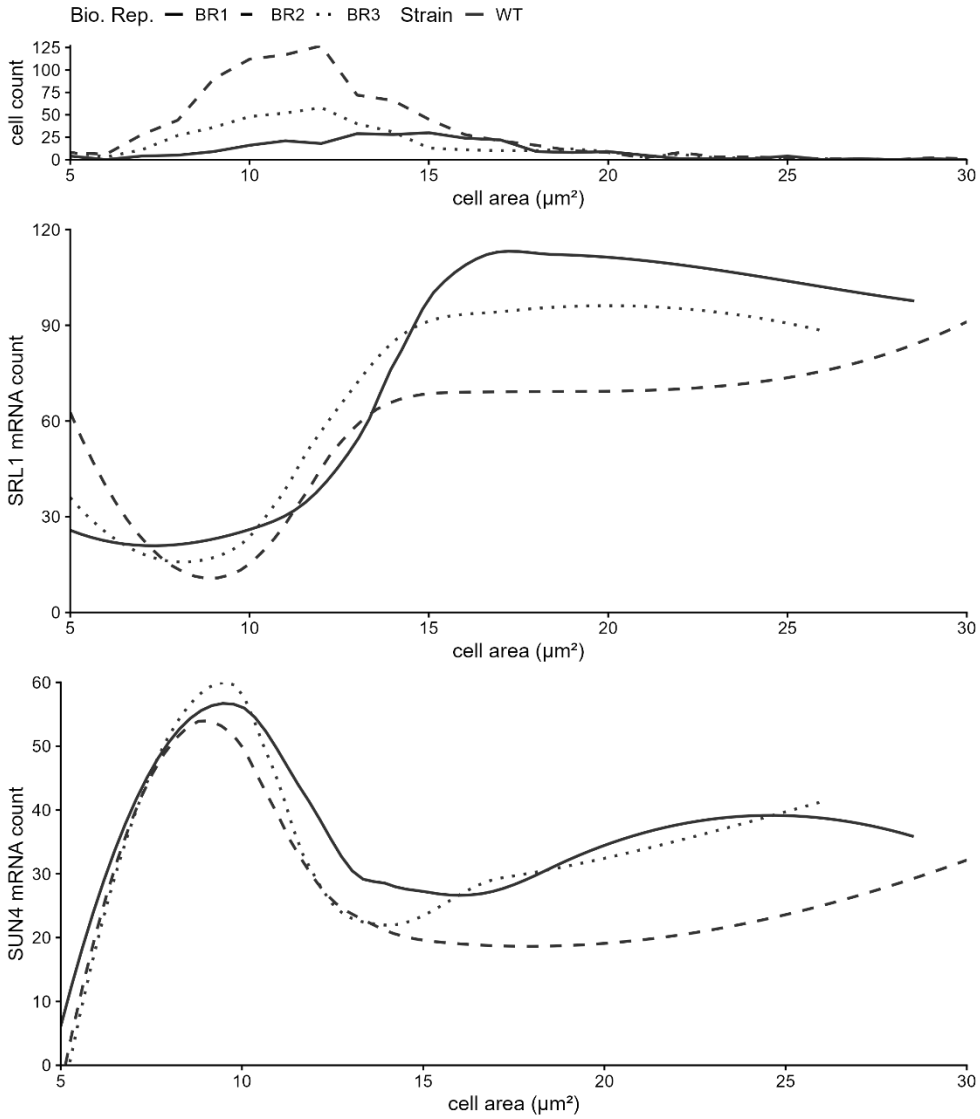

Figure 4.7. *SUN4* mRNA is more abundant in smaller cells, whereas *SRL1* mRNA counts are higher in larger cells. Plots generated from smFISH quantification of *SUN4* and *SRL1* mRNA. The top panel shows cell count (Y axis) against cell area in μm^2 (X axis) for each biological replicate. The middle and bottom plots show total *SRL1* and *SUN4* mRNA counts, respectively, per cell (Y axis) against cell area in μm^2 (X axis) for three biological replicates in the wild-type.

middle and bottom panels show results of total mRNA count per cell (Y-axis) against cell area (X-axis).

To further confirm these results, I show mRNA localization in the wild-type in mother and bud cells. As previously described, *SRL1* smFISH in the wild-type displays *SRL1* mRNA localization to the bud neck and to the tip of the emerging bud (**Fig. 4.8A**). My results in three biological replicates (only two replicates shown in microscopy panel) demonstrate that *SRL1* mRNA is not abundant in smaller single cells. Its levels seem to increase upon bud emergence in the mother cell, and are higher still in the growing bud. At the budding stage, I observe some mRNA in the mother cell migrating to the bud neck, while the majority of the *SRL1* mRNA is localized at the emerging bud tip.

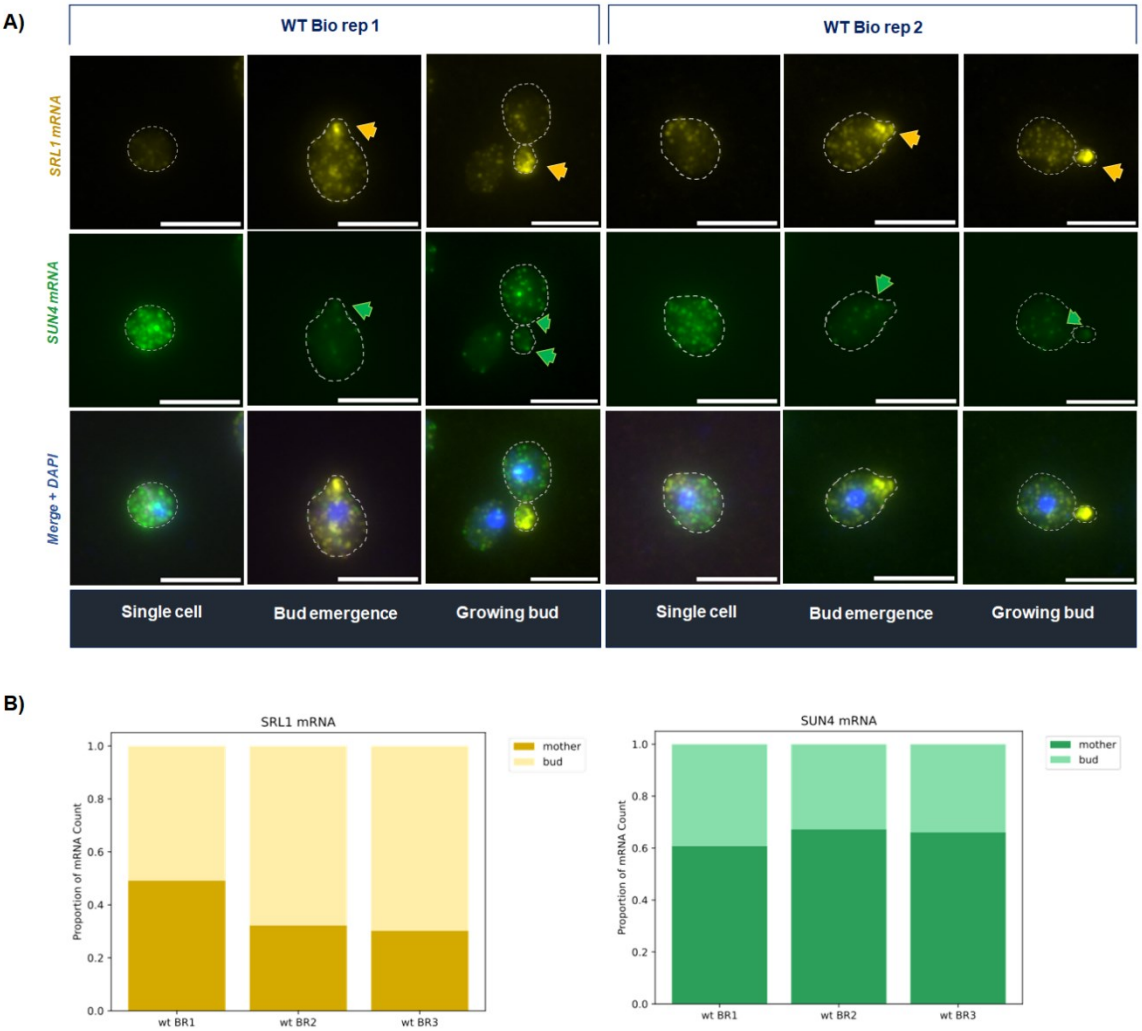

Figure 4.8. *SUN4* mRNA localizes mainly to the bud neck within the mother cell, whereas *SRL1* mRNA localizes to the apex of the budding daughter. A) smFISH microscopy images show localization of *SRL1* mRNA to the budding daughter (yellow arrows), while *SUN4* mRNA localizes to the bud neck with a smaller number of mRNA in the bud (green arrows). Scale bar is 5 µm. **B)** Proportion of respective *SRL1* and *SUN4* mRNA counts in the mother (dark colours) versus daughter cells (light colours) for three wild-type biological replicates.

Quantification of *SRL1* mRNA in segmented cells of three biological replicates (**Fig. 4.8B**), shows that *SRL1* mRNA proportion in the bud cell (mRNA count in bud divided by total mRNA count of mother plus bud) is higher than mRNA proportion in the mother cell (mRNA count in mother divided by total mRNA count of mother plus bud). Thus, confirming these observations on mRNA localization.

On the other hand, *SUN4* mRNA is more abundant in the cytoplasm in smaller single cells, compared to its expression in the growing bud. However, *SUN4* mRNA seems to migrate closer to the bud neck around the time of bud emergence in wild-type mother cells, and continues its localization near the bud neck and into the bud for growth (**Fig. 4.8A**). This localization is consistent with the role of Sun4 protein in septation and separation of the daughter from the mother cell. It is harder to see *SUN4* mRNA localization to the growing bud from microscopy images, solely due there being less of it than *SRL1* mRNA. However, quantification of mRNA shows that a proportion of *SUN4* mRNA exists in the bud, even though this mRNA is more abundant in mother cells (**Fig. 4.8B**). These localization patterns and quantification further confirm that both mRNAs localize in a cell cycle dependent manner.

4.3.4 *SUN4* mRNA localization might be affected by the RBP Ssd1

After observing localization in the wild-type, I investigated the effect of RNA-binding proteins of interest on the localization of my target mRNAs. To test this, I started by observing smFISH of *SUN4* and *SRL1* mRNAs in the Δ*ssd1* background, to compare them to my previous results in the wild-type.

My results show that *SRL1* mRNA remains localized at the tip of the developing bud in the Δ*ssd1* background, much like the wild-type (**Fig**. **4.9A**). *SRL1* mRNA largely shows a localization pattern similar to that of the wild-type throughout the cell cycle; with the mRNA seeming diffuse in small single cells, with less abundance, but accumulating in larger numbers and polarizing to the bud neck of the emerging bud at a later stage of the cell cycle. Similar to the wild-type, *SRL1* mRNA is localized to the apex of the growing bud as the cell cycle progresses. However, this localization does not seem as strong as the wild-type's, which is to say that there might be partial mis-localization. To test my observations, I quantified *SRL1* mRNA in the developing bud and mother cells of Δ*ssd1* and compared mRNA proportions between Δ*ssd1* and the wild-type cells. Although this quantification shows that the proportion of *SRL1* mRNA in the bud of Δ*ssd1* cells is close to *SRL1* proportions in buds in the wild-type; it is visible from **Fig.4.9B** that there is more *SRL1* mRNA in wild-type developing bud than in Δ*ssd1* cells (**Fig. 4.9B**)**.** However, performing an unpaired t-test on the *SRL1* mRNA proportion in three biological replicates of the buds of Δ*ssd1* [0.49673203, 0.49927902, 0.45730386] compared to the buds in wild-type [0.50832013, 0.67734807, 0.69761658] gives a p-value of 0.1334, thus these results indicate the difference is not significant between Δ*ssd1* and the wild-type strains.

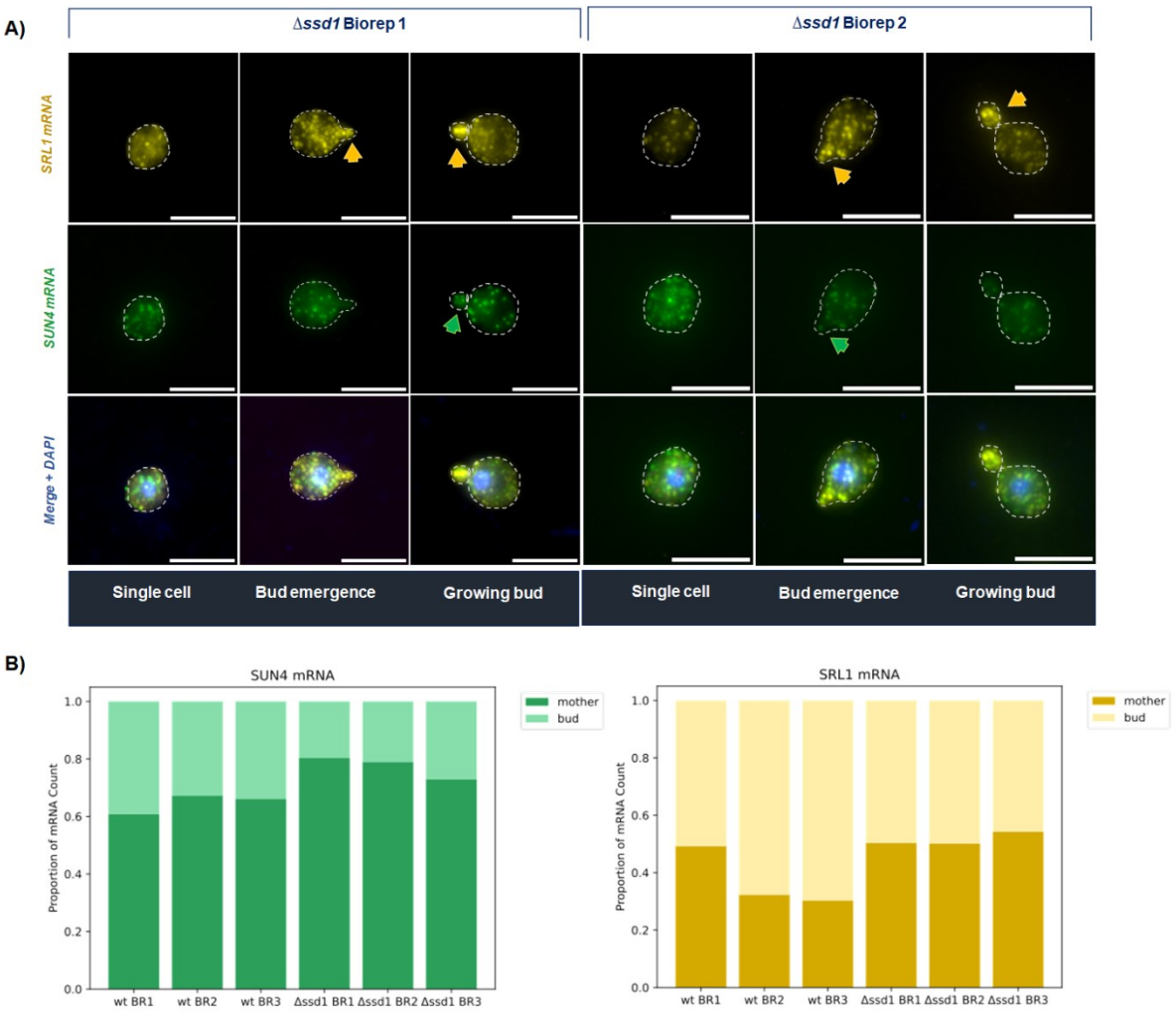

Figure 4.9. *SRL1* mRNA localization seems unaffected by deletion of the RBP Ssd1, whereas *SUN4* mRNA exhibits less localization to daughter cells. A) smFISH microscopy images show localization of *SRL1* mRNA to the budding daughter (yellow arrows) in Δ*ssd1*. *SUN4* mRNA localizes to the bud neck, with a very smal number of mRNA in the buddin daughter (green arrows). Scale bar is 5 µm. **B)** Proportion of respective *SRL1* and *SUN4* mRNA counts in the mother (dark colours) versus daughter cells (light colours) for three biological replicates of the wild-type, compared to three biological replicates of Δ*ssd1*.

As for *SUN4* mRNA, smFISH in Δ*ssd1* exhibits localization patterns akin to the wild-type when it comes to single cells (**Fig. 4.9A**). *SUN4* mRNA is more abundant in smaller single cells and shows a diffuse localization pattern in the cytoplasm. At the emergence of the bud, some of *SUN4* mRNA localizes closer to the budding neck. As the bud grows, a very small amount of *SUN4* mRNA makes its way to the bud, however the majority remains localized closer to the bud neck at the mother side (**Fig. 4.9A**). Quantification shows that *SUN4* mRNA proportions in the buds of the Δ*ssd1* strain are less than that of the wild-type (**Fig**. **4.9B**) (additional information on

total mRNA count per cell can be found in [supplementary figures 7.1. to 7.6.](). To check the significance of this difference, I performed an unpaired t-test on the *SUN4* mRNA proportion in three biological replicates of the growing buds of Δ*ssd1* [0.19573643, 0.21030043, 0.27086495] compared to the growing buds in wild-type

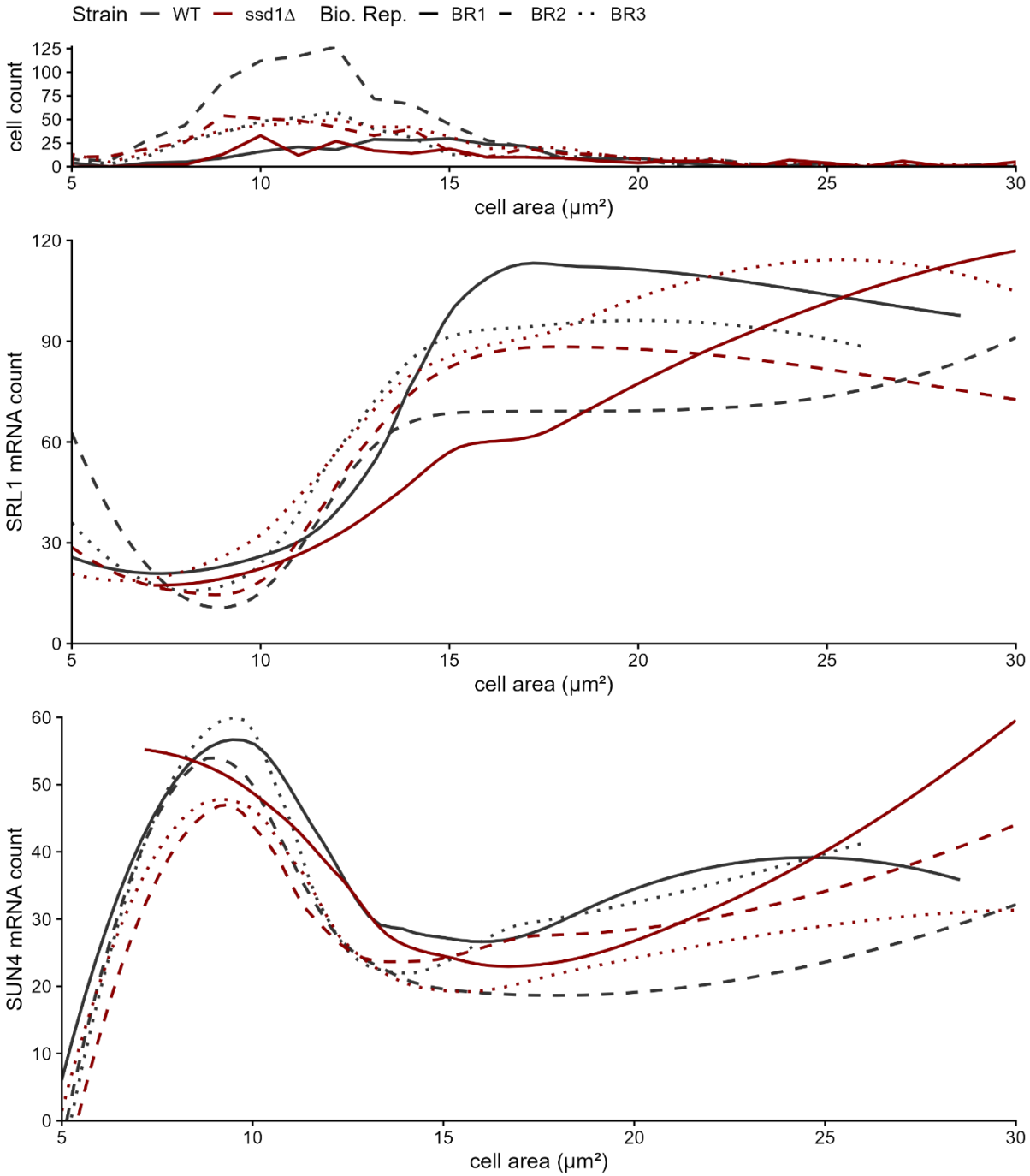

Figure 4.10. *SUN4* mRNA is more abundant in bigger cells in the wild-type than in Δ*ssd1*. Plots generated from smFISH quantification of *SUN4* and *SRL1* mRNA in the wild-type and Δ*ssd1*. The top panel shows cell count (Y axis) against cell area in μm^2 (X axis) for three biological replicates of each strain. The middle and bottom panels show *SRL1* and *SUN4* mRNA counts, respectively, compared to cell area (μm^2) for three biological replicates of each strain.

[0.3915592, 0.32797428, 0.33967248]. The t-test gives a p-value of 0.0142, thus the difference in *SUN4* localization is significant between the two strains.

This was a surprising result, as microscopy images do not show complete mis-localization of the *SUN4* mRNA, and comparison by eye did not make it immediately obvious. To double check this result, I plotted the mRNA count in whole cells for three biological replicates of Δ*ssd1* (dark red) and compared it to the previously shown wild-type plots (black) against cell area (μm^2) (Fig. **4.10**)**.** Going by the t-test results, I expected to see less of *SUN4* mRNA in larger cells in the Δ*ssd1* background (dark red) compared to the wild-type (black). This was partially true with two wild-type biological replicates exhibiting higher *SUN4* mRNA counts, around 15 μm^2 and above, than all three Δ*ssd1* replicates. However, there also seems to be more *SUN4* mRNA in these two wild-type biological replicates overall, including in smaller cells. Furthermore, one of the wild-type strains shows a lower *SUN4* mRNA count than all other replicates around this point. Another issue to address here is that the Δ*ssd1* background exhibits a larger cell size than the wild-type, as previously discussed in this thesis (3.4.). Therefore, comparison by cell area between wild-type and Δ*ssd1* is not the most reliable approach to interrogate the difference in abundance between Δ*ssd1* and the wild-type, and localization cannot be reliably inferred from it. However, these initial results suggest that the RBP Ssd1 might in fact be affecting the localization of its target mRNAs.

4.3.5 The RBP Mpt5 does not influence *SUN4* and *SRL1* mRNA localization

Following this, I tested the effect of the RBP Mpt5 on the localization of its target mRNAs. I utilized smFISH to investigate Mpt5's involvement in the transport mechanism of target mRNAs, by observing localization in the Δ*mpt5* background. *SRL1* smFISH of two biological replicates shows that Mpt5 does not affect the localization or expression of *SRL1* mRNA (**Fig**. **4.11A**). In the early budding stage, I observe that *SRL1* mRNA displays polarized localization to the bud neck and the tip of the emerging bud in Δ*mpt5*. In growing daughter cells, I see *SRL1* mRNA localizing to the tip of the budding daughter*,* similar to its localization in the wild-type strains. Furthermore, quantification of *SRL1* mRNA in this background revealed no significant difference between *SRL1* mRNA proportion in the daughter cells of Δ*mpt5* [0.62625972, 0.57973316] compared to wild-type cells [0.50832013, 0.67734807] (**Fig. 4.11B**). An unpaired t-test of these yielded a p-value of 0.9246. Similarly, *SUN4* smFISH in Δ*mpt5* shows localization in a cell cycle dependent manner with no apparent disturbance or mis-localization. This is confirmed through quantification of *SUN4* mRNA proportion in the daughter cells [0.2397892, 0.22514147] yielding a p-valueof 0.1409 when compared to *SUN4* mRNA in wild-type daughters [0.3915592, 0.32797428]. Overall, these results indicate that Mpt5 does not directly control the localization of *SRL1* and *SUN4* mRNA.

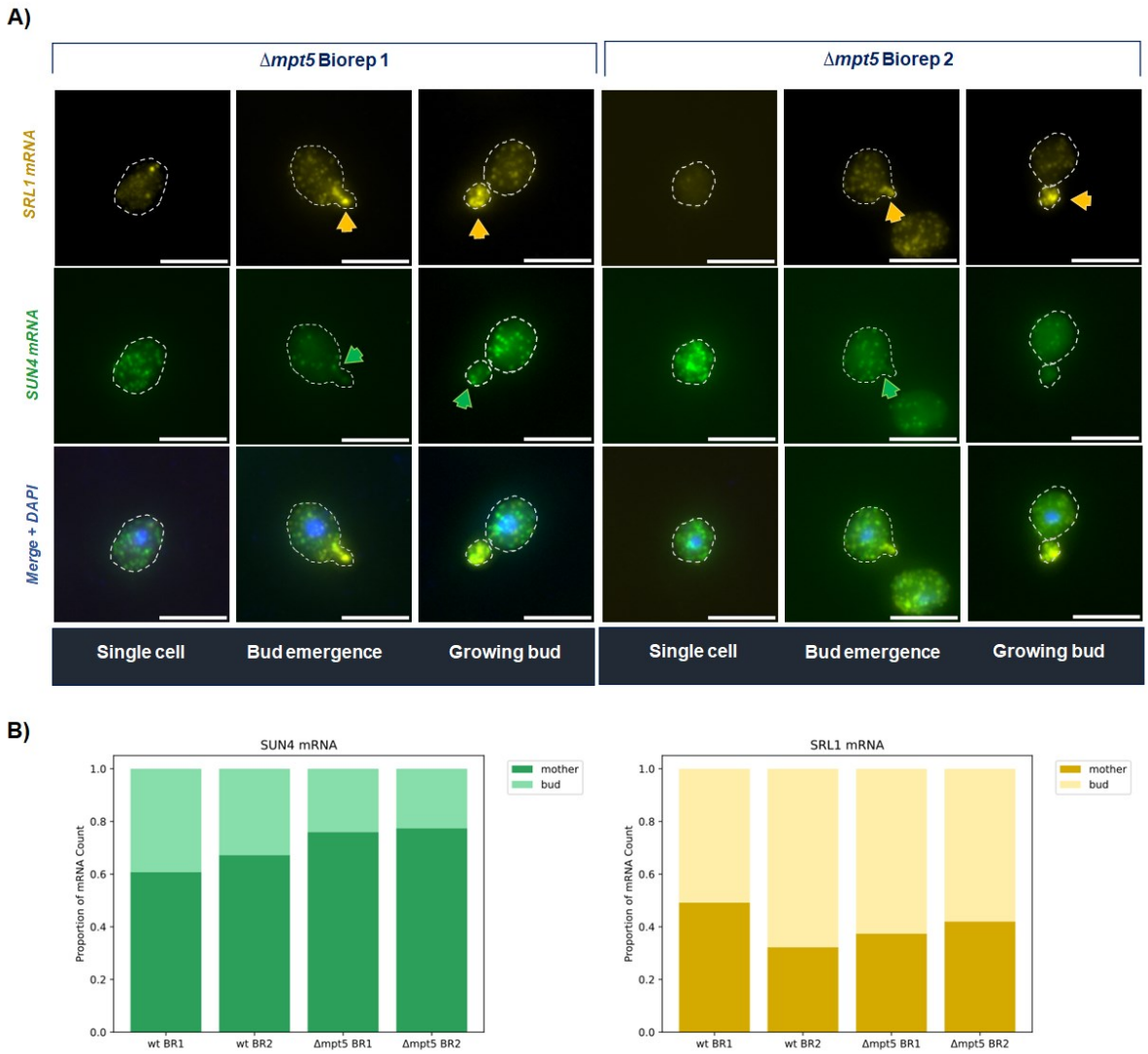

Figure 4.11. Deletion of the RBP Mpt5 does not affect *SUN4* and *SRL1* mRNA localization. A) smFISH microscopy images show localization of *SRL1* mRNA to the growing bud (yellow arrows) in Δ*mpt5*. *SUN4* mRNA localizes to the bud neck, with a very small number of mRNA in the growing bud (green arrows). Scale bar is 5 µm. **B)** Proportion of *SUN4* and *SRL1* mRNA counts in the mother (dark colours) versus buds (light colours) for two biological replicates of Δ*mpt5*, compared to two biological replicates of the wild-type.

4.3.6 The translocon component Sec72 does not affect *SRL1* mRNA localization

In a previous chapter, I replicated results showing that the translocon component Sec72 is involved in transporting the encoded cell wall proteins Sun4 and Srl1 (3.3.). In Δ*sec72* background, these protein products aggregate in the cytoplasm into distinct puncta. Following that observation, I additionally wanted to check if the role of Sec72 extends to the localization of the mRNAs encoding these proteins. My

smFISH microscopy results illustrate that Sec72 does not affect the localization or expression of *SRL1* mRNA (**Fig. 4.12**). *SRL1* smFISH of two biological replicates shows a similar localization to the apex of the budding daughter, similar to the wild-type. *SUN4* mRNA localization is harder to define, due to the very small number of mRNAs that localizes to the budding daughter, both in the wild-type and other strains. Unfortunately, I was unable to quantify mRNA for this strain background due to insufficient cell number in my smFISH datasets. Therefore, I cannot make any firm conclusions on the localization of *SUN4* mRNA in Δ*sec72*. This is an experiment that will be repeated in the future, to acquire more data from this background and quantify target mRNAs in the daughter and mother cells.

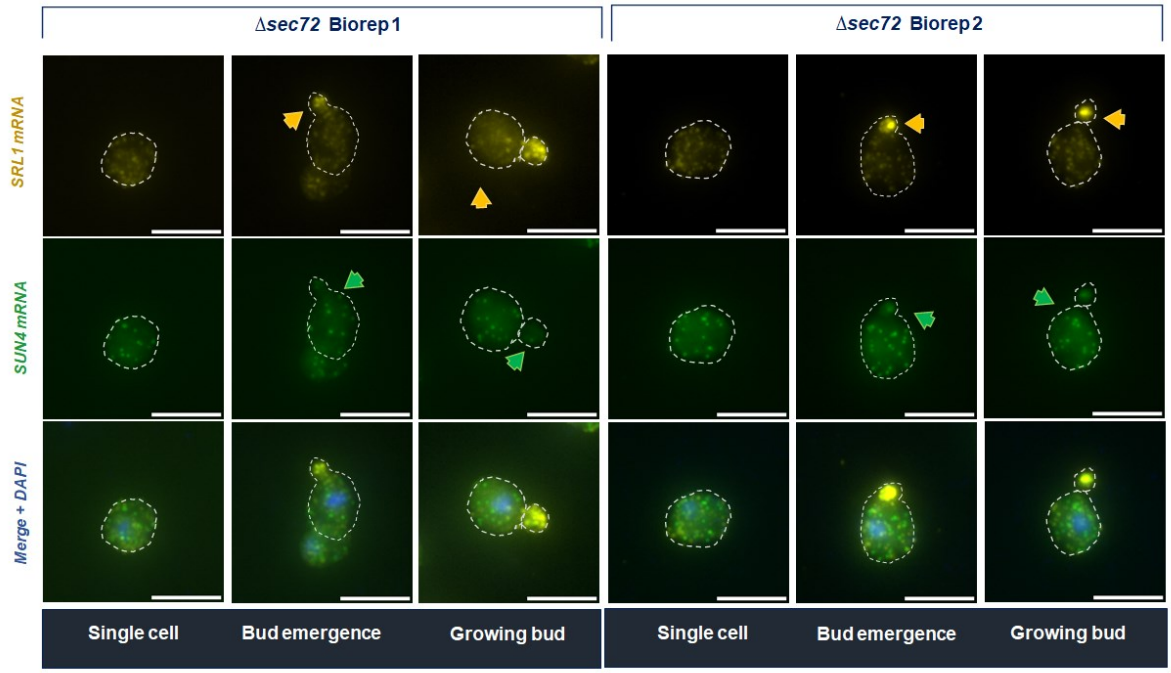

Figure 4.12. Deletion of the translocon component Sec72 does not seem to affect *SUN4* and *SRL1* mRNA localization. A) smFISH microscopy images show localization of *SRL1* mRNA to the growing bud (yellow arrows) similar to the wild-type. *SUN4* mRNA seems to localize to the bud neck and the developing bud (green arrows). Scale bar is 5 μm.

4.3.7 Deletion of the RBP She2 or the RBP She3 leads to mis-localization of *SRL1* mRNA

The final step of trying to understand the transport machinery at work for *SRL1* and *SUN4* RNA localization was to investigate the SHE proteins. As previously explained, She2 acts as a connector between its bound mRNA and a She3-Myo4 complex that shuttling of RNA from the mother cell and into the budding daughter, untranslated. Due to She2 binding of both of my mRNAs of interest, I expected to see partial or complete RNA mis-localization upon She2 deletion.

My first set of results confirm that *SRL1* does not localize to the budding daughter in absence of She2 (Fig. **4.13A**). smFISH of two biological replicates clearly shows that *SRL1* mRNA is unable to localize to the budding daughter in Δ*she2* background, compared to its localization to the apex of the bud in the wild-type. This phenotype can be seen from the onset of budding. Δ*she2* cells with an emerging bud show an abundance of *SRL1* in the mother's cytoplasm and hovering near the bud neck, without localizing to it. In Δ*she2* cells with a growing bud, a negligible amount of *SRL1* can be seen in the daughter, in stark contrast to abundant *SRL1* mRNA in the wild-type daughters (**Fig. 4.13A**)**.** These confirms that *SRL1* utilizes the RBP She2 for reaching the bud neck and the daughter cell, which is consistent with previous publications stating She2 dependent localization of *SRL1* RNA (Shepard *et al.*, 2003).

To further confirm this, I next imaged these mRNAs in the Δ*she3* background. As expected, the deletion of She3 led to a similar mis-localization phenotype for *SRL1* mRNA in two biological replicates (**Fig. 4.13B**). Although it is worth noting that more *SRL1* mRNA seems to reach the daughter cell in the Δ*she3* strain (**Fig. 4.13B**) compared to Δ*she2* (**Fig**. **4.13A)**. However, this result in combination with the Δ*she2* mis-localization phenotype confirms that *SRL1* utilizes She2 and She3 as part of their transport machinery. Previous studies show that *SRL1* physically interacts with the type I myosins Myo3 and Myo5 (Tong *et al.*, 2002; Tonikian *et al.*, 2009). I acquired Δ*myo3* and Δ*myo5* strains to test the effect of each deletion on RNA localization of *SRL1,* due to the interaction reported in the literature, but was unable to test these due to time constraints. Future experiments should also test *SRL1* mRNA localization in the Δ*myo4* background. It is highly likely that deletion of Myo4 will lead to mislocalization of *SRL1* mRNA.

As for *SUN4* mRNA, the mRNA does not seem able to reach the bud neck or the daughter cells in some of the Δ*she2* cells, while others show a small amount of *SUN4* similar to the wild-type (**Fig. 4.13A**)**.** Likewise**,** Δ*she3* cells display similar localization of *SUN4* to what is seen in the wild-type. To check the Δ*she2* results in particular, I examined quantification results to compare RNA proportion in the daughter cells between the wild-type and Δ*she2* in two biological replicates each (**Fig**. **4.13C**)**.**

For SRL1 mRNA **(Fig. 4.13C**)**,** it is clear that there's a bigger RNA proportion in the budding daughters of the wild-type, while in Δ*she2* the mothers display a higher proportion of mRNA. It is visible from the bar charts however that, in biological replicate one, Δ*she2* has more *SRL1* mRNA in the daughters. This is the result of a possible contamination which I also saw in microscopy images. Upon performing an unpaired t-test of mRNA proportion in both strains, the returned p-value was 0.1077, indicating an insignificant difference in *SRL1* mRNA proportions in Δ*she2* [0.34295685, 0.17343845], compared to the wild-type daughters [0.50832013, 0.67734807]. Nevertheless, due to the presented evidence and the possible contamination, this result might be different upon repeat of the experiment and the addition of a third biological replicate for Δ*she2*. Comparison between proportion of *SUN4* mRNA in the Δ*she2* daughters [0.32784538, 0.37380628] and the wild-type [0.3915592 , 0.32797428] also yielded an insignificant p-value of 0.8427. However,

the proportion of *SUN4* mRNA in daughter cells seemed consistent between the two biological replicates in ∆*she2.*

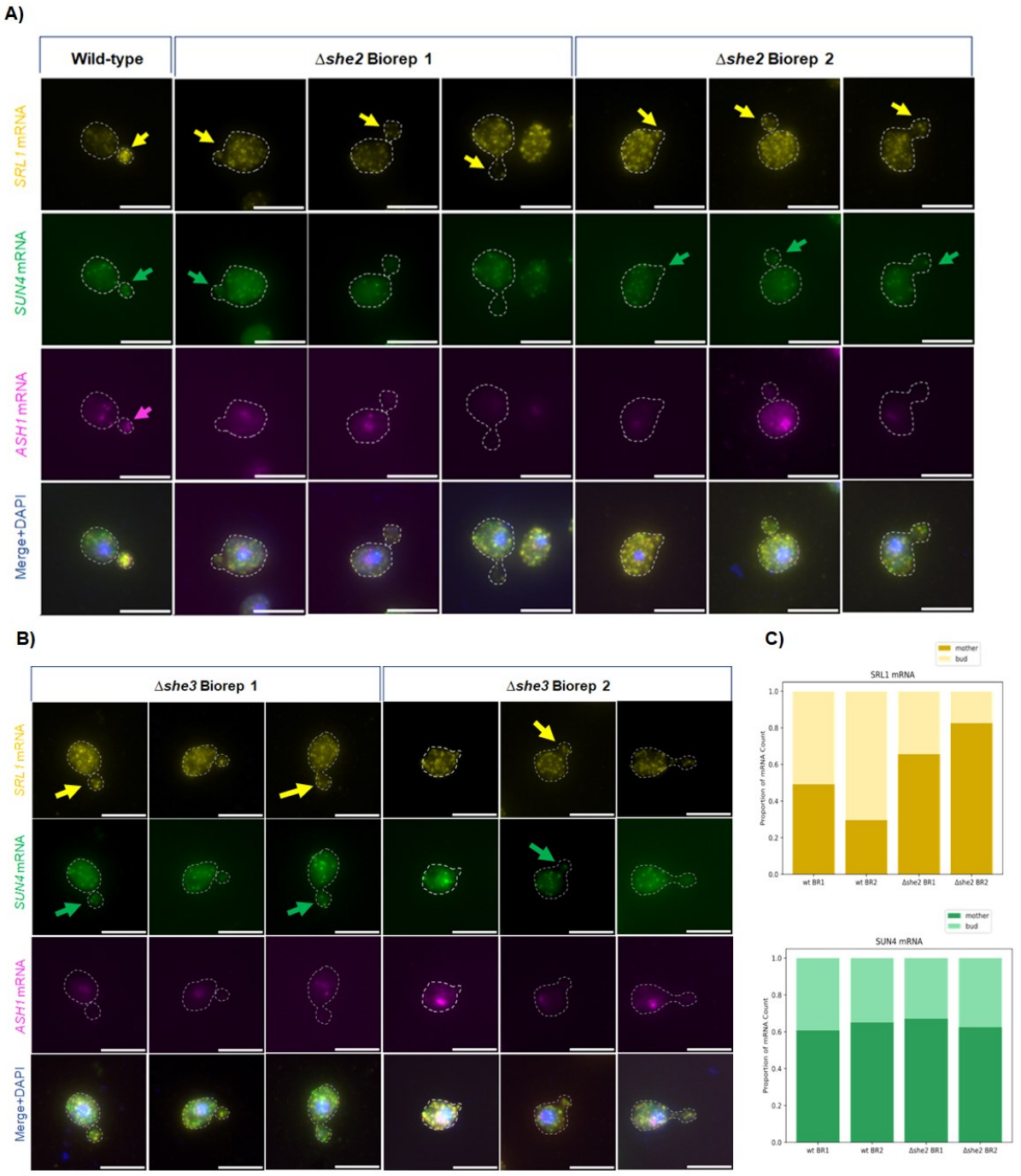

Figure 4.13. Deletion of She2 or She3 leads to *SRL1* mRNA mis-localization. A) smFISH microscopy images in two biological replicates show that *SRL1* mRNA cannot localize to the developing bud upon deletion of She2 (yellow arrows). *SUN4* mRNA seems unable to localizes in a small number of daughter cells in Δ*she2*, while localizing similar to the wild-type a in others (green arrows). Scale bar is 5 µm. **B)** SRL1 exhibits partial mis-localization in Δ*she3* cells with a very small number of *SRL1* mRNA reaching the growing buds. *SUN4* mRNA in this strain seems to localize similarly to the wild-type. **C)** Comparison of proportion of *SUN4* and *SRL1* mRNA in the mother (dark colours) and buds (light colours) in two biological replicates of Δ*she2* and the wild-type.

4.4 Discussion

4.4.1 *SUN4* and *SRL1* cell cycle dependent localization is part of the regulation of gene expression

Spatial and temporal mRNA localization is an essential part of regulating gene expression through localized protein translation (Gonsalvez, Urbinati and Long, 2005). In this chapter I investigate the localization of the mRNAs *SUN4* and *SRL1* which encode proteins associated with cell wall functions and cell cycle continuity. My results show that the localization of these mRNAs is dependent on the cell cycle. For *SUN4* mRNA, I observe that the mRNA can be found at a higher abundance in smaller cells, denoting the earlier stages of the cell cycle (G1 and S phase). I find that *SUN4* localizes near the bud neck in the mother cytoplasm, with a small proportion of mRNAs making their way into the daughter cell. These patterns are consistent with published studies previously identifying the role of Sun4 in septation and separation of daughter cells from the mother (Mouassite *et al.*, 2000), thus necessitating localized protein translation near the bud neck. However, the mechanism of *SUN4* mRNA localization has never been elucidated, and its connection to She2p (Oeffinger *et al.*, 2007) is not as widely reported as interactions between *SRL1* and She2p (Takizawa *et al.*, 2000; Shepard *et al.*, 2003; Oeffinger *et al.*, 2007). However, these two mRNAs sharing a considerable number of RBP regulators, the cell cycle coordinated localization, and their respective roles in cell wall functions indicate that they might also share the same mechanism of transport. From my microscopy results it is clear that *SRL1* localizes to the apex of the budding daughter in abundance during S phase and G2, however, by anaphase there is a considerably lower count of *SRL1* mRNA left in the budding daughter. This could be attributed to protein translation, but it could also be a result of mRNA degradation; another regulator of gene expression and cell cycle control.

4.4.2 How does Ssd1 contribute to cell cycle dependent regulation?

Previous studies have documented cell cycle regulation through mRNA turnover. For example, rapid mRNA decay of the cyclin Clb2p is necessary for the cell to finish mitosis. The entry into mitosis triggers this rapid decay, and its failure prevents the cells from finishing mitosis (Cai *et al.*, 2002; Gill *et al.*, 2004) (Cai et al 2002, Gill et al 2004). Single-molecule measurements of mRNA decay of *CLB2* reveal that its decay is promoter dependent, and carried out by the mitotic exist protein Dbf2.

Trcek *et al.* report that Dbf2p binds its target co-transcriptionally to enable this regulation at later stages of the cell cycle (Trcek *et al.*, 2011). The proposed model for this mechanism suggests that Dbf2p is exported with the mRNAs into the cytoplasm where, with assistance of its paralog Dbf20p, it maintains mRNA stability until the point of the cell cycle where mRNA decay is needed. At that point, Dbf2p and Dbf20p communicate cell-cycle cues onto the decay machinery, which in turn initiates the decay process (Trcek *et al.*, 2011). This mechanism is interesting as a model for possible Ssd1 function in maintaining mRNA stability and coordinating mRNA turnover with other regulators such as the PUF family proteins, including

Mpt5 (also known as Puf5). Due to the cell cycle dependent expression and localization of Ssd1 target mRNAs. It is possible that the decay of these targets is also coordinated with the cell cycle, and that an RBP such as Ssd1 regulates protein translation, while the release of Ssd1 via phosphorylation signals for localized translation of some mRNAs, and the degradation of others. Furthermore, Ssd1 binds the 5' UTR/promotor region of its targets, similarly to Dbf2. Interestingly enough, I also found evidence in the literature of negative genetic (severe fitness defect) interaction between Ssd1 and Dbf2 (Costanzo *et al.*, 2010), and a positive genetic interaction between Ssd1 and Dbf20 (Fiedler *et al.*, 2009). Dbf2 and Dbf20 belong to a subfamily of serine/threonine kinases which includes the Cbk1 kinase (Vitulo *et al.*, 2007). As previously explained in this thesis, phosphorylation by Cbk1 is predicted to release binding of Ssd1 from its target mRNAs to allow translation and cell polarization (Kurischko, Kim, *et al.*, 2011). Therefore, evidence indicates that Ssd1 might be part of a mechanism where it and others regulate mRNAs involved in the cell cycle. Where other components direct the mRNAs to polarized growth regions, and Ssd1 possibly acts as a translational repressor.

Future work could address the possibility of cell cycle dependent degradation of *SUN4* and *SRL1*, through mutating promoter regions of these mRNAs and detecting changes to expression and regulation by smFISH. Furthermore, to pinpoint the stage of the cell cycle where each mRNA is expressed and its localization within each stage, future experiments could utilise tubulin (Tub1) and *CLB2* as markers. The questions remain however regarding the role of current RBPs of interest: does Ssd1 act in regulating translation only, or does it also act in ensuring mRNA stability? Is the release and role of Ssd1 coordinated with RBPs such as Mpt5? And, how is it contributing to the transport machinery at work in mRNA localization?

4.4.3 How does Ssd1 contribute to localization of its target mRNAs via She2?

Previous research argued that Ssd1 contributes to the polarized localization of its target mRNAs. Kurischko *et al.* propose a mechanism of Ssd1 binding mRNA co-transcriptionally to export it to the cytoplasm, and to direct mRNAs to sites of localized translation (Kurischko, Kuravi, *et al.*, 2011). In the aforementioned study, Alanine substitution of a functional nuclear localization sequence (NLS) in the N-terminal of Ssd1 prevents Ssd1 nuclear entry. This leads to preventing mRNA binding and disruption of *SRL1* mRNA localization. Kurischko *et al.* also show that SRL1 mRNA localization is significantly diminished upon deletion of Δ*ssd1*. My results do not reflect this mis-localization in terms of statistical significance; however, this could be due to two possibilities.

The first possibility is that the previously used method altered mRNA localization, thus producing inaccurate results. Kurischko *et al.* methods alter the 3' UTR of SRL1, with an integration of a cassette containing 12 MS2-CP binding sites, together with the *S. pombe* HIS5+ gene as a selective marker. After deletion of the selective marker, the strain was transformed with the MS2-CP-GFP containing plasmid to visualize the tagged mRNA. This 12 MS2-CP method of tagging has been called into question for altering the 3' UTR, thus possibly altering mRNA decay and localization

and showing false positives (Garcia and Parker, 2015; Haimovich *et al.*, 2016), therefore it is possible that the previously reported *SRL1* mRNA localization is inaccurate. However, the smFISH technique could also pose some problems through the use of paraformaldehyde for cell fixation. The use of fixation in smFISH could cause high fluorescent background which might pose issues with single RNA detection and quantification (Patel, Brouwer and Lenstra, 2021), or affect the architecture of the cell and even the location of cellular structures (Perktold *et al.*, 2007; Li *et al.*, 2017). Problems could also arise due to over-digestion of the cells, or variations (in culture growth or cell digestion) between biological replicates of the same strain background causing mis-interpretation of biological results. Therefore, despite my own tests showing an insignificant t-test result, I am inclined towards a second possibility concerning *SRL1* localization; and that is a partial mis-localization of *SRL1* mRNA upon deletion of ∆*ssd1*, which can be seen in my microscopy images and the bar charts. In figure 9, it is visible that there is a smaller proportion of *SRL1* mRNA in the daughter cells of all three ∆*ssd1* biological replicates, than two of the wild-type biological replicates. The outlier seems to be wild-type biological replicate one, which exhibits different behaviour than the other two biological replicates. Furthermore, clear mis-localization of *SRL1* mRNA in ∆*she2* does not yield statistically significant results either in my datasets, which I believe is the result of technical issues while conducting the experiments. Therefore, I do not rule out the possibility of partial mis-localization of *SRL1* mRNA in ∆*ssd1*. Future work could replicate my experiment using smFISH, and reach a more definite conclusion.

To further interrogate the role of these RBPs of interest in the transport machinery, it is necessary to consider the interactions between *SRL1* mRNA, Ssd1, and the She2-She3 transport complex. To start, She2 binding of *SRL1* and *SUN4* mRNA must be examined more closely. Binding of *SRL1* by She2 has been documented in several studies, however, the exact location and motif of this binding remains unclear. During our collaboration on a project, Dr. Weronika Danecka screened the *SRL1* mRNA for suitable secondary structures, referring to published literature. An examination of the loop sequences of the identified structures somewhat matched the available literature (Jambhekar *et al.*, 2005; Olivier *et al.*, 2005). Dr. Danecka verified these structures by conservation analysis, and found that these structures and key loop features are conserved. This led to a prediction of the approximate She2 binding location, in the vicinity of the 3' UTR. Following a similar approach to Dr. Danecka's, I found a similar possible She2 binding site within *SUN4.* However, neither predicted binding site fully matches the available research. Therefore, future work could target these regions with point mutations within the predicted binding site. By observing if altering these sites prevents She2 binding and hinders *SRL1* and *SUN4* respective mRNA from bud localization, we can better understand the She2 binding motif and search for it in other cell cycle and bud-localized mRNAs.

5 Complementation of *S. cerevisiae*'s Ssd1 with Ssd1 homologs from different fungal species

5.1 Introduction

Saccharomyces cerevisiae Ssd1 (*Sc*Ssd1) belongs to the RNase II/RNB family; however, it is an RNA-binding protein (RBP) with no enzymatic activity. RNase II/RNB family enzymes exist across all domains of life and play a key role in RNA processing through the regulation of RNA maturation and degradation (Reis *et al.*, 2013; Lu and Taghbalout, 2014; Ballou, Cook and Wallace, 2021). *Escherichia coli* RNase II is a component of the RNA degradosome complex which is essential for RNA degradation in *E. coli* cells (Lu and Taghbalout, 2014). Members of this family, such as Dis3 and Dis3-like (Dis3L) enzymes, act in a similar processive capacity in mammals and eukaryotes (Malecki *et al.*, 2013; Ustianenko *et al.*, 2013). However, recent studies show that some proteins have evolved such that descendants of an enzyme become "pseudoenzymes", having conserved most of their structure but lost all catalytic activity (Chen *et al.*, 2015; Lazzaretti *et al.*, 2016; Ribeiro *et al.*, 2019; Ballou, Cook and Wallace, 2021). This suggests that a protein can evolve to change

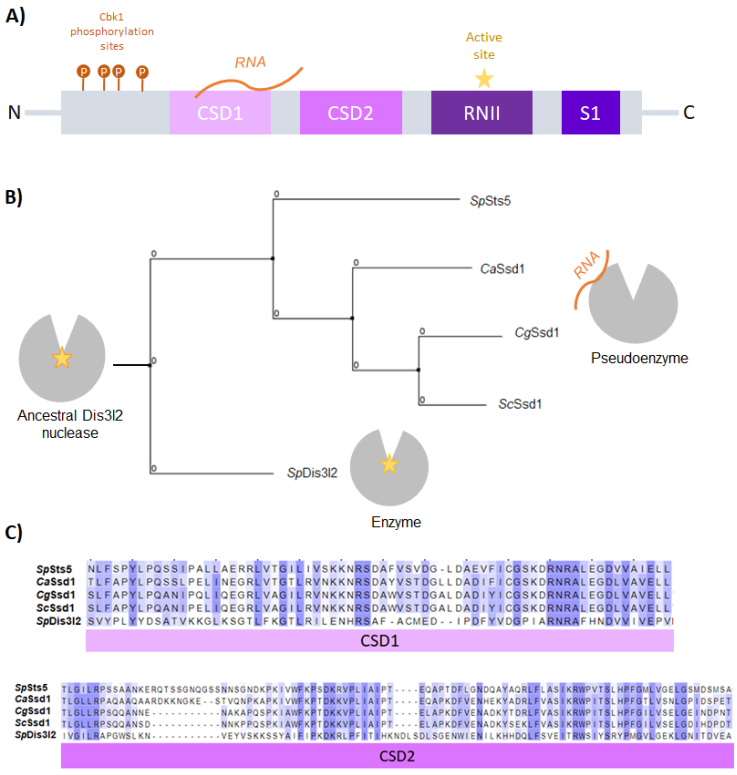

Figure 5.1. Conserved sequence features determine Ssd1 function. A) Schematic of Ssd1/Dis3L2 protein family features. **B)** Phylogenetic tree shows that *Sc*Ssd1 and Ssd1-like homologs evolved to gain an RNA-binding function and lose the ancestral active site, thus acting as pseudoenzymes. Whereas *Schizosaccharomyces pombe* (*Sp*Dis3L2) retained its active site and enzymatic function. **C)** Multiple sequence alignment of Cold Shock Domains (CSDs) shows high conservation between *Sc*Ssd1 and pseudoezyme homologs *Schizosaccharomyces pombe* Sts5 (*Sp*Sts5), *Candida albicans* Ssd1 (*Ca*Ssd1), and *Candida glabrata* Ssd1 (*Cg*Ssd1).

its structure and function. Phylogenetic analysis can be employed to determine the divergence of a protein from its predecessors. Through such analysis, the fungal Ssd1 protein has been shown to have evolved a change of function from an ancestral enzyme to a pseudoenzyme.

Among the characteristics of the RNase II family of enzymes are two N-terminal β-barrel cold-shock domains, and a central funnel-shaped domain known as RNII or the RNB domain (**Fig. 5.1A).** The RNII domain contains conserved catalytic residues that confer nuclease activity (active site) (**Fig.5.1A**). Analysis of the Ssd1 structure and sequence features reveals that some Ssd1 homologs have retained the RNII catalytic site, consisting of four conserved aspartic acid (D) residues, while others have lost it (Ballou, Cook and Wallace, 2021; Bayne *et al.*, 2022).

In eukaryotes: RNase II homologs Dis3, Dis3L, and Dis3-like2 retain the ancestral RNase II domain structure and catalytic site, whereas *Sc*Ssd1 and a number of Ssd1-like homologs resemble the Dis3L2 enzyme structurally but have evolved to lose the enzymatic active site (Ballou, Cook and Wallace, 2021; Bayne *et al.*, 2022). A good example of the diverging functions is Dis3-like 2 in *Schizosaccharomyces pombe* (*Sp*Dis3L2) and its Ssd1-like homolog *S. pombe* Sts5 (*Sp*Sts5). *Sp*Dis3L2 degrades poly(U)-tailed mRNAs and factors in RNA decay and degradation independently of the exosome (Malecki *et al.*, 2013), whereas its homolog *Sp*Sts5 acts as a translational repressor through binding mRNAs that encode proteins involved in cell growth and cytokinesis (Nuñez *et al.*, 2016). This demonstrates that *Sp*Sts5 and other Ssd1-like homologs have evolved an RNA-binding function through the conserved cold-shock domains (CSDs) (**Fig. 5.1A, Fig. 5C**), thus becoming RNA-binding “pseudoenzymes” (Ballou, Cook and Wallace, 2021; Bayne *et al.*, 2022). In *S. cerevisiae*, Ssd1 acts as a translational repressor on target mRNAs which have an Ssd1 binding motif (Jansen *et al.*, 2009). Bayne *et al*. (2022) have shown that this binding motif is highly conserved in homologous Ssd1 target transcripts, even at long evolutionary distances, which confirms that Ssd1-like homologs act in an RNA-binding capacity.

The eukaryotic RNase II/RNB family includes a number of Ssd1-like homologs that fall into the pseudoenzyme category, such as *Sp*Sts5, *Candida albicans* Ssd1 *(Ca*Ssd1*),* and *Candida glabrata* Ssd1 *(Cg*Ssd1*)* (**Fig. 5**.**1B)**.These homologs lost the catalytic RNII residue (Ballou, Cook and Wallace, 2021), but have highly conserved cold-shock domains, similar to *S. cerevisiae* Ssd1, (**Fig. 5**.**1C**) that allow them to bind RNA (Bayne *et al.*, 2022); thus acting as RNA-binding pseudoenzymes. Bayne *et al* (2022) concluded that the RNA binding site of Ssd1 is located on the outer surface of its CSDs, therefore after choosing the homologs, I ran a multiple sequence alignment on the CSD1 and CSD2 regions (**Fig. 5.1C**). I found that these regions are highly conserved in *Sp*Sts5, *Ca*Ssd1, and *Cg*Ssd1 with *Sc*Ssd1 as a reference, while *Sp*Dis3L2 shows lower identity to *Sc*Ssd1. Published studies show that *Sc*Ssd1 binds target mRNAs that have an Ssd1 binding motif (Hogan *et al.*, 2008), and that this binding motif is highly conserved in homologous Ssd1 target

transcripts in *C. glabrata*, *C. albicans*, and *S. pombe* (Bayne *et al.*, 2022). This confirms that insights into the conservation of structural features of proteins allows predictions into protein catalytic and molecular functions.

Such insights on sequence conservation and catalytic function, or lack thereof, can inform predictions about the conservation of the role of Ssd1 across fungal species. This is an important connection to investigate as Ssd1 homologs affect virulence in pathogenic fungi. I mentioned in the introduction that Ssd1 is known to function as a virulence factor in *C. albicans* and *C. glabrata*, however, the mechanism is unknown. Therefore, I aim to show in this chapter whether homologs of *Sc*Ssd1 can replace the native *S. cerevisiae* Ssd1 and maintain its native function. I propose that by showing whether the role of Ssd1 is conserved between these species, I can verify if *S. cerevisiae* can be used as a model organism to study Ssd1. I pursue this line of investigation by using phylogeny and known catalytic function to choose Ssd1 homologs and to predict their ability to substitute for *Sc*Ssd1 molecular function.

I chose Ssd1 homologs based on predicted catalytic function, conservation of structural features, and evolutionary distance. In order to address the question of the suitability of *Sc*Ssd1 as a model for understanding the mechanism of pathogenic Ssd1 homologs it was essential to include the pathogenic *C. albicans* and *C. glabrata* Ssd1. *Ca*Ssd1 and *Cg*Ssd1 both share conserved structural features with *Sc*Ssd1 and act as RBPs (Lee *et al.*, 2015; Healey *et al.*, 2020) (**Fig. 5.1B**). However, *Ca*Ssd1 is more evolutionary diverged from *Sc*Ssd1 compared to *Cg*Ssd1. For instance, *C. albicans* and *S. cerevisiae* diverged from a common ancestor 161-447 million years ago (MYA), while *C. glabrata* diverged from *S. cerevisiae* 80 MYA (Homann *et al.*, 2009; Shen *et al.*, 2018). This prompted us to choose a third homolog at an even greater evolutionary distance from *Sc*Ssd1 than both *Ca*Ssd1 and *Cg*Ssd1, to test if the conservation of Ssd1 function extends to such homologs. It was also important that this homolog is predicted to act as a pseudoenzyme, similarly to *Ca*Ssd1 and *Cg*Ssd1.

S. pombe is in the Taphrinomycotina, whose last common ancestor with the Saccharomycotina was 330-1100 MYA (Lum, Edwards and Wright, 1996; Wood *et al.*, 2002; Schmidt *et al.*, 2007), so I selected *Sp*Sts5 based on published structural features and its evolutionary distance from *Sc*Ssd1. Having chosen three pseudoenzyme Ssd1-like homologs, the next step was to test the effect of catalytic function on molecular function by phenotyping an enzymatic homolog. *Sp*Sts5 and *Sp*Dis3L2 both belong to Taphrinomycotina, however *Sp*Sts5 and *Sc*Ssd1 are more closely related than either is to *Sp*Dis3L2 (Ballou, Cook and Wallace, 2021). Ballou *et al* (2021) predict that *Sc*Ssd1 and *Sp*Dis3L2 proteins are the descendants of an ancient eukaryotic ancestor, however Ssd1-like homologs of *Sc*Ssd1 evolved to gain an RNA-binding function, becoming pseudoenzymes, while *Sp*Dis3L2 retained an ancestral enzymatic function (**Fig. 5.1B)**. Therefore, I included *Sp*Dis3L2 as the

enzymatic homolog to test the relationship between catalytic and other molecular functions.

To examine conservation of molecular function associated with the conservation of catalytic function, I constructed strains where I replaced *Sc*Ssd1 with the chosen homologs in *S. cerevisiae.* Next, I verified these strains as described in the methods (5.2.2.2), then performed phenotypic assays testing cell wall and heat sensitivity. The strain construction, verification, and phenotyping experiments in this chapter were all carried out in collaboration with Dr. Laura Tuck. The strain construction strategy and choice of phenotypic assays will be discussed in upcoming sections (5.2.1.).

5.2 Methods

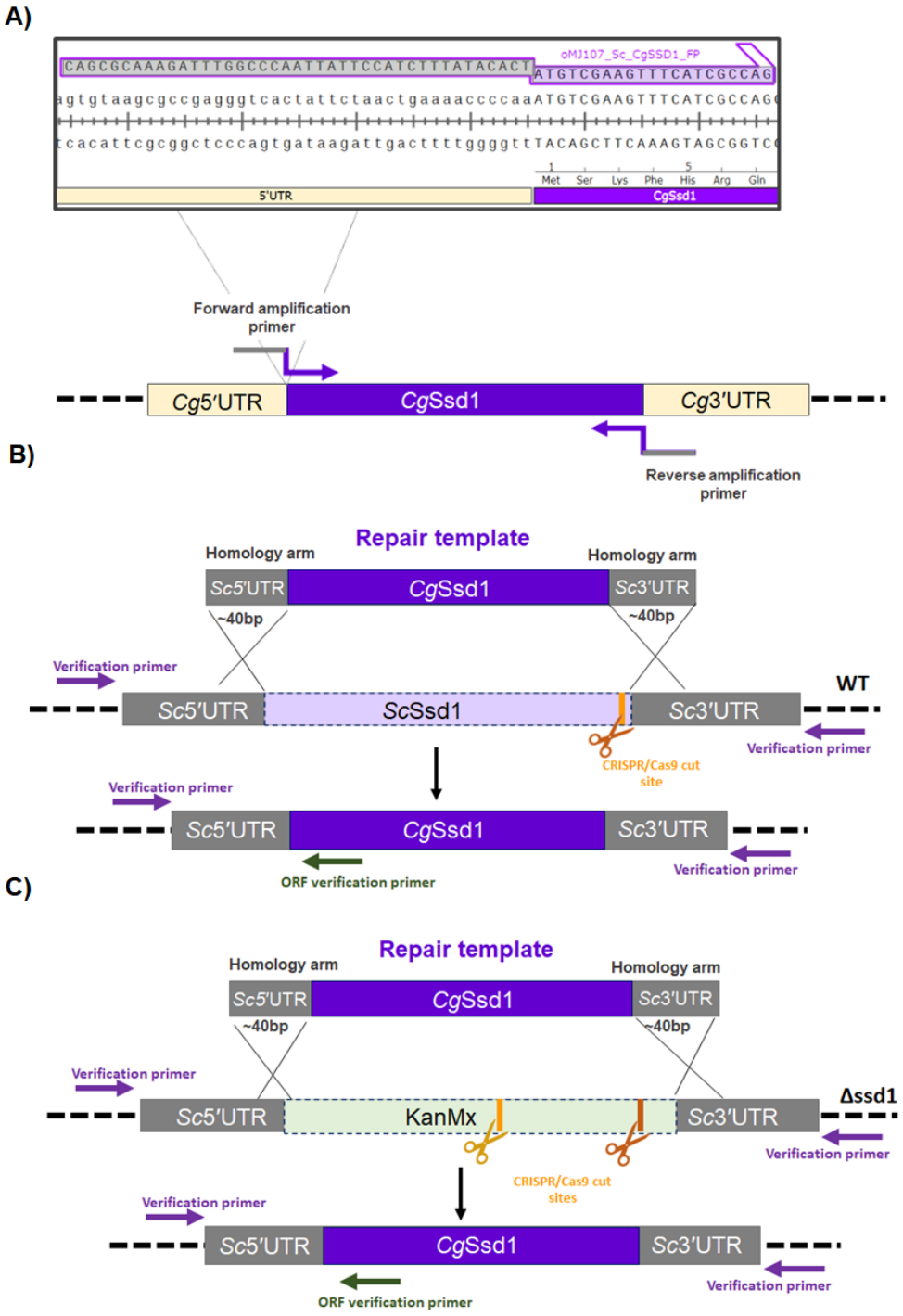

Figure 5.2. Construction strategy of *Sc*Ssd1 complemented strains.

A) Amplification of repair template with the addition of 40bp of homology arms on either side, to match the *Sc*Ssd1 UTRs. **B)** Insertion of the repair template in wild-type background, using a CRISPR/Cas9 gRNA to create a cut in ScSsd1 near the 3'UTR end. **C)** Insertion of the repair template in Δ*ssd1*background, using a CRISPR/Cas9 gRNA to create a cut either in the middle of KanMx selectable marker or near the 3'UTR end.

5.2.1 Strain construction

Ssd1 was replaced in *S. cerevisiae* with homologous sequences, using a CRISPR/Cas9 gRNA approach (Laughery and Wyrick, 2019). The repair templates were amplified using primer pairs that added homology arms upstream and downstream of the open reading frame (ORF). Each primer consisted of ~40 bp of homology to the appropriate untranslated region (UTR) of *S. cerevisiae* Ssd1 and ~29 bp homology to the target ORF (Fig. **5.2A**). These primers (**Table 5.1**) were used to amplify the repair template from extracted genomic DNA (2.7.) with Phusion polymerase (NEB) according to the manufacturer's PCR protocol. PCR products were verified on agarose gel to confirm correct product size (Fig. **5.3A**). Several PCR reactions were pooled and purified using Genomic DNA Clean & Concentrator-5 Kit (Zymo Research) to achieve a repair template concentration of around 100 ng/µl.

Primer ID	Primer sequence
SSD1_YDA	TGGTACCCTAAACATTTTGGTCTTA
SSD1_YDD	TTGTAAATATTGAAAAGAAGGCTGC
oMJ032_Sc_SpDIS3L2_FP	CAGCGCAAAGATTTGGCCCAATTATTCCATCTTTATACAC TATGGATTTAAAACCAAATATTAGAAG
oMJ033_SpDIS3L2_Sc_RP	GAAAAACAAGAAAAACAGCAATGACGATATTGGTAGAAGA GATTAATTCAAAGAAACTAGACTACAGCG
oMJ034_SpDIS3L2_5UTR_RP	GACTTTCTCGACACCATTCTG
oMJ035_SpDIS3L2_3UTR_FP	CCTCTATGGTACGACTCAGAAGC
oMJ036_Sc_SpSts5_FP	CAGCGCAAAGATTTGGCCCAATTATTCCATCTTTATACAC TATGGATGAGGAGTTTGAAAATGACTTTCC
oMJ037_SpSts5_Sc_RP	CAAGAAAAACAGCAATGACGATATTGGTAGAAGAGATCAA AACTCGACATTTGAAACGTTG
oMJ038_SpSts5_5UTR_RP	GGCATGAGTAGGACTATTCG
oMJ039_SpSts5_3UTR_FP	CGACAAAATCACTTTTACGC
oMJ172_CaSSD1_5'UTR_RP	CACCATTATTTGGAAGAAACT
oMJ173_CaSSD1_3'UTR_FP	CGGATTATTGTAACTTCAAGA
oMJ174_CgSSD1_5'UTR_RP	CAGATCTGGAGATACTGGCTC
oMJ175_CgSSD1_3'UTR_FP	GTGTCGAGATATTATTGTTCA

Table 5.1. Amplification and verification primers for strain construction. This table includes the primers mentioned in the methods section of this chapter.

For strain construction into the wild-type (**Fig. 5.2B**), yeast transformations were performed using CRISPR/Cas9. The gRNA **Ssd1_Cterm** (designed by Dr. Rosey Bayne) (**Table 5.2**) was used to make a cut in the Ssd1 ORF near the 3'UTR end (Fig. **5.2B**). 250 ng of the repair template and 500 ng of the gRNA were used, alongside fresh *S. cerevisiae* cells for transformation (2.7.). Each gRNA was previously transformed (2.4.) into pML104 plasmid backbones with a URA selection cassette, enabling selection of correct transformants on Synthetic complete -URA agar plates.

For transforming homologs into the Δ*ssd1* background (**Fig. 5.2C**), gRNAs were used to cut into the selectable marker conferring replacing *Sc*Ssd1 in this strain. The marker kanamycin resistance (KanMX) was targeted with two CRISPR gRNAs **gMJ026 (gRNA_1_KanMx4)** and **gMJ027 (gRNA_2_KanMx4)** (verified with sequencing as described in 2.4.) (**Table 5.2).** These gRNAs both cut within the selection cassette (**Fig. 5.2B, Fig.5.2C**). One gRNA was used per transformation to test their efficiency, by counting the number of resulting colonies on the selection plates. The KanMx selection marker only replaced *Sc*Ssd1 ORF without affecting the UTRs, therefore the same repair template was used for both strain backgrounds. The transformation and plating were carried out as described above.

5.2.2 Strain verification

5.2.2.1 PCR verification

gRNA ID	gRNA+PAM sequence	Oligo 1	Oligo 2
gMJ026 (gRNA_1_KanMx4)	ATGAAGGAGAAAACTCACCGAGG	GATCATGAAGGAGAAAACTCACCGGTTTTAGAGCTAG	CTAGCTCTAAAACCGGTGAGTTTTCTCCTTCAT
gMJ027 (gRNA_2_KanMx4)	GGTCAGACTAAACTGGCTGACGG	GATCGGTCAGACTAAACTGGCTGAGTTTTAGAGCTAG	CTAGCTCTAAAACTCAGCCAGTTTAGTCTGACC

Table 5.2. gRNA designed and used for strain construction. This table includes the gRNA mentioned in the methods section of this chapter, and the oligos for each gRNA (to be constructed as explained in general methods).

Constructed strains were verified using PCRs (**Fig.5.3B**). gDNA was extracted from transformants successfully grown on URA selection plates to use as PCR template. This was done per the gDNA extraction protocol (2.6.). The first verification step consisted of replicating the primers that were designed by the Yeast Knockout Collection to verify their strain collection. These verification primers, **SSD1_YDA** and **SSD1_YDD** (manufactured by Integrated DNA Technologies) (**Table 5.1**), were used to amplify the regions outside of the *Sc*Ssd1 UTRs to screen for correct band size for each transformant (**Fig. 5.2B, Fig .5.2C**). Due to *Ca*Ssd1 being close in size compared to *Sc*Ssd1, additional primers were designed within the ORF of each homolog near the 5' UTR as a second verification step (**Fig. 5.3B**). The verification PCRs were carried out using DreamTaq Green PCR Master Mix (Thermo Scientific) according to the manufacturer's protocol. All constructed strains are listed in **Table 5.3.**

ID	Description	Genotype
yMJ019	*S. pombe* Sts5, By4741	MATa; his3Δ1; leu2Δ0; met15Δ0; ura3Δ0; YDR293C:SPCC16C4.09
yMJ020	*S. pombe* Dis3l2, By4741	MATa; his3Δ1; leu2Δ0; met15Δ0; ura3Δ0; YDR293C:SPAC2C4.07c
yMJ021	*S. pombe* Sts5, *Δssd1*	MATa; his3Δ1; leu2Δ0; met15Δ0; ura3Δ0; YDR293C:SPCC16C4.09
yMJ022	*S. pombe* Dis3l2, *Δssd1*	MATa; his3Δ1; leu2Δ0; met15Δ0; ura3Δ0; YDR293C:SPAC2C4.07c
yMJ023	*C. albicans* Ssd1, *Δssd1*	MATa; his3Δ1; leu2Δ0; met15Δ0; ura3Δ0; YDR293C:C5_04730C_A
yMJ024	*C. glabrata* Ssd1, *Δssd1*	MATa; his3Δ1; leu2Δ0; met15Δ0; ura3Δ0; YDR293C:CAGL0J06072g
yMJ025	*C. albicans* Ssd1, BY4741	MATa; his3Δ1; leu2Δ0; met15Δ0; ura3Δ0; YDR293C:C5_04730C_A
yMJ026	*C. glabrata* Ssd1, BY4741	MATa; his3Δ1; leu2Δ0; met15Δ0; ura3Δ0; YDR293C:CAGL0J06072g

Table 5.3. Constructed and verified complementation strains. This table lists the strains made for this chapter, the inserted gene/homolog, and the background strains used for each.

5.2.2.2 Sanger sequencing

Strains were confirmed using Sanger sequencing (**Fig. 5.3C**). The previously mentioned verification primers were used to amplify the Ssd1 region with Platinum SuperFi II DNA Polymerase (Thermofisher Scientific) for PCRs, as per the manufacturer's protocol. PCR products were then purified using Monarch PCR & DNA Cleanup Kit (New England BioLabs), and diluted to a DNA concentration of 10-50 ng/µl as per the sequencing facility's instructions. Tubes containing 10 µl of purified product pre-mixed with 5 µl of primer (final concentration 5 µM) were sent to Genewiz, Azenta life sciences facility for Sanger sequencing. Results were viewed and aligned using Snapgene software (**Fig. 5.3C**).

5.2.3 Phenotyping assays

Phenotyping assays were performed to test the growth and heat sensitivity phenotypes of each of the strains. Single colonies of each of the complemented and control strains were grown overnight in 5 ml YPD broth in a 30 ºC shaking incubator at 180 rpm. The overnight cultures were made up to OD^{600} 1 to use for spotting neat cultures and for making ten-fold serial dilutions. These cultures were then treated and plated as required for each test, spotting 5 µl of each dilution.

5.2.3.1 Cell wall stress with Calcofluor White (CFW) assay

Serial ten-fold dilutions were made in water in flat bottom 48-well plate. These dilutions were spotted onto YPDA plates supplemented with 50 µM CFW (Kaeberlein and Guarente, 2002; Bayne *et al.*, 2022), and replica plated onto YPDA only plates. Two biological replicates were plated for each of the test and control strains. Plates were grown for 3 days at 30 ºC and imaged daily using Amersham™ ImageQuant™.

5.2.3.2 Induced thermotolerance assay

Serial ten-fold dilutions were made in water in 200 µl PCR strips. PCR strips of the dilutions were incubated at 37 ºC for 30 minutes followed by 50 ºC for another 30 minutes in a thermocycler (Mir, Fiedler and Cashikar, 2009; Bayne *et al.*, 2022). Two

biological replicates of the test and control strains were plated onto YPDA. Plates were grown for 3 days at 30 ºC and imaged daily.

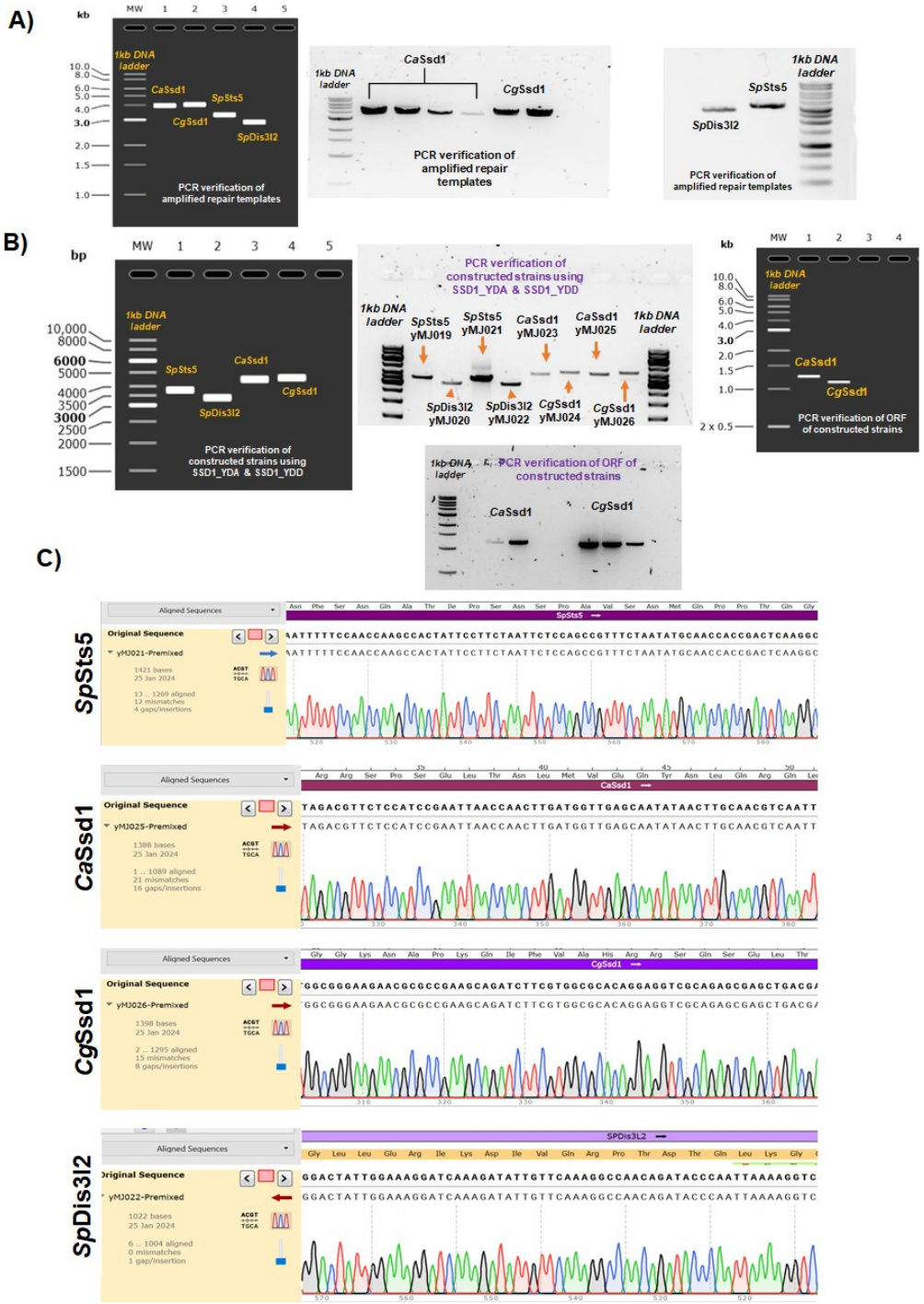

Figure 5.3. PCR and sequence alignment verification of constructed strains. A) PCR verifications (white gels) of the amplified repair templates that were used for CRISPR mediated yeast transformations. Each gel was simulated on Snapgene (black gels) to show the correct band size. **B)** PCR verification on agarose gels (white) of the constructed strains, with gels simulated using Snapgene (black) to show the expected band size. The first set using SSD1_YDA & SSD1_YDD primers to amplify the entire Ssd1 region in each strain. The second set using SSD1_YDA and primers within the ORF of *Ca*Ssd1 and *Cg*Ssd1 respectively to confirm the correct transformation, due to *Sc*Ssd1 being too close in size**. C)** Sequence alignments of the strains constructed in this chapter.

5.3 Results

Pseudoenzyme Ssd1-like homologs complement Ssd1 phenotype To test how sequence conservation can indicate the conservation of molecular function, I replaced Ssd1 in *S. cerevisiae* with copies of its pseudoenzyme and enzymatic homologs (*Sp*Sts5, *Ca*Ssd1, *Cg*Ssd1, and *Sp*Dis3L2). I carried out this replacement by inserting a homologous Ssd1 coding sequence under the native *Sc*Ssd1 promoter and terminator. The promoter and terminator regions of genes define the levels of gene expression, and are known to affect protein localization and stability (Tuller, Ruppin and Kupiec, 2009; Dvir *et al.*, 2013; Mayr, 2019). Thus, the replacement strategy was designed to ensure that the tested phenotypes are a product of conserved Ssd1 function and RNA-binding, without the results or binding being confounded by promoter and terminator regions foreign to *S. cerevisiae* Ssd1. I designed primers that only amplified the target ORF (~29 bp homology), and added homology arms (~40bp) on either side of this region. This enabled the insertion of a new ORF under the native UTR regions of *Sc*Ssd1 as illustrated in **Fig. 5.2**..This allows for production of a homologous Ssd1 protein with the native expression levels of *Sc*Ssd1.

In the wild-type, I used a CRISPR/Cas9 gRNA approach to create cuts at the insertion site, then transformed the amplified repair templates to replace the *Sc*Ssd1. To show preservation of function, I carried out the first set of replacements in the wild-type (BY4741) background using a gRNA that cuts near the 3'UTR end of *Sc*Ssd1 (**Fig. 5.2B**). Complementation in the wild-type shows whether homologous Ssd1 proteins behave similarly to the wild-type under phenotypic conditions.

The second strategy was to restore Ssd1 in a Δ*ssd1* background. To test if complementation of an Ssd1 homolog can restore Ssd1 function and prevent sensitivity under phenotypic conditions, compared to Δ*ssd1*. For this purpose, I used a Δ*ssd1* strain where the *Sc*Ssd1 was replaced with a selection cassette conferring kanamycin resistance (KanMX). The KanMX marker replaces the *Sc*Ssd1 ORF without disrupting the UTR regions, so I was able to use the same amplification primers and repair templates for both strain backgrounds. Dr. Laura Tuck and I designed two CRISPR gRNAs to trial them for transformation efficiency. This was done by comparing the number of transformants on selection plates resulting from using each gRNA. Both of these gRNAs cut within the KanMX marker. I then used the gRNAs (one at a time) to insert respective homologous Ssd1 sequences in place of this marker, under the native *Sc*Ssd1 promoter and terminator. I verified the constructed strains by PCR as previously described (**Fig. 5.2C**), using appropriate verification primers designed by the Yeast Knockout Collection. These primers amplify from outside the *Sc*Ssd1 UTRs towards the ORF, resulting in PCR products with a distinct size to compare to the inserted homolog. However, some homologs such as *Ca*Ssd1 and *Cg*Ssd1 were too close to *Sc*Ssd1 in size to be distinguished, and so I designed additional primers that anneal within the ORF of these homologs. These primers were used to amplify a region from within the ORF to the 5' UTR (**Fig. 5.2B, Fig.5.2C**), thus confirming the correct insertion size in each strain (**Fig. 5.3B**).

After strain verification, I tested the complemented strains for cell wall integrity and adaptation to heat stress using phenotypic spot assays. *Sc*Ssd1 has roles in cell wall integrity and induced thermotolerance (Kaeberlein and Guarente, 2002; Mir, Fiedler and Cashikar, 2009; Bayne *et al.*, 2022), thus I wanted to use assays for these sensitivities. I first tested the complemented strains under the cell wall stressor calcofluor white (CFW). Published studies show that Δ*ssd1* strains are sensitive to CFW concentrations in the range of 10–100 µM (Kaeberlein and Guarente, 2002), and cannot survive at 50 µM CFW (Kaeberlein and Guarente, 2002; Bayne *et al.*, 2022). Thus, I spotted two biological replicates of each of the test and control strains onto YPDA plates supplemented with 50 µM CFW.

The second phenotypic assay tested heat sensitivity. In *S. cerevisiae* treatment with mild heat temperatures induces tolerance to high temperatures and allow survival of the cells. Previous studies showed that Ssd1 genetically interacts with heat shock proteins, such as Hsp104, during heat stress and that *Sc*Ssd1 is required for induced thermotolerance (Mir, Fiedler and Cashikar, 2009). Therefore, the complemented and control strains were incubated at 37 ºC for 30 minutes, followed by 50 ºC for another 30 minutes in a thermocycler, then spotted onto YPDA plates to test for induced thermotolerance.

For these assays, I predict that homologs with the same non-catalytic function and conserved structural features such as *Cg*Ssd1, *Ca*Ssd1, and *Sp*Sts5, will conserve the *Sc*Ssd1 molecular function. Whereas the enzymatic *Sp*Dis3L2 will not complement the molecular function, due to its inability to bind target Ssd1 mRNAs. Thus, I expect Ssd1-like homologs to behave like the wild-type while *Sp*Dis3L2 shows a phenotype similar to Δ*ssd1*.

5.3.1 Genetic complementation in *S. cerevisiae* confirms conservation of Ssd1 function in closely related fungi

I selected *Ca*Ssd1 and *Cg*Ssd1 as the first homologs to complement into *S. cerevisiae*, due to their predicted pseudoenzyme nature and close evolutionary distance to *S. cerevisiae*. Published data show that these two species have lost the catalytic site in the RNB domain (Ballou, Cook and Wallace, 2021). This suggests that Ssd1 in these species acts as an RNA binding protein, and is consistent the reported conservation of the Ssd1-binding motif in target transcripts in *C. glabrata* and *C. albicans* (Bayne *et al.*, 2022).

I first tested these strains under cell wall stress, by spotting two biological replicates onto YPDA plates supplemented with 50 µM CFW. As expected, results show that *Ca*Ssd1 and *Cg*Ssd1, complemented into the wild-type (BY4741) background, retain cell wall integrity and grow normally in a manner similar to the wild-type strain, while

Δ*ssd1* cells do not survive under these conditions (**Fig. 5.4**). Following this, I tested *Ca*Ssd1 and *Cg*Ssd1 strains inserted into the Δ*ssd1* background. The *Ca* and *Cg* Ssd1 homologs restored the cell wall integrity function, as observed by colony growth, and behaved similarly to the wild-type strain. This clearly shows that *Ca*Ssd1 and *Cg*Ssd1 retain the functionality of *Sc*Ssd1 by supporting survival under cell wall stress.

Following these results, I tested the ability of the complemented strains to adapt and induce tolerance to high temperatures. I examined *Ca*Ssd1 and *Cg*Ssd1 complemented into the wild-type background. As predicted, the *Ca*Ssd1 and *Cg*Ssd1 were able to induce thermotolerance in their respective strains and exhibited a phenotype similar to the wild-type strain (**Fig. 5.4**). In contrast, the Δ*ssd1* strain showed less growth and a decreased survival rate. Following that, I tested *Ca*Ssd1 and *Cg*Ssd1 complemented into the Δ*ssd1* background and showed a restoration of the induced thermotolerance phenotype in these strains.

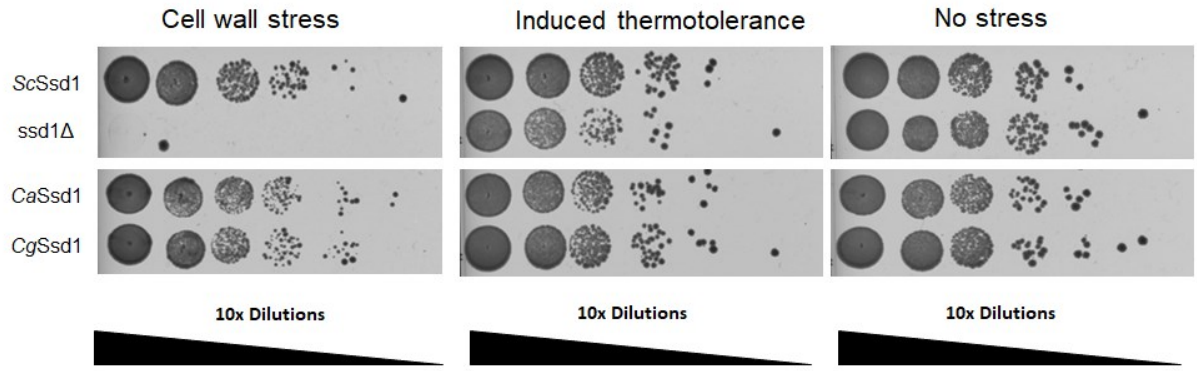

Figure 5.4. Pseudoenzyme Ssd1 homologs complement yeast's Ssd1 phenotypes under cell wall stress and heat stress. Cell wall stress: Wild-type, *ssd1*Δ, and complementation strains spotted on YPD plates supplemented with 50 µM CFW. *Ca*Ssd1 and *Cg*Ssd1 retain cell wall integrity and grow normally in a manner similar to the wild-type strain, while Δ*ssd1* cells show no growth. **Induced thermotolerance:** Strains were incubated at 37 ºC for 30 minutes followed by 50 ºC for another 30 minutes and then spotted onto YPD plates. *Ca*Ssd1 and *Cg*Ssd1 were able to induce thermotolerance and produce a phenotype similar to the wild-type strain, while Δ*ssd1* shows reduced growth. **No stress:** Strains spotted onto a YPD plate with no stress grow normally. The upper and lower panels of each set were imaged from different regions of the same plate –irrelevant intervening spots have been removed for clarity. These complementation strains were constructed in the wild-type background.

The results of these phenotypic assays illustrate that the tested homologs have the same molecular function and contribute to similar biological processes as *Sc*Ssd1, thus resulting in similar phenotypes. This shows that the study of Ssd1 in *S. cerevisiae* is informative for a molecular understanding of Ssd1 pseudoenzyme homologs in fungal pathogens.

.

5.3.2 *S. pombe* homologs of Ssd1 do not recapitulate Ssd1 activity in *S. cerevisiae*

My next aim was to examine the conservation of molecular function in light of a different enzymatic function. The fission yeast *S. pombe* includes Ssd1 homologs that act in both enzymatic and non-enzymatic capacity. As shown before, *Sp*Sts5 retains the structural features conferring the ability to bind RNA. Previous studies show that *Sp*Sts5 acts as an RBP, much like the budding yeast Ssd1 (Nuñez *et al.*, 2016; Bayne *et al.*, 2022). Ballou *et al.* (2012) reported that Sts5 is predicted to be a pseudoenzyme, unlike its distant paralogue *S. pombe* Dis3L2, which degrades cytoplasmic mRNA (Malecki *et al.*, 2013). These two paralogs with their differing functions, and at a further evolutionary distance to *S. cerevisiae* compared with *Candida*, were therefore the next set of complementation strains to test. I replaced *Sc*Ssd1 with *Sp*Sts5 and *Sp*Dis3L2 in the wild-type and Δ*ssd1* backgrounds as previously described. I hypothesized that *Sp*Sts5 would complement the function of *Sc*Ssd1 and retain the wild-type phenotype, much like the previously tested pseudoenzyme complementation, by restoring cell wall integrity under CFW (5.3.2.).

Surprisingly, my hypothesis proved to be partially wrong for the first set of phenotypic assays. Upon spotting *Sp*Sts5 and *Sp*Dis3L2 on YPDA + 50 µM CFW plates, I found that *Sp*Sts5 only partially complements the function of *Sc*Ssd1. Where the wild-type strain grows normally on the selection plate, the *Sp*Sts5 shows limited growth at the highest concentration of spotted cell culture, with a lower density of cells than the wild-type (**Fig. 5.5**). Meanwhile, *Sp*Dis3L2 behaves as expected and shows no surviving cells at all, phenocopying the Δ*ssd1* strain. To further confirm this, I also

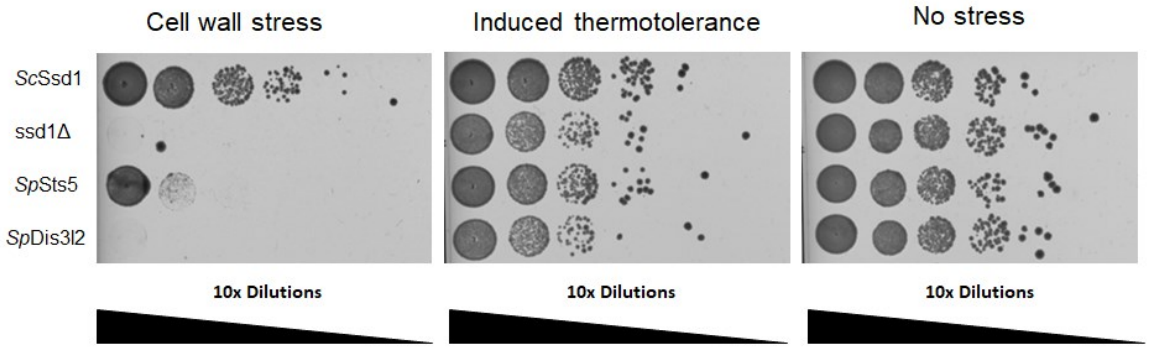

Figure 5.5. Pseudoenzyme *Sp*Sts5 partially complements *Sc*Ssd1 phenotype under cell wall stress and heat stress. Cell wall stress: Wild-type, *ssd1*Δ, and complementation strains spotted on YPD plates supplemented with 50 µM CFW. *Sp*Sts5 partially complements cell wall integrity, while *Sp*Dis3L2 resembles *ssd1*Δ cells with no growth. **Induced thermotolerance:** Strains were incubated at 37 ºC for 30 minutes followed by 50 ºC for another 30 minutes and then spotted onto YPD plates. *Sp*Sts5 partially complements this phenotype, showing reduced density compared to wild-type. *Sp*Dis3L2 shows reduced survival, similar to *ssd1*Δ phenotype. **No stress:** Strains spotted onto a YPD plate with no stress grow normally. The control spot assays are the same ones previously shown in Fig. 5.4. These complementation strains were constructed in the wild-type background.

tested the *Sp*Sts5 and *Sp*Dis3L2 complemented into the ∆*ssd1* background, and saw the same results.

The next step was to test the complemented strains for induced thermotolerance as previously described. My results for this test showed similar results to the Calcofluor white assay. The *Sp*Sts5 complementation strain partially complemented the function of *Sc*Ssd1: it prompted thermotolerance, but with a lower survival rate than the wild-type. Meanwhile, *Sp*Dis3L2 did not complement the function at all (**Fig.5.5**).

My results show a clear pattern of *Sp*Sts5 complementation strains displaying a phenotype similar to the wild-type strain but with lower cell density, while *Sp*Dis3L2 displays severely reduced growth much like ∆*ssd1*. These phenotypes were reproducible in strains complemented both into the wild-type and ∆*ssd1* backgrounds.

The results of these phenotypic tests tell us that phylogenetic predictions on sequence features can help predict conservation of some molecular functions. I was able to predict that *S. pombe* Dis3L2 would not complement the molecular function of ScSsd1 due to their structural differences. However, *Sp*Sts5 only partially complemented the role of Ssd1 in cell wall integrity and induced thermotolerance despite sharing a conserved structure and binding motif with *Sc*Ssd1.

5.4 Discussion

5.4.1 *Sc*Ssd1 can be used as a model to study the function of Ssd1 homologs in closely related fungi

Previous studies documented the role of Ssd1 in stress adaptation, virulence, cell wall integrity, and induced thermotolerance in different fungi (Kaeberlein and Guarente, 2002; Wheeler *et al.*, 2003; Gank *et al.*, 2008; Hogan *et al.*, 2008; Mir, Fiedler and Cashikar, 2009). Homologs of Ssd1 exist in fungi such as *C. glabrata, C. albicans*, *S. pombe, Cryptococcus neoformans,* and *Aspergillus fumigatus.* The loss of Ssd1 affects the fungal cell wall and leads to increased sensitivity to cell wall disrupters and to decreased cell survival. This phenotype was seen in *S. cerevisiae* and *C. albicans* upon deletion of Ssd1 and disruption with the chitin-binding CFW (Song *et al.*, 2008; Bayne *et al.*, 2022). *C. glabrata* similarly shows decreased resistance to the β(1,3)-d-glucan inhibitor, caspofungin, upon loss of Ssd1 (Healey *et al.*, 2020). Furthermore, a study published in 1998 showed that *Ca*Ssd1 functions similarly to *Sc*Ssd1 (Chen and Rosamondt, 1998). In this study, *Ca*Ssd1 was expressed from a plasmid in *S. cerevisiae* to test its ability to substitute for *Sc*Ssd1 and rescue a growth phenotype. The results showed that *Ca*Ssd1 can indeed suppress temperature-sensitive mutations and restore growth, much like an Ssd1-viable (Ssd1-v) strain (Sutton, Immanuel and Arndt, 1991; Evans and Stark, 1997; Chen and Rosamondt, 1998). My results clearly replicate the findings of this study on the ability of *Ca*Ssd1 to function in place of *Sc*Ssd1.

Additionally, my results confirm the role of Ssd1 for cell wall integrity. Under cell wall stress, complementation of *S. cerevisiae* Ssd1 with homologous *Ca*Ssd1 and *Cg*Ssd1*,* respectively, protects the cells under cell wall stress. Strains complemented with these homologs show a phenotype similar to the wild-type under both tested conditions; preserving *Sc*Ssd1 molecular function in the wild-type and restoring it in the *ssd1*Δ background. These results were expected in light of previously published phenotypes, and due to the conserved structural features in my tested homologs.

Another level of conservation that is worth noting is the likely conserved regulation of Ssd1 homologs. Homologous Ssd1 pseudoenzymes show conserved regulation by the cell wall biogenesis kinase (Cbk1), which is part of a network that regulates cell proliferation and morphogenesis (Jansen *et al.*, 2009; Kurischko, Kim, *et al.*, 2011). Cbk1 regulates morphogenesis and promotes a daughter-specific transcriptional program to regulate the asymmetry between mother and daughter cells (Colman-Lerner, Chin and Brent, 2001; Weiss *et al.*, 2002; Jansen *et al.*, 2009). The deletion of *Sc*Ssd1 suppresses the lethality of Cbk1 suppression (Jansen *et al.*, 2009). This is because Cbk1 regulates translation of mRNA by phosphorylating *Sc*Ssd1 at the N-terminus (**Fig. 5.5A)**, thus releasing the translational repression of target mRNAs and allowing production of the encoded proteins. This regulation by Cbk1 is conserved in the *Ca*Ssd1 homolog, where Cbk1 phosphorylates *Ca*Ssd1 at phosphorylation sites in the N-terminus to regulate hyphal growth and

morphogenesis (Lee *et al.*, 2015). This conservation extends to *S. pombe* where a Cbk1-ortholog Orb6 phosphorylates *Sp*Sts5 (Nuñez *et al.*, 2016) (5.4.2.).

The experiments in this chapter were carried out with the purpose of showing that the role of Ssd1 homologs is conserved across fungal species, in a way that allows the use of *Sc*Ssd1 as a model for studying Ssd1 mechanism of function. This is particularly important for investigating and attenuating the pathway of virulent Ssd1 homologs in pathogenic fungi. my results show that Ssd1 homologs from the pathogenic *C. albicans* and *C. glabrata* can replace *Sc*Ssd1 and restore its function in *S. cerevisiae.*

This further proves that *Sc*Ssd1 acts within pathways that *Ca*Ssd1 and *Cg*Ssd1 interact with, leading to the ability to act in place of *Sc*Ssd1. In combination with the conserved sequence features (**Fig. 5.1B, Fig.5.1C)**, and the previously published conserved Cbk1 regulation (Jansen *et al.*, 2009; Lee *et al.*, 2015; Nuñez *et al.*, 2016), this shows that clarifying the RNA-binding interactions and mechanism of *Sc*Ssd1 can offer insight into the homologous mechanisms of *Ca*Ssd1 and *Cg*Ssd1.

5.4.2 Dissimilar regulation hinders ability of *S. pombe* Sts5 to restore Ssd1 activity in *S. cerevisiae*

Despite the conserved structure features and RNA-binding function with other Ssd1-homologs, *Sp*Sts5 only partially complemented the role of *Sc*Ssd1 in cell wall integrity and induced thermotolerance. This was an unexpected result for *Sp*Sts5. Following this result, I consulted the literature and found that while Sts5 has a role in polarized growth, it is not required for cell wall integrity in *S. pombe,* unlike *Sc*Ssd1 in *S. cerevisiae* (Toda *et al.*, 1996; Kaeberlein and Guarente, 2002; Nuñez *et al.*, 2016). Perhaps it is reasonable then to assume that *Sp*Sts5 wouldn't complement a cell wall integrity phenotype in *S*c, but this partial complementation also extends to induced thermotolerance phenotype. Therefore, I wanted to pursue further differences between the homologs to understand what might be causing *Sp*Sts5 to behave differently. This investigation led us to another notable dissimilarity between *Sc*Ssd1 and *Sp*Sts5. Although *Sp*Sts5 is regulated by the Cbk1 ortholog Orb6, it exhibits some differences in number of phosphorylation motifs and related sequence features compared to *Sc*Ssd1 and Ssd1-like homologs (**Fig. 5.5B**).

Previous studies suggest that *Sp*Sts5 recruitment into ribonucleoprotein granules and P-bodies is negatively regulated by the Orb6 kinase (Nuñez *et al.*, 2016). This in turn controls the translational repression of mRNAs encoding proteins with roles in polarized growth and cell separation in *S. pombe*. Despite the conservation of this regulation step by Cbk1 and orthologous Orb6, Ssd1 homologs diverge in a sequence feature that confers the Cbk1 docking site. *Sc*Ssd1 alongside *Ca*Ssd1 and *Cg*Ssd1 all contain a Cbk1 docking site which enhances phosphorylation, while *Sp*Sts5 lacks this feature (**Fig. 5.6B**) (Ballou, Cook and Wallace, 2021). Furthermore, phosphorylation motifs are highly conserved in Ssd1 homologs despite a poorly aligned N-terminal domain (Ballou, Cook and Wallace, 2021). However, *Sc*Ssd1 has seven instances of the phosphorylation motif, whereas *Sp*Sts5 only has two phosphorylation motifs (Ballou, Cook and Wallace, 2021). Thus, it is a possibility that *Sp*Sts5 is not phosphorylated by Orb6/Cbk1 at the same rate as native *Sc*Ssd1 or the Candida Ssd1 homologs. If that is the case, it might cause a higher translational repression rate of target mRNAs, resulting in less protein products to act in cell wall biogenesis and stability. The other possibility is that *Sp*Sts5 might be binding a different set of mRNAs than *Sc*Ssd1, thus acting in different functions.

A)

B)

Ssd1 locus	Cbk1 dock site	RNA binding	RNII active site
*Sp*Dis3L2	+	-	-
*Sp*Sts5	-	+	-
*Ca*Ssd1	+	+	-
*Cg*Ssd1	+	+	-
*Sc*Ssd1	+	+	+

Figure 5.6. *Sp*Sts5 has similar sequence features to other Ssd1 pseudoenzymes, except for the loss of a Cbk1 docking site. A) Schematic of Ssd1/Dis3L2 protein family features. **B)** A table comparing features between Ssd1 homologs shows that *Sp*Sts5 has lost its active site and evolved an RNA-binding feature like other pseudoenzymes, however it has no Cbk1 docking site.

Another possibility is that *Sp*Sts5 is not expressed at the same level as *Sc*Ssd1 in my strains. Although I expressed the Ssd1 homologs under the native *Sc*Ssd1 promoter (5.3.1), I did not check protein expression levels in my complemented

strains compared to *Sc*Ssd1 in wild-type. It is therefore possible that *Sp*Sts5 was expressed at a lower level in these strains, leading to the partial complementation phenotype. Future work could address this by measuring Ssd1 expression in the complemented strains and the wild-type (4.3).

The induced thermotolerance phenotype was also partially complemented by *Sp*Sts5, while *Ca*Ssd1 and *Cg*Ssd1 retained wild-type behaviour. Previous studies show that Ssd1 is required for induced thermotolerance and affects the aggregation of heat shock protein 104 (Hsp104) during stress (Mir, Fiedler and Cashikar, 2009). Hsp104 is a heat shock protein, with a role in protein disaggregation, that is also required for induced thermotolerance in yeast (Lindquist and Kim, 1996). During stress, Hsp104 is diffuse in wild-type cells but appears in a punctate pattern in *ssd1*Δ cells (Mir, Fiedler and Cashikar, 2009). This suggests that Ssd1 might be required for Hsp104-mediated protein disaggregation in *S. cerevisiae*. A cell under stress would use available resources rather than synthesize new proteins (Martínez-Pastor and Estruch, 1996; Ashe, De Long and Sachs, 2000; Crawford and Pavitt, 2019), therefore, it is possible that the partial complementation phenotype in *Sp*Sts5 is also due to decreased phosphorylation which leads to a reduced number of “free” Sts5 proteins in the cell. However, it is not understood how *Sc*Ssd1 contributes to heat stress phenotypes. The role and mechanism of action of ScSsd1 in heat stress is likely different to its function in cell wall stress, and therefore it is also possible that this function is an *Sc*Ssd1 specific process that does not extend to the *S. pombe* homologs.

Meanwhile, the nuclease *Sp*Dis3L2 does not complement *Sc*Ssd1 function at all. This result was expected, because unlike the other Ssd1 homologs; *Sp*Dis3L2 retained the active site allowing catalytic activity. In fact, *Sp*Dis3L2 is a nuclease that is involved in cytoplasmic mRNA degradation in *S. pombe* (Malecki *et al.*, 2013). Therefore, it is possible that the structure and catalytic function of *Sp*Dis3L2 makes it unable to bind the mRNA transcripts usually bound by *Sc*Ssd1. If that is the case, Dis3L2 would be unable to protect the cell against cell wall or heat stress, which would lead to a reduced rate of survival of cells. However, more experiments are needed to test this hypothesis.

5.5 Future work

Several questions about Ssd1 mechanism and evolution remain unanswered. Here I propose further complementation studies that could address them. I postulate that experiments with a focus on protein expression, inter-molecular interactions, and phosphorylation, can be used to elucidate the mechanism of function of Ssd1 and its homologs. Additionally, complementation with informative homologs could further clarify the evolution of Ssd1, and the emergence of its RNA-binding function. I was unable to pursue these experiments due to time limitations. However, I propose that the strains from this chapter could be used for the following experiments or used for constructing more informative strains.

5.5.1 Is partial complementation by *Sp*Sts5 caused by reduced phosphorylation or lower *Sp*Sts5 expression levels?

Homologs can be tagged with a fluorescent protein or an epitope tag to measure expression levels, and to track the localization of the Ssd1-homolog population within the cell. This would be particularly useful in the case of *Sp*Sts5 and *Sc*Ssd1 to compare expression levels, and observe if there is a bigger proportion of *Sc*Ssd1 unbound from mRNA compared to unbound *Sp*Sts5. Ssd1 expression levels in test and control strains, as well as free vs bound Ssd1 populations, could also be measured using an epitope tag and western blot. Higher levels of free (unbound) *Sc*Ssd1 compared to *Sp*Sts5 might explain the partial complementation phenotype affected by Cbk1 phosphorylating and releasing *Sp*Sts5 at a decreased rate compared to the other homologs. The partial complementation could also be due to lower *Sp*Sts5 expression as previously discussed.

5.5.2 How conserved is the Ssd1 pathway: is the regulation of Ssd1 and its interactions with other RBPs similar in Ssd1 homologs?

Further experiments could also target phosphorylation motifs in the other homologs, or simply overexpress *Sp*Sts5 to observe the effect of overexpression on the complementation phenotype. This could be achieved through manipulations to the promoter and terminator regions, or by placing *Sp*Sts5 on an overexpression plasmid. Another set of experiments could tackle protein interactions by complementing into different mutant backgrounds, to observe the interactions with other RBPs and regulators such as Cbk1. In such experiments, complementation strains could be used as the background to tag Ssd1-homologs and RBPs of interest or Cbk1 with fluorescent reporter proteins to observe co-localization. These experiments would use *Sc*Ssd1 as a control/reference strain, and serve to clarify the network Ssd1 and its homologs work within. This knowledge can be carried out and implemented in other species such as *C. albicans* to observe if Ssd1-homologs work within the same networks and if there is a pathway to be targeted there to attenuate Ssd1 -thus attenuating virulence.

5.5.3 Do structural features or catalytic activity predict conservation of function in more distantly related fungi?

Another human pathogen of interest is the human pathogen *Cryptococcus neoformans.* The *C. neoformans* Ssd1 (*Cn*Ssd1) acts in growth and morphology of C. *neoformans* (Gerik *et al.*, 2005; Ballou, Cook and Wallace, 2021). It is also known that the *C. neoformans* Ssd1 homolog has a number of structural features resembling the inactive Ssd1 homolog, yet it retains a nuclease active site much like Dis3 enzymes (Ballou, Cook and Wallace, 2021). This makes *Cn*Ssd1 a homolog of interest to answer the question of whether structural features or catalytic activity can predict conservation of functionality. Which is to say: I don't know if *Cn*Ssd1 would complement the function of *Sc*Ssd1, but I did design primers with the intention of finding out (**Table 5.1**)**,** so this question could be tackled in the future.

5.5.4 What are the functions of Ssd1 homologs in filamentous fungi?

Another set of interesting Ssd1 homologs and orthologs that can be used for complementation are found in plant pathogens. It is known that the conservation of Ssd1 function extends to plant pathogens, as previous studies showed that a homolog of Ssd1 in *Fusarium oxysporum*, encoded in FOR3, can complement the *S. cerevisiae* Ssd1 (Lee *et al.*, 2010). This complementation confers resistance to the plant's defence protein osmotin to an osmotin-sensitive strain of *S. cerevisiae* (Lee *et al.*, 2010). Another study shows that orthologs of *Sc*Ssd1 work as regulators of cell wall assembly, and are required for pathogenicity in the cucumber anthracnose fungus, *Colletotrichum lagenarium*, and the rice blast fungus, *Magnaporthe grisea* (Tanaka *et al.*, 2007). This study shows that *C. lagenarium* SSD1 (*Cla*SSD1), expressed from a plasmid with an inducible GAL1 promoter, can functionally complement *Sc*Ssd1 and prevent caffeine hypersensitivity when complemented into *ssd1*Δ background (Tanaka *et al.*, 2007). Therefore, given more time, I would have extended my complementation experiments to include plant pathogens, to examine if *Sc*Ssd1 can be used as a model to study the functionality of its homologs in plants. This would be another avenue of pathways to target for attenuating virulence.

5.5.5 When did Ssd1 functions change in evolution?

The *Sp*Sts5 pseudoenzyme partially restores *Sc*Ssd1 function, while the *Sp*Dis3L2 enzyme does not. Despite *Sp*Sts5 and *Sp*Dis3L2 belonging to Taphrinomycotina, *Sp*Sts5 is more similar to the Saccharomycotina *Sc*Ssd1. This means that somewhere along the evolutionary path the function of Ssd1 diverged, however I do not know when or why that change happened. I propose that complementation studies using informative modern and ancestral Ssd1 homologs could address these questions. Dr Edward Wallace posits that complementation with ancestral proteins reconstructed from phylogenetic analysis (Harms and Thornton, 2010; Ballou, Cook and Wallace, 2021), could locate the emergence of the RNA-binding site in Ssd1 evolutionary history. Such results would answer the question of when Ssd1 evolved an RNA-binding function in fungal species, and might shed light on the life-style necessitating this evolution (Ballou, Cook and Wallace, 2021).

6 Conclusion and remaining future work

The regulation of fungal cell wall is an intricate process that requires precise spatial and temporal control. In my research project, I attempted to address some of the elements regulating fungal cell walls by investigating their specific targets, and examining the mechanisms by which these regulators operate. Below, I summarise some results and suggest future work that could build on my observations.

6.1 How do 3' UTRs contribute to transcriptional regulation?

I first started by investigating the role of RBPs and 3' UTRs on the localization and expression of the cell wall proteins Sun4 and Srl1. In chapter 3, I found that altering the 3' UTR leads to increased expression for Sun4, which suggests that such alteration hinders regulation of this protein. I also found that the deletion of Mpt5 increases Sun4 but not Srl1 expression. Suggesting that Mpt5 is more strongly involved in regulating Sun4, possibly through mRNA decay. This is particularly interesting in light of Mpt5 binding the 3' region of *SUN4* mRNA (Hogan *et al.*, 2008). In chapter 4, I tested the effect of deleting Mpt5 on the localization of its target mRNAs, and found no evidence that Mpt5 deletion leads to mis-localization. However, my smFISH experiments did not test 3' UTR alterations. I previously mentioned that other RBPs such as Puf2 also bind the 3' UTR of *SUN4* (Porter *et al.*, 2015). Puf2 can act as translational repressor or cause mRNA decay (Goldstrohm *et al.*, 2006). Therefore, using smFISH to visualize the localization and expression of *SUN4* with an altered 3' UTR could be informative on how 3' UTRs contribute to regulation at the transcriptional level for RNAs encoding cell wall and cell cycle proteins. My current results show that 3' UTRs contribute to post-transcriptional regulation, and should be considered when investigating protein expression or localization. Future work could build on the strains I constructed for chapter 3 and observe transcriptional regulation of *SRL1* and *SUN4* via 3' UTRs.

Another question that arises from my results is the effect of 3' UTRs on cell size.

6.2 Does bigger cell size caused by *SSD1* deletion affect the cell cycle and cell wall integrity?

In chapter 3, my first interesting result was that the deletion of the RBP Ssd1 leads to increased cell size, as does the deletion of the translocon complex Sec72. Deletion of Ssd1 increased protein expression for both Sun4 and Srl1 proteins. This led me to wonder whether the increased protein expression could be a burden to the cell, and leading to a weakened cell wall. It is unclear whether the cell wall defects in Δ*ssd1* are a product of increased cell size and protein overproduction, or if the increased cell size is the product of a weakened cell wall. Previous studies showed that cell size sensing and cell cycle initiation takes cell content into account (Talia *et al.*, 2007). This led me to wonder whether the deletion of Ssd1 drives cells into starting

the cell cycle, or budding before they are ready; either by increased cell size or increased protein expression.

Following the logic of protein overexpression leading to possible cell wall defects, naturally leads to question the combined effect of an altered 3' UTR and *SSD1* deletion on the cells. I showed in my results that proteins tagged with mNeonGreen and an altered terminator (tADH1) show the highest fluorescence, thus; highest tagged protein content, in the Δ*ssd1* background. This can be utilised for observing the effect of protein overexpression on the length of the cell cycle. Comparing the budding rate and the length of cell cycle between wild-type and Δ*ssd1*, with proteins tagged under native and altered terminators, could clarify the effect of Δ*ssd1* and protein overexpression on the cell cycle. These strains could be imaged, in combination with mCherry-labelled cell markers such as a Spc72, which is localized to the spindle pole body, or the α-tubulin gene (Tub1) (Maekawa *et al.*, 2017) could be used in combination to monitor the cell cycle stage and its duration. Meanwhile, experiments phenotyping cell wall sensitivity of these strains could elucidate whether the weakened cell wall phenotype is amplified or rescued by protein overexpression.

6.3 How are post-transcriptional and transcriptional regulators cooperating to regulate other target cell wall and cell cycle proteins?

In chapter 3, I did not find clear evidence implicating Ssd1 in the localization of the protein products of its target mRNAs. I found that, regardless of *SSD1* deletion, Sun4 localized to the bud neck while Srl1 localized to the periphery of the bud as described in previous studies (Mouassite *et al.*, 2000; Shepard *et al.*, 2003), which is consistent with their roles in cell septation and cell wall stability. Both transcript mRNAs of these proteins are also bound by transcriptional regulators from the PUF family (chapters 3 and 4). I discussed in previous chapter how future work could address transcriptional and post-transcriptional regulation in *SUN4* and *SRL1*, however; this question extends to other target Ssd1 transcripts. For instance, Ssd1 binds mRNAs encoding a glucanase (*DSE2*) and a chitinase (*CTS1*). *DSE2* and *CTS1* are both induced by the Ace2 transcription factor to contribute to cell separation by degrading the cell wall (Colman-Lerner, Chin and Brent, 2001). DSE2 interacts with Mpt5 (Miller *et al.*, 2017), and both *DSE2* and *CTS1* interact with Puf2 and Puf3 (Freeberg *et al.*, 2013; Porter *et al.*, 2015) which can cause mRNA decay. Thus, DSE2 and CTS1 are two more candidates to tackle in future work, to understand coordinated delivery and regulation of protein expression, via post-transcriptional (translational repression) and transcriptional (mRNA turnover) regulation.

Future work could address this regulation using smFISH. Mutations to binding sites of Ssd1 or/and PUF binding sites, coupled with extracting samples from defined time points, could elucidate mRNA expression and localization of these transcripts at different points of the cell cycle. Cell cycle markers discussed before, such as *TUB1* and *CLB2*, can be used for monitoring mRNA levels at different points in the cell cycle.

6.4 How do we define Sun4 localization throughout the cell cycle?

The precise localization of Sun4 protein throughout the cell cycle is still unknown. My results show Sun4 localization to the bud neck of the budding daughter in chapter 3 **(Fig. 6.1A**). Additionally, through the use of the fluorescent protein mNeongreen and pH as reporters on Sun4 localization (chapter 3), I also found that Sun4 is localized to the outer cell surface. However, it is difficult to decipher at which point of the cell cycle this happens, and whether some of the protein content I see is in the cytoplasm or on the cell surface. Future work could use markers such as Cdc10p to observe co-localization within of Sun4 and Cdc10 in the bud neck, and possibly at birth and bud scars (**Fig. 6.1B**). Bud scars can be stained with calcofluor white (CFW) to clarify protein localization to these scars on the cell surface as shown in previous studies (Sorokin, Knorre and Severin, 2014). This understanding of the localization of Sun4, will help us better understand its contribution to cell wall functions in *S. cerevisiae*, and how the protein localizes at different stages of the cell growth. Such knowledge could also be used to explore the implications for *SUN4* mRNA transport and localized translation.

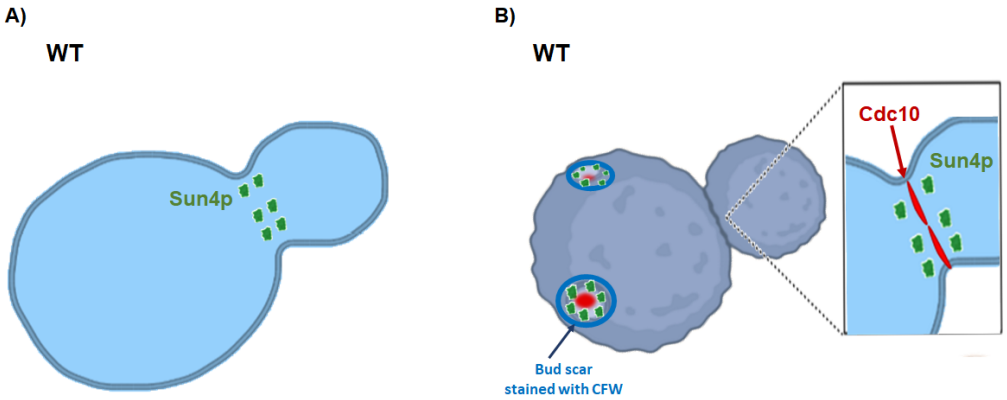

Figure 6.1. Monitoring Sun4 localization with relevant cell marker can elucidate localization patterns throughout the cell cycle. A) My results in previous chapters showed that Sun4 localizes to the bud neck. **B)** Future experiments utilising Cdc10 and CFW staining could elucidate Sun4 localization to the cell surface and bud scars.

6.5 In summary

In my results chapter on Ssd1 homologs and complementation; I showed that Ssd1 is a protein of interest for its existence across different fungal species, and its importance for virulence and cell wall integrity in each. The rationale of the experiments in that chapter was to show that conservation of the role and regulation of *Sc*Ssd1 exists as to allow using it as a model for studying other Ssd1 homologs.

My results in that chapter, combined with the discussed published studies on Ssd1, validate this approach. In previous chapters, my results indicated that Ssd1 might be acting as a translational repressor, but might also be contributing to polarized mRNA transport in cooperation with the RBPs She2 and She3. Flow cytometry results showed that deletion of the RBP Mpt5 causes increased protein expression of some Ssd1 targets. Combined with the localization of target mRNAs *SUN4* and *SRL1* is dependent on the cell cycle, observed by smFISH; this collection of results suggests that Ssd1 might be contributing to processes such as mRNA stability and localized degradation, in cooperation with Mpt5 and possibly other PUF family proteins, to regulate the *S. cerevisiae* cell cycle and consequently regulate the cell wall.

These results across my thesis only address a very small number of post-transcriptional regulators of the *S. cerevisiae* cell wall and its proteins, with a focus on Ssd1 conservation in other fungal species. Overall, my results should encourage future work and investment in elucidating the mechanism and evolution of RBPs such as Ssd1, in *S. cerevisiae* and their contribution to regulation of the fungal cell wall. Such studies in *S. cerevisiae* can be used as a guide for investigating homologous mechanisms in other fungal species.

7 Appendix

7.1 Supplementary figures

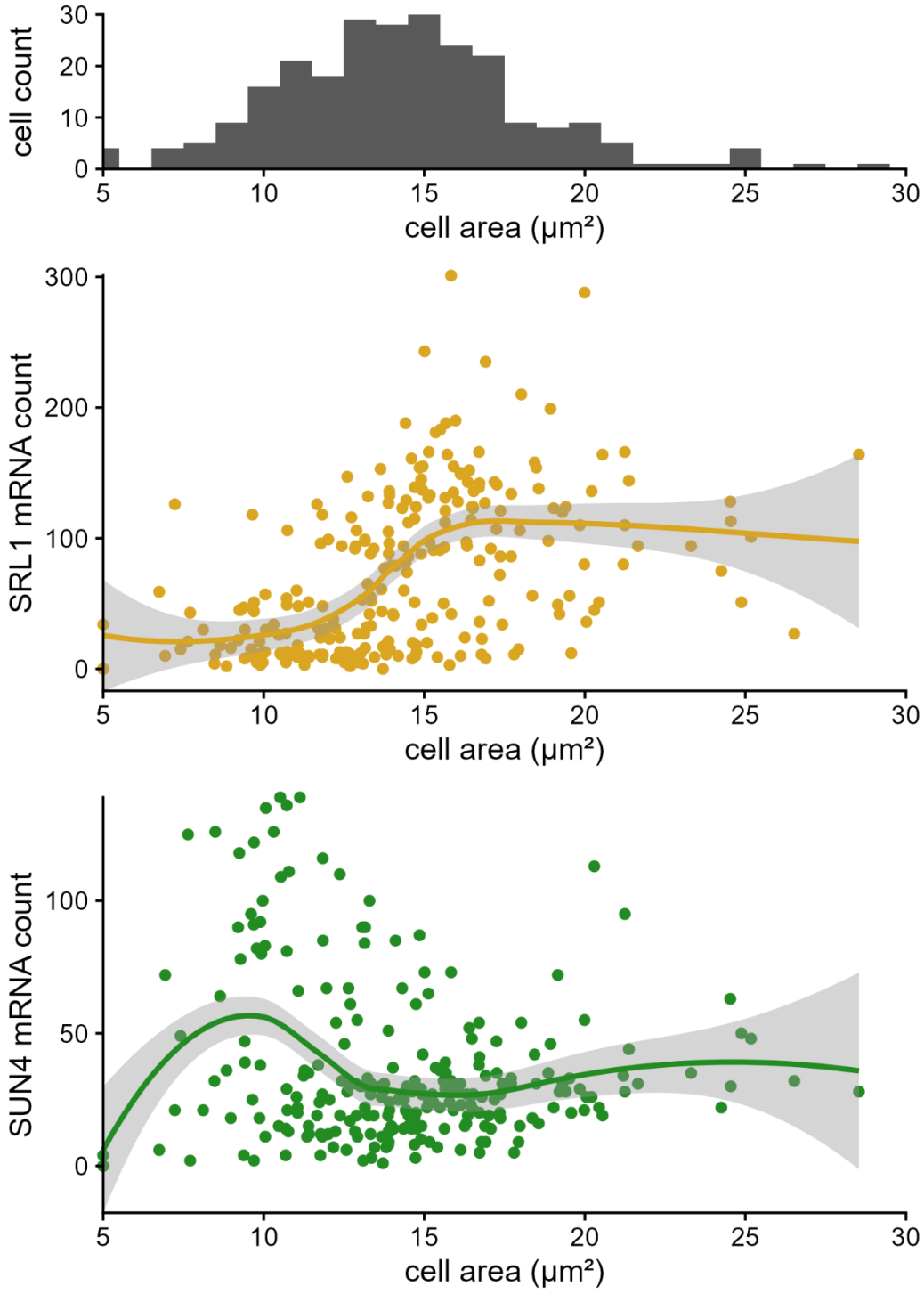

Figure 7.1. smFISH quantification: mRNA count per cell by cell area (μm²) in wild-type biological replicate one. Upper panel: Cell count of whole (mother and bud) cells on the Y axis by cell area (μm²) on the X axis. **Middle panel:** The Y axis shows total *SRL1* mRNA per cell in yellow, against the cell area in μm² on the X axis. **Bottom panel:** The Y axis shows total *SUN4* mRNA per cell in green, against the cell area in μm² on the X axis.

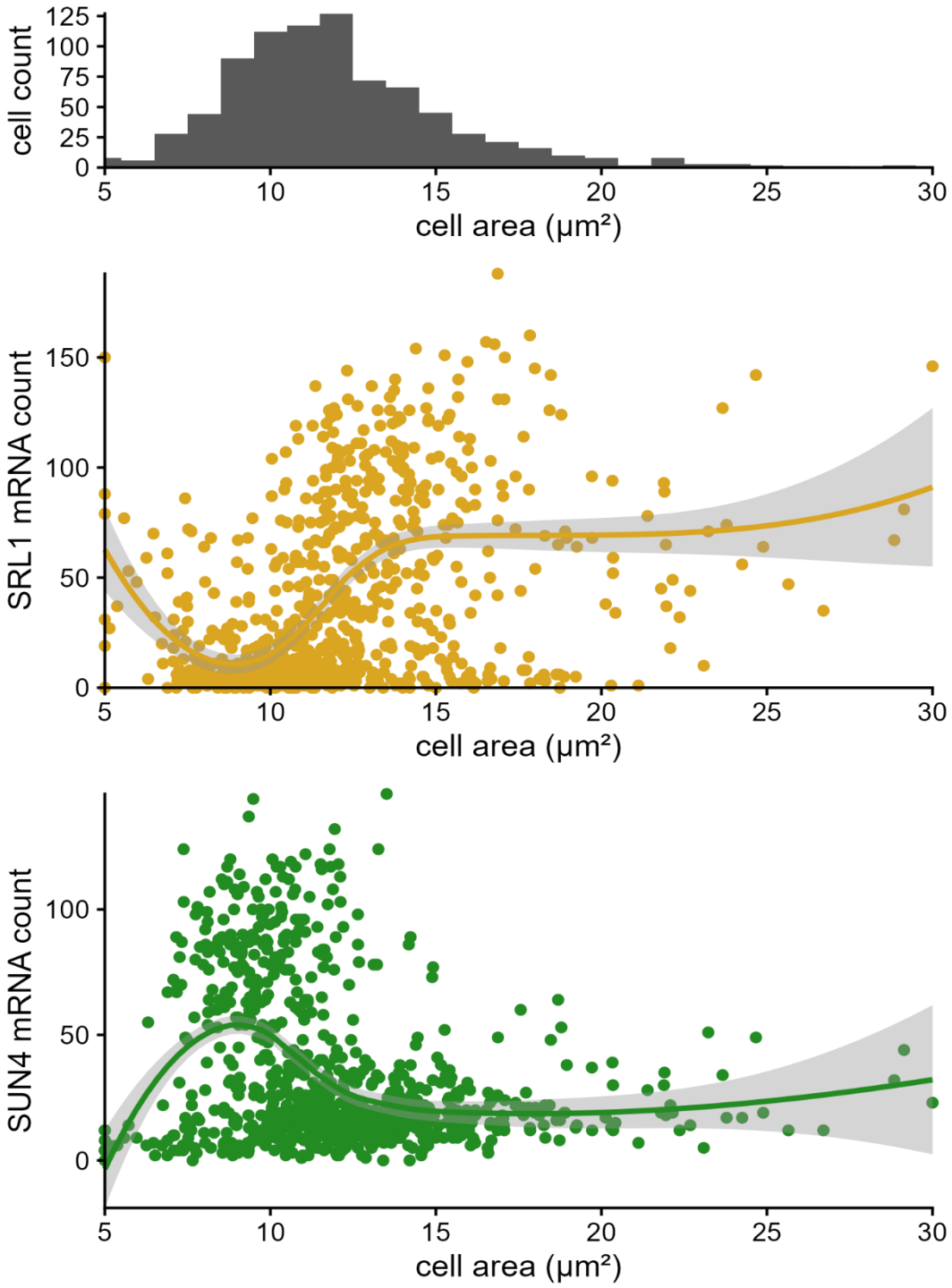

Figure 7.2. smFISH quantification: mRNA count per cell by cell area (μm^2) in wild-type biological replicate two. Upper panel: Cell count of whole cells on the Y axis by cell area (μm^2) on the X axis. **Middle panel:** The Y axis shows total *SRL1* mRNA per cell in yellow, against the cell area in μm^2 on the X axis. **Bottom panel:** The Y axis shows total *SUN4* mRNA per cell in green, against the cell area in μm^2 on the X axis.

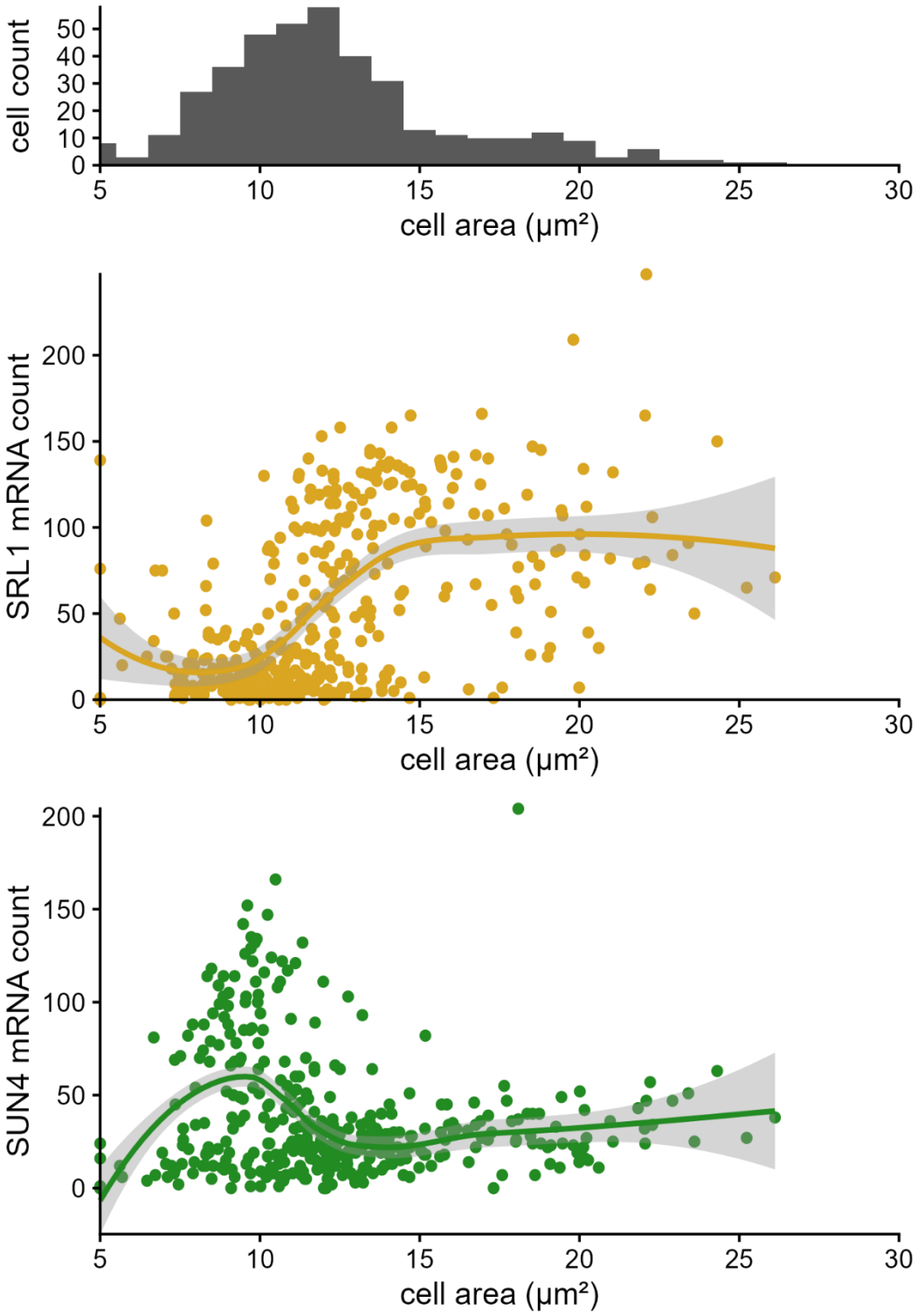

Figure 7.3. smFISH quantification: mRNA count per cell by cell area (μm²) in wild-type biological replicate three. Upper panel: Cell count of whole cells on the Y axis by cell area (μm²) on the X axis. **Middle panel:** The Y axis shows total *SRL1* mRNA per cell in yellow, against the cell area in μm² on the X axis. **Bottom panel:** The Y axis shows total *SUN4* mRNA per cell in green, against the cell area in μm² on the X axis.

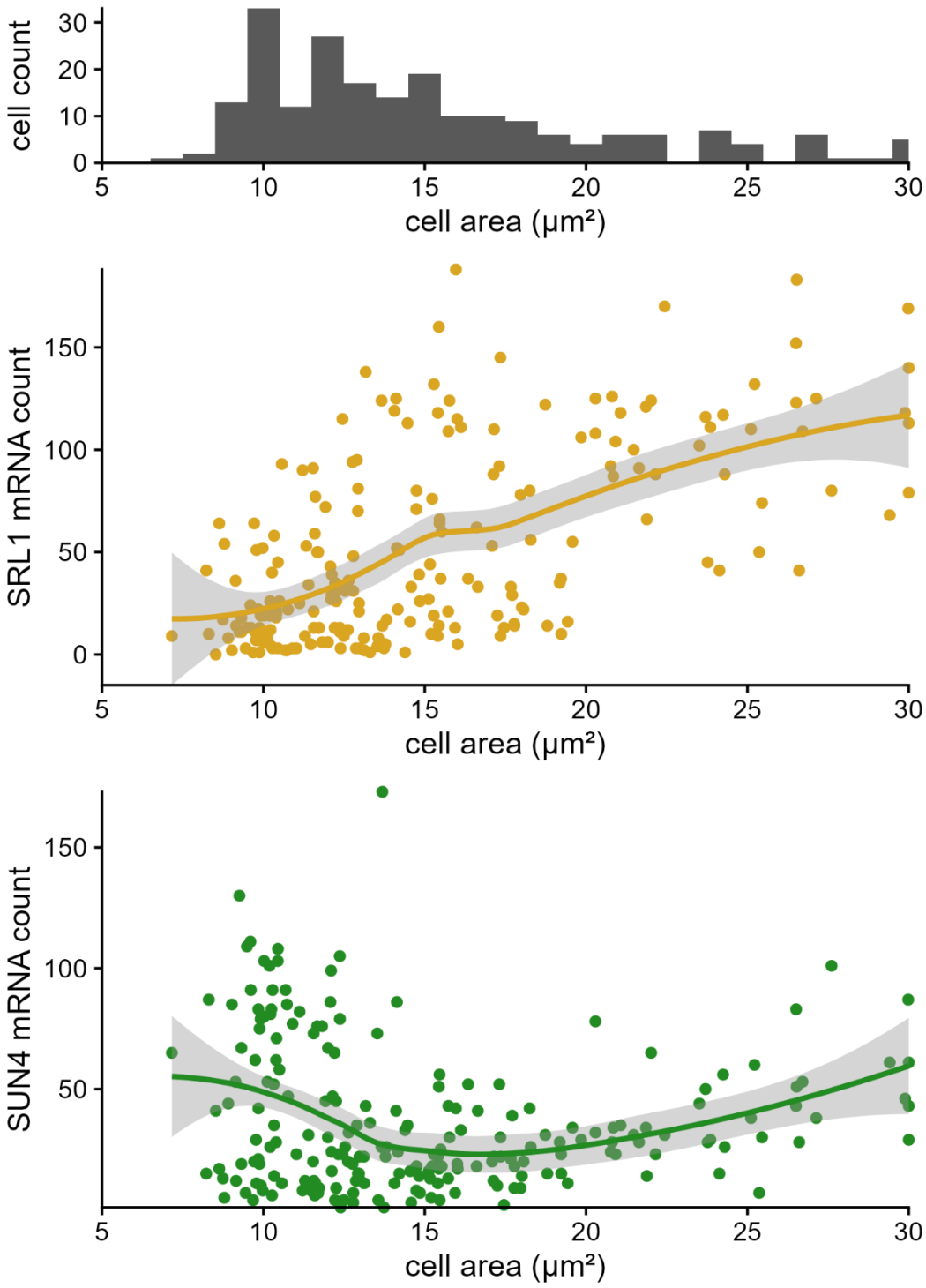

Figure 7.4. smFISH quantification: mRNA count per cell by cell area (μm²) in Δ*ssd1* biological replicate one. Upper panel: Cell count of whole cells on the Y axis by cell area (μm²) on the X axis. **Middle panel:** The Y axis shows total *SRL1* mRNA per cell in yellow, against the cell area in μm² on the X axis. **Bottom panel:** The Y axis shows total *SUN4* mRNA per cell in green, against the cell area in μm² on the X axis.

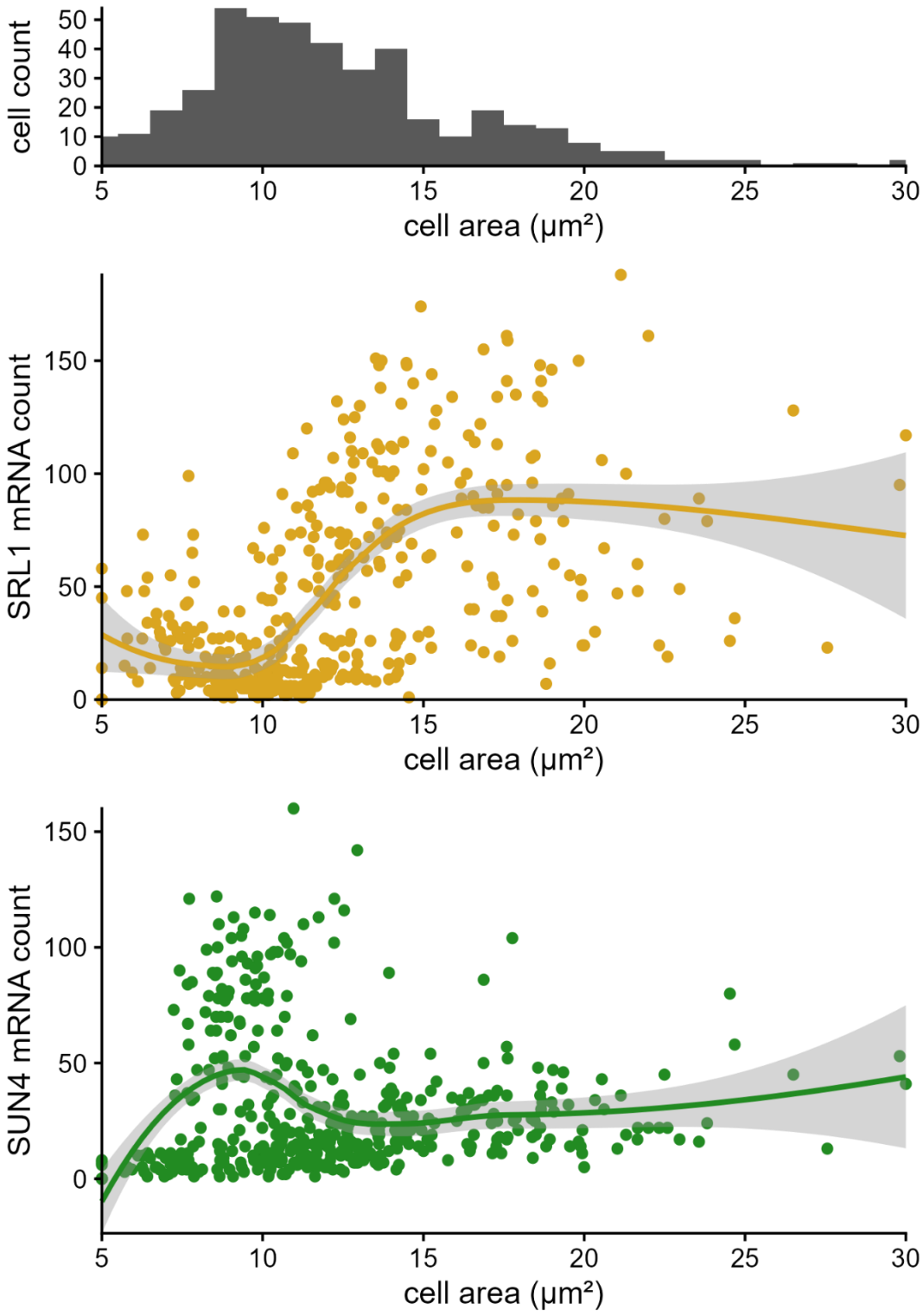

Figure 7.5. smFISH quantification: mRNA count per cell by cell area (μm²) in Δ*ssd1* biological replicate two. Upper panel: Cell count of whole cells on the Y axis by cell area (μm²) on the X axis. **Middle panel:** The Y axis shows total *SRL1* mRNA per cell in yellow, against the cell area in μm² on the X axis. **Bottom panel:** The Y axis shows total *SUN4* mRNA per cell in green, against the cell area in μm² on the X axis.

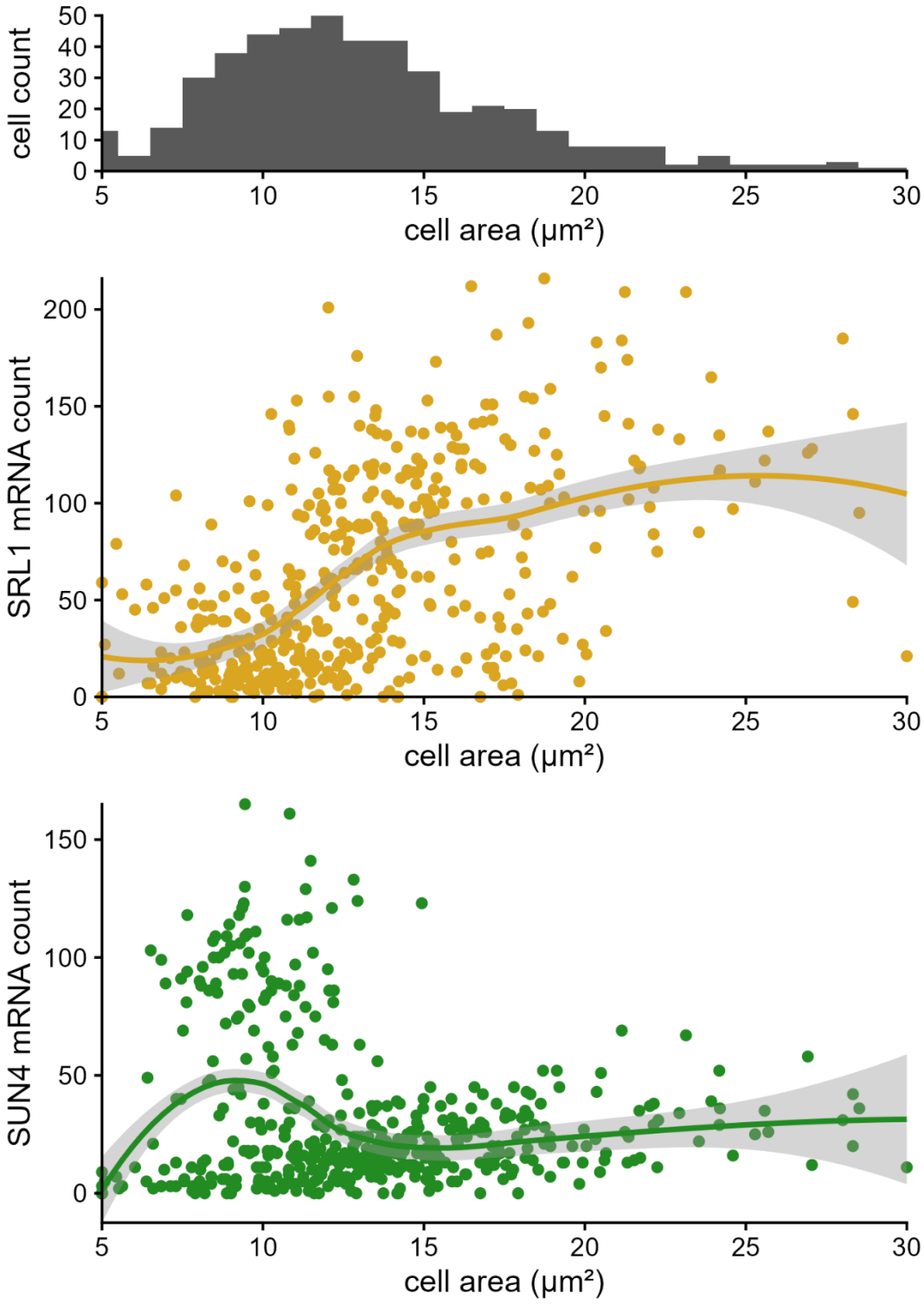

Figure 7.6. smFISH quantification: mRNA count per cell by cell area (μm²) in Δ*ssd1* biological replicate three. Upper panel: Cell count of whole cells on the Y axis by cell area (μm²) on the X axis. **Middle panel:** The Y axis shows total *SRL1* mRNA per cell in yellow, against the cell area in μm² on the X axis. **Bottom panel:** The Y axis shows total *SUN4* mRNA per cell in green, against the cell area in μm² on the X axis.

7.2 Strains used in this study

ID	Description	Genotype	Source
yMJ003	SUN4-mNeonGreen-tADH1, BY4741	*MATa ura3Δ0 leu2Δ0 his3Δ1 met15Δ0; SUN4-mNeonGreen-tADH1 HIS3MX*	This study
yMJ004	SCW4-mNeonGreen-tADH1, BY4741	*MATa ura3Δ0 leu2Δ0 his3Δ1 met15Δ0; SCW4-mNeongreen-tADH1 HIS3MX*	This study
yMJ005	SCW4-mNeonGreen-tADH1, BY4741	*MATa ura3Δ0 leu2Δ0 his3Δ1 met15Δ0; SCW4-mNeongreen-tADH1 HIS3MX*	This study
yMJ007	SRL1-mNeonGreen-tADH1, BY4741	*MATa ura3Δ0 leu2Δ0 his3Δ1 met15Δ0; SRL1-mNeongreen-tADH1 HIS3MX*	This study
yMJ008	SRL1-mNeonGreen-tADH1, BY4741	*MATa ura3Δ0 leu2Δ0 his3Δ1 met15Δ0; SRL1-mNeongreen-tADH1 HIS3MX*	This study
yMJ006	UTH1-mNeonGreen-tADH1, BY4741	*MATa ura3Δ0 leu2Δ0 his3Δ1 met15Δ0; UTH1-mNeongreen-tADH1 HIS3MX*	This study
yMJ009	PHO88-mNeonGreen-tADH1, BY4741	*MATa ura3Δ0 leu2Δ0 his3Δ1 met15Δ0; PHO88-mNeongreen-tADH1 HIS3MX*	This study
yMJ010	PHO88-mNeonGreen-tADH1, BY4741	*MATa ura3Δ0 leu2Δ0 his3Δ1 met15Δ0; PHO88-mNeongreen-tADH1 HIS3MX*	This study
yMJ011	SUN4-mNeonGreen-tADH1, *Δssd1*	*MATa; his3Δ1; leu2Δ0; met15Δ0; ura3Δ0; YDR293c::kanMX4; SUN4-mNeongreen-tADH1 HIS3MX*	This study
yMJ012	SRL1-mNeonGreen-tADH1, *Δssd1*	*MATa; his3Δ1; leu2Δ0; met15Δ0; ura3Δ0; YDR293c::kanMX4; SRL1-mNeongreen-tADH1 HIS3MX*	This study
yMJ013	SCW4-mNeonGreen-tADH1, *Δssd1*	*MATa; his3Δ1; leu2Δ0; met15Δ0; ura3Δ0; YDR293c::kanMX4; SCW4-mNeongreen-tADH1 HIS3MX*	This study
yMJ014	PHO88-mNeonGreen-tADH1, *Δssd1*	*MATa; his3Δ1; leu2Δ0; met15Δ0; ura3Δ0; YDR293c::kanMX4; PHO88-mNeongreen-tADH1 HIS3MX*	This study
yMJ015	SUN4-mNeonGreen, yRB002.3 (FH-SSD1(Nterm) N3) A	*yRB002.3; MATa ura3Δ0 leu2Δ0 his3Δ0 met15Δ0, FH-SSD1 (N-term FLAGAla_4His_8); SUN4_mNeongreen-HIS3*	This study
yMJ016	SUN4-mNeonGreen, Ssd1 Cluster2 mutants; R549E, R622E, R623E	*MATa ura3Δ0 leu2Δ0 his3Δ0 met15Δ0 ssd1-R622E,R623E (C-term His_8Ala_4FLAG); SUN4-mNeongreen-tADH1 HIS3MX*	This study

yMJ017	SUN4-mNeonGreen, Ssd1 Cluster3 mutants; W583E, W585A	*MATa ura3Δ0 leu2Δ0 his3Δ0 met15Δ0 ssd1-W583A,K585A (C-term His_8Ala_4FLAG); SUN4-mNeongreen-tADH1 HIS3MX*	This study
yMJ018	C-term SUN4-mNeonGreen, yRB027.5 (Cluster4 mutants) A	*yRB027.5; MATa ura3Δ0 leu2Δ0 his3Δ0 met15Δ0 ssd1-K505E,Q506E,Q510E (C-term His_8Ala_4FLAG); SUN4_mNeongreen-HIS3*	This study
yMJ019	*S. pombe* Sts5, BY4741	*MATa; his3Δ1; leu2Δ0; met15Δ0; ura3Δ0; YDR293C:SPCC16C4.09*	This study
yMJ020	*S. pombe* Dis3l2, BY4741	*MATa; his3Δ1; leu2Δ0; met15Δ0; ura3Δ0; YDR293C:SPAC2C4.07c*	This study
yMJ021	*S. pombe* Sts5, Δssd1	*MATa; his3Δ1; leu2Δ0; met15Δ0; ura3Δ0; YDR293C:SPCC16C4.09*	This study
yMJ022	*S. pombe* Dis3l2, Δssd1	*MATa; his3Δ1; leu2Δ0; met15Δ0; ura3Δ0; YDR293C:SPAC2C4.07c*	This study
yMJ023	*C. albicans* Ssd1, Δssd1	*MATa; his3Δ1; leu2Δ0; met15Δ0; ura3Δ0; YDR293C:C5_04730C_A*	This study
yMJ024	*C. glabrata* Ssd1, Δssd1	*MATa; his3Δ1; leu2Δ0; met15Δ0; ura3Δ0; YDR293C:CAGL0J06072g*	This study
yMJ025	*C. albicans* Ssd1, BY4741	*MATa; his3Δ1; leu2Δ0; met15Δ0; ura3Δ0; YDR293C:C5_04730C_A*	This study
yMJ026	*C. glabrata* Ssd1, BY4741	*MATa; his3Δ1; leu2Δ0; met15Δ0; ura3Δ0; YDR293C:CAGL0J06072g*	This study
BY4741	Wild-type	*MATa ura3Δ0 leu2Δ0 his3Δ1 met15Δ0*	Jean Beggs
Δ*ssd1*	ΔYDR293C	*MATa; his3Δ1; leu2Δ0; met15Δ0; ura3Δ0; YDR293C::kanMX4*	H. Tekotte
Δ*scw4*	ΔYGR279C	*MATa; his3Δ1; leu2Δ0; met15Δ0; ura3Δ0; YGR279C::kanMX4*	Edinburgh genome foundry
Δ*sun4*	ΔYNL066W	*MATa; his3Δ1; leu2Δ0; met15Δ0; ura3Δ0; YNL066W::kanMX4*	Edinburgh genome foundry
Δ*mpt5*	ΔYGL178W	*MATa; his3Δ1; leu2Δ0; met15Δ0; ura3Δ0; YGL178W::kanMX4*	Edinburgh genome foundry
Δ*sec72*	ΔYLR292C	*BY4741; MATa; his3Δ1; leu2Δ0; met15Δ0; ura3Δ0; YLR292C::kanMX4*	Edinburgh genome foundry
yMJ027	SUN4-mNeonGreen-tADH1, Δ*sec72*	*MATa; his3Δ1; leu2Δ0; met15Δ0; ura3Δ0; YLR292c::kanMX4; SUN4-mNeongreen-tADH1 HIS3MX*	This study

yMJ028	SUN4-mNeonGreen-tADH1, Δ*sec72*	*MATa; his3Δ1; leu2Δ0; met15Δ0; ura3Δ0; YLR292c::kanMX4; SUN4-mNeongreen-tADH1 HIS3MX*	This study
yMJ029	SRL1-mNeonGreen-tADH1, Δ*sec72*	*MATa; his3Δ1; leu2Δ0; met15Δ0; ura3Δ0; YLR292c::kanMX4; SRL1-mNeongreen-tADH1 HIS3MX*	This study
yMJ030.1	SUN4-yoHaloTag, BY4741	*BY4741; MATa; his3Δ1; leu2Δ0; met15Δ0; ura3Δ0; SUN4-yoHaloTag*	This study
yMJ030.2	SUN4-yoHaloTag, BY4741	*BY4741; MATa; his3Δ1; leu2Δ0; met15Δ0; ura3Δ0; SUN4-yoHaloTag*	This study
yMJ031.1	SUN4-yoHaloTag Δ*sec72*	*BY4741; MATa; his3Δ1; leu2Δ0; met15Δ0; ura3Δ0; YLR292C::kanMX4 SUN4-yoHaloTag*	This study
yMJ031.2	SUN4-yoHaloTag Δ*sec72*	*BY4741; MATa; his3Δ1; leu2Δ0; met15Δ0; ura3Δ0; YLR292C::kanMX4 SUN4-yoHaloTag*	This study
yMJ032	SUN4-yoHaloTag, BY4741	*BY4741; MATa; his3Δ1; leu2Δ0; met15Δ0; ura3Δ0; SUN4-yoHaloTag*	This study
yMJ033	SUN4-yoHaloTag Δssd1	*BY4741; MATa; his3Δ1; leu2Δ0; met15Δ0; ura3Δ0; YDR293C::kanMX4 SUN4-yoHaloTag*	This study
yMJ034	SUN4-yoHaloTag Δssd1	*BY4741; MATa; his3Δ1; leu2Δ0; met15Δ0; ura3Δ0; YDR293C::kanMX4 SUN4-yoHaloTag*	This study
yMJ035	SRL1-yoHaloTag, BY4741	*BY4741; MATa; his3Δ1; leu2Δ0; met15Δ0; ura3Δ0; SRL1-yoHaloTag*	This study
yMJ036	SRL1-yoHaloTag in Δssd1,	*BY4741; MATa; his3Δ1; leu2Δ0; met15Δ0; ura3Δ0; YDR293C::kanMX4 SRL1-yoHaloTag*	This study
yMJ037	SRL1-yoHaloTag, Δ*sec72*	*BY4741; MATa; his3Δ1; leu2Δ0; met15Δ0; ura3Δ0; YLR292C::kanMX4 SRL1-yoHaloTag*	This study
yMJ039	Sun4-mNeongreen scarless, BY4741	*BY4741; MATa; his3Δ1; leu2Δ0; met15Δ0; ura3Δ0; Sun4-mNeongreen*	This study
yMJ040	Sun4-mNeongreen scarless, BY4741	*BY4741; MATa; his3Δ1; leu2Δ0; met15Δ0; ura3Δ0; Sun4-mNeongreen*	This study
yMJ041	Sun4-mNeongreen scarless, *Δssd1*	*BY4741; MATa; his3Δ1; leu2Δ0; met15Δ0; ura3Δ0; YDR293C::kanMX4 Sun4-mNeongreen*	This study

yMJ042	Sun4-mNeongreen scarless, *Δssd1*	*BY4741; MATa; his3Δ1; leu2Δ0; met15Δ0; ura3Δ0; YDR293C::kanMX4 Sun4-mNeongreen*	This study
yMJ043	Sun4-mNeongreen scarless, *Δmpt5*	*BY4741; MATa; his3Δ1; leu2Δ0; met15Δ0; ura3Δ0; YGL178W::kanMX4 Sun4-mNeongreen*	This study
yMJ044	Sun4-mNeongreen scarless, *Δmpt5*	*BY4741; MATa; his3Δ1; leu2Δ0; met15Δ0; ura3Δ0; YGL178W::kanMX4 Sun4-mNeongreen*	This study
yMJ045	Sun4-mNeongreen scarless, *Δsec72*	*BY4741; MATa; his3Δ1; leu2Δ0; met15Δ0; ura3Δ0; YDR293C::kanMX4 Sun4-mNeongreen*	This study
yMJ046	Sun4-mNeongreen scarless, *Δsec72*	*BY4741; MATa; his3Δ1; leu2Δ0; met15Δ0; ura3Δ0; YDR293C::kanMX4 Sun4-mNeongreen*	This study
yMJ047	Sun4-mNeongreen scarless, *Δsec72*	*BY4741; MATa; his3Δ1; leu2Δ0; met15Δ0; ura3Δ0; YDR293C::kanMX4 Sun4-mNeongreen*	This study
yMJ048	Srl1-mNeongreen scarless, BY4741	*BY4741; MATa; his3Δ1; leu2Δ0; met15Δ0; ura3Δ0; Srl1-mNeongreen*	This study
yMJ049	Srl1-mNeongreen scarless, BY4741	*BY4741; MATa; his3Δ1; leu2Δ0; met15Δ0; ura3Δ0; Srl1-mNeongreen*	This study
yMJ050	Srl1-mNeongreen scarless, BY4741	*BY4741; MATa; his3Δ1; leu2Δ0; met15Δ0; ura3Δ0; Srl1-mNeongreen*	This study
yMJ051	Srl1-mNeongreen scarless, *Δssd1*	*BY4741; MATa; his3Δ1; leu2Δ0; met15Δ0; ura3Δ0; YDR293C::kanMX4 Srl1-mNeongreen*	This study
yMJ052	Srl1-mNeongreen scarless, *Δssd1*	*BY4741; MATa; his3Δ1; leu2Δ0; met15Δ0; ura3Δ0; YDR293C::kanMX4 Srl1-mNeongreen*	This study
yMJ053	Srl1-mNeongreen scarless, *Δmpt5*	*BY4741; MATa; his3Δ1; leu2Δ0; met15Δ0; ura3Δ0; YGL178W::kanMX4 Srl1-mNeongreen*	This study
yMJ054	Srl1-mNeongreen scarless, *Δmpt5*	*BY4741; MATa; his3Δ1; leu2Δ0; met15Δ0; ura3Δ0; YGL178W::kanMX4 Srl1-mNeongreen*	This study
yMJ055	Srl1-mNeongreen scarless, *Δsec72*	*BY4741; MATa; his3Δ1; leu2Δ0; met15Δ0; ura3Δ0; YLR292C::kanMX4 Srl1-mNeongreen*	This study

yMJ056	Srl1-mNeongreen scarless, *Δsec72*	*BY4741; MATa; his3Δ1; leu2Δ0; met15Δ0; ura3Δ0; YLR292C::kanMX4 Srl1-mNeongreen*	This study
yMJ057	Srl1-mNeongreen scarless, *Δsec72*	*BY4741; MATa; his3Δ1; leu2Δ0; met15Δ0; ura3Δ0; YLR292C::kanMX4 Srl1-mNeongreen*	This study

7.3 Primers designed for this study

Primer name	Sequence	Description
oMJ001_SUN4_mNG_FP	GTTTCCGTTACTGCTGGCAAAG CTAAGTTTGTTCTATACAACggtga cggtgctggttta	SUN4_C' tag_mNeonG_pFA6 FWD
oMJ002_SUN4_mNG_RP	ATACAATCAACTTACTCAACTGT TGATGCGCCTAAGTTTAtcgatgaat tcgagctcg	SUN4_C' tag_mNeonG_pFA6 REV
oMJ003_SRL1_mNG_FP	CAATGGTACAACACCACTTCGAT TACTAATTCGACCAGTTGGggtga cggtgctggttta	SRL1_C' tag_mNeonG_pFA6 FWD
oMJ004_SRL1_mNG_RP	CAAAAAGAACTTAAAAGGACACG TTTGAACTCATAATTCAtcgatgaatt cgagctcg	SRL1_C' tag_mNeonG_pFA6 REV
oMJ005_SCW4_mNG_FP	CTTACGGTGTTGAAAAATACTGG GGTATTCTATCCAATGAAggtgacg gtgctggttta	SCW4_C' tag_mNeonG_pFA6 FWD
oMJ006_SCW4_mNG_RP	CAAGATTTTTTTTGTTTTTTTTTA CAATTGAGTAGACTTAtcgatgaattc gagctcg	SCW4_C' tag_mNeonG_pFA6 REV
oMJ007_UTH1_mNG_FP	CTGTTTCAGTTACTTCTGGTTCT GCTAACTTTGTCTTCTACggtgacg gtgctggttta	UTH1_C' tag_mNeonG_pFA6 FWD
oMJ008_UTH1_mNG_RP	CTAGCAAAAGCTTATTTGCAATA TTCAAGGAAAAAAGGCCTAtcgatg aattcgagctcg	UTH1_C' tag_mNeonG_pFA6 REV
oMJ009_SP6_mod	atttaggtgacactatagaacg	Modified Sp6 primer to check pFA6 plasmids
oMJ010_SEQ_SUN4_FP	CAGTCAACGGTGAATGTATCTAT G	Seq_SUN4_Ctag_FWD to check mNeonGreen junction, this primer is upstream of the tag
oMJ011_SEQ_mNG_RP	ccatacccatgacgtcggtg	Sequencing primer to check mNeonGreen integration, this primer is at the end of mNeonGreen sequence (integrated from plasmid pFA6a-link-ymNeongreen-SpHis5). This primer will be used for all the proteins tagged using this plasmid
oMJ012_SEQ_SUN4_RP	CGGCGTGGGTTTTAGTGTATG	Seq_SUN4_Ctag primer to check the junction downstream of the tag
oMJ013_SEQ_HIS3_FP	ccaagcatacaaaccaaaaggg	Sequencing primer to check selection marker integration, this primer is at the start of HIS3 sequence (integrated from plasmid pFA6a-link-ymNeongreen-SpHis5). This primer will be used for all the proteins tagged using this plasmid
oMJ014_SEQ_SRL1_FP	CGACTACACAATACGTTACTGtc	Seq_SRL1 Ctag_FWD to check mNeonGreen junction, this primer is upstream of the tag

oMJ015_SEQ_SRL1_RP	CTGATGTATTTAGGTAGCAGAAGG	Seq_SRL1 Ctag_REV to check selectable marker junction, this primer is downstream of the tag
oMJ016_SEQ_SCW4_FP	GCTGATACCTTCTTATTCACTGCC	Seq_SCW4 Ctag_FWD to check mNeonGreen junction, this primer is upstream of the tag
oMJ017_SEQ_SCW4_RP	GAAAGCAGTCCTTTGATATAACAGAG	Seq_SCW4 Ctag_REV to check selectable marker junction, this primer is downstream of the tag
oMJ018_SEQ_UTH1_FP	GGCTCTACCGTCAATGGTGC	Seq_UTH1 Ctag_FWD to check mNeonGreen junction, this primer is upstream of the tag
oMJ019_SEQ_UTH1_RP	GGACTGTGTTTTTTTGTATTGTGGAAAAACG	Seq_UTH1 Ctag_REV to check selectable marker junction, this primer is downstream of the tag
oMJ020_SUN4_CP_FP	CAAAATTGTCGCCGCTGATGAC	Primer to amplify the region of the ORF upstream of 3' UTR, this will be used for colony PCR
oMJ021_SUN4_CP_RP	GTCTGGAAGAATGATAAATAGAAACAAAG	Primer to amplify upstream of 3' UTR, this will be used for colony PCR
oMJ022_SRL1_CP_FP	CAGTACGTTACAGTCACCCC	Primer to amplify the region of the ORF upstream of 3' UTR, this will be used for colony PCR
oMJ023_SRL1_CP_RP	GATAGTGAAAAATAAATACCAGTTGG	Primer to amplify upstream of 3' UTR, this will be used for colony PCR
oMJ024_SCW4_CP_FP	CTGTTTCCGCCATTACCAGCTC	Primer to amplify the region of the ORF upstream of 3' UTR, this will be used for colony PCR
oMJ025_SCW4_CP_RP	CAAATGAGATCATAAACGAACTAAAATAGG	Primer to amplify upstream of 3' UTR, this will be used for colony PCR
oMJ026_UTH1_CP_FP	CACCAAACTTTAACATCAAGATCG	Primer to amplify the region of the ORF upstream of 3' UTR, this will be used for colony PCR
oMJ027_UTH1_CP_RP	GCTATATATGATAATATCTAGTGGTATCTTAAAAAAG	Primer to amplify upstream of 3' UTR, this will be used for colony PCR
SSD1_YDA	TGGTACCCTAAACATTTTGGTCTTA	Primer from yeast deletion collection, this primer will be used to check insert with respective 5UTR_RP primer of each homolog
SSD1_YDD	TTGTAAATATTGAAAAGAAGGCTGC	Primer from yeast deletion collection, this primer will be used to check insert with respective 3UTR_FP primer of each homolog

oMJ028_Sc_CnSSD1_FP	CCTTTCAGCGCAAAGATTTGGCCCAATTATTCCATCTTTATACACTATGGCCGACCCTTTGTCCCCAGCTC	This primer is designed to replace yeast ssd1 with c. neoformans ssd1. The primer has 46 bp homology to 5'UTR of s. cerevisiae and 25 bp to CNAG_03345 ORF
oMJ029_CnSSD1_SC_RP	GTGAAAAACAAGAAAAACAGCAATGACGATATTGGTAGAAGAGACTACAGAGCGGAGCCCCTCAAATTTGAGTGC	This primer is designed to replace yeast ssd1 with c. neoformans ssd1. The primer has homology to 3'UTR of s. cerevisiae and to CNAG_03345 ORF
oMJ030_CnSSD1_5UTR_RP	GCTCGCAAGAGCATCACCAC	This primer is designed to check yeast ssd1 replacement with c. neoformans ssd1 near the 5UTR end
oMJ031_CnSSD1_3UTR_FP	CTAACGAAGTAAAATTCCTTATGGACAGG	This primer is designed to check yeast ssd1 replacement with c. neoformans ssd1 near the 3UTR end
oMJ032_Sc_SpDIS3L2_FP	CAGCGCAAAGATTTGGCCCAATTATTCCATCTTTATACACTATGGATTTAAAACCAAATATTAGAAG	This primer is designed to replace yeast ssd1 with S. pombe Dis3l2. The primer has homology to 5'UTR of s. cerevisiae and to S pombe Dis3l2 ORF
oMJ033_SpDIS3L2_Sc_RP	GAAAAACAAGAAAAACAGCAATGACGATATTGGTAGAAGAGATTAATTCAAAGAAACTAGACTACAGCG	This primer is designed to replace yeast ssd1 with S. pombe Dis3l2. The primer has homology to 3'UTR of s. cerevisiae and to S. pombe Dis3l2 ORF
oMJ034_SpDIS3L2_5UTR_RP	GACTTTCTCGACACCATTCTG	This primer is designed to check yeast ssd1 replacement with S. pombe Dis3l2 near the 5UTR
oMJ035_SpDIS3L2_3UTR_FP	CCTCTATGGTACGACTCAGAAGC	This primer is designed to check yeast ssd1 replacement with S. pombe Dis3l2 near the 3UTR end
oMJ036_Sc_SpSts5_FP	CAGCGCAAAGATTTGGCCCAATTATTCCATCTTTATACACTATGGATGAGGAGTTTGAAAATGACTTTCC	This primer is designed to replace yeast ssd1 with S. pombe Sts5. The primer has homology to 5'UTR of s. cerevisiae and to S. pombe Sts5 ORF
oMJ037_SpSts5_Sc_RP	CAAGAAAAACAGCAATGACGATATTGGTAGAAGAGATCAAAACTCGACATTTGAAACGTTG	This primer is designed to replace yeast ssd1 with S. pombe Sts5. The primer has homology to 3'UTR of s. cerevisiae and to S pombe Sts5 ORF
oMJ038_SpSts5_5UTR_RP	GGCATGAGTAGGACTATTCG	This primer is designed to check yeast ssd1 replacement with S pombe Sts5 near the 5UTR
oMJ039_SpSts5_3UTR_FP	CGACAAAATCACTTTTACGC	This primer is designed to check yeast ssd1 replacement with S pombe Sts5 near the 3UTR

oMJ040_Sc_NcGul1_FP	CAGCGCAAAGATTTGGCCCAATTATTCCATCTTTATACACTATGGATCAGCAACAGCAGCCTCAAGGAGG	This primer is designed to replace yeast ssd1 with N crassa gul1 (ssd1). The primer has homology to 5'UTR of s. cerevisiae and to NcGul1 ORF
oMJ041_NcGul1_SC_RP	GTGAAAAACAAGAAAAACAGCAATGACGATATTGGTAGAAGAGATTAGAGGGCATAGGGATTGAGCGAGC	This primer is designed to replace yeast ssd1 with N crassa gul1 (ssd1). The primer has homology to 3'UTR of s. cerevisiae and to NcGul1 ORF
oMJ042_NcGul1_5UTR_RP	CGACGATCCCTGAGCTATCTG	This primer is designed to check yeast ssd1 replacement with N crassa gul1 near the 5UTR
oMJ043_NcGul1_3UTR_FP	GCTTCGAGAAGCGTGTCCAC	This primer is designed to check yeast ssd1 replacement with N crassa gul1 near the 3UTR
oMJ044_SC_Rd1_FP	CAGCGCAAAGATTTGGCCCAATTATTCCATCTTTATACACTATGGAAGAATTTAAGAAAGATG	This primer is designed to replace yeast ssd1 with Rhizopus delemar 1 RO3G_04239. The primer has homology to 5'UTR of s. cerevisiae and to RO3G_04239 ORF
oMJ045_Rd1_SC_RP	GAAAAACAAGAAAAACAGCAATGACGATATTGGTAGAAGAGATTACATGAAAGGATTAATAGGGTAAACG	This primer is designed to replace yeast ssd1 with Rhizopus delemar 1 RO3G_04239. The primer has homology to 3'UTR of s. cerevisiae and to RO3G_04239 ORF
oMJ046_Rd1_5UTR_RP	CTCATTCTCTGTGTCTTTCC	This primer is designed to check yeast ssd1 replacement with RO3G_04239 near the 5UTR
oMJ047_Rd1_3UTR_FP	CACCTATTCGACGTTTTGCAG	This primer is designed to check yeast ssd1 replacement with RO3G_04239 near the 3UTR
oMJ048_SC_Rd3_FP	CAGCGCAAAGATTTGGCCCAATTATTCCATCTTTATACACTATGAACCATTTACTTGAACATCAAACTGCC	This primer is designed to replace yeast ssd1 with Rhizopus delemar 3 RO3G_03283. The primer has homology to 5'UTR of s. cerevisiae and to Rhizopus delemar 3 RO3G_03283 ORF
oMJ049_Rd3_SC_RP	GTGAAAAACAAGAAAAACAGCAATGACGATATTGGTAGAAGAGATTAGGAAAAGGGATTAACAGCTAATACACG	This primer is designed to replace yeast ssd1 with Rhizopus delemar 3 RO3G_03283. The primer has homology to 3'UTR of s. cerevisiae and to Rhizopus delemar 3 RO3G_03283 ORF
oMJ050_Rd3_5UTR_RP	GCGTCTTGACAAATTACGAGGAC	This primer is designed to check yeast ssd1 replacemnt with Rhizopus delemar 3 RO3G_03283 at 5'UTR

oMJ051_Rd3_3UTR_FP	GCTTGTCTACCAGTCTGGAG	This primer is designed to check yeast ssd1 replacemnt with Rhizopus delemar 3 RO3G_03283 at 3'UTR
oMJ052_SC_Rd5_FP	CAGCGCAAAGATTTGGCCCAATTATTCCATCTTTATACACTATGGACTATGAGACGCTAGAACAACAAACAGC	This primer is designed to replace yeast ssd1 with Rhizopus delemar 5 RO3G_14745. The primer has homology to 5'UTR of s. cerevisiae and to Rhizopus delemar 5 RO3G_14745 ORF
oMJ053_Rd5_SC_RP	GAAAAACAAGAAAAACAGCAATGACGATATTGGTAGAAGAGACTAAGCATAAGGATTAGCAGCAAATACTC	This primer is designed to replace yeast ssd1 with Rhizopus delemar 5 RO3G_14745. The primer has homology to 3'UTR of s. cerevisiae and to Rhizopus delemar 5 RO3G_14745 ORF
oMJ054_Rd5_5UTR_RP	CAAGCTCAAAGATTTGCTATTGATGG	This primer is designed to check replacement of yeast ssd1 with Rhizopus delemar 5 RO3G_14745 near 5'UTR
oMJ055_Rd5_3UTR_FP	GTACATCGTCAATTAGAAGCTGC	This primer is designed to check replacement of yeast ssd1 with Rhizopus delemar 5 RO3G_14745 near 3'UTR
oMJ060_SEC5_mCh_pMS_FP	CAATTTAAAAAGAACTGCTATTCAATTCGCCGCCTTCAGCggtgacggtgctggttta	SEC5_Ctag_mCherry_FWD using pMS278 from MS lab. These primers will be just to test if the PCR works with the insert on this plasmid, not to actually tag the target with
oMJ061_SEC5_mCh_pMS_RP	TAATAATCATTGTTAGTACATCTTTATACCTCTGTTTCTAGAATTCGAGCTCGTTTTCGACAC	SEC5_Ctag_mCherry_REV, the rev sequence has the 4bp insert we found while sequencing using pMS278 from MS lab. These primers will be just to test if the PCR works with the insert on this plasmid, not to actually tag the target with
oMJ062_Hsp104_mCh_FP	CGATAATGAGGACAGTATGGAAATTGATGATGACCTAGATgcaggtgctggagctggt	Hsp104_Ctag_mCherry_FWD using either mCherry_Kanx or mCherry_NAT plasmids (pFM571 & pFM699) https://academic.oup.com/femsyr/article/16/3/fow027/2467789
oMJ063_Hsp104_mCh_RP	CTTGTTCGAAAGTTTTTAAAAATCACACTATATTAAATTAtcgatgaattcgagctcg	Hsp104_Ctag_mCherry_REV using either mCherry_Kanx or mCherry_NAT plasmids (pFM571 & pFM699) https://academic.oup.com/femsyr/article/16/3/fow027/2467790
oMJ064_Hsp104_CP_FP	GGATAAGGAAACTGTCAATGTCGTC	Primer to amplify the region of the ORF upstream of 3' UTR, this will be used for colony PCR

oMJ065_Hsp104_CP_RP	CCAGTGGACTTTTTTGTCCATTG	Primer to amplify upstream of 3' UTR, this will be used for colony PCR
oMJ066_SEQ_Hsp104_FP	CGTGATGAAAATGTTCCTGAGG AAGCTG	Seq_Hsp104 Ctag_FWD to check mCherry junction, this primer is upstream of the tag
oMJ067_mCherry_RP	gtcctcggggtacatccgctc	This is a REV primer within the mCherry tag, to be used for sequencing
oMJ068_Hxt2_mNG_FP	TGGTAGCTGGATCTCAAAAGAAA AAAGAGTTTCCGAGGAAggtgacg gtgctggttta	HXT2_C' tag_mNeonG_pFA6 FWD, this is a negative control for Ssd1 control of gene expression. C-terminal mNeongreen tag of a protein not controlled by Ssd1, to verify that any effect of Ssd1 deletion on expression (and localisation) is specific and not global, nor dependent on mNeongreen.
oMJ069_Hxt2_mNG_RP	GCCTTAAAAAAATCAGTGCTAGT TTAAGTATAATCTCTTAtcgatgaatt cgagctcg	HXT2_C' tag_mNeonG_pFA6 REV, this is a negative control for Ssd1 control of gene expression. C-terminal mNeongreen tag of a protein not controlled by Ssd1, to verify that any effect of Ssd1 deletion on expression (and localisation) is specific and not global, nor dependent on mNeongreen.
oMJ070_Hxt2_CP_FP	GTGCAATTGGATTTTCATACGGG TATGTC	Primer to amplify the region of the ORF upstream of 3' UTR, this will be used for colony PCR
oMJ071_Hxt2_CP_RP	CTAGATAAATGAGTGGTACAAAT AAAAACATC	Primer to amplify upstream of 3' UTR, this will be used for colony PCR
oMJ072_SEQ_Hxt2_FP	GGCTGTTTGGTATTTTCATTCTT CTACGTG	Seq_Hxt2 Ctag_FWD to check mNeonGreen junction, this primer is upstream of the tag and will be used with oMJ011_SEQ_mNG_RP
oMJ073_Pho88_mNG_FP	AGAAGCTGAAAGAGCCGGTAAC GCTGGTGTTAAGGCTGAAggtgac ggtgctggttta	PHO88_C' tag_mNeonG_pFA6 FWD, this is a negative control for Ssd1 control of gene expression. C-terminal mNeongreen tag of a protein not controlled by Ssd1, to verify that any effect of Ssd1 deletion on expression (and localisation) is specific and not global, nor dependent on mNeongreen.
oMJ074_Pho88_mNG_RP	AAAACTAGGAAAAAAAAATACTT CGCTTTTGATCGAATCAtcgatgaat tcgagctcg	PHO88_C' tag_mNeonG_pFA6 REV, this is a negative control for Ssd1 control of gene expression. C-terminal mNeongreen tag of a

		protein not controlled by Ssd1, to verify that any effect of Ssd1 deletion on expression (and localisation) is specific and not global, nor dependent on mNeongreen.
oMJ075_PHO88_CP_FP	CACCTCTTCGGTAAGCCTGC	Primer to amplify the region of the ORF upstream of 3' UTR, this will be used for colony PCR
oMJ076_PHO88_CP_RP	GCAATTCTATGGCGATGTAGGAAAATAG	Primer to amplify upstream of 3' UTR, this will be used for colony PCR
oMJ077_SEQ_PHO88_FP	GAAGAGACCATTCAAGGCTCCATC	Seq_PHO88 Ctag_FWD to check mNeonGreen junction, this primer is upstream of the tag and will be used with oMJ011_SEQ_mNG_RP
oMJ078_SEC5_CP_FP	CTTGAAAAGGACACCGAGGCCAC	Primer to amplify the region of the ORF upstream of 3' UTR, this will be used for colony PCR
oMJ079_SEC5_CP_RP	CCCGTTATACAATGTTTCCTCG	
oMJ080_SEQ_SEC5_FP	GTGCTTACAAAACTGTTTCCAGAACGAC	Seq_SEC5 Ctag_FWD to check mCherry junction, this primer is upstream of the tag. This will be used with primer 0MJ081
oMJ081_SEQ_mCherry_RP	cttgtacagctcgtccatgcc	This is a REV primer within the mCherry tag, to be used for sequencing. This tag is from pMS278 plasmid
oMJ082_CDC12_mCh_FP	GCAGGTCAAAAGCTTGCAAGTAAAAAAATCCCATTTAAAAggtgacggtgctggttta	CDC12_Ctag_mCherry_FWD using mCherry_NAT pMS278
oMJ083_CDC12_mCh_RP	AAATTGACGAGACAAAGAGGAAGACATTAATTAATCATCACTGGATGGCGGCGTTAGTATC	CDC12_Ctag_mCherry_REV using mCherry_NAT pMS278
oMJ084_CDC12_CP_FP	GCATTGAAGAAGTATTTCACTGACCAAGTC	Primer to amplify the region of the ORF upstream of 3' UTR, this will be used for colony PCR
oMJ085_CDC12_CP_RP	CCGGTTTATTTTTGTTTTTACTGTTCGATTGTG	
oMJ086_SEQ_CDC12_FP	GGAGCAAAGATTTAGACAATGGGAGCAAAAC	Seq_CDC12 Ctag_FWD to check mCherry junction, this primer is upstream of the tag. This will be used with primer 0MJ081
oMJ087_Hsp104_mCh_FP_pMS	CGATAATGAGGACAGTATGGAAATTGATGATGACCTAGATggtgacggtgctggttta	Hsp104_Ctag_mCherry_FWD using mCherry_NAT plasmids pMS278 with the previously made primer oMJ063
pr1862 21 "Sec72-KO-F	AACTTGCGTTAAAGGCATACCAAAGCAAGCTTATTCAACCCGGATCCCCGGGTTAATTAA	Forward primer for KO Sec72 using pFA6a plasmids sec72
pr1863 21 "Sec72-KO-R	ACATATCAAGAAAAGGCTAAAATATCTTCGGTTATGCACCGAATTCGAGCTCGTTTAAAC	Reverse primer for KO Sec72 using pFA6a plasmids sec72

pr1881 22 "Sec72-CHK-F"	TGTTGTT GCACTATCTA CCG	Forward primer for Check PCR of Sec72, within ORF
pr1882 22 "Sec72-CHK-R"	ATTCACCGTTATATTCGGCC	Reverese primer for Check PCR of Sec72, within ORF
oMJ088_SEC72_CP_FP	CGGATGTAGGAGCACACGTAACAATTAG	Forward primer for Check PCR of Sec72, 5'UTR
oMJ089_SEC72_CP_RP	CTTGCTATGTAGTCGTGTGTAGC	REV primer for Check PCR of Sec72, 3'UTR
oMJ090_KanMX_CHK_FP	caggcgcaatcacgaatgaataacg	Primer to check KanMX cassette
oMJ091_KanMX_CHK_RP	cgcgatcgctgttaaaagg	Primer to check KanMX cassette
oMJ092_Sec72-KO-R	ACATATCAAGAAAAGGCTAAAATATCTTCGGTTATGCACCgaattcgagctcgttttcga	Reverse primer for KO Sec72 using pFA6a plasmid pAG35
oMJ093_NATMx_CHK_FP	cactcttgacgacacggcttacc	Primer to check NatMX cassette
oMJ094_NATMx_CHK_RP	catgtagagcgcctgctcgc	Primer to check NatMX cassette
oMJ095_Khd1_KO_Fp	GGGTAACTTAGAGACAGCATTAGTATATATACCAGCCATGcggatccccgggttaattaa	Khd1 knockout primer
oMJ096_khd1_KO_Rp	TTTGTCTGTGTGGGACGTGCGCACGCACACGTATATACTAgaattcgagctcgttttcga	Khd1 knockout primer
oMJ097_khd1_CP_FP	CATAAGTACCCGAGCATATATAACTACTTGGC	Khd1 colony PCR primer
oMJ098_khd1_CP_RP	GAATCATTTTTTTCCCTTTAATAAAAATACAGTTTAAACTAG	Khd1 colony PCR primer
oMJ099_Khd1_CHK_Fp	GGCTTCCAAGGACTTCTTAC	Khd1 check primer
oMJ100_Khd1_Chk_Rp	CGTCTTTATCATCGTCATCC	Khd1 check primer
oMJ101_MPT5_KO_FP	AATTTATAAATCAATTACGATTTTTCCAGTTTCTCTTATGcggatccccggttaattaa	Mpt5 knockout primer
oMJ102_MPT5_KO_RP	ACAGTAAGAAGGAAAGAAAAAGAAAGAAAAAAAAGTATTAgaattcgagctcgttttcga	Mpt5 knockout primer
oMJ103_MPT5_CP_fp	CTACGGATCAGCAAAAGCCTGC	Mpt5 colony PCR primer
oMJ104_MPT5_CP_Rp	GGGACTTTAGTAGGACGTCATTGC	Mpt5 colony PCR primer
oMJ105_Sc_CaSSD1_FP	CAGCGCAAAGATTTGGCCCAATTATTCCATCTTTATACACTATGAGCTCGTCACAAGATTAC	Repair template amplification primer to replace *S. cerevisiae* Ssd1 with *C. albicans* Ssd1
oMJ106_CaSSD1_Sc_RP	GAAAAACAAGAAAAACAGCAATGACGATATTGGTAGAAGAGATTACTGTTCTTCAGCAAATGG	Repair template amplification primer to replace *S. cerevisiae* Ssd1 with *C. albicans* Ssd1
oMJ107_Sc_CgSSD1_FP	AGCGCAAAGATTTGGCCCAATTATTCCATCTTTATACACTATGTCGAAGTTTCATCGCCAG	Repair template amplification primer to replace *S. cerevisiae* Ssd1 with *C. glabrata* Ssd1
oMJ108_CgSSD1_Sc_RP	GAAAAACAAGAAAAACAGCAATGACGATATTGGTAGAAGAGATTAGTGTTTTGGTTCCACTTT	Repair template amplification primer to replace *S. cerevisiae* Ssd1 with *C. glabrata* Ssd1
oMJ109_SUN4_pET264_FP	GTACCGTTTCCGTTACTGCTGGCAAAGCTAAGTTTGTTCTATACAACTAACCGCTCTAGAACTAGTGGATCC	
oMJ110_Sun4_pET264_RP	CAATAAAATGGACGGGCAGAAAAGAATGGaGTAATAATACAATCA	

	ACTTACTCAACTGTTGATGCGaCTAAGTGTTGTCGAGATCGATAGATCT	
oMJ111_Sun4_Kan_pET264	CAATAAAATGGACGGGCAGAAAAGAATGGaGTAATAATACAATCAACTTACTCAACTGTTGATGCGaCTAAGTGCATAGGCCACTAGTGGATCTG	
oMJ112_SRL1_pET264_FP	CACTACCTCTCCAGGTAACGTACAATGGTACAACACCACTTCGATTACTAATTCGACCAGTTGGTGACCGCTCTAGAACTAGTGGATCC	
oMJ113_SRL1_pET264_RP	GTCAATACAGATACAAAAAAGAAACAAAAAGAACTTAAAAGcACACGTTTGAACTCATAATGTTGTCGAGATCGATAGATCT	
oMJ114_SRL1_Kan_pET264	GTCAATACAGATACAAAAAAGAAACAAAAAGAACTTAAAAGtACACGTTTGAACTCATAATGCATAGGCCACTAGTGGATCTG	
oMJ115_SCW4_pET264_FP	ACGGTGCTTACGGTGTTGAAAAATACTGGGGTATTCTATCCAATGAATAACCGCTCTAGAACTAGTGGATCC	
oMJ116_SCW4_pET264_RP	AATTTAAAGTTAAAAATATTGtGTATCGTTTTTTAAATCAAGATTTTTTTTTGTTTTTTTTTACAATTGAGTAGACGTTGTCGAGATCGATAGATCT	
oMJ117_SCW4_KAN_pET264	AATTTAAAGTTAAAAATATTGtGTATCGTTTTTTAAATCAAGATTTTTTTTTGTTTTTTTTTACAATTGAGTAGACGCATAGGCCACTAGTGGATCTG	
oMJ118_Sun4_mNG_FP	CCGTTACTGCTGGCAAAGCTAAGTTTGTTCTATACAACatggtctctaagggtgaagaag	no linker, for scarless tagging
oMJ119_Sun4_mNG_RP	ATACAATCAACTTACTCAACTGTTGATGCGCCTAAGTTTActtgtacaattcgtccatac	no linker, for scarless tagging
oMJ120_SRL1_mNG_FP	GGTACAACACCACTTCGATTACTAATTCGACCAGTTGGatggtctctaaggtgaagaag	no linker, for scarless tagging
oMJ121_SRL1_mNG_RP	CAAAAAGAACTTAAAAGTACACGTTTGAACTCATAATTCActtgtacaattcgtccatac	no linker, for scarless tagging, mutated for gRNA_3UTR
oMJ122_SCW4_mNG_FP	CGGTGTTGAAAAATACTGGGGTATTCTATCCAATGAAatggtctctaaggtgaagaag	no linker, for scarless tagging
oMJ123_SCW4_mNG_RP	CAAGATTTTTTTTGTTTTTTTTTACAATTGAGTAGACTTActtgtacaattcgtccatac	no linker, for scarless tagging
oMJ124_UTH1_mNG_FP	CTGTTTCAGTTACTTCTGGTTCTGCTAACTTTGTCTTCTACatggtctctaagggtgaag	no linker, for scarless tagging
oMJ125_UTH1_mNG_RP	CTAGCAAAAGCTTATTTGCAATATTCAAGGAAAAAATGCCTActtgtacaattcgtccatac	no linker, for scarless tagging, mutated for gRNA_3UTR

oMJ126_Sun4_Amp_FP	GTACCGTTTCCGTTACTGCTGG	Primers used to amplify from pET264_ssd1_protein PCR product as template due to the two bands on the gel issue from original primers
oMJ127_Sun4_Amp_RP	CAATAAAATGGACGGGCAGAAAAG	Primers used to amplify from pET264_ssd1_protein PCR product as template due to the two bands on the gel issue from original primers
oMJ128_SRL1_Amp_FP	CACTACCTCTCCAGGTAACGTAC	Primers used to amplify from pET264_ssd1_protein PCR product as template due to the two bands on the gel issue from original primers
oMJ129_SRL1_Amp_RP	GAGTTACAGAAGGTGAAATTGTC	Primers used to amplify from pET264_ssd1_protein PCR product as template due to the two bands on the gel issue from original primers
oMJ130_SCW4_amp_FP	ACGGTGCTTACGGTGTTGAAAAATAC	Primers used to amplify from pET264_ssd1_protein PCR product as template due to the two bands on the gel issue from original primers
oMJ131_SCW4_Amp_RP	AATTTAAAGTTAAAAATATTGtGTATCGTTTTTTAAATCAAG	Primers used to amplify from pET264_ssd1_protein PCR product as template due to the two bands on the gel issue from original primers
oMJ132_SUN4_linker_HALO_FP	GCTAAGTTTGTTCTATACAACGGCGGCAGTGGAAGTGGCCTCCAggcagaaatcggtacaggtttccc	Primers used to add homology to SUN4+linker and amplify the halotag for C-term tagging
oMJ133_SUN4_HALO_RP	ACAATCAACTTACTCAACTGTTGATGCGCCTAAGTTTAacctgagatttctaatgtggacaaccatc	Primers used to add homology to SUN4 and amplify the halotag for C-term tagging
oMJ134_Halotag_REV	gatcgatgatcaactttctaccaac	Rev primer within the Halotag for confirmation
oMJ135_SRL1_Linker_FP_HALO	CGATTACTAATTCGACCAGTTGGGGCGGCAGTGGAAGTGGCCTCCAGatggcagaaatcggtacagg	Primers used to add homology to SRL1+linker and amplify the halotag for C-term tagging
oMJ136_SRL1_RP_HALO	GAACTTAAAAGGACACGTTTGAACTCATAATTCAacctgagatttctaatgtggacaaccatctggc	Primers used to add homology to SRL1 and amplify the halotag for C-term tagging
oMJ137_SCW4_Linker_FP_HALO	ACTGGGGTATTCTATCCAATGAAGGCGGCAGTGGAAGTGGCCTCCAGatggcagaaatcggtacagg	Primers used to add homology to SCW4+linker and amplify the halotag for C-term tagging
oMJ138_SCW4_RP_HALO	GTTTTTTTTTACAATTGAGTAGACTTAacctgagatttctaatgtggacaaccatctggc	Primers used to add homology to SCW4 and amplify the halotag for C-term tagging
oMJ139_PIR1_FP_Linker_Halo	GAGCACATTGGAACTCAATGTAATGCAGTACACCTACAAGCAATCGATTTACTCAACTGTGGCGGCA	Add homology to PIR1+linker and amplify the halotag for C-term tagging

	GTGGAAGTGGCCTCCAGgcagaaatcggtacaggtttccc	
oMJ140_PIR1_RP_Halo	CAGAATATGCTACGATGACTTTACGTTTTCATGCGAGTATGAGAAGTAAACTTATGATTAacctgagatttctaatgtggacaacc	Add homology to PIR1 and amplify the halotag for C-term tagging
oMJ141_PIR1C_CP_FP	CCAGAAGGTAACTTGGCCATCG	PIR1 C-terminus colony PCR
oMJ142_PIR1C_CP_RP	GGTTTCAAAAGAAAGCTTTATGAAATGAAGAGACG	PIR1 C-terminus colony PCR
oMJ143_PIR1C_SEQ_FP	CAGGAAACTTCTACAACTTATACGATGAGC	PIR1 C-terminus sequencing primer
oMJ144_PIR1C_SEQ_RP	CCCAAATTATGCCCTTTGGAGACAG	PIR1 C-terminus sequencing primer
oMJ145_HSP150_FP_Linker_Halo	CGAACACATTGGTAGTCAATGTACTCCAGTTCACTTGGAAGCAATCGATTTAATAGACTGTGGCGGCAGTGGAAGTGGCCTCCAGgcagaaatcggtacaggtttccc	Add homology to HSP150+linker and amplify the halotag for C-term tagging
oMJ146_HSP150_RP_Halo	TCTAATCAATGTAAATGAGAAAAAGTCGTCAGAATAAAAGAACTAATAGTTTTCTGCTTAacctgagatttctaatgtggacaacc	Add homology to HSP150 and amplify the halotag for C-term tagging
oMJ147_HSP150C_CP_FP	AGACGGTAACTTGGCTATTGGTG	HSP150 C-terminus colony PCR
oMJ148_HSP150C_CP_RP	ACCGCAGAAAAGATAAATGCAAAGG	HSP150 C-terminus colony PCR
oMJ149_HSP150C_SEQ_FP	TGTCTTCTACCAATGTTTGTCCGG	HSP150 C-terminus sequencing primer
oMJ150_HSP150C_SEQ_RP	GCGACTAGAGTAGTAGTAGAAAAGGACAC	HSP150 C-terminus sequencing primer
oMJ151_SUN4_mNG_REV	ATACAATCAACTTACTCAACTGTTGATGCGCCTAAGTTTActtgtacaattcgtccatacc	Scarless tagging of SUN4 with mNeongreen
oMJ152_SRL1_mNG_REV	CAAAAAGAACTTAAAAGGACACGTTTGAACTCATAATTCActtgtacaattcgtccatacc	Scarless tagging of SRL1 with mNeongreen
oMJ153_Linker_FP_HALO	GGCGGCAGTGGAAGTGGCCTCCAGatggcagaaatcggtacagg	Adds a GGSGSGLQ linker to yoHaloTag. Can be used as FP to amplify the yoHaloTag for C-terminal fusions.
oMJ154_SCW4_Linker_FP_HALO	CTTACGGTGTTGAAAAATACTGGGGTATTCTATCCAATGAAGGCGGCAGTGGAAGTGGCCTCCAGatggcagaaatcggtacagg	40bp homology to SCW4 ORF, GGSGSGLQ, and amplify yoHaloTag for C-term tagging
oMJ155_SCW4_RP_HALO	ATCAAGATTTTTTTTGTTTTTTTTTACAATTGAGTAGACTTAacctgagatttctaatgtggacaaccatctg	42bp homology to SCW4 3'UTR, and amplify yoHaloTag for C-term tagging
oMJ156_SRL1_Linker_FP_HALO	ATGGTACAACACCACTTCGATTACTAATTCGACCAGTTGGGGCGGCAGTGGAAGTGGCCTCCAGatggcagaaatcggtacagg	40bp homology to SRL1 ORF, GGSGSGLQ, and amplify yoHaloTag for C-term tagging
oMJ157_SRL1_RP_HALO	CAAAAAGAACTTAAAAGGACACGTTTGAACTCATAATTCAacctgagatttctaatgtggacaaccatctg	40bp homology to SRL1 3'UTR, and amplify yoHaloTag for C-term tagging
oMJ158_SUN4_mGL_FP	CCGTTACTGCTGGCAAAGCTAAGTTTGTTCTATACAACggtgacggtgctggtttaattaacatggtttctaaaggtgaagaattattc	Amplify mGreenLantern with homology to SUN4, forward primer

oMJ159_SUN4_mGL_RP	GTAATAATACAATCAACTTACTCAACTGTTGATGCGCCTAAGTTTAggatcctttgtacaattcatcc	Amplify mGreenLantern with homology to SUN4, reverse primer
oMJ160_SRL1_mGL_FP	GGTACAACACCACTTCGATTACTAATTCGACCAGTTGGggtgacggtgctggtttaattaacatggtttctaaaggtgaagaattattc	Amplify mGreenLantern with homology to SRL1, forward primer
oMJ161_SRL1_mGL_RP	GAAACAAAAAGAACTTAAAAGGACACGTTTGAACTCATAATTCAggatcctttgtacaattcatcc	Amplify mGreenLantern with homology to SRL1, reverse primer
oMJ162_SHE2_SEQ_FP	TCTCTTATAGAATGGTTCTTCGTGC	Primers from YKO collection https://horizondiscovery.com/en/non-mammalian-research-tools/products/yeast-knockout#resources
oMJ163_SHE2_SEQ_RP	AGGCTTCATTTTAGGCTATAGTTCC	Primers from YKO collection https://horizondiscovery.com/en/non-mammalian-research-tools/products/yeast-knockout#resources
oMJ164_SHE3_SEQ_FP	TTTAGAATGTATTTTTGGTTCCACG	Primers from YKO collection https://horizondiscovery.com/en/non-mammalian-research-tools/products/yeast-knockout#resources
oMJ165_SHE3_SEQ_RP	CCTGCTATCATTGGTCTTATGAAAT	Primers from YKO collection https://horizondiscovery.com/en/non-mammalian-research-tools/products/yeast-knockout#resources
oMJ166_MYO3_SEQ_FP	AATAGAGTGGATGGAATAAAACCCT	Primers from YKO collection https://horizondiscovery.com/en/non-mammalian-research-tools/products/yeast-knockout#resources
oMJ167_MYO3_SEQ_RP	AACTAATTCACAAGTTCCAGGAGTG	Primers from YKO collection https://horizondiscovery.com/en/non-mammalian-research-tools/products/yeast-knockout#resources
oMJ168_MYO5_SEQ_FP	AAACTAATGACGGCTAAAATTAAGTCA	Primers from YKO collection https://horizondiscovery.com/en/non-mammalian-research-tools/products/yeast-knockout#resources
oMJ169_MYO5_SEQ_RP	TTACCCTTTTTATGAGATACCCTCC	Primers from YKO collection https://horizondiscovery.com/en/non-mammalian-research-tools/products/yeast-knockout#resources
oMJ170_KanB_YKO	CTGCAGCGAGGAGCCGTAAT	Primers from YKO collection https://horizondiscovery.com/en/non-mammalian-research-tools/products/yeast-knockout#resources
oMJ171_KanC_YKO	TGATTTTGATGACGAGCGTAAT	Primers from YKO collection https://horizondiscovery.com/en/non-mammalian-research-tools/products/yeast-knockout#resources

oMJ172_CaSSD1_5'UTR_RP	CACCATTATTTGGAAGAAACT	Please note that the 100uM tube in primers box was mislabelled as CaSSD1_5'UTR_RP only
oMJ173_CaSSD1_3'UTR_FP	CGGATTATTGTAACTTCAAGA	Please note that the 100uM tube in primers box was mislabelled as CaSSD1_3'UTR_FP only
oMJ174_CgSSD1_5'UTR_RP	CAGATCTGGAGATACTGGCTC	Please note that the 100uM tube in primers box was mislabelled as CgSSD1_5'UTR_RP only
oMJ175_CgSSD1_3'UTR_FP	GTGTCGAGATATTATTGTTCA	Please note that the 100uM tube in primers box was mislabelled as CgSSD1_3'UTR_FP only

7.4 gRNAs designed for this study

ID	Description	Oligos	Oligo1	Oligo2	gRNA+PAM
gMJ001_Sun4_gRNA_3UTR	in 3UTR, 42bp from stop codon, minus strand	ogMJ001_SUN4_3UTR & ogMJ002_SUN4_3UTR	GATCTGGACGGGCAGAAAAGAATGGTTTTAGAGCTAG	CTAGCTCTAAAACCATTCTTTTCTGCCCGTCCA	TGGACGGGCAGAAAAGAATGGGG
gMJ002_Sun4_gRNA_orf_3UTR	overlaps stop codon	ogMJ003_SUN4_stop & ogMJ004_SUN4_stop	GATCTGTTCTATACAACTAAACTTGTTTTAGAGCTAG	CTAGCTCTAAAACAAGTTTAGTTGTATAGAACA	TGTTCTATACAACTAAACTTAGG
gMJ003_SRL1_gRNA_orf_3UTR	overlaps stop codon	ogMJ005_SRL1_stop & ogMJ006_SRL1_stop	GATCTGAACTCATAATTCACCAACGTTTTAGAGCTAG	CTAGCTCTAAAACGTTGGTGAATTATGAGTTCA	TGAACTCATAATTCACCAACTGG
gMJ004_SRL1_gRNA_3UTR	in 3UTR, 19bp from stop codon, minus strand	ogMJ007_SRL1_3UTR & ogMJ008_SRL1_3UTR	GATCAGAAACAAAAAGAACTTAAAGTTTTAGAGCTAG	CTAGCTCTAAAACTTTAAGTTCTTTTTGTTTCT	AGAAACAAAAAGAACTTAAAAGG
gMJ005_SCW4_gRNA_orf_3UTR	overlaps stop codon	ogMJ011_SCW4_stop & ogMJ012_SCW4_stop	GATCAATTGAGTAGACTTATTCATGTTTTAGAGCTAG	CTAGCTCTAAAACATGAATAAGTCTACTCAATT	AATTGAGTAGACTTATTCATTGG
gMJ006_SCW4_gRNA_3UTR	in 3UTR, 52bp from stop codon, minus strand	ogMJ009_Scw4_3UTR & ogMJ010_Scw4_3UTR	GATCAATTTAAAGTTAAAAATATTGTTTTAGAGCTAG	CTAGCTCTAAAACAATATTTTTAACTTTAAATT	AATTTAAAGTTAAAAATATTGGG
gMJ007_UTH1_gRNA_orf_3UTR	overlaps stop codon	ogMJ013_UTH1_stop & ogMJ014_UTH1_stop	GATCTGCTAACTTTGTCTTCTACTGTTTTAGAGCTAG	CTAGCTCTAAAACAGTAGAAGACAAAGTTAGCA	TGCTAACTTTGTCTTCTACTAGG
gMJ008_UTH1_gRNA_3UTR	in 3UTR, overlaps stop codon, minus strand	ogMJ015_UTH1_3UTR & ogMJ016_UTH1_3UTR	GATCTTGCAATATTCAAGGAAAAAGTTTTAGAGCTAG	CTAGCTCTAAAACTTTTTCCTTGAATATTGCAA	TTGCAATATTCAAGGAAAAAAGG
gMJ026	complementation gRNA: gRNA_1_KanMx4	gRNA_1_KanMX4_fwd & gRNA_1_KanMX4_rev	GATCATGAAGGAGAAAACTCACCGGTTTTAGAGCTAG	CTAGCTCTAAAACCGGTGAGTTTTCTCCTTCAT	ATGAAGGAGAAAACTCACCGAGG
gMJ027	complementation gRNA: gRNA_2_KanMx4	gRNA_2_KanMX4_fwd & gRNA_2_KanMX4_rev	GATCGGTCAGACTAAACTGGCTGAGTTTTAGAGCTAG	CTAGCTCTAAAACTCAGCCAGTTTAGTCTGACC	GGTCAGACTAAACTGGCTGACGG

8 Bibliography

Ahlers, J. *et al.* (2023) 'napari: a multi-dimensional image viewer for Python'. Zenodo. Available at: https://doi.org/10.5281/zenodo.8100286.

Aibara, S. *et al.* (2015) 'Domain organization within the nuclear export factor Mex67:Mtr2 generates an extended mRNA binding surface', *Nucleic Acids Research*, 43(3), pp. 1927–1936. Available at: https://doi.org/10.1093/nar/gkv030.

Alberts, B. *et al.* (2022) *Molecular biology of the cell.* Seventh edition / Bruce Alberts [and six others]; with problems by John Wilson, Tim Hunt. New York: W. W. Norton & Company.

Alcázar-Román, A.R. *et al.* (2006) 'Inositol hexakisphosphate and Gle1 activate the DEAD-box protein Dbp5 for nuclear mRNA export', *Nature Cell Biology*, 8(7), pp. 711–716. Available at: https://doi.org/10.1038/ncb1427.

Anderson, J.S. and Parker, R.P. (1998) 'The 3' to 5' degradation of yeast mRNAs is a general mechanism for mRNA turnover that requires the SKI2 DEVH box protein and 3' to 5' exonucleases of the exosome complex.', *The EMBO Journal*, 17(5), pp. 1497–1506. Available at: https://doi.org/10.1093/emboj/17.5.1497.

Araujo, P.R. *et al.* (2012) 'Before It Gets Started: Regulating Translation at the 5' UTR', *Comparative and Functional Genomics*, 2012, p. 475731. Available at: https://doi.org/10.1155/2012/475731.

Ariyachet, C. *et al.* (2017) 'Post-translational modification directs nuclear and hyphal tip localization of C andida albicans mRNA-binding protein Slr1', *Molecular Microbiology*, 104(3), pp. 499–519. Available at: https://doi.org/10.1111/mmi.13643.

Aronov, S. *et al.* (2007) 'mRNAs Encoding Polarity and Exocytosis Factors Are Cotransported with the Cortical Endoplasmic Reticulum to the Incipient Bud in Saccharomyces cerevisiae', *Molecular and Cellular Biology*, 27(9), pp. 3441–3455. Available at: https://doi.org/10.1128/MCB.01643-06.

Arribere, J.A. and Gilbert, W.V. (2013) 'Roles for transcript leaders in translation and mRNA decay revealed by transcript leader sequencing', *Genome Research*, 23(6), pp. 977–987. Available at: https://doi.org/10.1101/gr.150342.112.

Ashe, M.P., De Long, S.K. and Sachs, A.B. (2000) 'Glucose Depletion Rapidly Inhibits Translation Initiation in Yeast', *Molecular Biology of the Cell*, 11(3), pp. 833–848.

Ast, T., Cohen, G. and Schuldiner, M. (2013) 'A Network of Cytosolic Factors Targets SRP-Independent Proteins to the Endoplasmic Reticulum', *Cell*, 152(5), pp. 1134–1145. Available at: https://doi.org/10.1016/j.cell.2013.02.003.

Axelrod, S. *et al.* (2021) 'starfish: scalable pipelines for image-based transcriptomics', *Journal of Open Source Software*, 6(61), p. 2440. Available at: https://doi.org/10.21105/joss.02440.

Bähler, J. *et al.* (1998) 'Heterologous modules for efficient and versatile PCR-based gene targeting in Schizosaccharomyces pombe', *Yeast*, 14(10), pp. 943–951. Available at: https://doi.org/10.1002/(SICI)1097-0061(199807)14:10<943::AID-YEA292>3.0.CO;2-Y.

Bain, J.M. *et al.* (2014) 'Candida albicans Hypha Formation and Mannan Masking of β-Glucan Inhibit Macrophage Phagosome Maturation', *mBio*, 5(6), p. 10.1128/mbio.01874-14. Available at: https://doi.org/10.1128/mbio.01874-14.

Baladrón, V. *et al.* (2002) 'Eng1p, an Endo-1,3-β-Glucanase Localized at the Daughter Side of the Septum, Is Involved in Cell Separation in Saccharomyces cerevisiae', *Eukaryotic Cell*, 1(5), pp. 774–786. Available at: https://doi.org/10.1128/ec.1.5.774-786.2002.

Ballou, E.R., Cook, A.G. and Wallace, E.W.J. (2021) 'Repeated Evolution of Inactive Pseudonucleases in a Fungal Branch of the Dis3/RNase II Family of Nucleases', *Molecular Biology and Evolution*, 38(5), pp. 1837–1846. Available at: https://doi.org/10.1093/molbev/msaa324.

Banks, I.R. *et al.* (2005) 'A Chitin Synthase and Its Regulator Protein Are Critical for Chitosan Production and Growth of the Fungal Pathogen Cryptococcus neoformans', *Eukaryotic Cell*, 4(11), pp. 1902–1912. Available at: https://doi.org/10.1128/ec.4.11.1902-1912.2005.

Bashirullah, A., Cooperstock, R.L. and Lipshitz, H.D. (1998) 'RNA LOCALIZATION IN DEVELOPMENT', *Annual Review of Biochemistry*, 67(Volume 67, 1998), pp. 335–394. Available at: https://doi.org/10.1146/annurev.biochem.67.1.335.

Baumann, S. *et al.* (2012) 'Kinesin-3 and dynein mediate microtubule-dependent co-transport of mRNPs and endosomes', *Journal of Cell Science*, 125(11), pp. 2740–2752. Available at: https://doi.org/10.1242/jcs.101212.

Bayne, R.A. *et al.* (2022) 'Yeast Ssd1 is a non-enzymatic member of the RNase II family with an alternative RNA recognition site', *Nucleic Acids Research*, 50(5), pp. 2923–2937. Available at: https://doi.org/10.1093/nar/gkab615.

Becht, P., König, J. and Feldbrügge, M. (2006) 'The RNA-binding protein Rrm4 is essential for polarity in Ustilago maydis and shuttles along microtubules', *Journal of Cell Science*, 119(23), pp. 4964–4973. Available at: https://doi.org/10.1242/jcs.03287.

Bi, E. *et al.* (1998) 'Involvement of an Actomyosin Contractile Ring in Saccharomyces cerevisiae Cytokinesis', *The Journal of Cell Biology*, 142(5), pp. 1301–1312.

Bobola, N. *et al.* (1996) 'Asymmetric Accumulation of Ash1p in Postanaphase Nuclei Depends on a Myosin and Restricts Yeast Mating-Type Switching to Mother Cells', *Cell*, 84(5), pp. 699–709. Available at: https://doi.org/10.1016/S0092-8674(00)81048-X.

Botman, D. *et al.* (2019) 'In vivo characterisation of fluorescent proteins in budding yeast', *Scientific Reports*, 9, p. 2234. Available at: https://doi.org/10.1038/s41598-019-38913-z.

Bradski, G. (2000) *The Opencv Library*, *Dr. Dobb's J. Softw. Tools*.

Brand, A. (2012) 'Hyphal Growth in Human Fungal Pathogens and Its Role in Virulence', *International Journal of Microbiology*, 2012, p. 517529. Available at: https://doi.org/10.1155/2012/517529.

Brar, G.A. (2016) 'Beyond the Triplet Code: Context Cues Transform Translation', *Cell*, 167(7), pp. 1681–1692. Available at: https://doi.org/10.1016/j.cell.2016.09.022.

Brar, G.A. and Weissman, J.S. (2015) 'Ribosome profiling reveals the what, when, where, and how of protein synthesis', *Nature reviews. Molecular cell biology*, 16(11), pp. 651–664. Available at: https://doi.org/10.1038/nrm4069.

Breker, M., Gymrek, M. and Schuldiner, M. (2013) 'A novel single-cell screening platform reveals proteome plasticity during yeast stress responses', *The Journal of Cell Biology*, 200(6), pp. 839–850. Available at: https://doi.org/10.1083/jcb.201301120.

Brown, C.E. and Sachs, A.B. (1998) 'Poly(A) Tail Length Control in Saccharomyces cerevisiae Occurs by Message-Specific Deadenylation', *Molecular and Cellular Biology*, 18(11), pp. 6548–6559.

Brown, T.A. (2002) *Genomes / T.A. Brown.* Second edition. Oxford: Bios Scientific Publishers.

Bulik, D.A. *et al.* (2003) 'Chitin Synthesis in Saccharomyces cerevisiae in Response to Supplementation of Growth Medium with Glucosamine and Cell Wall Stress', *Eukaryotic Cell*, 2(5), pp. 886–900. Available at: https://doi.org/10.1128/EC.2.5.886-900.2003.

Burd, C.G. and Dreyfuss, G. (1994) 'Conserved Structures and Diversity of Functions of RNA-Binding Proteins', *Science*, 265(5172), pp. 615–621. Available at: https://doi.org/10.1126/science.8036511.

Caballero-Lima, D. *et al.* (2014) 'In andida albicans hyphae, Sec2p is physically associated with mRNA on secretory vesicles', *Molecular Microbiology*, 94(4), pp. 828–842. Available at: https://doi.org/10.1111/mmi.12799.

Cabib, E. (2004) 'The septation apparatus, a chitin-requiring machine in budding yeast', *Archives of Biochemistry and Biophysics*, 426(2), pp. 201–207. Available at: https://doi.org/10.1016/j.abb.2004.02.030.

Cai, T. *et al.* (2002) 'The Saccharomyces cerevisiae RNase mitochondrial RNA processing is critical for cell cycle progression at the end of mitosis.', *Genetics*, 161(3), pp. 1029–1042.

Carpenter, A.E. *et al.* (2006) 'CellProfiler: image analysis software for identifying and quantifying cell phenotypes', *Genome Biology*, 7(10), p. R100. Available at: https://doi.org/10.1186/gb-2006-7-10-r100.

Chang, P. *et al.* (2004) 'Localization of RNAs to the Mitochondrial Cloud in Xenopus Oocytes through Entrapment and Association with Endoplasmic Reticulum', *Molecular Biology of the Cell*, 15(10), pp. 4669–4681. Available at: https://doi.org/10.1091/mbc.E04-03-0265.

Chen, C.-Y. and Rosamondt, J. (1998) 'Candida albicans SSDl can suppress multiple mutations in Saccharomyces cere visiae', *Microbiology*, 144(11), pp. 2941–2950. Available at: https://doi.org/10.1099/00221287-144-11-2941.

Chen, K.-M. *et al.* (2015) 'Metazoan Maelstrom is an RNA-binding protein that has evolved from an ancient nuclease active in protists', *RNA*, 21(5), pp. 833–839. Available at: https://doi.org/10.1261/rna.049437.114.

Chen, X., Zaro, J. and Shen, W.-C. (2013) 'Fusion Protein Linkers: Property, Design and Functionality', *Advanced drug delivery reviews*, 65(10), pp. 1357–1369. Available at: https://doi.org/10.1016/j.addr.2012.09.039.

Christensen, J.R. and Reck-Peterson, S.L. (2022) 'Hitchhiking Across Kingdoms: Cotransport of Cargos in Fungal, Animal, and Plant Cells', *Annual Review of Cell and Developmental Biology*, 38(Volume 38, 2022), pp. 155–178. Available at: https://doi.org/10.1146/annurev-cellbio-120420-104341.

Cohen, N., Aviram, N. and Schuldiner, M. (2023) 'A systematic proximity ligation approach to studying protein-substrate specificity identifies the substrate spectrum of the Ssh1 translocon', *The EMBO Journal*, 42(11), p. e113385. Available at: https://doi.org/10.15252/embj.2022113385.

Colman-Lerner, A., Chin, T.E. and Brent, R. (2001) 'Yeast Cbk1 and Mob2 activate daughter-specific genetic programs to induce asymmetric cell fates', *Cell*, 107(6), pp. 739–750. Available at: https://doi.org/10.1016/s0092-8674(01)00596-7.

Colomina, N. *et al.* (2008) 'Whi3, a Developmental Regulator of Budding Yeast, Binds a Large Set of mRNAs Functionally Related to the Endoplasmic Reticulum * ♦', *Journal of Biological Chemistry*, 283(42), pp. 28670–28679. Available at: https://doi.org/10.1074/jbc.M804604200.

Colomina, N. *et al.* (2009) 'Whi3 regulates morphogenesis in budding yeast by enhancing Cdk functions in apical growth', *Cell Cycle (Georgetown, Tex.)*, 8(12), pp. 1912–1920. Available at: https://doi.org/10.4161/cc.8.12.8740.

Cormack, B.P., Ghori, N. and Falkow, S. (1999) 'An Adhesin of the Yeast Pathogen Candida glabrata Mediating Adherence to Human Epithelial Cells', *Science*, 285(5427), pp. 578–582. Available at: https://doi.org/10.1126/science.285.5427.578.

Costanzo, M. *et al.* (2010) 'The Genetic Landscape of a Cell', *Science (New York, N.Y.)*, 327(5964), pp. 425–431. Available at: https://doi.org/10.1126/science.1180823.

Crane, M.M. *et al.* (2014) 'A Microfluidic System for Studying Ageing and Dynamic Single-Cell Responses in Budding Yeast', *PLOS ONE*, 9(6), p. e100042. Available at: https://doi.org/10.1371/journal.pone.0100042.

Cranfill, P.J. *et al.* (2016) 'Quantitative assessment of fluorescent proteins', *Nature Methods*, 13(7), pp. 557–562. Available at: https://doi.org/10.1038/nmeth.3891.

Crawford, R.A. and Pavitt, G.D. (2019) 'Translational regulation in response to stress in Saccharomyces cerevisiae', *Yeast (Chichester, England)*, 36(1), pp. 5–21. Available at: https://doi.org/10.1002/yea.3349.

Cross, B.C.S. *et al.* (2009) 'Delivering proteins for export from the cytosol', *Nature Reviews Molecular Cell Biology*, 10(4), pp. 255–264. Available at: https://doi.org/10.1038/nrm2657.

Das, S., Sarkar, D. and Das, B. (2017) 'The interplay between transcription and mRNA degradation in *Saccharomyces cerevisiae*', *Microbial Cell*, 4(7), pp. 212–228. Available at: https://doi.org/10.15698/mic2017.07.580.

Dassi, E. (2017) 'Handshakes and Fights: The Regulatory Interplay of RNA-Binding Proteins', *Frontiers in Molecular Biosciences*, 4. Available at: https://doi.org/10.3389/fmolb.2017.00067.

Dee, J.M. *et al.* (2015) 'Cytology and molecular phylogenetics of Monoblepharidomycetes provide evidence for multiple independent origins of the hyphal habit in the Fungi', *Mycologia*, 107(4), pp. 710–728. Available at: https://doi.org/10.3852/14-275.

Deng, Y., Singer, R.H. and Gu, W. (2008) 'Translation of ASH1 mRNA is repressed by Puf6p–Fun12p/eIF5B interaction and released by CK2 phosphorylation', *Genes & Development*, 22(8), pp. 1037–1050. Available at: https://doi.org/10.1101/gad.1611308.

Desai, J.V. (2018) 'Candida albicans Hyphae: From Growth Initiation to Invasion', *Journal of Fungi*, 4(1), p. 10. Available at: https://doi.org/10.3390/jof4010010.

Dichtl, K., Samantaray, S. and Wagener, J. (2016) 'Cell wall integrity signalling in human pathogenic fungi', *Cellular Microbiology*, 18(9), pp. 1228–1238. Available at: https://doi.org/10.1111/cmi.12612.

Dickson, R.M. *et al.* (1997) 'On/off blinking and switching behaviour of single molecules of green fluorescent protein', *Nature*, 388(6640), pp. 355–358. Available at: https://doi.org/10.1038/41048.

van Dijk, E. *et al.* (2002) 'Human Dcp2: a catalytically active mRNA decapping enzyme located in specific cytoplasmic structures', *The EMBO Journal*, 21(24), pp. 6915–6924. Available at: https://doi.org/10.1093/emboj/cdf678.

Ding, D. *et al.* (1993) 'Dynamic Hsp83 RNA localization during Drosophila oogenesis and embryogenesis.', *Molecular and Cellular Biology*, 13(6), pp. 3773–3781.

Dreyfuss, G., Choi, Y.D. and Adam, S.A. (1984) 'Characterization of heterogeneous nuclear RNA-protein complexes in vivo with monoclonal antibodies.', *Molecular and Cellular Biology*, 4(6), pp. 1104–1114.

Droettboom, M. *et al.* (2015) 'matplotlib: v1.4.3'. Zenodo. Available at: https://doi.org/10.5281/zenodo.15423.

Dunckley, T. and Parker, R. (1999) 'The DCP2 protein is required for mRNA decapping in Saccharomyces cerevisiae and contains a functional MutT motif.', *The EMBO Journal*, 18(19), pp. 5411–5422. Available at: https://doi.org/10.1093/emboj/18.19.5411.

Dvir, S. *et al.* (2013) 'Deciphering the rules by which 5'-UTR sequences affect protein expression in yeast', *Proceedings of the National Academy of Sciences of the United States of America*, 110(30), pp. E2792–E2801. Available at: https://doi.org/10.1073/pnas.1222534110.

Eguchi, Y. *et al.* (2010) 'Estimating the protein burden limit of yeast cells by measuring the expression limits of glycolytic proteins', *eLife*, 7, p. e34595. Available at: https://doi.org/10.7554/eLife.34595.

Elson, S.L. *et al.* (2009) 'An RNA Transport System in Candida albicans Regulates Hyphal Morphology and Invasive Growth', *PLOS Genetics*, 5(9), p. e1000664. Available at: https://doi.org/10.1371/journal.pgen.1000664.

Evans, DRH. and Stark, MJR. (1997) 'Mutations in the Saccharomyces Cerevisiae Type 2a Protein Phosphatase Catalytic Subunit Reveal Roles in Cell Wall Integrity, Actin Cytoskeleton Organization and Mitosis', *Genetics*, 145(2), pp. 227–241.

Feldheim, D. and Schekman, R. (1994) 'Sec72p contributes to the selective recognition of signal peptides by the secretory polypeptide translocation complex.', *Journal of Cell Biology*, 126(4), pp. 935–943. Available at: https://doi.org/10.1083/jcb.126.4.935.

Femino, A.M. *et al.* (1998) 'Visualization of Single RNA Transcripts in Situ', *Science*, 280(5363), pp. 585–590. Available at: https://doi.org/10.1126/science.280.5363.585.

Fiedler, D. *et al.* (2009) 'Functional Organization of the S. cerevisiae Phosphorylation Network', *Cell*, 136(5), pp. 952–963. Available at: https://doi.org/10.1016/j.cell.2008.12.039.

Frantsuzov, P. *et al.* (2008) 'Universal emission intermittency in quantum dots, nanorods and nanowires', *Nature Physics*, 4(7), pp. 519–522. Available at: https://doi.org/10.1038/nphys1001.

Free, S.J. (2013) 'Chapter Two - Fungal Cell Wall Organization and Biosynthesis', in T. Friedmann, J.C. Dunlap, and S.F. Goodwin (eds) *Advances in Genetics*. Academic Press, pp. 33–82. Available at: https://doi.org/10.1016/B978-0-12-407677-8.00002-6.

Freeberg, M.A. *et al.* (2013) 'Pervasive and dynamic protein binding sites of the mRNA transcriptome in Saccharomyces cerevisiae', *Genome Biology*, 14(2), p. R13. Available at: https://doi.org/10.1186/gb-2013-14-2-r13.

Frost, D.J. *et al.* (1994) 'Characterization of (1,3)-β-glucan synthase in Candida albicans: microsomal assay from the yeast or mycelial morphological forms and a permeabilized whole-cell assay', *Microbiology*, 140(9), pp. 2239–2246. Available at: https://doi.org/10.1099/13500872-140-9-2239.

Fundakowski, J., Hermesh, O. and Jansen, R.-P. (2012) 'Localization of a Subset of Yeast mRNAs Depends on Inheritance of Endoplasmic Reticulum', *Traffic*, 13(12), pp. 1642–1652. Available at: https://doi.org/10.1111/tra.12011.

Galán-Díez, M. *et al.* (2010) 'Candida albicans β-Glucan Exposure Is Controlled by the Fungal CEK1-Mediated Mitogen-Activated Protein Kinase Pathway That Modulates Immune Responses Triggered through Dectin-1', *Infection and Immunity*, 78(4), pp. 1426–1436. Available at: https://doi.org/10.1128/iai.00989-09.

Gank, K.D. *et al.* (2008) 'SSD1 Is Integral to Host Defense Peptide Resistance in Candida albicans', *Eukaryotic Cell*, 7(8), pp. 1318–1327. Available at: https://doi.org/10.1128/ec.00402-07.

Garcia, J.F. and Parker, R. (2015) 'MS2 coat proteins bound to yeast mRNAs block 5' to 3' degradation and trap mRNA decay products: implications for the localization of mRNAs by MS2-MCP system', *RNA*, 21(8), pp. 1393–1395. Available at: https://doi.org/10.1261/rna.051797.115.

García, R. *et al.* (2019) 'Signalling through the yeast MAPK Cell Wall Integrity pathway controls P-body assembly upon cell wall stress', *Scientific Reports*, 9(1), p. 3186. Available at: https://doi.org/10.1038/s41598-019-40112-9.

Garcia-Rubio, R. *et al.* (2020) 'The Fungal Cell Wall: Candida, Cryptococcus, and Aspergillus Species', *Frontiers in Microbiology*, 10. Available at: https://doi.org/10.3389/fmicb.2019.02993.

George, L. *et al.* (2018) 'Intracellular RNA-tracking methods', *Open Biology*, 8(10), p. 180104. Available at: https://doi.org/10.1098/rsob.180104.

Gerik, K.J. *et al.* (2005) 'Cell wall integrity is dependent on the PKC1 signal transduction pathway in Cryptococcus neoformans', *Molecular Microbiology*, 58(2), pp. 393–408. Available at: https://doi.org/10.1111/j.1365-2958.2005.04843.x.

Gerstberger, S., Hafner, M. and Tuschl, T. (2014) 'A census of human RNA-binding proteins', *Nature Reviews Genetics*, 15(12), pp. 829–845. Available at: https://doi.org/10.1038/nrg3813.

Gilbert, W.V. *et al.* (2007) 'Cap-Independent Translation Is Required for Starvation-Induced Differentiation in Yeast', *Science*, 317(5842), pp. 1224–1227. Available at: https://doi.org/10.1126/science.1144467.

Gill, T. *et al.* (2004) 'RNase MRP Cleaves the CLB2 mRNA To Promote Cell Cycle Progression: Novel Method of mRNA Degradation', *Molecular and Cellular Biology*, 24(3), pp. 945–953. Available at: https://doi.org/10.1128/MCB.24.3.945-953.2004.

Gillies, S. (2023) '"Shapely: manipulation and analysis of geometric objects".' Available at: https://github.com/shapely/shapely.

Goldstrohm, A.C. *et al.* (2006) 'PUF proteins bind Pop2p to regulate messenger RNAs', *Nature Structural & Molecular Biology*, 13(6), pp. 533–539. Available at: https://doi.org/10.1038/nsmb1100.

Gonsalvez, G.B. and Long, R.M. (2012) 'Spatial regulation of translation through RNA localization', *F1000 Biology Reports*, 4, p. 16. Available at: https://doi.org/10.3410/B4-16.

Gonsalvez, G.B., Urbinati, C.R. and Long, R.M. (2005) 'RNA localization in yeast: moving towards a mechanism', *Biology of the Cell*, 97(1), pp. 75–86. Available at: https://doi.org/10.1042/BC20040066.

González, M. and Fernando, A. (2023) 'Phenotyping single cells of Saccharomyces cerevisiae using an end-to-end analysis of high-content time-lapse microscopy'. Available at: https://doi.org/10.7488/era/3596.

Goss, D.J. and Theil, E.C. (2011) 'Iron Responsive mRNAs: A Family of Fe2+ Sensitive Riboregulators', *Accounts of chemical research*, 44(12), pp. 1320–1328. Available at: https://doi.org/10.1021/ar2001149.

Gow, N.A.R., Latge, J.-P. and Munro, C.A. (2017) 'The Fungal Cell Wall: Structure, Biosynthesis, and Function', *Microbiology Spectrum*, 5(3), p. 10.1128/microbiolspec.funk-0035–2016. Available at: https://doi.org/10.1128/microbiolspec.funk-0035-2016.

de Groot, P.W.J. *et al.* (2008) 'The Cell Wall of the Human Pathogen Candida glabrata: Differential Incorporation of Novel Adhesin-Like Wall Proteins', *Eukaryotic Cell*, 7(11), pp. 1951–1964. Available at: https://doi.org/10.1128/EC.00284-08.

Guo, B. *et al.* (2000) 'A Saccharomyces gene family involved in invasive growth, cell–cell adhesion, and mating', *Proceedings of the National Academy of Sciences of the United States of America*, 97(22), pp. 12158–12163.

Guo, Z. and Sherman, F. (1996) 'Signals Sufficient for 3'-End Formation of Yeast mRNA', *Molecular and Cellular Biology*, 16(6), pp. 2772–2776. Available at: https://doi.org/10.1128/MCB.16.6.2772.

Hagen, I. *et al.* (2004) 'Sed1p and Srl1p are required to compensate for cell wall instability in Saccharomyces cerevisiae mutants defective in multiple GPI-anchored mannoproteins', *Molecular Microbiology*, 52(5), pp. 1413–1425. Available at: https://doi.org/10.1111/j.1365-2958.2004.04064.x.

Haimovich, G. *et al.* (2016) 'Use of the MS2 aptamer and coat protein for RNA localization in yeast: A response to "MS2 coat proteins bound to yeast mRNAs block 5' to 3' degradation and trap mRNA decay products: implications for the localization of mRNAs by MS2-MCP system"', *RNA*, 22(5), pp. 660–666. Available at: https://doi.org/10.1261/rna.055095.115.

Haimovich, G. and Gerst, J.E. (2018) 'Single-molecule Fluorescence in situ Hybridization (smFISH) for RNA Detection in Adherent Animal Cells', *Bio-protocol*, 8(21), p. e3070. Available at: https://doi.org/10.21769/BioProtoc.3070.

Haim-Vilmovsky, L. and Gerst, J.E. (2009) 'm-TAG: a PCR-based genomic integration method to visualize the localization of specific endogenous mRNAs in vivo in yeast', *Nature Protocols*, 4(9), pp. 1274–1284. Available at: https://doi.org/10.1038/nprot.2009.115.

Hall, R.A. and Wallace, E.W.J. (2022) 'Post-transcriptional control of fungal cell wall synthesis', *The Cell Surface*, 8, p. 100074. Available at: https://doi.org/10.1016/j.tcsw.2022.100074.

Harms, M.J. and Thornton, J.W. (2010) 'Analyzing protein structure and function using ancestral gene reconstruction', *Current opinion in structural biology*, 20(3), pp. 360–366. Available at: https://doi.org/10.1016/j.sbi.2010.03.005.

Harris, C.R. *et al.* (2020) 'Array programming with NumPy', *Nature*, 585(7825), pp. 357–362. Available at: https://doi.org/10.1038/s41586-020-2649-2.

Harris, S.D. (2011) 'Hyphal morphogenesis: an evolutionary perspective', *Fungal Biology*, 115(6), pp. 475–484. Available at: https://doi.org/10.1016/j.funbio.2011.02.002.

Hartwell, L.H. *et al.* (1974) 'Genetic Control of the Cell Division Cycle in Yeast', *Science*, 183(4120), pp. 46–51. Available at: https://doi.org/10.1126/science.183.4120.46.

Hartwell, L.H. and Unger, M.W. (1977) 'Unequal division in Saccharomyces cerevisiae and its implications for the control of cell division', *The Journal of Cell Biology*, 75(2 Pt 1), pp. 422–435. Available at: https://doi.org/10.1083/jcb.75.2.422.

Healey, K.R. *et al.* (2020) 'Differential Regulation of Echinocandin Targets Fks1 and Fks2 in Candida glabrata by the Post-Transcriptional Regulator Ssd1', *Journal of Fungi*, 6(3), p. 143. Available at: https://doi.org/10.3390/jof6030143.

Heasman, J., Quarmby, J. and Wylie, C.C. (1984) 'The mitochondrial cloud of *Xenopus* oocytes: The source of germinal granule material', *Developmental Biology*, 105(2), pp. 458–469. Available at: https://doi.org/10.1016/0012-1606(84)90303-8.

Hentze, M.W. *et al.* (2018) 'A brave new world of RNA-binding proteins', *Nature Reviews Molecular Cell Biology*, 19(5), pp. 327–341. Available at: https://doi.org/10.1038/nrm.2017.130.

Hibbett, D.S. *et al.* (2007) 'A higher-level phylogenetic classification of the *Fungi*', *Mycological Research*, 111(5), pp. 509–547. Available at: https://doi.org/10.1016/j.mycres.2007.03.004.

Hickey, S.M. *et al.* (2022) 'Fluorescence Microscopy—An Outline of Hardware, Biological Handling, and Fluorophore Considerations', *Cells*, 11(1), p. 35. Available at: https://doi.org/10.3390/cells11010035.

Hinnebusch, A.G. (2011) 'Molecular Mechanism of Scanning and Start Codon Selection in Eukaryotes', *Microbiology and Molecular Biology Reviews*, 75(3), pp. 434–467. Available at: https://doi.org/10.1128/mmbr.00008-11.

Hinnebusch, A.G. and Lorsch, J.R. (2012) 'The Mechanism of Eukaryotic Translation Initiation: New Insights and Challenges', *Cold Spring Harbor Perspectives in Biology*, 4(10), p. a011544. Available at: https://doi.org/10.1101/cshperspect.a011544.

Hogan, D.J. *et al.* (2008) 'Diverse RNA-binding proteins interact with functionally related sets of RNAs, suggesting an extensive regulatory system', *PLoS biology*, 6(10), p. e255. Available at: https://doi.org/10.1371/journal.pbio.0060255.

Holmes, K.J. *et al.* (2013) 'Whi3, an S. cerevisiae RNA-Binding Protein, Is a Component of Stress Granules That Regulates Levels of Its Target mRNAs', *PLOS ONE*, 8(12), p. e84060. Available at: https://doi.org/10.1371/journal.pone.0084060.

Homann, O.R. *et al.* (2009) 'A Phenotypic Profile of the Candida albicans Regulatory Network', *PLoS Genetics*, 5(12), p. e1000783. Available at: https://doi.org/10.1371/journal.pgen.1000783.

Hose, J. *et al.* (2020) 'The genetic basis of aneuploidy tolerance in wild yeast', *eLife*. Edited by H. Klein et al., 9, p. e52063. Available at: https://doi.org/10.7554/eLife.52063.

Hsin, J.-P. and Manley, J.L. (2012) 'The RNA polymerase II CTD coordinates transcription and RNA processing', *Genes & Development*, 26(19), pp. 2119–2137. Available at: https://doi.org/10.1101/gad.200303.112.

Hsu, C.L. and Stevens, A. (1993) 'Yeast cells lacking 5'-->3' exoribonuclease 1 contain mRNA species that are poly(A) deficient and partially lack the 5' cap structure.', *Molecular and Cellular Biology*, 13(8), pp. 4826–4835.

Huh, W.-K. *et al.* (2003) 'Global analysis of protein localization in budding yeast', *Nature*, 425(6959), pp. 686–691. Available at: https://doi.org/10.1038/nature02026.

Hüttelmaier, S. *et al.* (2005) 'Spatial regulation of β-actin translation by Src-dependent phosphorylation of ZBP1', *Nature*, 438(7067), pp. 512–515. Available at: https://doi.org/10.1038/nature04115.

Imbert, A. *et al.* (2022) 'FISH-quant v2: a scalable and modular tool for smFISH image analysis', *RNA*, 28(6), pp. 786–795. Available at: https://doi.org/10.1261/rna.079073.121.

Ingolia, N.T. *et al.* (2009) 'Genome-Wide Analysis in Vivo of Translation with Nucleotide Resolution Using Ribosome Profiling', *Science*, 324(5924), pp. 218–223. Available at: https://doi.org/10.1126/science.1168978.

Iraqui, I. *et al.* (2005) 'The Yak1p kinase controls expression of adhesins and biofilm formation in Candida glabrata in a Sir4p-dependent pathway', *Molecular Microbiology*, 55(4), pp. 1259–1271. Available at: https://doi.org/10.1111/j.1365-2958.2004.04475.x.

Jabra-Rizk, M.A. *et al.* (2016) 'Candida albicans Pathogenesis: Fitting within the Host-Microbe Damage Response Framework', *Infection and Immunity*, 84(10), pp. 2724–2739. Available at: https://doi.org/10.1128/IAI.00469-16.

Jackson, R.J., Hellen, C.U.T. and Pestova, T.V. (2010) 'THE MECHANISM OF EUKARYOTIC TRANSLATION INITIATION AND PRINCIPLES OF ITS REGULATION', *Nature reviews. Molecular cell biology*, 11(2), pp. 113–127. Available at: https://doi.org/10.1038/nrm2838.

Jambhekar, A. *et al.* (2005) 'Unbiased selection of localization elements reveals cis-acting determinants of mRNA bud localization in Saccharomyces cerevisiae', *Proceedings of the National Academy of Sciences of the United States of America*, 102(50), pp. 18005–18010. Available at: https://doi.org/10.1073/pnas.0509229102.

Jansen, J.M. *et al.* (2009) 'Cbk1 regulation of the RNA binding protein Ssd1 integrates cell fate with translational control', *Current biology : CB*, 19(24), pp. 2114–2120. Available at: https://doi.org/10.1016/j.cub.2009.10.071.

Jansen, R.-P. (2001) ‘mRNA localization: message on the move’, *Nature Reviews Molecular Cell Biology*, 2(4), pp. 247–256. Available at: https://doi.org/10.1038/35067016.

Jiang, S. *et al.* (2012) ‘A proteomics approach to the cell-surface interactome using the enzyme-mediated activation of radical sources reaction’, *Proteomics*, 12(1), pp. 54–62. Available at: https://doi.org/10.1002/pmic.201100551.

Juanes, M.A. and Piatti, S. (2016) ‘The final cut: cell polarity meets cytokinesis at the bud neck in S. cerevisiae’, *Cellular and Molecular Life Sciences*, 73(16), pp. 3115–3136. Available at: https://doi.org/10.1007/s00018-016-2220-3.

Jurado, A.R. *et al.* (2014) ‘Structure and Function of Pre-mRNA 5′-End Capping Quality Control and 3′-End Processing’, *Biochemistry*, 53(12), pp. 1882–1898. Available at: https://doi.org/10.1021/bi401715v.

Kadosh, D. (2016) ‘Control of Candida albicans morphology and pathogenicity by post-transcriptional mechanisms’, *Cellular and molecular life sciences : CMLS*, 73(22), pp. 4265–4278. Available at: https://doi.org/10.1007/s00018-016-2294-y.

Kaeberlein, M. and Guarente, L. (2002) ‘Saccharomyces cerevisiae MPT5 and SSD1 function in parallel pathways to promote cell wall integrity’, *Genetics*, 160(1), pp. 83–95. Available at: https://doi.org/10.1093/genetics/160.1.83.

Katahira, J. *et al.* (1999) ‘The Mex67p-mediated nuclear mRNA export pathway is conserved from yeast to human.’, *The EMBO Journal*, 18(9), pp. 2593–2609. Available at: https://doi.org/10.1093/emboj/18.9.2593.

Kaur, R. *et al.* (2005) ‘A yeast by any other name: *Candida glabrata* and its interaction with the host’, *Current Opinion in Microbiology*, 8(4), pp. 378–384. Available at: https://doi.org/10.1016/j.mib.2005.06.012.

Keene, J.D. and Tenenbaum, S.A. (2002) ‘Eukaryotic mRNPs May Represent Posttranscriptional Operons’, *Molecular Cell*, 9(6), pp. 1161–1167. Available at: https://doi.org/10.1016/S1097-2765(02)00559-2.

Kelliher, C.M. *et al.* (2016) ‘Investigating Conservation of the Cell-Cycle-Regulated Transcriptional Program in the Fungal Pathogen, Cryptococcus neoformans’, *PLOS Genetics*, 12(12), p. e1006453. Available at: https://doi.org/10.1371/journal.pgen.1006453.

Keppler, A. *et al.* (2003) ‘A general method for the covalent labeling of fusion proteins with small molecules in vivo’, *Nature Biotechnology*, 21(1), pp. 86–89. Available at: https://doi.org/10.1038/nbt765.

Kiss, E. *et al.* (2019) ‘Comparative genomics reveals the origin of fungal hyphae and multicellularity’, *Nature Communications*, 10(1), p. 4080. Available at: https://doi.org/10.1038/s41467-019-12085-w.

Klis, F.M., Boorsma, A. and De Groot, P.W.J. (2006) ‘Cell wall construction in Saccharomyces cerevisiae’, *Yeast*, 23(3), pp. 185–202. Available at: https://doi.org/10.1002/yea.1349.

Kloc, M. *et al.* (2000) ‘The Targeting of Xcat2 mRNA to the Germinal Granules Depends on a *cis*-Acting Germinal Granule Localization Element within the 3′UTR’, *Developmental Biology*, 217(2), pp. 221–229. Available at: https://doi.org/10.1006/dbio.1999.9554.

Kloc, M. and Etkin, L.D. (2005) 'RNA localization mechanisms in oocytes', *Journal of Cell Science*, 118(2), pp. 269–282. Available at: https://doi.org/10.1242/jcs.01637.

Kloc, M., Larabell, C. and Etkin, L.D. (1996) 'Elaboration of the Messenger Transport Organizer Pathway for Localization of RNA to the Vegetal Cortex of*Xenopus*Oocytes', *Developmental Biology*, 180(1), pp. 119–130. Available at: https://doi.org/10.1006/dbio.1996.0289.

Kloc, M., Zearfoss, N.R. and Etkin, L.D. (2002) 'Mechanisms of Subcellular mRNA Localization', *Cell*, 108(4), pp. 533–544. Available at: https://doi.org/10.1016/S0092-8674(02)00651-7.

Kluyver, T. *et al.* (2016) 'Jupyter Notebooks – a publishing format for reproducible computational workflows', in F. Loizides and B. Scmidt (eds). *20th International Conference on Electronic Publishing (01/01/16)*, IOS Press, pp. 87–90. Available at: https://doi.org/10.3233/978-1-61499-649-1-87.

Kolitz, S.E., Takacs, J.E. and Lorsch, J.R. (2009) 'Kinetic and thermodynamic analysis of the role of start codon/anticodon base pairing during eukaryotic translation initiation', *RNA*, 15(1), pp. 138–152. Available at: https://doi.org/10.1261/rna.1318509.

Kollár, R. *et al.* (1997) 'Architecture of the Yeast Cell Wall: β(1→6)-GLUCAN INTERCONNECTS MANNOPROTEIN, β(1→3)-GLUCAN, AND CHITIN *', *Journal of Biological Chemistry*, 272(28), pp. 17762–17775. Available at: https://doi.org/10.1074/jbc.272.28.17762.

König, J. *et al.* (2012) 'Erratum: Protein–RNA interactions: new genomic technologies and perspectives', *Nature Reviews Genetics*, 13(3), pp. 220–220. Available at: https://doi.org/10.1038/nrg3183.

Kradin, R. (2017) *Diagnostic Pathology Of Infectious Disease*. 2nd edn.

Kurischko, C., Kuravi, V.K., *et al.* (2011) 'Nucleocytoplasmic shuttling of Ssd1 defines the destiny of its bound mRNAs', *Molecular microbiology*, 81(3), pp. 831–849. Available at: https://doi.org/10.1111/j.1365-2958.2011.07731.x.

Kurischko, C., Kim, H.K., *et al.* (2011) 'The yeast Cbk1 kinase regulates mRNA localization via the mRNA-binding protein Ssd1', *The Journal of Cell Biology*, 192(4), pp. 583–598. Available at: https://doi.org/10.1083/jcb.201011061.

Kuznetsov, E. *et al.* (2013) 'SUN Family Proteins Sun4p, Uth1p and Sim1p Are Secreted from Saccharomyces cerevisiae and Produced Dependently on Oxygen Level', *PLoS ONE*, 8(9), p. e73882. Available at: https://doi.org/10.1371/journal.pone.0073882.

Kuznetsov, E., Váchová, L. and Palková, Z. (2016) 'Cellular localization of Sun4p and its interaction with proteins in the yeast birth scar', *Cell Cycle*, 15(14), pp. 1898–1907. Available at: https://doi.org/10.1080/15384101.2016.1189043.

Lapointe, C.P. *et al.* (2017) 'Architecture and dynamics of overlapped RNA regulatory networks', *RNA*, 23(11), pp. 1636–1647. Available at: https://doi.org/10.1261/rna.062687.117.

Latgé, J.-P., Beauvais, A. and Chamilos, G. (2017) 'The Cell Wall of the Human Fungal Pathogen Aspergillus fumigatus: Biosynthesis, Organization, Immune Response, and Virulence', *Annual Review of Microbiology*, 71(1), pp. 99–116. Available at: https://doi.org/10.1146/annurev-micro-030117-020406.

Laughery, M.F. and Wyrick, J.J. (2019) 'Simple CRISPR-Cas9 Genome Editing in Saccharomyces cerevisiae', *Current Protocols in Molecular Biology*, 129(1), p. e110. Available at: https://doi.org/10.1002/cpmb.110.

Lazzaretti, D. *et al.* (2016) 'The bicoid mRNA localization factor Exuperantia is an RNA-binding pseudonuclease', *Nature Structural & Molecular Biology*, 23(8), pp. 705–713. Available at: https://doi.org/10.1038/nsmb.3254.

Lee, F.C.Y. and Ule, J. (2018) 'Advances in CLIP Technologies for Studies of Protein-RNA Interactions', *Molecular Cell*, 69(3), pp. 354–369. Available at: https://doi.org/10.1016/j.molcel.2018.01.005.

Lee, H. *et al.* (2010) 'Use of the Plant Defense Protein Osmotin To Identify Fusarium oxysporum Genes That Control Cell Wall Properties', *Eukaryotic Cell*, 9(4), pp. 558–568. Available at: https://doi.org/10.1128/EC.00316-09.

Lee, H.C. and Bernstein, H.D. (2001) 'The targeting pathway of Escherichia coli presecretory and integral membrane proteins is specified by the hydrophobicity of the targeting signal', *Proceedings of the National Academy of Sciences of the United States of America*, 98(6), pp. 3471–3476. Available at: https://doi.org/10.1073/pnas.051484198.

Lee, H.-J. *et al.* (2015) 'The NDR Kinase Cbk1 Downregulates the Transcriptional Repressor Nrg1 through the mRNA-Binding Protein Ssd1 in Candida albicans', *Eukaryotic Cell*, 14(7), pp. 671–683. Available at: https://doi.org/10.1128/EC.00016-15.

Li, F. and Palecek, S.P. (2003) 'EAP1, a Candida albicans Gene Involved in Binding Human Epithelial Cells', *Eukaryotic Cell*, 2(6), p. 1266. Available at: https://doi.org/10.1128/EC.2.6.1266-1273.2003.

Li, Y. *et al.* (2017) 'The effects of chemical fixation on the cellular nanostructure', *Experimental cell research*, 358(2), pp. 253–259. Available at: https://doi.org/10.1016/j.yexcr.2017.06.022.

Li, Z. and Nielsen, K. (2017) 'Morphology Changes in Human Fungal Pathogens upon Interaction with the Host', *Journal of Fungi*, 3(4), p. 66. Available at: https://doi.org/10.3390/jof3040066.

Lindquist, S. and Kim, G. (1996) 'Heat-shock protein 104 expression is sufficient for thermotolerance in yeast.', *Proceedings of the National Academy of Sciences of the United States of America*, 93(11), pp. 5301–5306.

Lomakin, I.B. *et al.* (2006) 'The fidelity of translation initiation: reciprocal activities of eIF1, IF3 and YciH', *The EMBO Journal*, 25(1), pp. 196–210. Available at: https://doi.org/10.1038/sj.emboj.7600904.

Long, R.M. *et al.* (2000) 'She2p is a novel RNA-binding protein that recruits the Myo4p–She3p complex to ASH1 mRNA', *The EMBO Journal*, 19(23), pp. 6592–6601. Available at: https://doi.org/10.1093/emboj/19.23.6592.

Longtine, M.S. *et al.* (1998) 'Additional modules for versatile and economical PCR-based gene deletion and modification in Saccharomyces cerevisiae', *Yeast*, 14(10), pp. 953–961. Available at: https://doi.org/10.1002/(SICI)1097-0061(199807)14:10<953::AID-YEA293>3.0.CO;2-U.

López-Franco, R., Howard, R.J. and Bracker, C.E. (1995) 'Satellite Spitzenkörper in growing hyphal tips', *Protoplasma*, 188(1), pp. 85–103. Available at: https://doi.org/10.1007/BF01276799.

Lord, P.G. and Wheals, A.E. (1981) 'Variability in individual cell cycles of Saccharomyces cerevisiae', *Journal of Cell Science*, 50(1), pp. 361–376. Available at: https://doi.org/10.1242/jcs.50.1.361.

Los, G.V. *et al.* (2008) 'HaloTag: a novel protein labeling technology for cell imaging and protein analysis', *ACS chemical biology*, 3(6), pp. 373–382. Available at: https://doi.org/10.1021/cb800025k.

Lu, F. and Taghbalout, A. (2014) 'The Escherichia coli major exoribonuclease RNase II is a component of the RNA degradosome', *Bioscience Reports*, 34(6). Available at: https://doi.org/10.1042/BSR20140113.

Lum, P.Y., Edwards, S. and Wright, R. (1996) 'Molecular, functional and evolutionary characterization of the gene encoding HMG-CoA reductase in the fission yeast, Schizosaccharomyces pombe', *Yeast*, 12(11), pp. 1107–1124. Available at: https://doi.org/10.1002/(SICI)1097-0061(19960915)12:11<1107::AID-YEA992>3.0.CO;2-E.

Lunde, B.M., Moore, C. and Varani, G. (2007) 'RNA-binding proteins: modular design for efficient function', *Nature Reviews Molecular Cell Biology*, 8(6), pp. 479–490. Available at: https://doi.org/10.1038/nrm2178.

Maekawa, H. *et al.* (2017) 'Polo-like kinase Cdc5 regulates Spc72 recruitment to spindle pole body in the methylotrophic yeast Ogataea polymorpha', *eLife*. Edited by A. Akhmanova, 6, p. e24340. Available at: https://doi.org/10.7554/eLife.24340.

Maekiniemi, A., Singer, R.H. and Tutucci, E. (2020) 'Single molecule mRNA fluorescent in situ hybridization combined with immunofluorescence in S. cerevisiae: Dataset and quantification', *Data in Brief*, 30, p. 105511. Available at: https://doi.org/10.1016/j.dib.2020.105511.

Magidson, V. and Khodjakov, A. (2013) 'Chapter 23 - Circumventing Photodamage in Live-Cell Microscopy', in G. Sluder and D.E. Wolf (eds) *Methods in Cell Biology*. Academic Press (Digital Microscopy), pp. 545–560. Available at: https://doi.org/10.1016/B978-0-12-407761-4.00023-3.

Malecki, M. *et al.* (2013) 'The exoribonuclease Dis3L2 defines a novel eukaryotic RNA degradation pathway', *The EMBO Journal*, 32(13), pp. 1842–1854. Available at: https://doi.org/10.1038/emboj.2013.63.

Marchese, D. *et al.* (2016) 'Advances in the characterization of RNA-binding proteins', *Wiley Interdisciplinary Reviews. RNA*, 7(6), pp. 793–810. Available at: https://doi.org/10.1002/wrna.1378.

Mardis, E.R. (2008) 'The impact of next-generation sequencing technology on genetics', *Trends in Genetics*, 24(3), pp. 133–141. Available at: https://doi.org/10.1016/j.tig.2007.12.007.

Markham, J. and Conchello, J.-A. (2001) 'Artefacts in restored images due to intensity loss in three-dimensional fluorescence microscopy', *Journal of Microscopy*, 204(2), pp. 93–98. Available at: https://doi.org/10.1046/j.1365-2818.2001.00961.x.

Martin, F. *et al.* (2011) 'Cap-Assisted Internal Initiation of Translation of Histone H4', *Molecular Cell*, 41(2), pp. 197–209. Available at: https://doi.org/10.1016/j.molcel.2010.12.019.

Martínez-Pastor, M. t. and Estruch, F. (1996) 'Sudden depletion of carbon source blocks translation, but not transcription, in the yeast Saccharomyces cerevisiae', *FEBS Letters*, 390(3), pp. 319–322. Available at: https://doi.org/10.1016/0014-5793(96)00683-7.

Mayr, C. (2017) ‘Regulation by 3’-Untranslated Regions’, *Annual Review of Genetics*, 51(Volume 51, 2017), pp. 171–194. Available at: https://doi.org/10.1146/annurev-genet-120116-024704.

Mayr, C. (2019) ‘What Are 3’ UTRs Doing?’, *Cold Spring Harbor Perspectives in Biology*, 11(10), p. a034728. Available at: https://doi.org/10.1101/cshperspect.a034728.

Mayya, V.K. and Duchaine, T.F. (2019) ‘Ciphers and Executioners: How 3’-Untranslated Regions Determine the Fate of Messenger RNAs’, *Frontiers in Genetics*, 10. Available at: https://doi.org/10.3389/fgene.2019.00006.

McDonald, J.C. *et al.* (2000) ‘Fabrication of microfluidic systems in poly(dimethylsiloxane)’, *ELECTROPHORESIS*, 21(1), pp. 27–40. Available at: https://doi.org/10.1002/(SICI)1522-2683(20000101)21:1<27::AID-ELPS27>3.0.CO;2-C.

Mellado, E. *et al.* (2003) ‘Cell wall biogenesis in a double chitin synthase mutant (*chs*G−/*chs*E−) of *Aspergillus fumigatus*’, *Fungal Genetics and Biology*, 38(1), pp. 98–109. Available at: https://doi.org/10.1016/S1087-1845(02)00516-9.

Miller, J.E. *et al.* (2017) ‘Genome-Wide Mapping of Decay Factor–mRNA Interactions in Yeast Identifies Nutrient-Responsive Transcripts as Targets of the Deadenylase Ccr4’, *G3: Genes|Genomes|Genetics*, 8(1), pp. 315–330. Available at: https://doi.org/10.1534/g3.117.300415.

Mir, S.S., Fiedler, D. and Cashikar, A.G. (2009) ‘Ssd1 is required for thermotolerance and Hsp104-mediated protein disaggregation in Saccharomyces cerevisiae’, *Molecular and Cellular Biology*, 29(1), pp. 187–200. Available at: https://doi.org/10.1128/MCB.02271-07.

Molino, J.V. (2020) ‘Agarose pads for microscopy’. Available at: https://www.protocols.io/view/agarose-pads-for-microscopy-bkn8kvhw (Accessed: 24 March 2024).

Moore, M.J. and Proudfoot, N.J. (2009) ‘Pre-mRNA Processing Reaches Back toTranscription and Ahead to Translation’, *Cell*, 136(4), pp. 688–700. Available at: https://doi.org/10.1016/j.cell.2009.02.001.

Mori, A. *et al.* (2015) ‘Signal peptide optimization tool for the secretion of recombinant protein from *Saccharomyces cerevisiae*’, *Journal of Bioscience and Bioengineering*, 120(5), pp. 518–525. Available at: https://doi.org/10.1016/j.jbiosc.2015.03.003.

Mosquera, L. *et al.* (1993) ‘A mRNA localized to the vegetal cortex of Xenopus oocytes encodes a protein with a nanos-like zinc finger domain’, *Development*, 117(1), pp. 377–386. Available at: https://doi.org/10.1242/dev.117.1.377.

Mouassite, M. *et al.* (2000) ‘The “SUN” family: yeast SUN4/SCW3 is involved in cell septation’, *Yeast*, 16(10), pp. 905–919. Available at: https://doi.org/10.1002/1097-0061(200007)16:10<905::AID-YEA584>3.0.CO;2-1.

Moyes, D.L. *et al.* (2016) ‘Candidalysin is a fungal peptide toxin critical for mucosal infection’, *Nature*, 532(7597), pp. 64–68. Available at: https://doi.org/10.1038/nature17625.

Mueller, F. *et al.* (2013) ‘FISH-quant: automatic counting of transcripts in 3D FISH images’, *Nature Methods*, 10(4), pp. 277–278. Available at: https://doi.org/10.1038/nmeth.2406.

Muhlrad, D. and Parker, R. (1992) 'Mutations affecting stability and deadenylation of the yeast MFA2 transcript.', *Genes & Development*, 6(11), pp. 2100–2111. Available at: https://doi.org/10.1101/gad.6.11.2100.

Muhlrad, D. and Parker, R. (1994) 'Premature translational termination triggers mRNA decapping', *Nature*, 370(6490), pp. 578–581. Available at: https://doi.org/10.1038/370578a0.

Munro, C.A. *et al.* (2003) '*CHS8*—a fourth chitin synthase gene of *Candida albicans* contributes to in vitro chitin synthase activity, but is dispensable for growth', *Fungal Genetics and Biology*, 40(2), pp. 146–158. Available at: https://doi.org/10.1016/S1087-1845(03)00083-5.

Ng, D.T., Brown, J.D. and Walter, P. (1996) 'Signal sequences specify the targeting route to the endoplasmic reticulum membrane.', *Journal of Cell Biology*, 134(2), pp. 269–278. Available at: https://doi.org/10.1083/jcb.134.2.269.

Nuñez, I. *et al.* (2016) 'Spatial control of translation repression and polarized growth by conserved NDR kinase Orb6 and RNA-binding protein Sts5', *eLife*. Edited by J.P. Taylor, 5, p. e14216. Available at: https://doi.org/10.7554/eLife.14216.

Nurse, P. (1980) 'Cell cycle control — both deterministic and probabilistic?', *Nature*, 286(5768), pp. 9–10. Available at: https://doi.org/10.1038/286009a0.

Oeffinger, M. *et al.* (2007) 'Comprehensive analysis of diverse ribonucleoprotein complexes', *Nature Methods*, 4(11), pp. 951–956. Available at: https://doi.org/10.1038/nmeth1101.

Oh, D. and Houston, D.W. (2017) 'RNA Localization in the Vertebrate Oocyte: Establishment of Oocyte Polarity and Localized mRNA Assemblages', *Results and problems in cell differentiation*, 63, pp. 189–208. Available at: https://doi.org/10.1007/978-3-319-60855-6_9.

Ohyama, Y., Kasahara, K. and Kokubo, T. (2010) 'Saccharomyces cerevisiae Ssd1p promotes CLN2 expression by binding to the 5'-untranslated region of CLN2 mRNA', *Genes to Cells*, 15(12), pp. 1169–1188. Available at: https://doi.org/10.1111/j.1365-2443.2010.01452.x.

Olivier, C. *et al.* (2005) 'Identification of a Conserved RNA Motif Essential for She2p Recognition and mRNA Localization to the Yeast Bud', *Molecular and Cellular Biology*, 25(11), pp. 4752–4766. Available at: https://doi.org/10.1128/MCB.25.11.4752-4766.2005.

Orlean, P. (2012) 'Architecture and Biosynthesis of the Saccharomyces cerevisiae Cell Wall', *Genetics*, 192(3), pp. 775–818. Available at: https://doi.org/10.1534/genetics.112.144485.

Panzner, S. *et al.* (1995) 'Posttranslational protein transport in yeast reconstituted with a purified complex of Sec proteins and Kar2p', *Cell*, 81(4), pp. 561–570. Available at: https://doi.org/10.1016/0092-8674(95)90077-2.

Paquin, N. *et al.* (2007) 'Local Activation of Yeast *ASH1* mRNA Translation through Phosphorylation of Khd1p by the Casein Kinase Yck1p', *Molecular Cell*, 26(6), pp. 795–809. Available at: https://doi.org/10.1016/j.molcel.2007.05.016.

Parker, R. (2012) 'RNA Degradation in Saccharomyces cerevisae', *Genetics*, 191(3), pp. 671–702. Available at: https://doi.org/10.1534/genetics.111.137265.

Patel, H.P., Brouwer, I. and Lenstra, T.L. (2021) 'Optimized protocol for single-molecule RNA FISH to visualize gene expression in S. cerevisiae', *STAR Protocols*, 2(3), p. 100647. Available at: https://doi.org/10.1016/j.xpro.2021.100647.

Patel, P.K. and Free, S.J. (2019) 'The Genetics and Biochemistry of Cell Wall Structure and Synthesis in Neurospora crassa, a Model Filamentous Fungus', *Frontiers in Microbiology*, 10. Available at: https://doi.org/10.3389/fmicb.2019.02294.

Perktold, A. *et al.* (2007) 'Organelle association visualized by three dimensional ultrastructural imaging of the yeast cell', *FEMS Yeast Research*, 7(4), pp. 629–638. Available at: https://doi.org/10.1111/j.1567-1364.2007.00226.x.

Phan, Q.T. *et al.* (2007) 'Als3 Is a Candida albicans Invasin That Binds to Cadherins and Induces Endocytosis by Host Cells', *PLOS Biology*, 5(3), p. e64. Available at: https://doi.org/10.1371/journal.pbio.0050064.

Pietsch, J.M. *et al.* (2023) 'Determining growth rates from bright-field images of budding cells through identifying overlaps', *eLife*. Edited by A.M. Moses and M.B. Eisen, 12, p. e79812. Available at: https://doi.org/10.7554/eLife.79812.

Piñol-Roma, S. *et al.* (1988) 'Immunopurification of heterogeneous nuclear ribonucleoprotein particles reveals an assortment of RNA-binding proteins.', *Genes & Development*, 2(2), pp. 215–227. Available at: https://doi.org/10.1101/gad.2.2.215.

Pizzinga, M. *et al.* (2019) 'Translation factor mRNA granules direct protein synthetic capacity to regions of polarized growth', *The Journal of Cell Biology*, 218(5), pp. 1564–1581. Available at: https://doi.org/10.1083/jcb.201704019.

Pollard, T.D. (2024) *Cell biology / Thomas D. Pollard, William C. Earnshaw, Jennifer Lippincott-Schwartz, Graham T. Johnson.* Fourth edition. Philadelphia, PA: Elsevier.

Popolo, L. *et al.* (1997) 'Increase in chitin as an essential response to defects in assembly of cell wall polymers in the ggp1delta mutant of Saccharomyces cerevisiae.', *Journal of Bacteriology*, 179(2), pp. 463–469.

Porter, D.F. *et al.* (2015) 'Target selection by natural and redesigned PUF proteins', *Proceedings of the National Academy of Sciences*, 112(52), pp. 15868–15873. Available at: https://doi.org/10.1073/pnas.1508501112.

Poulin, F. and Sonenberg, N. (2013) 'Mechanism of Translation Initiation in Eukaryotes', in *Madame Curie Bioscience Database [Internet]*. Landes Bioscience. Available at: https://www.ncbi.nlm.nih.gov/books/NBK6597/ (Accessed: 4 August 2024).

Pruyne, D.W., Schott, D.H. and Bretscher, A. (1998) 'Tropomyosin-containing Actin Cables Direct the Myo2p-dependent Polarized Delivery of Secretory Vesicles in Budding Yeast', *Journal of Cell Biology*, 143(7), pp. 1931–1945. Available at: https://doi.org/10.1083/jcb.143.7.1931.

Rabani, M. *et al.* (2017) 'Massively parallel reporter assay of 3'UTR sequences identifies in vivo rules for mRNA degradation', *Molecular cell*, 68(6), pp. 1083-1094.e5. Available at: https://doi.org/10.1016/j.molcel.2017.11.014.

Raj, A. *et al.* (2008) 'Imaging individual mRNA molecules using multiple singly labeled probes', *Nature Methods*, 5(10), pp. 877–879. Available at: https://doi.org/10.1038/nmeth.1253.

Rancati, G. *et al.* (2008) 'Aneuploidy and polyploidy underlie adaptive evolution of yeast cells deprived of a conserved cytokinesis motor', *Cell*, 135(5), pp. 879–893. Available at: https://doi.org/10.1016/j.cell.2008.09.039.

Rapoport, T.A. (2007) 'Protein translocation across the eukaryotic endoplasmic reticulum and bacterial plasma membranes', *Nature*, 450(7170), pp. 663–669. Available at: https://doi.org/10.1038/nature06384.

Rees, J.S. *et al.* (2015) 'Protein Neighbors and Proximity Proteomics', *Molecular & Cellular Proteomics : MCP*, 14(11), pp. 2848–2856. Available at: https://doi.org/10.1074/mcp.R115.052902.

Reis, F.P. *et al.* (2013) 'The RNase II/RNB family of exoribonucleases: putting the "Dis" in disease', *WIREs RNA*, 4(5), pp. 607–615. Available at: https://doi.org/10.1002/wrna.1180.

Reuter, J.A., Spacek, D. and Snyder, M.P. (2015) 'High-Throughput Sequencing Technologies', *Molecular cell*, 58(4), pp. 586–597. Available at: https://doi.org/10.1016/j.molcel.2015.05.004.

Ribeiro, A.J.M. *et al.* (2019) 'Emerging concepts in pseudoenzyme classification, evolution, and signaling', *Science Signaling*, 12(594), p. eaat9797. Available at: https://doi.org/10.1126/scisignal.aat9797.

Ritch, J.J. *et al.* (2010) 'The Saccharomyces SUN gene, UTH1, is Involved in Cell Wall Biogenesis', *FEMS yeast research*, 10(2), pp. 168–176. Available at: https://doi.org/10.1111/j.1567-1364.2009.00601.x.

Rodríguez-Peña, J.M. *et al.* (2000) 'A Novel Family of Cell Wall-Related Proteins Regulated Differently during the Yeast Life Cycle', *Molecular and Cellular Biology*, 20(9), pp. 3245–3255.

Röhm, M. *et al.* (2013) 'A family of secreted pathogenesis-related proteins in Candida albicans', *Molecular Microbiology*, 87(1), pp. 132–151. Available at: https://doi.org/10.1111/mmi.12087.

van Rossum, G. (1995) 'Python reference manual'. Available at: https://ir.cwi.nl/pub/5008 (Accessed: 5 February 2024).

Rougemaille, M. *et al.* (2008) 'THO/Sub2p Functions to Coordinate 3'-End Processing with Gene-Nuclear Pore Association', *Cell*, 135(2), pp. 308–321. Available at: https://doi.org/10.1016/j.cell.2008.08.005.

Roux, K.J. *et al.* (2012) 'A promiscuous biotin ligase fusion protein identifies proximal and interacting proteins in mammalian cells', *The Journal of Cell Biology*, 196(6), pp. 801–810. Available at: https://doi.org/10.1083/jcb.201112098.

Samacoits, A. *et al.* (2018) 'A computational framework to study sub-cellular RNA localization', *Nature Communications*, 9(1), p. 4584. Available at: https://doi.org/10.1038/s41467-018-06868-w.

Savinov, A. *et al.* (2021) 'Effects of sequence motifs in the yeast 3' untranslated region determined from massively parallel assays of random sequences', *Genome Biology*, 22(1), p. 293. Available at: https://doi.org/10.1186/s13059-021-02509-6.

Schmid, M. *et al.* (2006) 'Coordination of Endoplasmic Reticulum and mRNA Localization to the Yeast Bud', *Current Biology*, 16(15), pp. 1538–1543. Available at: https://doi.org/10.1016/j.cub.2006.06.025.

Schmidt, M.W. *et al.* (2007) 'Comparative proteomic and transcriptomic profiling of the fission yeast Schizosaccharomyces pombe', *Molecular Systems Biology*, 3, p. 79. Available at: https://doi.org/10.1038/msb4100117.

Schwarzmüller, T. *et al.* (2014) 'Systematic Phenotyping of a Large-Scale Candida glabrata Deletion Collection Reveals Novel Antifungal Tolerance Genes', *PLOS Pathogens*, 10(6), p. e1004211. Available at: https://doi.org/10.1371/journal.ppat.1004211.

Semotok, J.L. *et al.* (2005) 'Smaug Recruits the CCR4/POP2/NOT Deadenylase Complex to Trigger Maternal Transcript Localization in the Early Drosophila Embryo', *Current Biology*, 15(4), pp. 284–294. Available at: https://doi.org/10.1016/j.cub.2005.01.048.

Shalem, O. *et al.* (2013) 'Measurements of the Impact of 3' End Sequences on Gene Expression Reveal Wide Range and Sequence Dependent Effects', *PLoS Computational Biology*, 9(3), p. e1002934. Available at: https://doi.org/10.1371/journal.pcbi.1002934.

Shaner, N.C. *et al.* (2013) 'A bright monomeric green fluorescent protein derived from Branchiostoma lanceolatum', *Nature Methods*, 10(5), pp. 407–409. Available at: https://doi.org/10.1038/nmeth.2413.

Shashkova, S. and Leake, M.C. (2017) 'Single-molecule fluorescence microscopy review: shedding new light on old problems', *Bioscience Reports*, 37(4), p. BSR20170031. Available at: https://doi.org/10.1042/BSR20170031.

Shen, X.-X. *et al.* (2018) 'Tempo and Mode of Genome Evolution in the Budding Yeast Subphylum', *Cell*, 175(6), pp. 1533-1545.e20. Available at: https://doi.org/10.1016/j.cell.2018.10.023.

Shen, Z. *et al.* (2009) 'Nuclear Shuttling of She2p Couples ASH1 mRNA Localization to its Translational Repression by Recruiting Loc1p and Puf6p', *Molecular Biology of the Cell*, 20(8), pp. 2265–2275. Available at: https://doi.org/10.1091/mbc.E08-11-1151.

Shepard, K.A. *et al.* (2003) 'Widespread cytoplasmic mRNA transport in yeast: Identification of 22 bud-localized transcripts using DNA microarray analysis', *Proceedings of the National Academy of Sciences*, 100(20), pp. 11429–11434. Available at: https://doi.org/10.1073/pnas.2033246100.

Sil, A. and Herskowitz, I. (1996) 'Identification of an Asymmetrically Localized Determinant, Ash1p, Required for Lineage-Specific Transcription of the Yeast HO Gene', *Cell*, 84(5), pp. 711–722. Available at: https://doi.org/10.1016/S0092-8674(00)81049-1.

Singh, G. *et al.* (2015) 'The Clothes Make the mRNA: Past and Present Trends in mRNP Fashion', *Annual Review of Biochemistry*, 84(1), pp. 325–354. Available at: https://doi.org/10.1146/annurev-biochem-080111-092106.

Skinner, S.O. *et al.* (2013) 'Measuring mRNA copy number in individual Escherichia coli cells using single-molecule fluorescent in situ hybridization', *Nature Protocols*, 8(6), pp. 1100–1113. Available at: https://doi.org/10.1038/nprot.2013.066.

Skotheim, J.M. *et al.* (2008) 'Positive feedback of G1 cyclins ensures coherent cell cycle entry', *Nature*, 454(7202), pp. 291–296. Available at: https://doi.org/10.1038/nature07118.

Song, Y. *et al.* (2008) 'Role of the RAM network in cell polarity and hyphal morphogenesis in Candida albicans', *Molecular Biology of the Cell*, 19(12), pp. 5456–5477. Available at: https://doi.org/10.1091/mbc.e08-03-0272.

Sorokin, M.I., Knorre, D.A. and Severin, F.F. (2014) 'Early manifestations of replicative aging in the yeast *Saccharomyces cerevisiae*.', *Microbial Cell*, 1(1), pp. 37–42. Available at: https://doi.org/10.15698/mic2014.01.122.

Stadler, C. *et al.* (2013) 'Immunofluorescence and fluorescent-protein tagging show high correlation for protein localization in mammalian cells', *Nature Methods*, 10(4), pp. 315–323. Available at: https://doi.org/10.1038/nmeth.2377.

Steiger, M. *et al.* (2003) 'Analysis of recombinant yeast decapping enzyme', *RNA*, 9(2), pp. 231–238. Available at: https://doi.org/10.1261/rna.2151403.

Steitz, J.A. (1969) 'Polypeptide chain initiation: nucleotide sequences of the three ribosomal binding sites in bacteriophage R17 RNA', *Nature*, 224(5223), pp. 957–964. Available at: https://doi.org/10.1038/224957a0.

Stewart, G.G. (2017) 'The Structure and Function of the Yeast Cell Wall, Plasma Membrane and Periplasm', in G.G. Stewart (ed.) *Brewing and Distilling Yeasts*. Cham: Springer International Publishing (The Yeast Handbook), pp. 55–75. Available at: https://doi.org/10.1007/978-3-319-69126-8_5.

Stringer, C. *et al.* (2021) 'Cellpose: a generalist algorithm for cellular segmentation', *Nature Methods*, 18(1), pp. 100–106. Available at: https://doi.org/10.1038/s41592-020-01018-x.

Sudbery, P.E. (2011) 'Growth of Candida albicans hyphae', *Nature Reviews Microbiology*, 9(10), pp. 737–748. Available at: https://doi.org/10.1038/nrmicro2636.

Sundstrom, P. (2002) 'Adhesion in Candida spp', *Cellular Microbiology*, 4(8), pp. 461–469. Available at: https://doi.org/10.1046/j.1462-5822.2002.00206.x.

Sutton, A., Immanuel, D. and Arndt, K.T. (1991) 'The SIT4 protein phosphatase functions in late G1 for progression into S phase.', *Molecular and Cellular Biology*, 11(4), pp. 2133–2148.

Sy, B. *et al.* (2018) 'High-Resolution, High-Throughput Analysis of Hfq-Binding Sites Using UV Crosslinking and Analysis of cDNA (CRAC)', in V. Arluison and C. Valverde (eds) *Bacterial Regulatory RNA: Methods and Protocols*. New York, NY: Springer, pp. 251–272. Available at: https://doi.org/10.1007/978-1-4939-7634-8_15.

Takizawa, P.A. *et al.* (2000) 'Plasma Membrane Compartmentalization in Yeast by Messenger RNA Transport and a Septin Diffusion Barrier', *Science*, 290(5490), pp. 341–344. Available at: https://doi.org/10.1126/science.290.5490.341.

Talia, S.D. *et al.* (2007) 'The effects of molecular noise and size control on variability in the budding yeast cell cycle', *Nature*, 448(7156), pp. 947–951. Available at: https://doi.org/10.1038/nature06072.

Tanaka, S. *et al.* (2007) 'Saccharomyces cerevisiae SSD1 orthologues are essential for host infection by the ascomycete plant pathogens Colletotrichum lagenarium and Magnaporthe grisea', *Molecular Microbiology*, 64(5), pp. 1332–1349. Available at: https://doi.org/10.1111/j.1365-2958.2007.05742.x.

Taylor, R.J., Tagiltsev, G. and Briggs, J.A.G. (2023) 'The structure of COPI vesicles and regulation of vesicle turnover', *FEBS Letters*, 597(6), pp. 819–835. Available at: https://doi.org/10.1002/1873-3468.14560.

Terashima, H. *et al.* (2002) 'Sequence-based approach for identification of cell wall proteins in Saccharomyces cerevisiae', *Current Genetics*, 40(5), pp. 311–316. Available at: https://doi.org/10.1007/s00294-001-0264-9.

Teunissen, A.W.R.H. and Steensma, H.Y. (1995) 'The dominant flocculation genes of Saccharomyces cerevisiae constitute a new subtelomeric gene family', *Yeast*, 11(11), pp. 1001–1013. Available at: https://doi.org/10.1002/yea.320111102.

Thammahong, A. *et al.* (2019) 'An Ssd1 Homolog Impacts Trehalose and Chitin Biosynthesis and Contributes to Virulence in Aspergillus fumigatus', *mSphere*, 4(3), pp. e00244-19. Available at: https://doi.org/10.1128/mSphere.00244-19.

Toda, T. *et al.* (1996) 'The fission yeast STS5+ gene is required for maintenance of growth polarity and functionally interacts with protein kinase C and an osmosensing MAP-kinase pathway', *Journal of Cell Science*, 109(9), pp. 2331–2342. Available at: https://doi.org/10.1242/jcs.109.9.2331.

Toikkanen, J.H. *et al.* (2003) 'The β Subunit of the Sec61p Endoplasmic Reticulum Translocon Interacts with the Exocyst Complex in *Saccharomyces cerevisiae**', *Journal of Biological Chemistry*, 278(23), pp. 20946–20953. Available at: https://doi.org/10.1074/jbc.M213111200.

Tong, A.H.Y. *et al.* (2002) 'A Combined Experimental and Computational Strategy to Define Protein Interaction Networks for Peptide Recognition Modules', *Science*, 295(5553), pp. 321–324. Available at: https://doi.org/10.1126/science.1064987.

Tonikian, R. *et al.* (2009) 'Bayesian Modeling of the Yeast SH3 Domain Interactome Predicts Spatiotemporal Dynamics of Endocytosis Proteins', *PLOS Biology*, 7(10), p. e1000218. Available at: https://doi.org/10.1371/journal.pbio.1000218.

Trautwein, M. *et al.* (2004) 'Arf1p Provides an Unexpected Link between COPI Vesicles and mRNA in Saccharomyces cerevisiae', *Molecular Biology of the Cell*, 15(11), pp. 5021–5037. Available at: https://doi.org/10.1091/mbc.e04-05-0411.

Trcek, T. *et al.* (2011) 'Single-Molecule mRNA Decay Measurements Reveal Promoter- Regulated mRNA Stability in Yeast', *Cell*, 147(7), pp. 1484–1497. Available at: https://doi.org/10.1016/j.cell.2011.11.051.

Tsanov, N. *et al.* (2016) 'smiFISH and FISH-quant – a flexible single RNA detection approach with super-resolution capability', *Nucleic Acids Research*, 44(22), p. e165. Available at: https://doi.org/10.1093/nar/gkw784.

Tucker, M. *et al.* (2001) 'The Transcription Factor Associated Ccr4 and Caf1 Proteins Are Components of the Major Cytoplasmic mRNA Deadenylase in Saccharomyces cerevisiae', *Cell*, 104(3), pp. 377–386. Available at: https://doi.org/10.1016/S0092-8674(01)00225-2.

Tuller, T., Ruppin, E. and Kupiec, M. (2009) 'Properties of untranslated regions of the S. cerevisiae genome', *BMC Genomics*, 10, p. 391. Available at: https://doi.org/10.1186/1471-2164-10-391.

Tutol, J.N., Kam, H.C. and Dodani, S.C. (2019) 'Identification of mNeonGreen as a pH-Dependent, Turn-On Fluorescent Protein Sensor for Chloride', *Chembiochem : a European journal of chemical biology*, 20(14), pp. 1759–1765. Available at: https://doi.org/10.1002/cbic.201900147.

Tutucci, E. *et al.* (2022) 'Cyclin CLB2 mRNA localization determines efficient protein synthesis to orchestrate bud growth and cell cycle progression'. bioRxiv, p. 2022.03.01.481833. Available at: https://doi.org/10.1101/2022.03.01.481833.

Tutucci, E. and Singer, R.H. (2020) 'Simultaneous Detection of mRNA and Protein in S. cerevisiae by Single-Molecule FISH and Immunofluorescence', in M. Heinlein (ed.) *RNA Tagging: Methods and Protocols*. New York, NY: Springer US (Methods in Molecular Biology), pp. 51–69. Available at: https://doi.org/10.1007/978-1-0716-0712-1_4.

Ustianenko, D. *et al.* (2013) 'Mammalian DIS3L2 exoribonuclease targets the uridylated precursors of let-7 miRNAs', *RNA*, 19(12), pp. 1632–1638. Available at: https://doi.org/10.1261/rna.040055.113.

Verstrepen, K.J. and Klis, F.M. (2006) 'Flocculation, adhesion and biofilm formation in yeasts', *Molecular Microbiology*, 60(1), pp. 5–15. Available at: https://doi.org/10.1111/j.1365-2958.2006.05072.x.

Vitulo, N. *et al.* (2007) 'Characterization and Evolution of the Cell Cycle-Associated Mob Domain-Containing Proteins in Eukaryotes', *Evolutionary Bioinformatics Online*, 3, pp. 121–158.

Wahle, E. and Winkler, G.S. (2013) 'RNA decay machines: Deadenylation by the Ccr4–Not and Pan2–Pan3 complexes', *Biochimica et Biophysica Acta (BBA) - Gene Regulatory Mechanisms*, 1829(6), pp. 561–570. Available at: https://doi.org/10.1016/j.bbagrm.2013.01.003.

Walker, L.A. *et al.* (2008) 'Stimulation of Chitin Synthesis Rescues Candida albicans from Echinocandins', *PLOS Pathogens*, 4(4), p. e1000040. Available at: https://doi.org/10.1371/journal.ppat.1000040.

Walt, S. van der *et al.* (2014) 'scikit-image: image processing in Python', *PeerJ*, 2, p. e453. Available at: https://doi.org/10.7717/peerj.453.

Wang, Z. *et al.* (2019) 'Novel insights into global translational regulation through Pumilio family RNA-binding protein Puf3p revealed by ribosomal profiling', *Current genetics*, 65(1), pp. 201–212. Available at: https://doi.org/10.1007/s00294-018-0862-4.

Wanless, A.G., Lin, Y. and Weiss, E.L. (2014) 'Cell morphogenesis proteins are translationally controlled through UTRs by the Ndr/LATS target Ssd1', *PloS One*, 9(1), p. e85212. Available at: https://doi.org/10.1371/journal.pone.0085212.

Waskom, M. (2021) 'seaborn: statistical data visualization', *Journal of Open Source Software*, 6(60), p. 3021. Available at: https://doi.org/10.21105/joss.03021.

Weiss, E.L. *et al.* (2002) 'The Saccharomyces cerevisiae Mob2p-Cbk1p kinase complex promotes polarized growth and acts with the mitotic exit network to facilitate daughter cell-specific localization of Ace2p transcription factor', *The Journal of Cell Biology*, 158(5), pp. 885–900. Available at: https://doi.org/10.1083/jcb.200203094.

Weissman, Z. and Kornitzer, D. (2004) 'A family of Candida cell surface haem-binding proteins involved in haemin and haemoglobin-iron utilization', *Molecular Microbiology*, 53(4), pp. 1209–1220. Available at: https://doi.org/10.1111/j.1365-2958.2004.04199.x.

Werner-Washburne, M. *et al.* (1993) 'Stationary phase in the yeast Saccharomyces cerevisiae.', *Microbiological Reviews*, 57(2), pp. 383–401.

Wheeler, E.C., Van Nostrand, E.L. and Yeo, G.W. (2018) 'Advances and challenges in the detection of transcriptome-wide protein–RNA interactions', *Wiley Interdisciplinary Reviews. RNA*, 9(1), p. e1436. Available at: https://doi.org/10.1002/wrna.1436.

Wheeler, R.T. *et al.* (2003) 'A Saccharomyces cerevisiae mutant with increased virulence', *Proceedings of the National Academy of Sciences of the United States of America*, 100(5), pp. 2766–2770. Available at: https://doi.org/10.1073/pnas.0437995100.

Wickens, M. *et al.* (2002) 'A PUF family portrait: 3'UTR regulation as a way of life', *Trends in Genetics*, 18(3), pp. 150–157. Available at: https://doi.org/10.1016/S0168-9525(01)02616-6.

Wood, V. *et al.* (2002) 'The genome sequence of Schizosaccharomyces pombe', *Nature*, 415(6874), pp. 871–880. Available at: https://doi.org/10.1038/nature724.

Xie, Y. and Ren, Y. (2019) 'Mechanisms of nuclear mRNA export: a structural perspective', *Traffic (Copenhagen, Denmark)*, 20(11), pp. 829–840. Available at: https://doi.org/10.1111/tra.12691.

Yeaman, M.R. *et al.* (2004) 'Susceptibility to Thrombin-Induced Platelet Microbicidal Protein Is Associated with Increased Fluconazole Efficacy against Experimental Endocarditis Due to Candida albicans', *Antimicrobial Agents and Chemotherapy*, 48(8), pp. 3051–3056. Available at: https://doi.org/10.1128/AAC.48.8.3051-3056.2004.

Yofe, I. *et al.* (2016) 'One library to make them all: Streamlining yeast library creation by a SWAp-Tag (SWAT) strategy', *Nature methods*, 13(4), pp. 371–378. Available at: https://doi.org/10.1038/nmeth.3795.

Yosefzon, Y. *et al.* (2011) 'Divergent RNA binding specificity of yeast Puf2p', *RNA*, 17(8), pp. 1479–1488. Available at: https://doi.org/10.1261/rna.2700311.

Young, B.P. *et al.* (2001) 'Sec63p and Kar2p are required for the translocation of SRP-dependent precursors into the yeast endoplasmic reticulum in vivo', *The EMBO Journal*, 20(1–2), pp. 262–271. Available at: https://doi.org/10.1093/emboj/20.1.262.

Zacharias, D.A. *et al.* (2002) 'Partitioning of Lipid-Modified Monomeric GFPs into Membrane Microdomains of Live Cells', *Science*, 296(5569), pp. 913–916. Available at: https://doi.org/10.1126/science.1068539.

Zakhartsev, M. and Reuss, M. (2018) 'Cell size and morphological properties of yeast Saccharomyces cerevisiae in relation to growth temperature', *FEMS Yeast Research*, 18(6), p. foy052. Available at: https://doi.org/10.1093/femsyr/foy052.

Zenklusen, D. *et al.* (2002) 'Stable mRNP Formation and Export Require Cotranscriptional Recruitment of the mRNA Export Factors Yra1p and Sub2p by Hpr1p', *Molecular and Cellular Biology*, 22(23), pp. 8241–8253. Available at: https://doi.org/10.1128/MCB.22.23.8241-8253.2002.

Zhao, W. *et al.* (2014) 'Massively parallel functional annotation of 3' untranslated regions', *Nature biotechnology*, 32(4), pp. 387–391. Available at: https://doi.org/10.1038/nbt.2851.

Zhou, Z.D. and Tan, E.-K. (2017) 'Iron regulatory protein (IRP)-iron responsive element (IRE) signaling pathway in human neurodegenerative diseases', *Molecular Neurodegeneration*, 12(1), p. 75. Available at: https://doi.org/10.1186/s13024-017-0218-4.